Development of an Improved Design Procedure for Unbonded Concrete Overlays

Lev Khazanovich, Ph.D, Principal Investigator
Department of Civil and Environmental Engineering
University of Pittsburgh

February 2020

MnROAD
Safer, Smarter, Sustainable Pavements Through Innovative Research

Technical Report Documentation Page

1. Report No. MN 2020-08	2.	3. Recipients Accession No.	
4. Title and Subtitle Development of an Improved Design Procedure for Unbonded Concrete Overlays		5. Report Date February 2020	
		6.	
7. Author(s) Lev Khazanovich, Julie Vandenbossche, John DeSantis and Steve Sachs		8. Performing Organization Report No.	
9. Performing Organization Name and Address Department of Civil and Environmental Engineering University of Pittsburgh 3700 O'Hara Street, Pittsburgh, PA 15261-2294		10. Project/Task/Work Unit No.	
		11. Contract (C) or Grant (G) No. (c) 1003327 (wo) 2	
12. Sponsoring Organization Name and Address Minnesota Department of Transportation Office of Research & Innovation 395 John Ireland Boulevard, MS 330 St. Paul, Minnesota 55155-1899		13. Type of Report and Period Covered Final Report	
		14. Sponsoring Agency Code	
15. Supplementary Notes http://mndot.gov/research/reports/2020/202008.pdf			

16. Abstract (Limit: 250 words)

An unbonded portland cement concrete overlay of concrete pavements (UBOL) is a rehabilitation technique in which the new overlay is isolated from the existing distressed pavement using a separator layer. Typically, a 1-to 2-in asphalt separator layer (or interlayer) is used. Recent innovations in the unbonded overlay technology have led to the adoption of new types of interlayers, such as non-woven geotextile fabric, as well as the use of overlays with joint spacings and layouts that are much shorter than conventional joint spacings. The effect of these design alternatives on the performance of the UBOL cannot be accounted for using currently available design procedures. This report documents the development of a new mechanistic-empirical design procedure for UBOL. It presents the results of laboratory and field studies; the calibration of an advanced structural (Totski) model that better captures the effects of the interlayer and separation between the overlay and the existing pavement; and the development of cracking and faulting performance prediction models for UBOL. The performance prediction models were incorporated into a rudimentary software tool, Pitt UBOL-ME, that can be used for the design and analysis of UBOL. Unlike prior UBOL design procedures, Pitt UBOL-ME can be used to quantify the effect of the performance of the interlayer on the performance of the UBOL and can be used for both conventional and short joint spacings.

17. Document Analysis/Descriptors concrete overlays, pavement interlayers, pavement cracking, faulting, erosion		18. Availability Statement No restrictions. Document available from: National Technical Information Services, Alexandria, Virginia 22312	
19. Security Class (this report) Unclassified	20. Security Class (this page) Unclassified	21. No. of Pages 328	22. Price

DEVELOPMENT OF AN IMPROVED DESIGN PROCEDURE FOR UNBONDED CONCRETE OVERLAYS

FINAL REPORT

Prepared by:

Lev Khazanovich, Ph.D.
Julie M. Vandenbossche, Ph.D., P.E.
Steve Sachs, Ph.D.
John W. DeSantis
Department of Civil and Environmental Engineering
University of Pittsburgh

FEBRUARY 2020

TABLE OF CONTENTS

LIST OF FIGURES

LIST OF TABLES

EXECUTIVE SUMMARY

Pooled Fund study TPF-5(269), *Development of an Improved Design Procedure for Unbonded Concrete Overlays*, is sponsored by the Georgia, Iowa, Kansas, Michigan, Minnesota (lead state), Missouri, North Carolina, and Oklahoma departments of Transportation. An unbonded Portland cement concrete (PCC) overlay is a type of rehabilitation method in which the new overlay is isolated from the existing pavement using a separator layer. Typically, hot mix asphalt (HMA) with 1-to 2-inch thickness is used as a separator layer, or interlayer. This type of rehabilitation is usually cost-effective when pre-overlay repairs can be minimized by using a separator layer, especially for moderately to severely distressed pavements. Although unbonded concrete overlays (UBOLs) have been used since 1916, there is still lack of reliable procedures or guidance on the design and construction features that can make them a more cost-effective rehabilitation solution. Recent innovations in the unbonded overlay technology have led to introduction of new types of interlayers, such as non-woven geotextiles, as well as the use of overlays with joint spacings and layouts that are much shorter than conventional joint spacings. These design alternatives cannot be characterized by the currently available design procedures.

The objective of this eight-state pooled fund study was development of a standalone national design procedure that would result in improved performance and life-span prediction of UBOLs constructed over existing concrete or composite pavements. To achieve the objective of this project, the research team reviewed literature pertaining to design and performance of unbonded concrete overlays, performed laboratory and field studies, developed improved mechanistic-empirical performance prediction models for UBOLs, and developed rudimentary software for design and performance prediction of UBOLs.

A comprehensive literature review identified a variety of design factors currently considered by the existing overlay design methods including traffic, interface conditions, material properties, condition of the existing pavement, temperature curling or moisture warping, joint spacing, load transfer, and failure criteria. The available design methods, including the current American Association of State Highway and Transportation Officials (AASHTO) *Mechanistic-Empirical Pavement Design Guide* (*MEPDG*), do not consider the same design factors. The existing procedures include different ways of accounting for these factors; some procedures ignore the influence of some of the design factors believed to be important by others. The currently available design procedures do not account directly for structural contribution of the interlayer.

A survey was developed to evaluate the past and current practices transportation agencies are using for UBOLs and to assess the performance of those in service. Data collected on design and performance of UBOLs in several participating states showed a variety of overlay geometry, interlayer materials and presence of distresses. Common distresses seen in UBOLs include pumping and erosion of the HMA interlayer, minor cracking after 5-20 years, and joint deterioration due to freeze-thaw damage after 5-10 years. However, most of the overlays exhibited very good performance for 20-plus years after construction, showing this to be a sound rehabilitation alternative. The transportation agencies also suggested the following recommendations developed based on their experience with UBOLs:

- Clear drainage paths should be provided in design and drainage maintenance should be performed with regularity.
- Crown corrections to encourage drainage should be made in the concrete overlay and not in the HMA layer to prevent "punch down" failures and stripping.
- Dowels improve performance of overlays experiencing pumping and erosion, especially in thick overlays.
- Pre-overlay repairs are deemed only to be necessary for severely distressed areas.
- Widened slabs with thick UBOLs can cause longitudinal cracking.
- A knife-edge technique can be used successfully to create longitudinal joints for 6-ft by 6-ft panel pavements.

Field pavement surveys were conducted to determine distresses associated with UBOLs. The predominant distress in these pavements was longitudinal cracking and different cracking mechanisms, and causes were identified, including erosion of the interlayer between the lane shoulder joint and the wheel path, as well as consolidation of the HMA interlayer or localized erosion at the intersection of the wheel path and the transverse joint. It was found that ensuring adequate drainage and maintaining edge drains were significantly important to the structures where the interlayer was susceptible to erosion. If the drainage system backs up, then water will remain trapped in the interlayer. Corner breaks were also observed in many sections in what could also be the result of drainage issues. Moreover, faulting was identified on some sections indicating pumping of the HMA interlayer, resulting in a loss of support due to interlayer material breakdown that must be accounted for in the design process.

A laboratory investigation was conducted to examine the effects of the interlayer on the response of the pavement structure under load and to investigate the interlayer's ability to prevent reflective cracking. HMA and nonwoven geotextile (thick and thin fabric) interlayer systems were considered. The specimens with asphalt interlayers were sawed from in-service pavements to ensure that mixture proportioning and density of the asphalt interlayers were typical of those found in the field. These asphalt-concrete composite beams were obtained from the Minnesota and Michigan departments of Transportation.

The laboratory study revealed that a discrete joint or crack in the existing pavement will tend not to reflect up into the overlay under normal wheel loads when the existing pavement is fully supported. However, when a void is simulated under the discontinuity in the existing pavement, a reflective crack is possible. The measured deflection characteristics were used to establish stiffness for validating the structural models. Specimens with a fabric interlayer exhibited lower stiffness than the specimens with an HMA interlayer. In the latter, permanent compression developed in the HMA over time. High values of interlayer compression indicate that either damage or displacement occurred in the interlayer.

The results of the laboratory study were used to establish parameters for these interlayers for structural modeling of UBOLs required for development of a mechanistic-empirical design procedure for UBOLs. In this study, the Totski model was adapted for structural modeling of UBOLs. This model simulates an UBOL and a slab resting on a spring interlayer supported by a slab resting on the Winkler subgrade. The

advantage of this model is that it is capable of explicitly modeling the "cushioning" property of the interlayer. This model was developed specifically for modeling of UBOLs but has not been widely used due to lack of data needed to verify the procedure for selection of the spring interlayer stiffness parameter. The laboratory research conducted and field testing gathered during this study provided the information needed for this task.

The structural model calibrated with lab and field data was used for development of mechanistic-empirical design performance prediction models for UBOLs: fatigue cracking model and joint faulting model. Both models utilize the current AASHTO *MEPDG* incremental damage framework but offer significant enhancements compared to the currently available models.

The UBOL cracking prediction model developed in this study considers four mechanisms of cracking: (i) initiating at the bottom overlay surface near mid-slab overlay/shoulder joint and propagating upward and transversely; (ii) initiating at the top overlay surface near mid-slab overlay/shoulder joint and propagating downward and transversely; (iii) initiating at the bottom of the overlay transverse joint and propagating upward and longitudinally; and (iv) initiating at the top of the overlay transverse joint and propagating downward and longitudinally. Neural Networks for bottom and top stresses in two critical locations were developed for conventional and short width UBOLs. The modifications of the temperature data linearization and built-in curl analyses were incorporated into the model. The model was successfully calibrated using the Long-Term Pavement Performance (LTPP) data and validated using a variety of design inputs, vehicle and environmental loading. The effect of different design parameters was studied in a sensitivity study. The model quantifies the influence of dowels, overlay thickness, interlayer material (stiffness), joint spacing, shoulder type, and dowel diameter.

The current *MEPDG* faulting model assumed that overlay faulting was the result of subgrade erosion below the existing pavement slab. Based on the results of laboratory and field observations, the UBOL faulting model developed in this study assumed that overlay faulting was the result of erosion of the interlayer. Thus, relating interlayer erosion potential with the interlayer material properties through the interlayer erodibility index was an important part of the faulting model development. Neural Networks were developed to predict critical overlay responses: the slab curling corner deflections and the deflection basins. The 2-ft by 6-ft basin size was selected to characterize overlay structural response under axial loading instead of deflections at the corner, because the basin was able to more accurately represent the difference in energy density on both sides of the joint. The model was calibrated using the performance data from the LTPP, MnROAD, and Michigan Department of Transportation (MDOT) pavement sections.

To facilitate implementation of the design procedure developed in this study, a standalone rudimentary software was developed with a full user guide. The software can perform two types of analyses: performance prediction and reliability. If the performance prediction option is selected, the program predicts the percentage of cracked slabs and mean joint faulting at the end of the design life for a given overlay thickness. If the reliability analysis option is selected, the program finds the overlay thickness meeting the specified cracking reliability level and predicts joint faulting for the specified faulting reliability level.

The final report also discusses advantages and disadvantages of various interlayer types. Dense-graded HMA is relatively resistant to internal breakdown and stripping because water does not flow through the interlayer. However, it is not drainable, and trapped water can cause erosion and stripping at the interfaces. Open-graded HMA allows water to drain, but the material is often more susceptible to degradation due to stripping and raveling. Excessively porous open-graded HMA may have insufficient strength and stability to resist severe deformation or degradation. Nonwoven geotextile fabric is not erodible and allows drainage through in-plane fabric permittivity. These fabrics are generally highly effective at reducing friction or bond between the overlay and underlying pavement. The use of tie bars or structural concrete fibers is sometimes required to prevent longitudinal joints from opening. Due to the lack of bond with the older concrete, thinner overlays may be free to curl up when placed on a fabric interlayer.

CHAPTER 1: INTRODUCTION

An unbonded Portland cement concrete (PCC) overlay is a type of rehabilitation method in which the new overlay is isolated from the existing pavement using a separator layer (Smith et al., 2002). Typically, Hot Mix Asphalt (HMA) with 1-to 2-inch thickness is used as a separator layer, or interlayer. Recently, non-woven geotextile fabrics have also become a popular interlayer option for unbonded concrete overlays (UBOLs). An interlayer is installed to ensure the overlay behaves independently from the existing pavement. By providing a shear plane for differential movement, the separator layer prevents the formation of reflective cracking and serves as a debonding layer between the two concrete layers (Torres et al., 2012). The interlayer provides a level surface for the overlay and isolates the overlay from the underlying distresses and irregularities (Smith et al., 2002). As a result, the existing pavement behaves as a stable foundation for the UBOL. This type of rehabilitation is usually cost-effective when pre-overlay repairs can be minimized by using a separator layer, especially for moderately to severely distressed pavements (Torres et al., 2012).

Although UBOLs have been used since 1916 as a successful method of rehabilitation, there is still a lack of reliable procedures and guidance on the design and construction features that can make it a more cost-effective rehabilitation solution. Consequently, even though highway agencies in California, Indiana, Iowa, Illinois, Michigan, Minnesota, Michigan, Missouri, Texas, and other states routinely use this type of overlay, there are a number of agencies that do not even consider rehabilitation with UBOLs; many are unfamiliar with its design and construction.

Recent innovations in the UBOL technology led to introduction of new types of interlayers, such as non-woven geotextiles, as well as the use of overlays with joint spacings and layouts that are much shorter than conventional joint spacings. These design alternatives cannot be characterized by the currently available design procedures.

The objective of this eight-state pooled fund study was development of a standalone national design procedure that would result in improved performance and life-span prediction of UBOLs constructed over existing concrete or composite pavements. The new procedure incorporates the best features from existing UBOL designs, as well as improved structural and fatigue models that consider the effects from the environment and the behavior of the wide range of interlayer systems currently in use.

To achieve the objective of this research, the research team:

1. Reviewed literature pertaining to design and performance of UBOLs;
2. Performed laboratory and field studies;
3. Developed improved mechanistic-empirical cracking and faulting models for UBOLs;
4. And developed rudimentary software for design and performance prediction UBOLs.

This document contains eleven chapters. Chapter 1 gives a brief introduction to the research performed. Chapter 2 provides a literature review of available design procedures and performance studies. Chapter 3 summarizes information on design and performance of UBOLs in several states participating in this pooled fund study. Chapter 4 presents results of the laboratory investigation employed to examine the effects of the interlayer on the response of the UBOL structure under load. Chapter 5 describes the results of the calibration of the structural model for UBOLs. The developments of the cracking and faulting models for UBOLs are documented in Chapters 6 and 7, respectively. Chapter 8 discusses suitability of existing project to receive a UBOL as a rehabilitation alternative. Chapter 9 provides guidelines for selection of a suitable interlayer for a UBOL. Chapter 10 summarizes the basic inputs to the software procedure UBOLDesign. Chapter 11 summaries the accomplishments of the study and recommendations for future research.

CHAPTER 2: LITERATURE REVIEW

This chapter summarizes a review of the design procedures and performance studies of unbonded concrete overlays available prior to this study.

2.1 EXISTING DESIGN PROCEDURES

Several design procedures for unbonded concrete overlays reviewed in this study represent the major approaches available for the analysis and design of concrete overlays placed on non-fractured existing concrete pavements. The procedures include the following:

- Corps of Engineers (departments of the Army and the Air Force 1979; Army Corps of Engineers 2001)
- AASHTO (1993)
- Portland Cement Association (PCA) (Tayabji and Okamoto 1985)
- Minnesota DOT (1993)
- FAA (Rollings 1988)
- MEPDG (NCHRP 2004)

Other current overlay design procedures are closely associated with one of the above.

Table 1 presents an overview of the major features of the six design procedures. As the table shows, these procedures do not consider the same design factors. They include different ways of considering the influence of these factors, and some procedures ignore the influence of some of the design factors believed to be important by others. Brief descriptions of these design procedures are provided below.

Table 1: Design factors considered in unbonded overlay design methods

Design Factors	AASHTO	Corps of Engineers	Rollings	PCA	Minnesota DOT	*MEPDG*
Analytical Model	Empirical equation ($h^n = h^n - h_e^n$)	Empirical equation ($h^n = h^n - h_e^n$)	Layered elastic theory	Plate theory/finite element model JSLAB	Corps of Engineers/PCA	Plate theory/finite element model ISLAB2000
2. Failure criteria	Deterioration in terms of serviceability loss	Cracking in 50% of slabs	Deterioration in terms of a Structural Condition Index (SCI)	Depends on failure criterion for full depth concrete design procedure	Not applicable	Transverse cracking and joint faulting
3. Interface condition	Considers overlay to be fully unbonded, n=2	Power in design equation is adjusted to account for level of bonding	Varies between full bonding and completely unbonded	Unbonded	Power in design equation is adjusted to account for level of bonding	Unbonded
4. Material properties	Modulus of elasticity and flexural strength for overlay concrete, k-value for subgrade	Equivalent required thickness, "h," as input to empirical equation	Modulus of elasticity and Poisson's ratio for all materials, and flexural strength of overlay concrete	Modulus of elasticity and modulus of rupture for overlay concrete, k-value for subgrade	Modulus of elasticity and modulus of rupture for overlay concrete, k-value for subgrade	Modulus of elasticity and Poisson's ratio for all materials, flexural strength, coefficient of thermal expansion for overlay concrete
5. Difference in strength/modulus of overlay and base pavement concrete	Not considered	Thickness of base pavement is adjusted	Included directly in calculation of stresses and design factors	Included directly in calculation of stresses and design factors	Not considered	Included directly in calculation of stresses and deflections

Design Factors	AASHTO	Corps of Engineers	Rollings	PCA	Minnesota DOT	*MEPDG*
6. Cracking in base pavement before overlay	Effective thickness of base pavement is reduced	Effective thickness of base pavement is reduced	Modulus of elasticity of base pavement is reduced	Included directly in calculation of stresses using soft elements	Thickness of base pavement is reduced	PCC damage in the existing slab is considered through a reduction in its elastic modulus
7. Fatigue effects of traffic on uncracked base pavement	Effective thickness of base pavement is reduced	Effective thickness of base pavement is reduced	Included in terms of equivalent traffic	Not considered	Not considered	Not considered
8. Cracking of base after overlay	Not directly considered	Not directly considered	Modulus of elasticity of base is reduced to compensate for cracking under traffic	Not considered	Not considered	Not considered
9. Temperature curling or moisture warping	Assumes AASHTO Road Test conditions	Not considered	Not considered	Does not affect thickness selection	Not considered	Included directly in calculation of stresses and deflections
10. Joint spacing	Maximum joint spacing 1.75*hOL (JPCP)	No recommendation provided	No recommendation provided	Maximum joint spacing in feet is 1.75*h_OL(in) (JPCP)	15 ft if 7 in < hOL < 10.5 in; 20 ft if hOL > 10.5 in	Included directly in calculation of stresses and deflections
11. Joint load transfer	Thickness increased if not doweled	Dowels assumed	Not considered	Not specified for overlay but considered in evaluation of base pavement	Dowels assumed	Included directly in calculation of deflections

Design Factors	AASHTO	Corps of Engineers	Rollings	PCA	Minnesota DOT	MEPDG
12. Drainage	Included in thickness design by empirical coefficient	Not considered	Requires retrofit of drainage system (if necessary)	Edge drains are recommended where pumping and erosion has occurred in the existing slab.	Edge drains and permeable interlayer for all pavements, interceptor drains when overlay is wider than the base pavement.	Requires retrofit of drainage system (if necessary)
13. Interlayer	Recommends 1-in min. thick AC interlayer or permeable open graded interlayer	No recommendation provided	No recommendation provided	Thin interlayer (<0.5 in) if extensive repair work performed. Thick (>0.5 in) otherwise.	>1 in >2 in if base pavement is badly faulted and/or has a rough profile	

2.1.1 Army Corps of Engineers Rigid Overlays for Airfields

In the Army Corps of Engineers (COE) method, the thickness of the overlay is a function of the structural capacity/thickness required for a new pavement and the effective structural capacity/thickness of the existing pavement. As the pavement deteriorates, its structural capacity drops. The effective thickness is defined as the required thickness of a pavement fabricated with new materials that can provide a capacity equivalent to the structural capacity of the existing pavement (Army Corps of Engineers 2001). This method is known as Effective Thickness Approach (Huang 2004). The general equation for this method is as follows.

$$h_{OL}^n = h_n^n - C * h_e^n \qquad\qquad (1)$$

where:

> n is a function of the degree of bond between the overlay and the existing pavement. This value is usually 2 for unbonded overlays.
>
> C is a function of the condition of the existing pavement.
>
> h_{OL} is the required thickness of the overlay.
>
> h_n is the design thickness of the new pavement.
>
> h_e is the effective thickness of the existing pavement

Depending on the type of the overlay, the C value varies. For example, for the condition of an existing rigid pavement, C can equal 1, 0.75, and 0.35, for good, moderate, and bad conditions, respectively (Corps of Engineers 2001). According to the Army Corps of Engineers (2001), the use of an unbonded concrete overlay is appropriate when:

- a plain concrete overlay is used to overlay an existing reinforced concrete pavement;
- a continuously reinforced or pre-stressed concrete overlay is used to overlay an existing plain concrete or reinforced concrete pavement;
- a plain concrete overlay is being used to overlay an existing plain concrete pavement with C less than or equal to 0.35; and/or
- matching joints in a plain concrete overlay with those in the existing plain concrete pavement cause undue construction difficulties.

The minimum required thickness of plain concrete unbonded overlay according to the COE method is 6 in (150 mm). When it is impractical to match the joints in the overlay to joints in the existing rigid pavement, a bond-breaking medium will be used in order to design the overlay as an unbonded overlay. For an unbonded concrete, the design and spacing of transverse contraction joints will be similar to requirements for plain concrete pavements on grade. In terms of material properties, the effective

modulus of subgrade, K-value, and the flexural strength of the existing and overlay concrete are required for the thickness design (Army Corps of Engineers 2001).

2.1.2 Association of American State Highway and Transportation Officials

Similar to the Corps of Engineers, AASHTO utilizes the Effective Thickness Approach summarized above. According to Section 5.9 of the AASHTO guide (AASHTO 1993), *n* in Equation (1) will have a value of 2 for an unbonded PCC overlay. Note that the structural contribution of the HMA interlayer is disregarded because of its negligible structural capacity in the resultant pavement. The required parameters for design are extensive.

The procedure requires important factors that are used to approximate the structural contribution of the existing pavement, including the load transfer efficiency of the existing pavement, the effective modulus of subgrade reaction, and the elastic modulus of the existing concrete. The thickness design of the new concrete overlay requires the modulus of elasticity of the new concrete, the mean concrete modulus of rupture (S_C), drainage coefficient (C_d), serviceability loss of the existing pavement (ΔPSI), reliability (I), Standard Deviation (s_0), and future traffic (Hall and Banihatti 1998). It appears that R of 95% and S of 0.39 for any type of PCC overlay lead to appropriate thicknesses consistent with the recommended values (Huang 2004). However, different values can be adopted as suggested by the AASHTO Supplement to the 1993 guide (AASHTO 1998). Two methods are recommended by AASHTO to estimate the effective thickness of the existing pavement, as described below.

2.1.2.1 Condition Survey Method

In this method, the thickness of the unbonded concrete overlay can be obtained from

$$h_{OL} = \sqrt{h_n^2 - h_e^2}$$
(2)

$$h_e = (F_{jcu}) * h$$
(3)

where *h* is the slab thickness of the existing pavement, and F_{jcu} is the joints and cracks adjustment factor for unbonded concrete overlay. F_{jcu} varies from 1 to 0.9 as a function of deteriorated joints and cracks per mile. Values of 0.98, 0.94, and 0.9 may be used for less than 20, 100, and 200 deteriorated joints and cracks per mile, respectively. Having this value, h_e can be calculated using Equation 3. Consequently, the required thickness of the unbonded concrete overlay can be calculated by Equation 2.

2.1.2.2 Remaining Life Method

The main difference between this method and condition survey method is related to the procedure for calculating the effective thickness of the existing pavement (h_e). This method is based on the premise that the traffic history of the existing pavement is available. The Remaining Life, *RL*, of the existing pavement (expressed as a decimal portion of the original design life) can be estimated using Equation 4.

$$RL = 1 - \frac{N_P}{N_{1.5}} \tag{4}$$

Where N_P is the number of passes of the design axle (18-kip single axle) accumulated on the existing pavement and $N_{1.5}$ is the number of passes of the design axle (18-kip single axle) required that the original pavement was designed to sustain before reaching a present serviceability level of 1.5.

$N_{1.5}$ can be estimated using the design charts or equations available in AASHTO guide. As the next step, the calculated value RL can be used in Equation (5) or in Figure 5.2 in the 1993 AASHTO guide to obtain the Condition Factor (CF).

$$CF = 1 - 0.7 * e^{-(RL+0.85)^2} \tag{5}$$

Similar to F_{jcu}, CF would be used to calculate the effective thickness of the existing pavement and, consequently, the required thickness of the unbonded concrete overlay.

2.1.3 Portland Cement Association Method

The PCA method for unbonded concrete overlay design strives to achieve structural equivalency between a new full-depth concrete pavement and a system comprising the existing concrete pavement and the unbonded concrete overlay (Tayabji and Okamoto 1985, APCA 1990). Structural equivalency is evaluated by comparing the edge stress at the bottom of a new full-depth concrete pavement with that at the bottom of the unbonded overlay (above the existing pavement and the interlayer). The design criteria is to have this overlay edge stress be less than or equal to the edge stress of the equivalent new pavement, thereby producing similar fatigue damage accumulation and similar performance life. The design charts that are used with this procedure were developed by the JSLAB finite element analysis program; cracks in the existing pavement were taken into consideration by incorporating the soft elements theory.

Design charts were developed for three different cases of existing pavement distress: 1) heavily distressed, 2) moderately distressed, and 3) lightly distressed. The following assumptions were also used:

- all loads are applied by 18-kip (80-kN) single-axles,
- concrete overlay modulus of elasticity = 5×10^6 psi (35 Gpa),
- existing concrete modulus of elasticity = $3\text{-}4 \times 10^6$ psi (21-28 Gpa),
- existing pavement slab length = 20 ft (6.1 m), and
- no tied concrete shoulders.

If a tied shoulder exists, the overlay thickness may be reduced by 1 in. (25 mm), and 6 in. (150 mm) is considered to be the minimum allowable thickness of the overlay. A comparison between the PCA method and the Army Corps of Engineers approach shows that the three PCA distress cases correspond well with the COE condition values I of 0.3-0.5 (heavy distress), 0.5-0.7 (moderate distress), and 0.7-0.9 (light distress). In terms of material property inputs, the effective modulus of subgrade reaction (k-

value) and the elastic modulus of the existing and overlay concrete are needed (Huang 2004; Harrington 2008).

2.1.4 Minnesota Department of Transportation Method

The Minnesota design procedure for unbonded concrete overlays considers unbonded concrete overlays to be a feasible rehabilitation alternative for Portland Cement Concrete (PCC) pavements of all conditions. However, there are some limitations to the feasibility of the unbonded PCC overlay when:

- the severity and amount of distresses in the existing pavement is not large enough and can be addressed using other concrete pavement rehabilitation methods;
- the existing pavement experiences large heaves or settlements;
- alignment changes are involved, which results in short segments of unbonded overlays (a constructability consideration);
- it is not economical to raise the curb and the gutter;
- the existing pavement is 20 ft (6 m) wide or less and the new pavement must be 24 ft (7.3m) or more in width; and
- traffic cannot be detoured for sufficient time period to accommodate construction needs.

The current minimum design period is 15 years, and minimal pre-overlay repairs are needed to restore the structural integrity, load transfer, and continuity. Detailed descriptions of the specific types of repairs that are suitable for unbonded concrete overlays of existing Jointed Plain, Jointed Reinforced, and Continuously Reinforced Concrete Pavements (JPCP, JRCP, and CRCP) are provided in the design manual. Rubblizing is recommended for pavements with serious durability problems or pavements that require repairs of more than 50 percent of the pavement surface area. When rubblizing of the old pavement is used, the unbonded concrete pavement must be designed as a new pavement over a high-quality base and not as an unbonded concrete overlay over concrete.

MnDOT determines the required overlay thickness as the average of the previously described Corps of Engineers and Portland Cement Association methods (MnDOT 2010).

2.1.5 FAA Rigid Overlays for Airfields

The FAA design method, as described in Rollings (1988), utilizes an iterative procedure that is based on the fatigue capacity of the pavement, as illustrated in Figure 1. Trial overlay designs are selected and analyzed. If the resulting SCI at the end of the analysis period is too low, a thicker overlay must be selected; if the SCI it is more than the design objective, the overlay thickness must be reduced in the next trial (Rollings 1988).
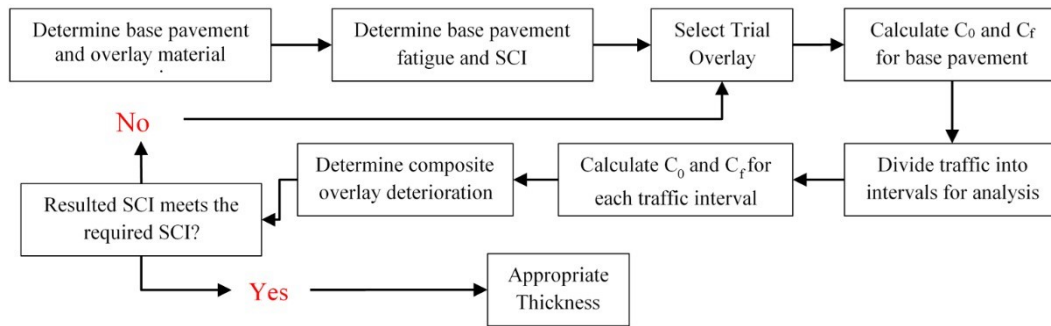
Figure 1: 1988 FAA Design Procedure [from Rollings (1988)]

In Figure 1, C_0 is the coverage level at which the Structural Condition Index (SCI) begins to decrease from 100 and C_f is coverage level at which SCI becomes 0. Overall, this design procedure uses a layered elastic analytical model to evaluate the load-induced tensile stresses in the base pavement and the overlay. Using these stresses, the deterioration of the base and overlay pavements can be predicted in terms of SCI. The analysis also takes into consideration the fatigue damage and progressive cracking of the base pavement, as well as deficiencies in joint load transfer (Rollings 1988).

The analysis requires (among other things) input of the elastic modulus and Poisson's ratio for each layer in the pavement. It is not necessary to measure the Poisson's ratio directly; recommended values are commonly estimated to be 0.15 to 0.2 for concrete, 0.3 for granular materials, and 0.4 to 0.5 for cohesive soil materials. The flexural strengths of the base and overlay concrete are required (due to their major influence on the pavement performance), and the degree of bonding between the pavement layers must also be considered. Except for the interface of the layers in contact with concrete, all the layers are generally considered to be fully bonded, while the interfaces between concrete layers and any other materials are usually considered to be frictionless. The interface between the existing concrete pavement and the overlay pavement is considered to be either fully bonded or partially bonded, depending upon the SCI value. For unbonded concrete overlays, a bond-breaking layer must be used to hinder the reflection of existing cracks. It is necessary to include the bond-breaking layer in the layered elastic analysis if the thickness of that layer is greater than or equal to 1 inch (25 mm).

2.1.6 Ohio Department of Transportation

In Ohio, the first stage of rehabilitation of the PCC consists of using a 3-inch HMA overlay to create what is often referred to as a "composite pavement." After the HMA overlay has provided service for some time, an unbonded concrete overlay can be used. Two strategies may be considered for preparing the composite pavement for the new overlay: 1) mill-off required portions of the HMA if the underlying PCC is in a good condition or HMA is still thick enough, or 2) remove the HMA and repair severe distress in the underlying PCC before placing a thin layer (1-inch) of HMA to serve as an interlayer for the new unbonded concrete overlay.

In order to appropriately implement the first alternative, Ohio DOT has performed a study on understanding and quantifying the impact of milling off portions of the existing composite pavement on the structural capacity of the remaining pavement (Mallela et al. 2008). Ohio DOT implements its own design procedure and software (DOITOVER) to calculate the overlay thickness needed for an existing composite pavement using Equations (6) through (8).

$$D_{OL} = \sqrt{D^2_{required} - D^2_{effective}} \tag{6}$$

$$D_{effective} = \frac{D_{new}}{\left(\frac{E_{effective}}{E_P}\right)^{0.33}} \tag{7}$$

$$D_{new} = \frac{H_{AC}}{2} + H_{PCC} \tag{8}$$

Where:

- $D_{required}$ is the required thickness of a new PCC pavement to resist the design traffic;
- H_{AC} is the thickness of the existing asphalt pavement and H_{PCC} is the thickness of the existing PCC layers;
- E_P is the effective elastic modulus of the existing pavement system, including all of the layers above the subgrade; and
- $E_{effective}$ is the effective elastic modulus of the combined HMA and PCC layers.

FWD and Dynaflect test results were analyzed to evaluate the structural capacity of the milled off composite pavements for 6 different projects. The results showed a decrease in structural capacity due to the removal of HMA by milling. The FWD provided more consistent and reasonable results than the Dynaflect (Mallela et al.,2008).

2.1.7 Mechanistic Empirical Pavement Design Guide

The *MEPDG* uses field performance data and a mechanistic-based approach to predict the performance of the overlaid pavement. The design of unbonded concrete overlays is covered in detail in the *MEPDG* reporting (NCHRP 2004), specifically in the Chapter titled "PCC Rehabilitation Design of Existing Pavements." Many different factors can be used as the inputs for the *MEPDG* design of unbonded concrete overlays, including:

- rehabilitation type
- design life

- pavement failure criteria (i.e., limits on panel cracking, joint faulting, International Roughness Index (IRI))
- design reliability
- traffic
- climate
- pavement cross-section and layer properties
- slab geometry
- joint and shoulder type
- concrete properties (strength, mixture proportions, coefficient of thermal expansion, etc.), and
- drainage and surface properties.

The *MEPDG* uses an iterative procedure to identify designs that meet the selected design criteria for the specified site conditions and overlay panel sizes (Torres et al.,2012). Also, it helps the engineer to predict the performance of the overlay by using indicators such as IRI, slab transverse cracking, and joint faulting for JPCP overlays, and IRI, crack spacing and width, and number of punchouts for CRCP overlays. One study showed that the *MEPDG* is capable of making reasonable predictions for concrete overlays that are 6 in (152 mm) or more in thickness (Darter et al.,2009).

Darter et al. (2009) conducted a case study and simulated JPCP concrete overlay over existing concrete pavement over a range of conditions and design using the *MEPDG*. The effect of the existing condition of the pavement was reflected in the effective modulus of the existing slab, which was estimated using the following formula:

$$EBASE/DESIGN = CBD \times ETEST \qquad\qquad\qquad (9)$$

where C_{BD} is the Coefficient Reduction Factor for the existing pavement – given as 0.42 to 0.75 for "Good" condition, 0.22 to 0.42 for "Moderate" condition, and 0.042 to 0.22 for "Severe" condition – and E_{TEST} is the elastic modulus of the existing uncracked concrete slab (lbf/in^2).

 The analysis showed that as the existing pavement condition varied from "Good" to "Severe," the performance of the JPCP overlay was significantly reduced. The composite behavior of the existing and new layers and the reduced modulus of the existing pavement were the reasons for this observation. Also, the thickness of the JPCP overlay had a significant effect on the predicted performance. The effects of selected specific design features and construction processes are summarized below:

- An increase of 1 ft to the typical 12 ft lane width improved the performance considerably.
- Increasing the thickness of the interlayer from 1 in. to 3 in. had a moderate impact on improved pavement performance.
- A decrease in the effective modulus of the existing pavement increased the amount of faulting for all panel sizes.
- Rubblizing the existing pavement resulted in a significant drop of the effective modulus of the slab, resulting in additional overlay thickness (in this case 2 in.).

2.2 PERFORMANCE STUDIES

Performance of unbonded concrete overlays was a subject of many past studies. Several of them are summarized below.

2.2.1 Performance Evaluation of Concrete Pavement Overlays, Final Report (Simonsen and Price 1989)

This report follows the one discussed above and provides performance data on the two overlays constructed in 1984. The overlays were evaluated based on observations, cores, and load testing, and their performance was deemed satisfactory. The asphalt interlayer was not found to create a totally unbonded system and movement between the two concrete layers was not independent. Coring showed that cracks in the overlay tended to be located near cracks or joints in the original pavement. Based on the overall performance of the two overlays, this report recommends the use of unbonded concrete overlays as a pavement rehabilitation method.

2.2.2 Chojnacki (2000)

The Missouri Department of Transportation (MODOT) investigated the use of fiber-reinforced concrete (FRC) in UBOL (Chojnacki 2000). The investigation took place in 8 test sections (2500' in length) along Interstate 29 in Atchinson County, Missouri. Two test sections used conventional concrete, three used steel fibers in the PCC mix, and three used polyolefin fibers. Variables in the study also included thickness, joint spacing, and texture, otherwise the test sections shared materials and a cross-section. The test sections were placed using an interlayer atop the existing PCC pavement, which had been repaired in preparation for UBOL (although some cracks and joints were left unrepaired – the author did not indicate locations of those unrepaired distresses in the existing pavement).

Figure 2 summarizes the performance of these sections at the conclusion of the first year of service life. As is evident in the figure, it is difficult to assess the influence of FRC on overall UBOL performance in terms of transverse cracking.

Transverse Cracking by Entire Test Section
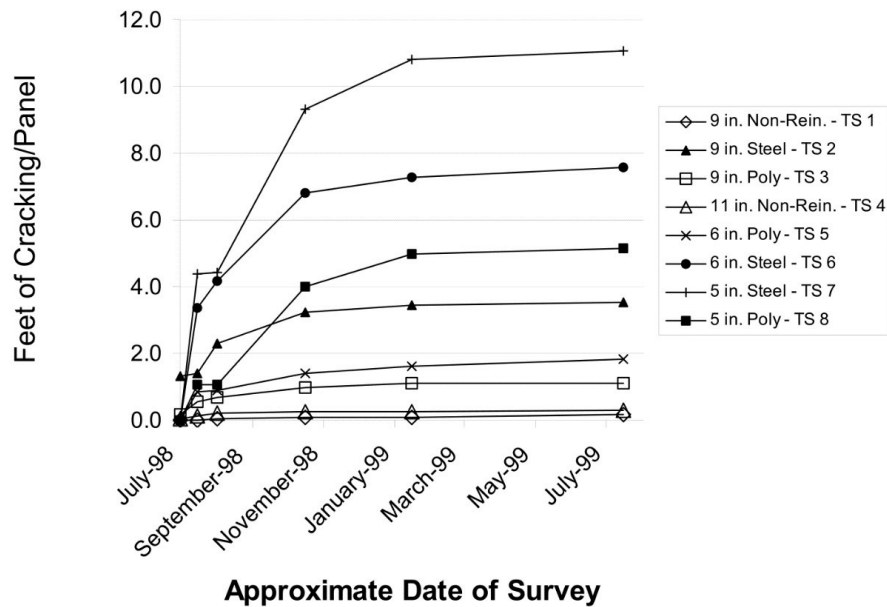
Figure 2: Transverse cracking in fiber-reinforced UBOL test sections along I-29 in Missouri [from Chojnacki (2000)]

Chojnacki notes that the cracking observed was typically not reflective cracking, and thus concluded that – at least on the basis of one year of performance – a one-inch thick asphalt interlayer was sufficient.

The study also had general observations on thickness and joint spacing. First, as expected, more cracking was observed in thinner sections; the author points to a comparison of 6" and 9" polyolefin FRC as indicating possible benefits of FRC in thickness reduction yet also acknowledges the limits of the performance data and conclusions that can be drawn for thickness design. The study also questioned the feasibility of dowels in thin overlays, as spalling was observed over some dowels in the thinner (5") test sections. In addition, considerably more cracking was observed in long panels (60' and 200') than in the short panels (15' and 30').

2.2.3 Hansen and Liu (2013)

Hansen and Liu performed a study to evaluate the performance of existing unbonded concrete overlays in Michigan (Hansen and Liu 2013). The older overlays were mostly JRCP, but overlays constructed since the mid-1990s were JPCP. Overall, the Michigan overlays have performed acceptably, but the recent development of some premature distresses with signs of pumping resulted in this study to investigate whether drainage problems were primarily responsible for these distresses. The outcome of this study is intended to justify additional efforts for improving the drainage systems of unbonded concrete overlays in order to extend the service lives of these pavements.

15

To accomplish the objectives, eight projects were selected with varying ages and performance levels that ranged from good to poor. A series of tests and assessments were conducted on the test sections, including a distress survey, surface profiling, and FWD testing. Coring was done to identify the type of cracking (i.e., bottom-up or top-down), to evaluate the effects of pumping and erosion, and to assess the quality of the drainage system. In addition, core specimens were examined for salt-frost deterioration, and drainage pipe outlets were checked for running water. Finite element analysis was performed using the EverFE program to support the findings of the forensic observations.

A summary of some of the findings of this study include:

- Pumping was the major cause of distress. The pumping was a result of inadequate drainage, causing erosion of the interlayer and, consequently, loss of support. This phenomenon was most often observed along the outer longitudinal edge.
- Doweled joints provide more uniform slab deflections on both sides of transverse joints and are helpful in reducing pumping.
- Laboratory tests on the retrieved cores showed that the primary cause of the rapid development of concrete joint spalling was the low air content of the concrete (< 3%), which results in poor salt scaling resistance and freeze-thaw durability.
- A connection between the International Roughness Index (IRI) and the development of pumping was found. This was believed to be useful in selecting the best time for implementing preventive maintenance measures.
- Finite element analyses showed that unbonded PCC overlays are more sensitive to loss of support than is conventional JPCP on aggregate bases. This added sensitivity is due to the increased stiffness of the overlay slab support system.
- The two drainage systems shown in Figure 3 and Figure 4 were recommended to improve the effectiveness of the drainage system and to prevent the early occurrence of distresses due to pumping.
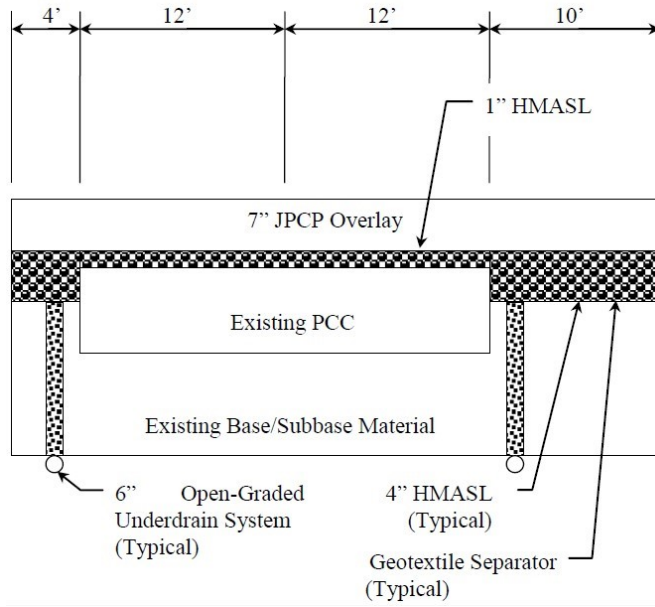
Figure 3: Thickened Shoulder Design with Open-Graded Underdrains [From Hansen and Liu (2013)]
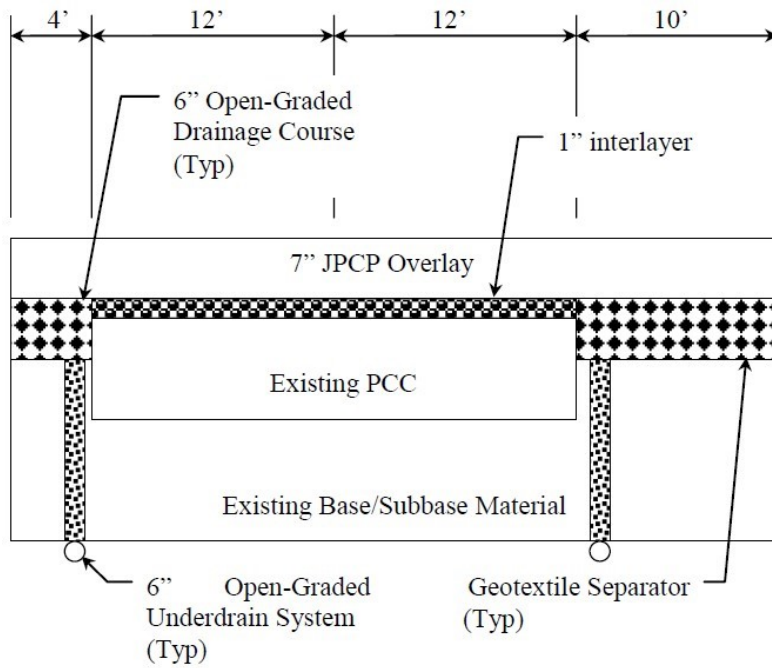
Figure 4: Open-Graded Drainage Course Shoulder Design [From Hansen and Liu (2013)]

2.2.4 Heckel (2002)

Heckel (2002) summarized the first six-years of performance of UBOL constructed along Interstate 74 near Galesburg, IL, by the Illinois Department of Transportation (ILDOT). A 9-inch UBOL was constructed over existing 7-inch thick CRCP, which had been rehabilitated previously using an AC overlay. The existing CRCP exhibited extensive D-cracking and punchouts. Heckel notes that the previous AC overlay, with milling and patching with additional AC to the grade of the previous AC overlay where required, was left in place to function as an interlayer for this project (7 miles of UBOL along I-74).

In terms of performance, the I-74 UBOL showed little to no distress after its first six years of service life. ILDOT monitored the pavement using visual distress surveys to assess cracking, IRI to assess roughness, and FWD testing to determine structural response. In every measure, the UBOL showed little degradation in overall performance. While transverse cracking was observed to have increased in 2001, that cracking was low in severity and expected given the traffic levels. The only notable distress was the development of a few, unrelated, small punchout-like distresses near the end of the observation – these small punchouts were so small as to not require repair or concern. No maintenance or patching of the unbonded concrete overlay was conducted in that time.

2.2.5 Tighe et al. (2005)

Tighe et al. (2005) discusses the rehabilitation of a pavement at an intersection in Toronto by the City of Toronto in 2003. The existing pavement was a distressed AC overlay of a PCC pavement. Unlike the UBOL discussed in Heckel (2002), which retained the AC overlay to act as the interlayer, the City of Toronto chose to completely mill off the pre-existing AC overlay down to the original PCC pavement. Repairs (routing and sealing) were conducted on the existing PCC, and then a new 25 mm (1") AC layer was placed to act as the interlayer. In this case, a tack coat was used in the hopes of improving bond between the PCC and interlayer. The project was finished with the placement of a 150 mm (6"), doweled UBOL.

An important feature of the placed UBOL in this study is that the authors, in cooperation with the City of Toronto, were able to instrument the UBOL with 12 strain gauges placed at specific locations and depths in the rehabilitated intersection. Tighe et al. report on two years of monitoring. The pavement was found to perform well, and the strain data was collected and analyzed. The data analysis and subsequent conclusions from the study were particularly focused on the performance of UBOL given different traffic behavior; this focus is due to the intersection being subjected to a great deal of metropolitan bus and "stop/start" traffic.

The authors observed, based on strain data, that UBOL performance was mostly dictated by traffic rather than environment; in other words, strains in the UBOL were more extreme given traffic loads than thermal shifts. However, for locations where traffic did not stop (i.e. non-bus stop locations), the authors observed that temperature effects were more pronounced on strains than traffic loads. The authors conclude by noting that future studies would include additional data from these sections.

2.2.6 Smith et al. (2002)

Smith, Yu, and Peshkin (2002) reported that then-current pavement design practices were moving away from the use of JRCP unbonded overlays and that this pavement type was rarely constructed. The general performance of the unbonded PCC was described as being good, but some unresolved design issues exist, such as quantification of the effects of pre-overlay preparation and repair, and the impacts of separator layer design on the performance of the overlay.

The report notes that traditional thinking is that any amount of bonding between the overlay and underlying pavement could cause performance problems, but the current thinking is that a certain amount of bond between the layers may actually improve the overlay performance. The important related factors were briefly discussed, including different types of existing pavement evaluation methods, pre-overlay repair considerations, thickness design, separator layer design, joint spacing, load transfer design, and jobsite consideration.

Some important findings and recommendations from this study include the following:

- Evaluation of the existing pavement evaluation can include visual survey, Falling Weight Deflectometer (FWD) testing, and coring. FWD test results can be used to back-calculate subgrade k-value and PCC modulus, measure subgrade variability, determine joint load transfer efficiency, and identify the presence of voids under joints and cracks. Coring is necessary when Material Related Distress (MRD) is an issue.
- One of the existing thickness design shortages is lack of consideration of the structural contribution of the interlayer and the friction between the overlay and interlayer, and the interlayer and the existing pavement in the design of the overlay. It is noted that the 1998 AASHTO Interim Design Guide Supplement considers the effects of interlayer friction (AASHTO 1998), but 1) excessive credit is given to the existing pavement, and 2) there is a lack of consideration of the effects of curling and warping, which is a particular deficiency for unbonded JPCP and often leads to unconservative overlay thickness designs. For this reason, shorter joint spacings are recommended for unbonded concrete overlays to reduce the high curling stresses.

It is also noted that the joint load transfer of unbonded PCC overlays is generally significantly better than that of a new JPCP due to the contribution of the underlying layer to reducing pavement deflections. Finally, this report recommended mismatching the joints of the existing pavement and those of the overlay (offsetting them by a minimum of 3 ft (1 m)) to maximize the benefits of the load transfer provided by the existing pavement.

CHAPTER 3: UNBONDED OVERLAY PERFORMANCE REVIEW

The research team has collected information on design and performance of unbonded overlays in several states participating in this pooled fund study. The summary of this information is provided below.

3.1 MINNESOTA UBOL EXPERIENCE

The Minnesota Department of Transportation (MnDOT) has used UBOL extensively and has continuously collected pavement condition information from these pavements over their service lives. MnDOT provided data on 619 rehabilitated sections in the worksheet made available to the research team. Of these 619 sections, 11 sections were rehabilitated using asphalt overlays and were thus irrelevant to the project work. The remaining 608 sections were UBOL, and these 608 sections represent a total of 6327 records taken over the service lives of all sections, where service life is measured as the period of time initiated with UBOL construction. Figure 5 and Figure 6 provide an overview of the available UBOL section data by number of surface rating (SR) records per section and section UBOL age.
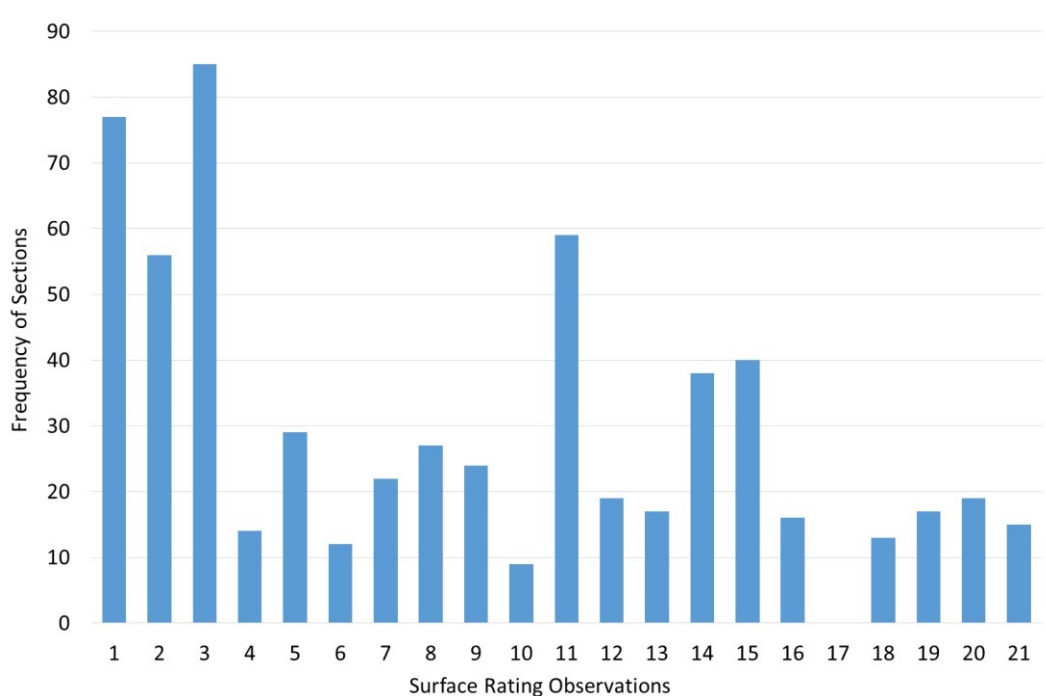
Figure 5: Number of surface rating records per UBOL section for MnDOT pavement management data
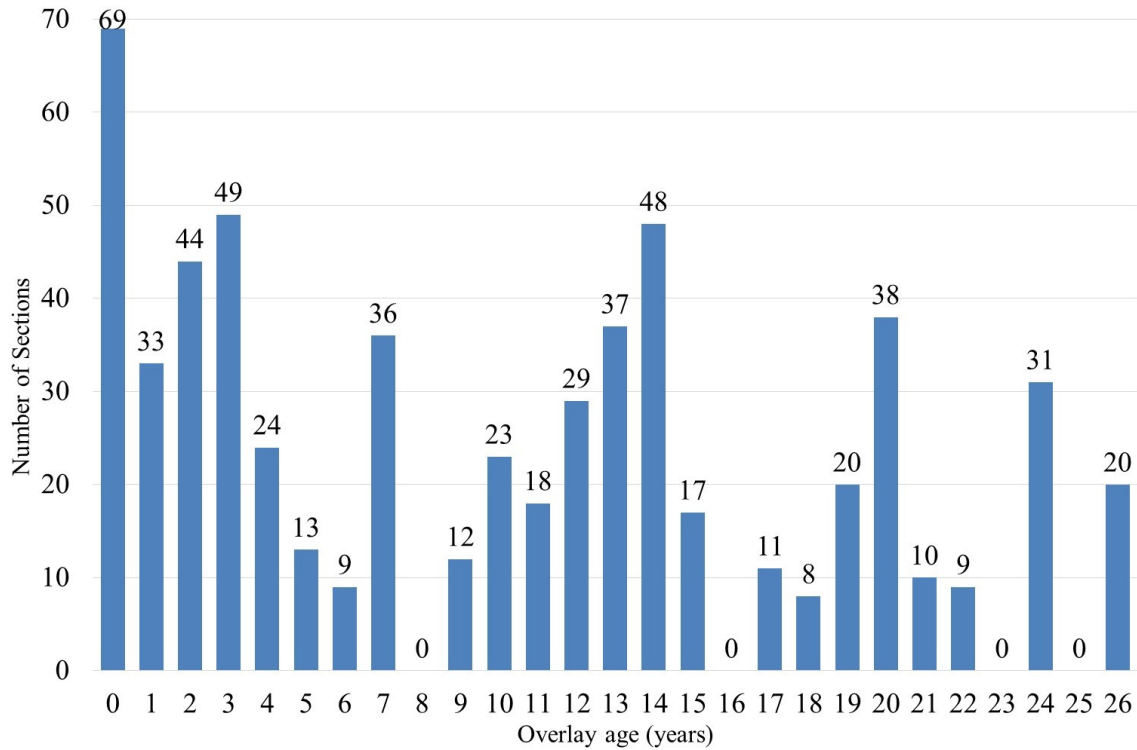
Figure 6: Frequency of sections by overlay age for MnDOT pavement management

MnDOT also provided pavement condition data collected using a Pathway Services, Inc. Digital Inspection Vehicle (DIV), as shown in Figure 8. The collected data are processed and reported in terms of the three indices – Ride Quality Index (RQI), Surface Rating (SR) and Pavement Quality Index (PQI). Descriptions of these indices and their ranges are presented in Table 2. For each index, a higher value indicates better pavement condition.

Figure 7: MnDOT's Pathway Services, Inc. Digital Inspection Vehicle (DIV) [from Janisch (2006)]

Table 2: MnDOT Pavement Condition Indices (Janisch 2006)

Index name	Pavement attribute measured by index	Rating scale (bad-good)
Ride Quality Index (RQI)	Pavement Roughness	0.0 – 5.0
Surface Rating (SR)	Pavement Distress	0.0 – 4.0
Pavement Quality Index (PQI)	Overall Pavement Quality $$PQI = \sqrt{(RQI)(SR)}$$	0.0 – 4.5
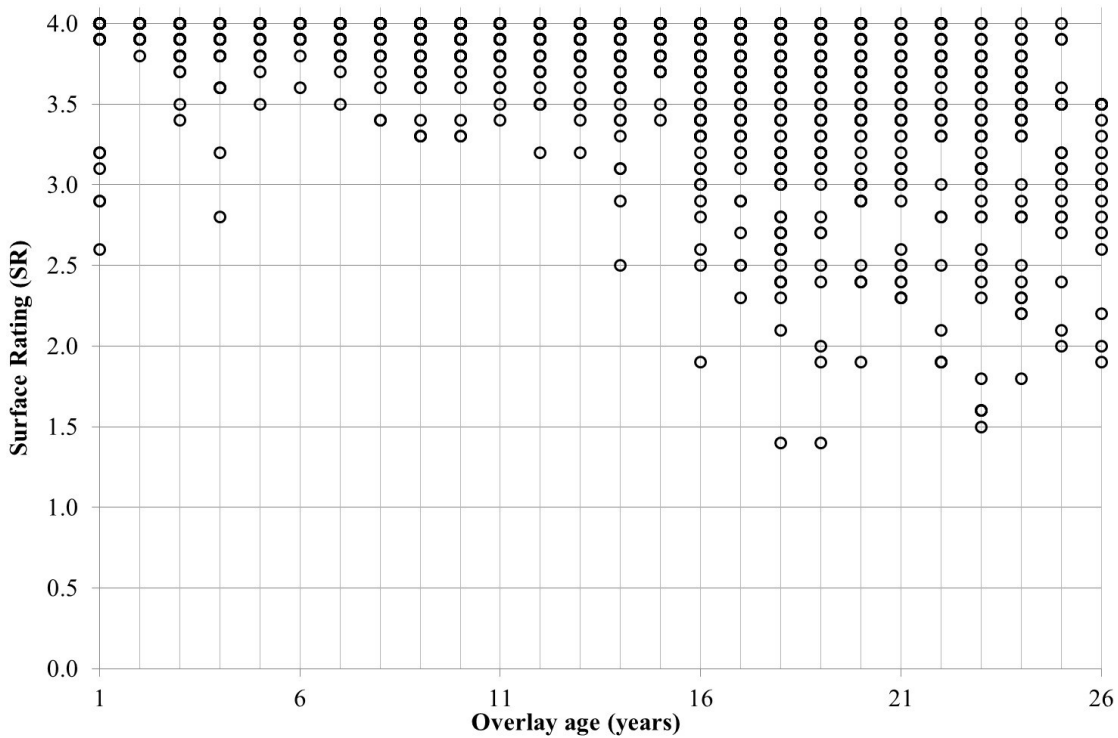
Figure 8: Performance values (SR) for all 6327 observations on all relevant sections in MnDOT database

The reported performance (surface rating) for all records for all sections are shown in Figure 8. Generally, one can observe deterioration in SR with increasing overlay age. The relationship between SR and pavement age varies widely by section, and overlay performance is influenced by many design, construction, traffic, materials, environmental and other factors.

Monitored distresses that can influence SR in UBOL include transverse or longitudinal joint spalling; faulting; or cracked, broken, faulted, patched, or D-cracked panels. SR is calculated based on Equation 10, in which *TWD* is the Total Weighted Distress.

$$SR = e^{1.386 - 0.045TWD} \qquad (10)$$

TWD is a metric that takes into account the individual low, medium, or high severity distresses that influence ride quality. To compute *TWD*, the amount and severity level of each distress type is converted to a percentage, and *TWD* is the sum of the individually weighted distresses (MnDOT 2011). For more information on the Surface Rating (*SR*) and the calculation of the total weighted distress (*TWD*), consult either Jansich (2006) or the MnDOT Distress Identification Manual (MnDOT 2011).

23

3.2 MICHIGAN UBOL EXPERIENCE

The Michigan Department of Transportation (MDOT) provided data on almost 30 overlays constructed between 1984 and 2013. These overlays were designed using the AASHTO-93 design method, which is the same method used to design new concrete pavements in Michigan. Typical overlay thicknesses in Michigan were 6-8 inches, though more recently, some 4-inchthick overlays have been constructed. These thinner overlays had a smaller joint spacing of 5.5 ft, while the 6-8 inch thick overlays had joint spacings of 12-14 feet. Some of the older overlays (pre-1995) had joint spacings ranging from 27 to 41 ft. Most of the overlays featured 1 inch or 1.25-inch dowels, although the 4-inch overlays were undoweled.

Overlays were constructed on pavements of varying quality (from good to poor). Full depth repairs were conducted on some pavements prior to overlay construction, although the number of full-depth repairs constructed on any given project did not seem to correlate well with the condition of the original pavements. Dense-graded HMA was used as the interlayer material until 2003, when a switch was made to open-graded HMA interlayers on most overlays; open-graded HMA interlayers continue to be used on the thin overlays.

The current condition of overlays built prior to 2003 varies between "poor" and "good" while the current condition of overlays built after 2003 (when MDOT began to use open-graded HMA interlayers) was consistently rated as "good" with the exception of one overlay. 2003 was also the year in which MDOT began the frequent use of 1-inch dowels in their overlays (as opposed to 1.5-nch dowels). Major distresses observed in Michigan unbonded concrete overlays include:

- Pumping and erosion of the HMA interlayer
- Cracking and spalling due to dowel bar misalignment
- Minor reflective cracking after 5-20 years on some projects
- Joint deterioration due to freeze thaw damage after 5-10 years on some projects

MDOT provided several observations about (and recommendations concerning) unbonded concrete overlay performance, including:

- An emphasis on providing clear drainage paths in design and drainage maintenance improved performance;
- Crown corrections to encourage drainage should be made in the concrete overlay and not in the HMA layer to prevent "punch down" failures;
- Dowels improved performance of overlays experiencing pumping and erosion;
- Pre-overlay repairs were deemed only to be necessary for severely distressed areas where support conditions are affected across the entire lane and when voids are present; and
- Lower levels of traffic were associated with better performance.

3.3 MISSOURI UBOL EXPERIENCE

The Missouri Department of Transportation provided data on 10 overlays ranging in age from 1 to 22 years. The AASHTO-86 and AAHSTO-93 methods were used to design most of the older overlays, while the ACPA design method was used for overlays built in the last 5 years. It was indicated that some of the older overlays were designed using "AASHTO 93 / *MEPDG*". Missouri DOT currently uses the *MEPDG* and AASHTO Pavement ME Design programs for new concrete pavement (but not overlay) design.

The typical overlay thickness used in Missouri was 8 inches for overlays built more than 5 years ago. When the switch was made to using the ACPA design method, thicknesses dropped to 5 inches. The older, thicker overlays had a joint spacing of 15 feet, while the newer, thinner overlays use 6ft by 6ft panels. Most of the 8-inch thick overlays featured 1.25-inch dowels, while none of the 5-inch thick overlays were doweled.

Overlays were constructed on pavements with condition ranging from "good" to "poor". Full-depth repairs were performed on some pavements prior to overlay construction, though the number of full-depth repairs used did not seem to correlate well with the condition of the original pavement. The types of interlay used varied by project and included geotextiles, new HMA, and using the existing HMA (with or without milling).

The current condition of the majority of the overlays was considered to be mostly "very good" to "excellent", with one overlay rated as "good" and one rated as "poor". These last two projects experienced significant cracking or faulting. Both had most or all of the following characteristics: no dowel bars, loss of edge support, asphalt interlayer stripping and thin pavement. The Missouri DOT provided several observations about overlay performance, including:

- It is preferable to avoid the use of widened slabs with thick unbonded overlays because longitudinal cracking can result, especially if the existing pavement is a composite pavement.
- Cross-slope adjustments should be made in the concrete overlay, not in the asphalt layer, particularly if the asphalt is prone to stripping.
- Dowels improve performance in thicker overlays.
- A knife-edge technique can be used successfully to create longitudinal joints for "big block" (6 ft by 6 ft panel) pavements.
- When design thickness is met in construction, unbonded overlays appear to be insensitive to traffic levels.

In addition to these observations, the research team incorporated reporting by Chojnacki (2000) into the case studies of the literature review above.

3.4 DELAWARE UBOL EXPERIENCE

The Delaware rehabilitation project included over 40 miles of CRCP and JRCP along I495. A major concern with the pre-existing pavements was alkali-silica reactivity (ASR) in both pavement types and joint deterioration in the JRCP. These pavements were rehabilitated using both asphalt and concrete overlays, the concrete overlay being a 10-inch unbonded overlay (Tayabji et al., 1994)

3.5 IOWA UBOL EXPERIENCE

The Iowa Department of Transportation responded with detailed information on UBOL pavements in the state roadway system, while noting that there also exist many overlays in the county system. These sections utilize the PCA design method, although the representative noted that Iowa is working toward implementing *MEPDG* for UBOL design. The Iowa DOT representative noted that UBOL design has been modified locally by the inclusion of rebar in the UBOL layer when placed over widening joints in a pre-existing pavement. Many of the trends observed by Iowa pavement engineers also deal with the effects of widening units included in the UBOL construction. The techniques developed for the design of UBOL that includes widening is detailed in Cable et al. (2005).

Details on eight UBOL projects are summarized in Table 3 below. Overall, the respondent noted that for these UBOL sections, few distresses were observed, but those distresses that were observed (and their likely causes) were:

- Low/medium severity longitudinal cracking in Year 3 (after UBOL construction) of one project, possibly due to the fact that the jointing did not match the old widening joint on that particular project;
- Transverse/corner cracking on in Year 3 of a project, possibly due to an unexpected increase in truck traffic volume; and
- Low severity longitudinal cracking in Year 2 of another project whose potential cause was unidentified.

Table 3: Reported section design for Iowa UBOL

Pvmt	UBOL Age (yrs)	Pre-existing Pavement			UBOL Design							Current condition (2014)
		Thickness	*Condition*	*Repairs*	*Design Method*	*Thickness*	*Dowel? (in)*	*Joint spacing*	*Shoulder type*	*Interlayer*	*Traffic level*	
IA 13	12	5" HMA over 10"-7"-10" PCC thickened edge	Old HMA overlay with deteriorated reflective cracks	Minimal full depth patching	ACPA/ Jim Cable	3.5"-4.5"	No	4.5'x4.5' 4.5'x5'	2' PCC/6' granular, Widening placed integral w/overlay	Existing HMA ~3'"	AADT = 3,000 9% trucks	Some minimal panel cracking
IA 175	7	4" HMA over 10"-7.5"-10" PCC thickened edge	Old HMA overlay with deteriorated reflective cracks, rutting	Patching deteriorated joints	ACPA/ Jim cable	4.5"	No	7' x 7'	2' PCC/8' granular, Widening placed integral w/overlay	Existing HMA 3.5"	AADT = 2,100 20% trucks	Longitudinal crack developed over old widening joint
I-29	6	3" HMA over 10" PCC	Old HMA overlay with deteriorated reflective cracks	Full depth Patching	PCA & AASHTO 1993 (WinPAS)	9"	Yes 1.25"	15' x 12'	6' & 8' PCC	Existing HMA/new 1" HMA	AADT = 17,000 22% trucks	Good. Some fine longitudinal cracking near shoulder
IA 9	5	4.5" HMA over 10"-7"-10" PCC thickened edge	Old HMA overlay with deteriorated reflective cracks, block cracking	Patching deteriorated joints	ACPA/ Jim Cable	5.5"	No	5' x 5' 5' x 6'	4' PCC/6' granular Widening placed integral w/overlay	Existing HMA 3"	AADT = 2,000 20% trucks	Good
I-29	5	4" HMA over 8" CRCP	CRCP with spot HMA overlays, longitudinal ¼ pt crack in CRCP	Milled off old HMA and placed new interlayer	PCA & AASHTO 1993 (WinPAS)	9"	Yes 1.25"	15' x 12'	6' & 8' PCC	New 1" HMA	AADT = 22,000 20% trucks	Good
IA 14	1	10"-8"-10" PCC thickened edge	Spot HMA overlays, some joint deterioration	Milled off spot HMA and placed new interlayer	ACPA/ Jim Cable	4.5"	No	5'x 5.5' 5' x 4'	2' PCC/8' granular Widening placed integral w/overlay	New 1" HMA	AADT = 2,300 18% trucks	New

Pvmt	UBOL Age (yrs)	Pre-existing Pavement			UBOL Design							Current condition (2014)
		Thickness	*Condition*	*Repairs*	*Design Method*	*Thick ness*	*Dowel? (in)*	*Joint spacing*	*Shoulder type*	*Interlayer*	*Traffic level*	
US 65	5	5" HMA over 10"-7"-10" PCC thickened edge	Deteriorated joints in HMA overlay were heaving in the winter.	Full depth patching deteriorated joints	ACPA/ Jim Cable	5"	No	5'x5' 5'x6'	4' PCC/6' granular Widening placed integral w/overlay	Existing HMA 4"	AADT = 2,400 16% trucks	Good. Some cracking on a portion due to increased loads from quarry
US 18	3	6"-10" HMA over 10"-7"-10" PCC thickened edge	Deteriorated joints in HMA overlay were heaving in the winter.	Full depth patched deteriorated joints.	ACPA/ Jim Cable	4.5"	No	4.5'x4. 5' 4.5'x5'	2' PCC/8' granular Widening placed integral w/overlay	Existing HMA 5" -8"	AADT =1,950 20% trucks	Good.

3.6 LTPP DATABASE

The Long-Term Pavement Performance (LTPP) database has provided an informative and user-friendly website (www.infopave.com) that contains a directory of numbers of projects. The LTPP GPS-9 projects (Unbonded PCC Overlay of PCC Pavement) are applicable to the project effort. There are 26 GPS-9 sections (of the total 2509 sections in the LTPP database). Figure 15 lists the locations of the relevant LTPP projects; only one of the sections is located in Canada, the rest are distributed in the US.

Figure 9: Location of LTPP UBOL Projects

A comprehensive and detailed information on each project is available on this website as listed below. Each description in the following subsections describes the data available; these data are extractable from the LTPP InfoPave website after submitting a request.

3.7 SURVEYS OF IN-FIELD PAVEMENTS

3.7.1 Unbonded Overlays in Michigan

Members of the research team surveyed in-field sections of unbonded concrete overlays in Michigan with the cooperation of the Michigan Department of Transportation (MDOT). A summary of these in-field pavements is provided in Table 4.

Table 4: Unbonded overlays surveyed in Michigan (2014)

Road	Location	CMS	Year Constructed	Age	Interlayer
US-131	Plainwell	3111	1998	16	1 in dense graded HMA
US-23		47014	1999	15	1 in dense graded HMA
I-69	North of I-94	13074	1999	15	1 in dense graded HMA
I-69	Charlotte	13074 & 23061	2000	14	1 in dense graded HMA
US-131	Rockford	41132 & 41133	2000	14	1.25-1.75 in open graded HMA

US-23		47014	2001	13	1 in dense graded HMA
I-75 NB	West Branch	65041	2003	11	1 in open graded HMA
US-131	Kalamazoo	39014 & 03111	2004	10	1 in dense graded HMA
I-96	Coopersville	70063	2004	10	1 in open graded HMA
I-75		25032 & 73171	2004 & 2005	10/9	Existing HMA from composite pavement
I-94		77111	2006	8	1 in open graded HMA
I-96	Walker	70063 & 41026	2006 & 2007	8/7	1 in open graded HMA

The oldest in-service UBOLs in Michigan were built in 1984. Their designs consist of between 6 to 8-inch jointed plain concrete pavements overlays with conventional joint spacing and between 1 to 1.75 inches of either dense or open graded hot mix asphalt (HMA) interlayers. Please note that in 1995 and prior the overlay was constructed as a jointed reinforce concrete pavement (JRCP) with either, 27 ft, 41ft, or a random joint spacing.

Michigan has constructed a large number of concrete overlays with a wide range of different design parameters much of which are performing very well. This provides a good opportunity to evaluate the effect of these parameters on performance. A site visit was performed with the focus of identifying characteristics in the design that might contribute to poor performance so the summary below highlights these findings. It should be noted that the majority of these UBOLs are performing quite well but the focus of the review below will be on the design features that contributed to a reduction in performance. After viewing 13 different UBOLs in Michigan in August 2014 and 8 additional sections in September 2015, the following observations, discussed in terms of relevant distresses or issues, were made.

3.7.1.1 Longitudinal Cracking

The predominant distress in these pavements was longitudinal cracking. Three separate mechanisms are believed to contribute the development of each of the three different types of longitudinal cracks.

Erosion longitudinal cracks. A contributing cause to the development of some of the longitudinal cracks is erosion of the interlayer between the lane shoulder joint and the wheel path, as shown in Figure 10.

Figure 10: Longitudinal cracking due to erosion of the HMA interlayer in surveyed Michigan sections

These longitudinal cracks tend to gradually meander towards the lane/shoulder joint. For example, on I-96, drainage was not included as part of the overlay. This resulted in water build up in the interlayer and longitudinal cracking in the overlay. MDOT has found that ensuring adequate drainage, as well as maintaining edge drains, is therefore significantly important to these structures where the interlayer is susceptible to erosion. If the drainage system backs up, then water will remain trapped in the interlayer, as shown in Figure 11.

Figure 11: Plugged edge drain near surveyed Michigan sections

Longitudinal cracks in the wheel path. Longitudinal fatigue cracking can also develop along the wheel path. This may propagate from one transverse joint to the next along the wheel path or begin propagating along a diagonal to the lane/shoulder joint, as illustrated in Figure 12.

Figure 12: Longitudinal (or diagonal) cracking in the wheel path in sections surveyed in Michigan

A gap created due to consolidation of the HMA interlayer or localized erosion at the intersection of the wheel path and the transverse joint might contribute to the initiation of these longitudinal/diagonal cracks. Once the crack has propagated along one side of the transverse joint, it will tend to propagate on the other as well as since high shear stresses can develop as the wheel moves off the crack slab on to the uncracked slab on the opposing side of the joint.

Midslab longitudinal cracks. Midslab longitudinal cracking was also observed, as shown in Figure 13. This appears to be top-down cracking related to fatigue. The shorter joint spacings of 10 or 12 ft can result in fatigue cracking preferentially occurring in the longitudinal direction in lieu of the transverse direction.

Figure 13: Midslab longitudinal cracking in surveyed Michigan sections

3.7.1.2 Wide Working Joints

In some sections every fifth or sixth joint was wider than the others indicating that they were the working joints. Distress frequently developed at these wider joints and consisted of longitudinal cracks propagating from the transverse joint. Possible causes of this include:

1.   Not all joints deployed initially (observed for both open and dense graded interlayers) and/or
2.   The use of dowel bar inserters could have contributed to joint lock-up.

One of these wider distressed working joints is shown in Figure 14.

Figure 14: Wider working joint exhibiting distress in surveyed Michigan sections

3.7.1.3 Corner Breaks

Corner breaks were also observed in many sections. A few instances of the corner breaks observed are illustrated in Figure 15. The observed corner breaks could be the result of drainage issues. If water only enters on part of the lane, and becomes trapped at the edge, a corner break may develop. This water will cause an asphalt interlayer to strip and ravel, leading to loss of support. MDOT now installs edge drain systems when constructing unbonded concrete overlays.
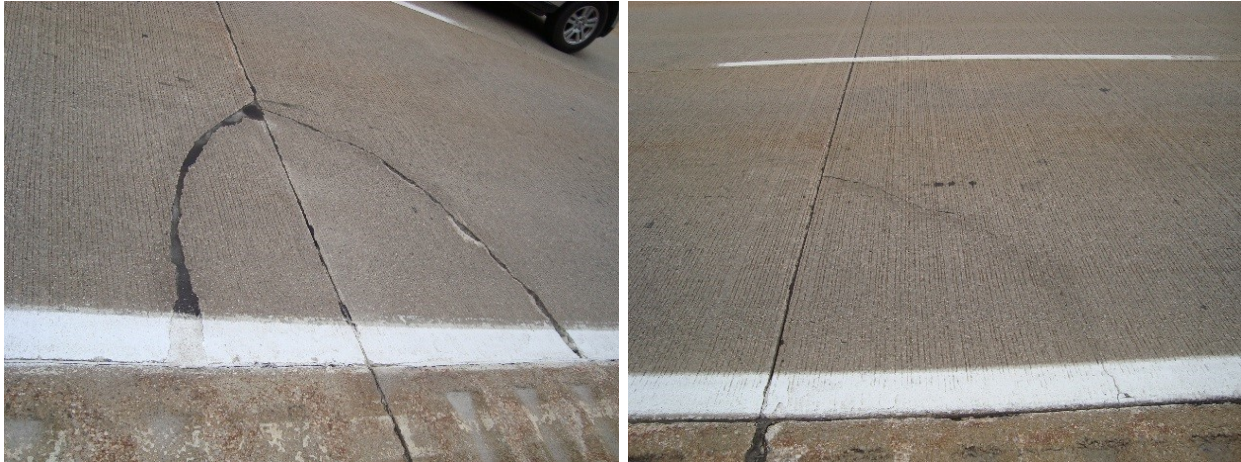
Figure 15: Corner breaks observed in Michigan

3.7.1.4 Transverse Cracking

Transversely cracked slabs can be classed according to the following sub-distresses:

Fatigue cracking. This is not a commonly observed distress even for relatively thin structures (6-8 in) on heavily trafficked roadways. This is most likely due to the shorter transverse joint spacing of 10 or 12 ft that is typically used.

Reflective distress. A transverse crack in the overlay can develop as the result of a region of reduced support in the existing pavement such as a severely distressed region. On US-131 in Plainwell, transverse cracking was more prevalent than in any other section. The existing PCC pavement was severely distressed, and no pre-overlay repairs were performed. The interlayer is 1-inch thick dense graded HMA. The cause of this transverse cracking is therefore most likely reflective distress from the existing PCC pavement up into the overlay. A confirmed case of reflective distress was observed on I-96 near Portland, where a tight mid-slab transverse crack was cored. The core revealed that the crack was above a distressed region in the existing pavement.

Reflective cracking. Reflective cracking is a transverse crack in the overlay directly above a well-defined joint or crack in the existing pavement. The laboratory study revealed that a discrete joint or crack in the existing pavement will tend to not reflect up into the overlay under normal wheel loads if the existing pavement is fully supported. However, when a void is simulated under the discontinuity in the existing pavement a reflective crack is possible. No instances of reflective cracking were observed in Michigan.

Transverse cracking near joints. Transverse cracking just on the leave side of the joint also appears to be common and does not appear to be a reflective crack. Examples of this can be seen in Figure 16. Further investigation is needed to determine the cause of these cracks.
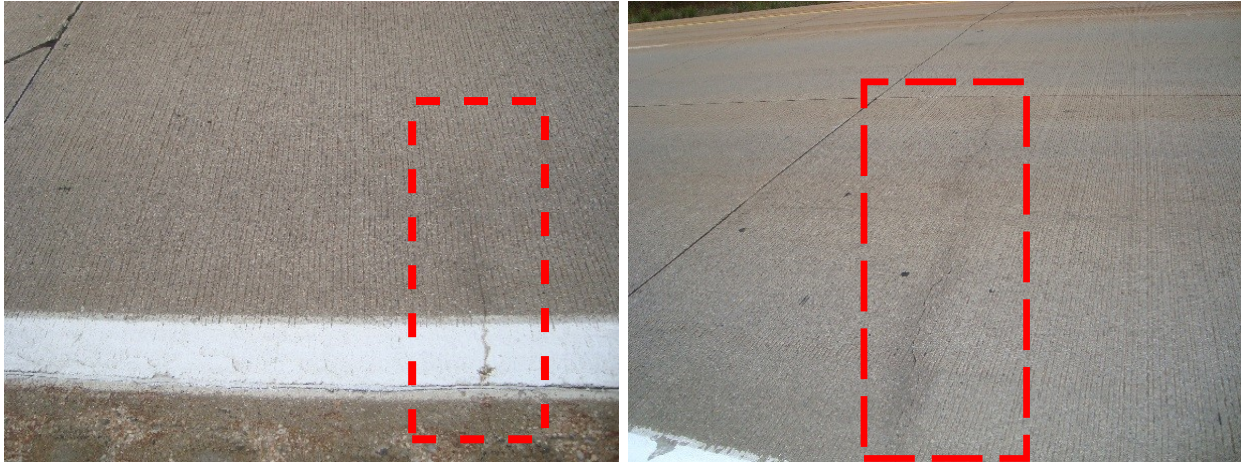
Figure 16: Transverse cracking on leave side of joint

3.7.1.5 Joint Faulting

Joint faulting is a distress also observed in UBOLs in Michigan. Faulting data was examined and between 0.3 and 1.3 inches/mile of faulting were recorded on the sections in which faulting data was available. This indicates that faulting can develop due to pumping of the HMA interlayer, resulting in a loss of support due to interlayer material breakdown that must be accounted for in the design process.

3.7.2 Observations of Section Using Interlayer Fabric

One nonwoven geotextile fabric was constructed in Michigan as part of a test section within a project where an UBOL was constructed with a 1-inch thick open graded HMA interlayer. This project is along US 10 near Coleman. The structure is a 6 in doweled JPCP with a 12 ft joint spacing and a tied shoulder. Early age longitudinal cracking was observed near the location where the fabric meets the asphalt. This could be due to a backup of water at the interface of the two interlayers leading to the crack initiation. The water could become trapped at the interface between the fabric and HMA resulting in a buildup of pressure resulting in the observed cracking. Additionally, the abrupt change in support condition between the asphalt and fabric could have resulted in additional stresses leading to the crack development. This longitudinal crack continued to develop in adjacent panels down the roadway, as would be expected without isolating the adjacent panels. This cracking is shown in

Figure 17 below.
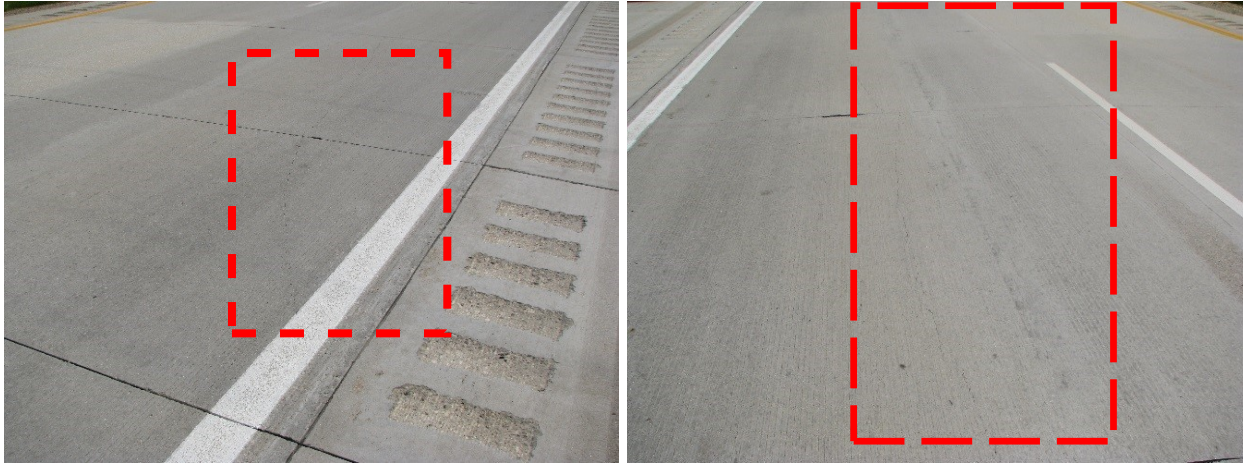
Figure 17: Longitudinal cracks on US-10 near Coleman, MI

CHAPTER 4: LABORATORY TESTING

In this study, a laboratory investigation was employed to examine the effects of the interlayer on the response of the pavement structure under load. Beam specimens were tested to evaluate three different mechanisms. Both hot mix asphalt and nonwoven geotextile fabric interlayer systems were considered. The objective of this investigation was to establish parameters for these interlayers that can be used to develop structural models, which in turn can be used to develop a mechanistic-empirical design procedure for unbonded concrete overlays.

Four mechanisms were being examined using four separate test setups. The mechanisms considered are:

1. Deflection characteristics of the interlayer
2. Friction developed along the interface between the interlayer and the overlay
3. Ability of the interlayer to prevent reflective cracking
4. Bond strength at the interfaces of the interlayer

The specimens for evaluating mechanisms 1 through 3 consisted of an overlay beam cast on top of the interlayer and existing concrete beam. The depth and width of both the overlay and the existing beams was chosen to be 6 inches. The measured deflection characteristics and interface friction were used to establish stiffness and shear transfer for validating the structural models. Mechanism 4 was used to evaluate resistance to upward curl. The results from mechanism 3 testing will be used to assess the potential for reflective cracking and, if necessary, to develop a reflective cracking model.

4.1 MATERIALS

The following subsections describe the materials used in the laboratory study described in the following sections. Note that any mention of named products in this report is not an endorsement of that product.

4.1.1 Interlayers

The nonwoven geotextile fabrics used for this study were manufactured by Propex and consisted of a thick and a thin fabric. The thick fabric, Reflectex, weighs 15 oz/yd^2 and is bleached white. The thinner fabric, made specifically for this study, weighs 10 oz/yd^2 and is black. In this report, the fabrics will be called F15 and F10 for the thick and the thin fabrics, respectively. These fabrics can be seen in Figure 18. For this study, the fabrics are attached to the existing concrete beams according to two methods:

- Pins: Fabric interlayers were pinned to the existing concrete using a gas-powered gun to attach two fasteners to each beam approximately 6 inches from the edge. This approximates methods used in the field. Fastening geotextile fabric using adhesives is a practice gaining popularity.
- Glue: Fabric interlayers were glued to the existing concrete using a geotextile glue made by 3M called Scotch-Weld HoldFast 70 Adhesive.

Figure 18: F10 on the Left and F15 on the Right

The specimens with asphalt interlayers were sawed from in-service pavements to ensure that mixture proportioning, and density of the asphalt interlayers are typical of those found in the field. These asphalt-concrete composite beams were obtained from the Minnesota and Michigan departments of Transportation (MNDOT and MDOT, respectively).

- MDOT provided beams with dense graded asphalt interlayers as well as beams with open graded asphalt mix interlayers. The dense graded asphalt interlayer is approximately 1 inch thick and the open graded interlayer is approximately 2 inches thick.
- MNDOT provided specimens from a concrete pavement that had previously been overlaid with asphalt. Some of the beams were cut prior to milling the dense graded asphalt overlay and the others were cut after some of the asphalt had been milled. MNDOT also provided beams cut immediately after an open graded asphalt was placed on a distressed existing pavement.

A summary of asphalt specimen sources, ages, and average asphalt thicknesses is provided in Table 5. To determine surface texture for each of the beam specimens, sand patch testing (ASTM E965) was performed and dimensions were measured. This information is summarized in Appendix A.

Table 5: Sources of Asphalt Samples Collected

Roadway	Asphalt Description	Ave. Asphalt Thickness
US-131, MI	Old, dense graded	1 in
US-131, MI	Old, open-graded	2 in
I-94, MnROAD	Old, dense graded, milled	0.875 in
I-94, MnROAD	Old, dense graded, unmilled	2.75 in
US-169, MN	New, open graded (PASSRC)	1.75 in

4.1.2 Specimen Designation

All specimens consisted of a bottom beam representing the existing concrete being overlaid, an interlayer, and a concrete beam on the top of the interlayer representing the overlay. The specimens with the fabric interlayers were made by first casting the bottom beam using a high strength mix representative of concrete properties for a 30-year old paving mix. Next, the fabric interlayer was either glued or pinned to the top surface of the bottom beam. Finally, a beam was cast on top of the fabric using a PCC paving mix specified in Section 4.1.3. For the specimens with the asphalt interlayer, the top beam was cast using the same PCC paving mix used for casting the top beam of the fabric layer specimens.

Each finished specimen had its own code identifying when each layer was cast (if it was not obtained in the field) and a description of the interlayer. The nomenclature is shown in Figure 19. From left to right, the first four numbers represent the month and date of cast, the middle letters and numbers are the interlayer designation, and the last letter indicates the batch number for the day of casting. The labeling designating each asphalt interlayer is defined as follows:

- MIDAU: unmilled, aged dense graded asphalt from Michigan
- MIOAU: unmilled, aged open graded asphalt from Michigan
- MNDAU: unmilled, aged dense graded asphalt from Minnesota
- MNDAM: milled, aged dense graded asphalt from Minnesota
- MNONU: unmilled, new open graded asphalt from Minnesota

For the fabric interlayer specimens, the letter following the fabric designation indicated whether the concrete layer represented an existing pavement or an overlay, as both had to be cast for each fabric specimen.
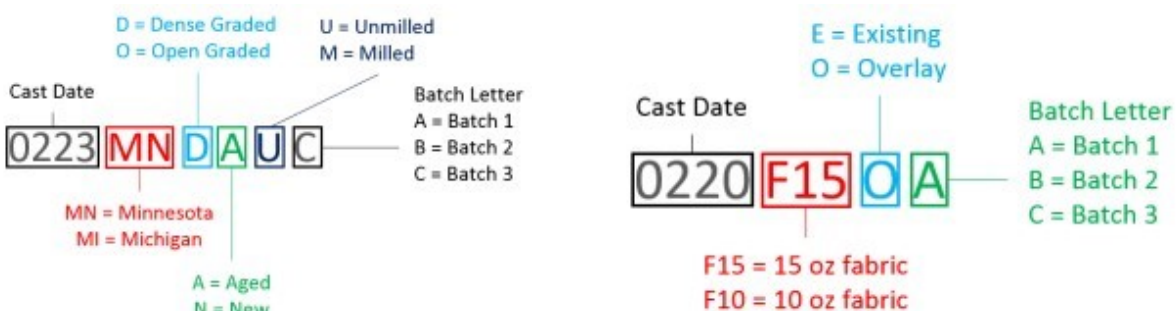
Figure 19: Asphalt Specimen Designation (Left) and Fabric Specimen Designation (Right)

4.1.3 PCC Mix Design

The concrete mixture design for the lower beam of the specimens with the fabric interlayer has a water to cementitious material ratio (w/cm) of 0.36 and a target flexural strength of approximately 850 psi. The overlay (top beam) mixture design for all specimens has a w/cm of 0.42 and a target flexural strength of 650 psi. The bottom beam flexural strength is higher than the overlay flexural strength to

simulate aged concrete being overlaid with a traditional overlay mix. Table 6 summarizes the final mixture design information for the two mixes. All material test data (including compressive strengths, elastic modulus, and modulus of rupture) are summarized in Appendix A. All specimens were made and cured according to ASTM C192.

Finally, an important note to the mix designs is that, due to a calibration error in the air meter used during the first four cast days, the overlay mix had a high air content and therefore reduced strengths. Once this error was noted and the air meter was recalibrated, the volume of air entraining admixture was adjusted, and the desired strengths were achieved. All overlay beams tested at 28 days and cast between 2/20/15 and 3/3/15 had a high air content. All specimens tested for reflective cracking with the high air mixture were replicated using the corrected mix.

Table 6: Target Mixture Design

Mixture Design for Casting Beams Representative of the Existing Slab			
Material	Weight (lb/cy)	Volume (cft/cy)	Volume fraction
Coarse aggregate, Limestone	1918	11.34	0.42
Fine aggregate	1163	6.98	0.26
Cement, Cemex Type I	650	3.31	0.12
Water	234	3.75	0.14
Air content	-	1.62	0.06
Superplasticizer, Sikament SPMN	17 oz per 100 lbs of cement		
Air entrainer, Sika AIR-360	3 oz per 100 lbs of cement		
Mixture Design for Casting Beams Representative of the Overlay			
Material	Weight (lb/cy)	Volume (cft/cy)	Volume fraction
Coarse aggregate Limestone	2053	12.15	0.45
Fine aggregate	1023	6.14	0.23
Cement, Cemex Type I	600	3.05	0.11
Water	252	4.04	0.15
Air content	-	1.62	0.06
Air entrainer, Sika AIR-360	2 oz per 100 lbs of cement		

4.2 DEFLECTION CHARACTERIZATION

The deflection characteristics of the interlayer were established using the setup shown in Figure 20.
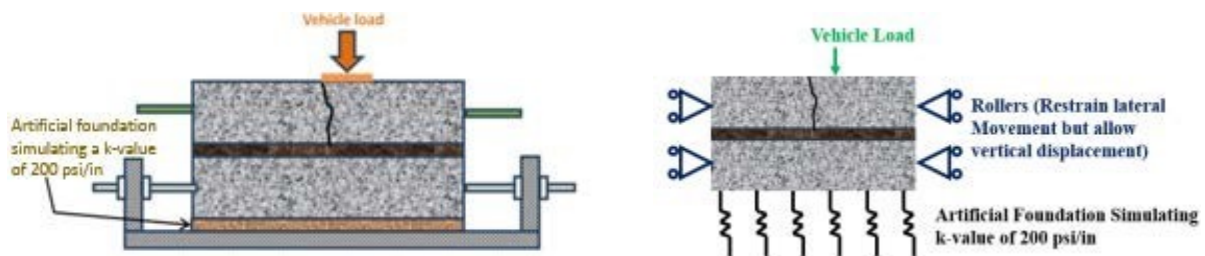
Figure 20: At left, a schematic of Deflection Characteristic Test Setup; at right, the boundary Conditions of Test Setup

The composite section consists of a beam representing the existing slab (in strength and stiffness), the interlayer system, and a beam representing the overlay (in strength and stiffness). A load was applied to one side of a joint sawed in the overlay and deflections in the overlay and existing beams are measured by linear variable displacement transducers (LVDTs). A brief discussion of the finite element modeling performed to ensure the beam test is representative of the response (deflection and rotation) of the pavement structure is provided. This is followed by a discussion of the hardware used in the setup, the loading regime, and the material properties for the beams tested.

4.2.1 Initial Test Planning

Finite element analysis software was used to establish and confirm an appropriate setup and boundary conditions for the specimens. The goal of the finite element modeling was to establish the specimen length, boundary conditions, and load magnitude and location required to create deflections and rotations representative of those in an overlay loaded by a 9,000 lb design load.

In the computational model, all components were assumed to be elastic solids, no load transfer was provided across the joint, and the three contact conditions between the layers were assumed. Contact conditions included fully bonded, unbonded, and an intermediate level of bond where some shear transfer was allowed. The contact for both interfaces at the interlayer was modified such that every reasonable permutation of contact condition at the interfaces was considered.

Before any analyses were conducted, it was determined that that rods would be cast into the ends of the beams so they could be connected to the testing frame to provide restraint in the transverse directions. This restraint helps the short beam respond in a more similar nature to a longer slab. At the start of modelling, a few elementary analyses were conducted to determine how to restrain the beam specimen so that it remained in contact with the support layer when a dynamic load was applied. It was eventually determined from a number of analyses that bearings would need to be placed through the overlay beam when testing for deflection at the interface. Mechanism 1 consists of a joint in the overlay and the load placed to one side of the beam to determine deflection characteristics as well as load transfer as seen in Figure 20. Also, a roller bearing was applied to create a pinned condition for facilitating rotation.

Next, the required length of the beam was determined. Three lengths were considered: 24 inches, 30 inches, and 36 inches. Since a modulus of rupture beam is 24 inches long, this was chosen as the minimum value. Due to the considerable depth (slightly over one foot since the depth of both the overlay and existing are 6 inches) of the two beam high structure, it was thought that the length of the overlay specimen should be increased to maintain a length to height ratio similar to a modulus of rupture beam. However, the length should remain as short as possible due to the significant increase in the weight of the stacked beam structure that would have to be moved on and off of the testing frame for each test. Neglecting the interlayer, the specimens would weight approximately 150 and 225 pounds for the 24 and 36-inch-long specimens, respectively. All three beam lengths (24, 30, and 36 inches) were considered in the finite element analyses, and it was found that the beam had to be at least 30 inches

long to maintain deflection and rotation characteristics similar to those of a slab. Therefore, it was decided to make each overlay specimen 30 inches long.

4.2.2 Final Test Setup

Figure 21 shows a specimen in the testing frame used to isolate the deflection at the interface.

Figure 21: Test setup used to characterize deflection at the interface

The loading head contains a ball joint and is the same loading head used for testing the modulus of rupture beams. The foundation support provided by the lower layers under the concrete slab in an in-service pavement was replicated by an artificial foundation of two layers of neoprene pads, known as Fabcel 25. Figure 22 shows the Fabcel 25 waffle-shaped neoprene pads.

Figure 22: Neoprene pads used to simulate support conditions

The stiffness of the two combined Fabcel layers was determined by conducting a plate load test (ASTM D1195/D1195M), and was found as 200 psi/in. The bearing assembly used to initiate points of rotation can be seen in Figure 23.
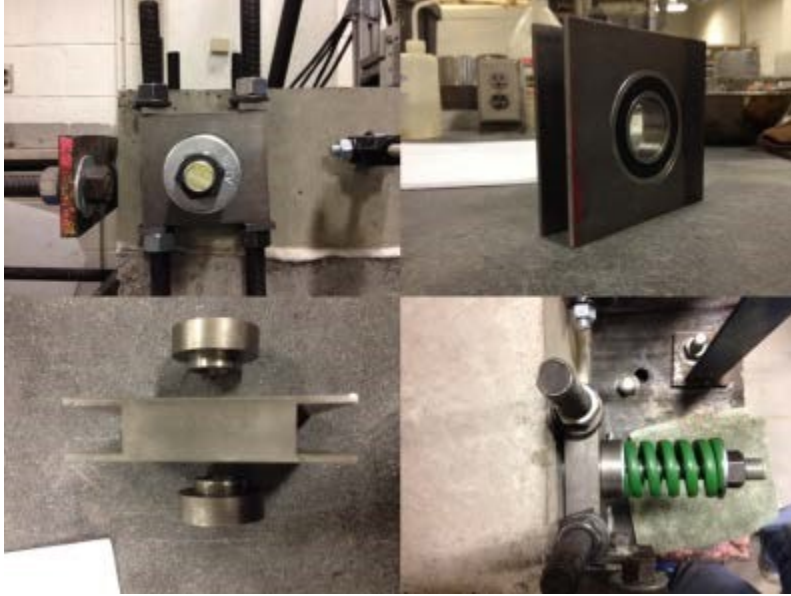
Figure 23: Bearing assembly

The green spring is used in conjunction with a torque wrench to apply the same compression every time. A torque of 40 inch-pounds was applied to the bearings for all specimens.

Additional restraint was provided by vertical rollers on both the loaded and unloaded sides of the beam on the front and back to prevent horizontal displacement of the specimen. Figure 24 shows the components of this assembly.

Figure 24: Roller assembly

Displacement in this configuration is measured using eight LVDTs. The LVDT locations are as shown in Figure 25.
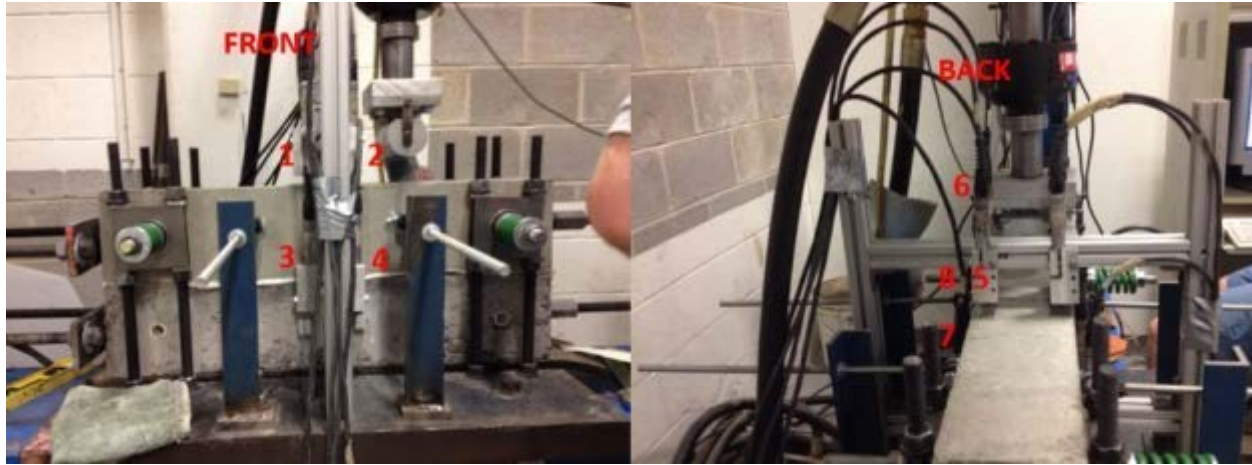
Figure 25: LVDT locations in deflection test setup

Displacement was measured at 1.5 inches from the center saw cut joint on the top of the overlay beam and at mid depth of the lower beam representing the slab being overlaid. The locations of LVDTs 5, 6, 7, and 8 were opposite of 1, 2, 3, and 4. Therefore, displacements measured by LVDTs 2 and 6 were averaged to obtain the overlay loaded (OL) deflection, 1 and 5 were averaged to obtain the overlay unloaded (OU) deflection, 3 and 7 were averaged to obtain the existing unloaded (EU) deflection, and 4 and 8 are averaged to obtain the existing loaded deflection (EL).

4.2.3 Test Protocol, Loading Conditions, and Specimens

The dynamic load applied to the specimen to test Mechanism 1 was intended to simulate a vehicle traveling 65 mph over 10 inches and the specimen is loaded at a rate of 7 Hz. 7 Hz was chosen as the loading frequency as it enables testing of specimens to occur in a reasonable time while still allowing for data to be sampled and show a clear time history of load and displacement. A constant 25 lbs minimum load was maintained for a 0.134 second rest period. A haversine load which approximates the stress pulse of a moving vehicle is applied over a 0.0087 second duration with a peak load of 600 lbs.

Testing was carried out for at least 300,000 cycles for each specimen. A static sweep from the seat load of 25 lbs to 600 pounds is conducted at 50, 100, 500, 1000, 2000, 5000, 10k, 20k, and every 10k loading cycles afterwards. The 600 lbs load induced a similar deflection and angular rotation in the beam to that of a 9-kip falling weight deflectometer load applied to an overlay in the field.

A total of 16 specimens were tested using the setup and loading described above. Table 7 provides summary information about each Mechanism 1 specimen. Displacement vs. load cycle, interlayer compression vs. load cycle, and LTE vs. load cycle plots for each specimen can be found in Appendix A.

Table 7: Summary Information for Specimens used in deflection testing

Specimen	Test Date	Overlay Elastic Modulus and Compressive Strength	Temp and Rel Humidity @ Test Time
0211F15EA 0220F150A	3/20/15	E = 3.11 million psi f'$_c$ = 2666 psi	69.4°F (51%)
0302F15EA 0303F150A	4/1/15	E = 3.04 million psi f'$_c$ = 2156 psi	70.2°F (51%)
0312F10EA 0330F10OB	4/8/15	E = 3.81 million psi f'$_c$ = 3881 psi	71.5°F (52%)
0316F10EB 0402F10OB	4/9/15	E = 3.88 million psi f'$_c$ = 4512 psi	71.9°F (51%)
0223MNDAUA	3/25/15	E = 3.28 million psi	69.8°F (48%)
0417MNDAUC	4/23/15	E = 3.88 million psi	70.8°F (47%)
0319MNDAMA	4/2/15	E = 4.94 million psi	71.7°F (49%)
0422MNDAMA	4/28/15	E = 4.3 million psi	71.4°F (45%)
0226MNONUA	3/27/15	E = 3.11 million psi	70.7°F (59%)
0522MNONUA	5/27/15	E = 4.65 million psi	72.2°F (51%)
0424MIDAUB	4/29/15	E = 4.23 million psi	72.6°F (41%)
0515MIDAUC	5/20/15	E = 4.78 million psi	71.3°F (36%)
0513MIOAUB	5/19/15	E = 4.71 million psi	72.3°F (58%)
0520MIOAUA	5/26/15	E = 4.62 million psi	72.6°F (53%)

4.2.4 Summary of Interlayer Deflection Test Results

As can be seen from the plots for both the 10 and 15 oz/yd^2 fabrics (F10 and F15) in Appendix A, the response of specimens with fabric interlayers remains relatively constant throughout the duration of the test and are therefore more consistent in time than the HMA specimens. F15 and F10 deflect approximately 6 and 4 mils respectively on the loaded side of the overlay. The LTE and interlayer compression (as defined in Appendix A) for F15 remains around 15% and 4 – 5 mils, respectively. For F10, LTE fluctuates between 20 and 40% while the interlayer compression is consistently around 3 mils. F10 is thinner than F15, so it does not compress as much.

For the specimens with an HMA interlayer, permanent compression developed in the HMA over time. The open graded asphalt interlayer from Minnesota had a LTE of 50 – 60% for first specimen and 60 –

75% for the second. Interlayer compression at the end of the test was approximately 19 mils and 13 mils for the first and second specimens, respectively. These high values of interlayer compression indicate that either damage or displacement occurred within the interlayer.

For the specimens with the unmilled dense graded HMA interlayer from Minnesota, LTE began at approximately 40% to 50% and decreased to approximately zero over the test and interlayer compression increased from approximately 2 mils to 8 mils. For the specimens with the milled dense graded HMA interlayer from Minnesota, LTE decreased from approximately 75% to 40% and interlayer compression increased from approximately 4 mils to 6 mils. The difference in thickness between the thicker unmilled and the thinner milled HMA could be part of the reason for the difference.

The specimens with the dense graded asphalt interlayer from Michigan had LTEs that fluctuated between 60% to 80% and peak interlayer compression was approximately 4 mils. The specimens with the open graded HMA interlayer from Michigan had basically constant LTEs of approximately 70% for first specimen and 60% for the second. Additionally, the final interlayer compression was approximately 4 mils for both specimens.

4.3 INTERLAYER FRICTION CHARACTERIZATION

Shear transfer at the interlayer is a critical parameter in the design of unbonded overlays because the interlayer system must be able to provide a slip plane to allow the overlay to move freely with respect to the existing pavement. On the other hand, field observations have indicated that some interlayer systems do not provide sufficient restraint to allow for joint deployment. This can lead to high curling stresses, and the joints that actually do crack are wide. Therefore, an unbonded overlay interlayer system must both have sufficient slip to allow free movement of the overlay and proide sufficient restraint for joint deployment.

Interaction between a concrete slab and a granular or stabilized base layer is traditionally characterized using the Push-Off Test (Maitra, Reddy, and Ramachandra, 2009; Ruiz, Kim, Schindler, and Rasmussen, 2001; Rasmussen and Rozycki, 2001). In this test, a small section of pavement is cast a short distance away from a paved lane. The paved lane acts as a rigid support and a hydraulic jack or actuator is used to displace the test section. The displacement of the test section is measured using a displacement measurement device rigidly fixed to the subgrade. The resistance to sliding is reported either as a force per unit area of interface or as a friction coefficient. The friction coefficient is the frictional force divided by the weight of the slab. When a chemical bond exists between the slab and the base, the sliding resistance will not be proportional to the slab weight, therefore it is more logical to report the force per unit area than the friction coefficient.

4.3.1 Initial Test Planning and Test Setup

In order to characterize the resistance to sliding of each interlayer system, a modified push-off test was performed in the laboratory. In this test, a joint is sawn in the overlay of a 30-inch beam. The bottom beam is not sawn, and both ends of this beam are restrained to prevent translational displacement. One

side of the overlay is also restrained against displacement. The other side of the overlay is attached to a threaded rod instrumented with strain gauges to record force. Two LVDTs attached to the loading frame are used to measure displacement of the loaded section. A thrust bearing attached to the vertical actuator is placed on the top of the loaded section of the overlay beam near the joint to prevent vertical displacement. The actuator is used in a displacement control mode to ensure no vertical displacement of the test block occurs near the joint during a test. The variable force provided by the actuator prevents rotation of the loaded half of the overlay and subsequent tensile debonding failure near the joint. A schematic of the test setup can be seen in Figure 26, and the test setup in the laboratory is shown in Figure 27.
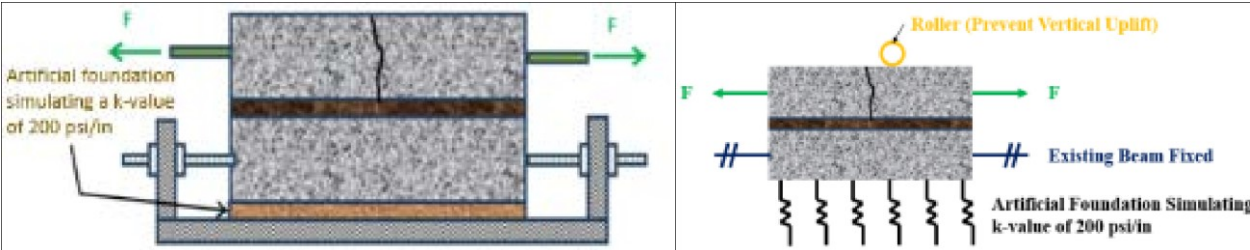
Figure 26: At left, Schematic of Modified Push Off Test Setup; At right, Boundary Conditions of Modified Push Off Test
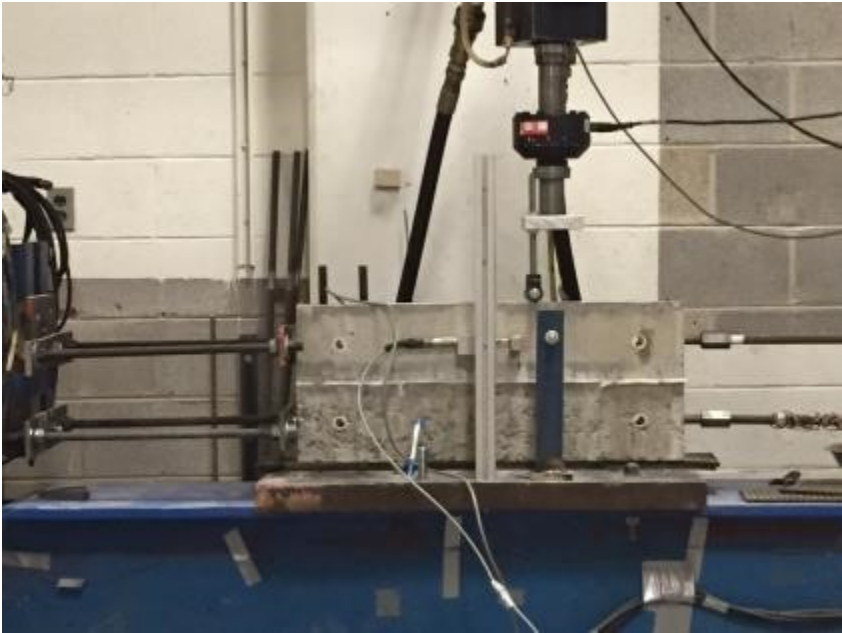
Figure 27: Laboratory setup for the modified push-off test

4.3.2 Test Loading Conditions and Specimens

The horizontal push-off load is applied by manually tightening the instrumented threaded rod. The modified push-off test has two phases. Phase 1 is the cyclic loading phase. In this phase, load is applied until the loaded portion of overlay reaches approximately 80 mils of displacement. The 80-mil displacement corresponds to a 100-degree Fahrenheit drop in temperature for a 12 foot slab cast of concrete with a thermal coefficient of expansion of 5.3 microstrain per degree F. The load is then held constant to observe the relaxation of the interlayer system until the force is relatively constant over time. The load is then removed from the rod. To account for non-elastic displacement, a load is applied in the opposite direction of the initial load until the overlay section returns to its initial position. This position is then held until the force is relatively constant over time. The load, relaxation, opposite load cycle is repeated between 6 to 8 times for each test. Phase 2 is the ultimate loading phase. In this phase, load is applied until the interlayer system fails, or very large displacements (over one inch) are observed.

The modified push-off test was performed on nine different interlayer systems. The details of these systems are shown in Table 8. The attachment to the existing concrete sample taken from the field could be an either an "asphaltic bond" or a "cementitious bond":

- For an asphaltic bond, the HMA was placed on hardened concrete.
- For a cementitious bond, the wet concrete was placed directly onto the asphalt.

The test date, elastic modulus for the concrete overlay, and temperature and relative humidity at the time of testing for each specimen are recorded in Table 9.

Table 8: Summary of Interlayers Tested in Modified Push-off Test

Label	Source	Grading	Surface	Age	Fabric Weight	Attachment to Existing Concrete
F15-Glued	Propex	n/a	n/a	n/a	15 lb/yd^2	Glued
F15-Pinned	Propex	n/a	n/a	n/a	15 lb/yd^2	Pinned
F10-Glued	Propex	n/a	n/a	n/a	10 lb/yd^2	Glued
F10-Pinned	Propex	n/a	n/a	n/a	10 lb/yd^2	Pinned[1]
MNDAU	MnDOT	Dense	Unmilled	Aged	n/a	Asphaltic Bond
MNDAM	MnDOT	Dense	Milled	Aged	n/a	Asphaltic Bond
MNONU	MnDOT	Open	Unmilled	New	n/a	Asphaltic Bond
MIDAU	MDOT	Dense	Unmilled	Aged	n/a	Cementitious Bond
MIOAU	MDOT	Open	Unmilled	Aged	n/a	Cementitious Bond

Table 9: Summary Information for Modified Push-off Test Beams

Corresponding Beam Nomenclature	Test Date (Time)	Overlay Elastic Modulus and Compressive Strength	Temp and Rel Humidity @ Test Time
0211F15EB 0220F150 (Glued)	3/20/15 (12:15 PM)	E = 3.11 million psi f′$_c$ = 2666 psi	69.6°F (51%)
0302F15EB 0303F10B (Glued)	4/1/15 (9:15 AM)	E = 3.04 million psi f′$_c$ = 2156 psi	70.0°F (51%)
0413F15EA 0506F15OA (Pinned)	5/11/15 (5:00 PM)	E = 4. 63 million psi f′$_c$ = 5334 psi	71.4°F (56%)
0413F15EB 0506F15OB (Pinned)	5/12/15 (12:15 PM)	E = 4. 63 million psi f′$_c$ = 5334 psi	71.8°F (54%)
0312F10EB 0330F10OC (Glued)	4/10/15 1:30 PM	E = 3.81 million psi f′$_c$ = 3881 psi	71.7°F (52%)
0316F10EB 0402F10OC (Glued)	4/10/15 (2:45 PM)	E = 3.88 million psi f′$_c$ = 4512 psi	71.7°F (52%)
0406F10EB 0506F10OB (Pinned)	5/11/15 (3:30 PM)	E = 4.63 million psi f′$_c$ = 5334 psi	71.9°F (55%)
0223MNDAUB	3/24/15 (1:30 PM)	E = 3.28 million psi f′$_c$ = 2326 psi	69.6°F (48%)
0417MNDAUB	4/23/15 (3:00 PM)	E = 3.88 million psi f′$_c$ = 4590 psi	70.9°F (47%)
0319MNDAMB	4/3/15 (11:00 AM)	E = 4.94 million psi f′$_c$ = 6833 psi	71.8°F (50%)
0422MNDAMB	4/27/15 (1:00 PM)	E = 4.3 million psi f′$_c$ = 4696 psi	71.2°F (45%)
0226MNONUB	3/30/15 (10:30 AM)	E = 3.11 million psi f′$_c$ = 2237 psi	70.2°F (59%)
0522MNONUB	5/26/15 (4:30 PM)	E = 4.65 million psi f′$_c$ = 5131 psi	71.1°F (55%)
0424MIDAUA	4/29/15 (12:00 PM)	E = 4.23 million psi f′$_c$ = 4694 psi	72.5°F (42%)
0515MIDAUA	5/20/15 (3:30 PM)	E = 4.78 million psi f′$_c$ = 5357 psi	70.6°F (37%)
0513MIOAUB	5/18/15 (4:45 PM)	E = 4.71 million psi f′$_c$ = 5013 psi	71.0°F (59%)
0520MIOAUA	5/26/15 (2:40 PM)	E = 4.62 million psi f′$_c$ = 5073 psi	71.0°F (56%)

4.3.3 Test Protocol and Response Measurement

The first cycle of each test provided information on the material properties relevant in determining when and where joints in the overlay would deploy. The average stiffness of the interlayer system for

49

the first load cycle was calculated as the force over displacement at a displacement of 80 mils. If the first cycle did not reach 80 mils displacement, the stiffness was calculated using the maximum displacement. The average initial stiffness of each interlayer system is provided in Table 10.

During testing it was determined that the interlayer system stiffness stabilized between 5 and 8 load cycles. This stiffness is relevant when calculating the stress in the overlay caused by the interlayer resisting uniform volume changes due to a decrease in temperature and/or moisture. An overly stiff unbonded overlay system can prevent true debonding, cause high stresses to develop in the overlay, and prevent proper joint deployment. The average final stiffness for each interlayer is summarized in Table 7. The definition of the initial and final stiffness is shown in Figure 28.

Finally, the ultimate strength of each interlayer system was tested to establish the ultimate resistance to sliding for each interlayer system. The average ultimate resistance is provided in Table 10 for each specimen. When reviewing Table 10, note that for one of the tests on the F10 Glued interlayer, a delay in the initial loading cycle caused the first load cycle to appear less stiff than several subsequent load cycles. For this test, the initial stiffness was estimated using the second load cycle. Data for each modified push-off beam are plotted in Appendix A (Mechanism 2 plots).
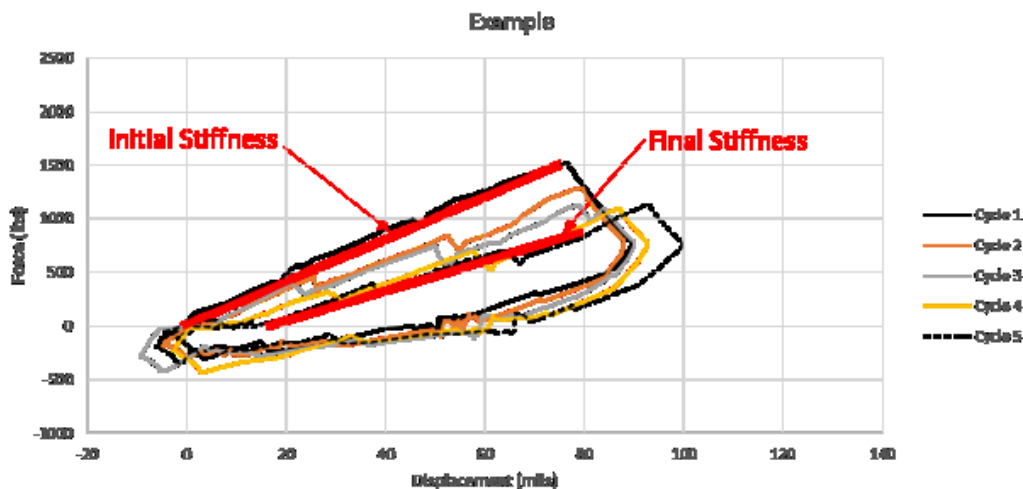
Figure 28: Example of Initial and Final Stiffness determination

Table 10: Summary Results from Modified Push-Off Test

Interlayer (Code)	Interlayer & interlayer thickness	Initial Stiffness (psi/in)	Final Stiffness (psi/in)	Ultimate Resistance (psi)
F15-Glued	Fabric (15 oz/yd^2)	61	37	13
F15-Pinned	Fabric (15 oz/yd^2)	50	40	26
F10-Glued	Fabric (10 oz/yd^2)	104	87	22
F10-Pinned	Fabric (10 oz/yd^2)	98	29	21
MNDAU	HMA (2.75 in)	234	167	39
MNDAM	HMA (0.875 in)	333	263	59

MIDAU	HMA (1 in)	336	317	>62
MNONU	HMA (1.75 in)	217	55	16
MIOAU	HMA (2 in)	169	136	63

4.3.4 Summary of Interlayer Friction Test Results

Results in Table 9 show that specimens with a fabric interlayer have a lower stiffness than the specimens with an HMA interlayer. Within the fabric specimens, the F10 specimens had a higher stiffness than the F15 specimens. This is most likely due to the smaller thickness of F10 that limits in-plane deformation of the interlayer (the thickness being smaller than that of F15).

The specimens with the milled interlayer from Minnesota have a higher initial and final stiffness than the specimens with the unmilled interlayer. It can also be seen that the ultimate resistance of the specimens with the milled interlayer was much greater that for the specimens with the unmilled interlayer. This is possibly due to the decreased thickness of the milled specimens. The largest reduction in stiffness among asphalt specimens occurs with the open graded asphalt interlayer from Minnesota which was visibly distressed during testing and had a very small ultimate resistance.

The specimens with the open and dense graded asphalt interlayers from Michigan exhibited the smallest decreases in stiffness and also had the largest ultimate resistance. The ultimate resistance for the thicker asphalt interlayers was lower with the exception of the open graded interlayer for the specimens from Minnesota, which damaged due to the lower strength.

In general, with the exception of the specimens with the open graded HMA interlayer from Minnesota, the fabric interlayers provide less restraint than the asphalt layers.

4.4 REFLECTIVE CRACKING CHARACTERIZATION

4.4.1 Test Setup

Reflective cracking is a potential concern for unbonded overlays. The reflective cracking test setup is designed to assess the ability of the interlayer system in deterring cracks in the existing pavement from reflecting up into the overlay. For this test setup, a saw cut is made in the lower beam at midspan to represent a joint or crack in the existing concrete. The beam was loaded directly above the sawed joint in the middle of the 30-inch beam using the same loading head used for the deflection test setup. Figure 29 below illustrates the schematic used in the planning of the reflective cracking test setup, while Figure 30 illustrates the as-built apparatus in the laboratory.
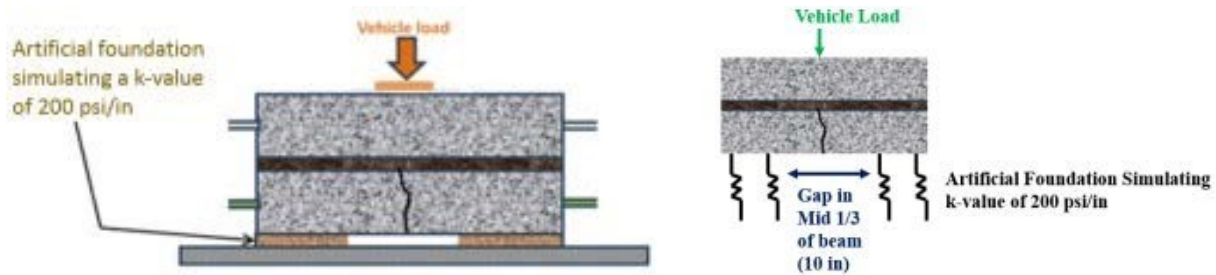
Figure 29: At left, Schematic of Reflective Cracking Test Setup; at right, Boundary Conditions of Reflective Cracking Test Setup

Figure 30: Final test apparatus for reflective cracking

4.4.2 Test Loading Conditions and Specimens

The load in the test configuration is applied at a constant rate until a reflective crack is generated in the overlay beam. The load rate was chosen to be 30 lbs per second, which is the loading rate specified when performing modulus of rupture testing for concrete beams (ASTM C78).

LVDTs record the displacement at the front and back of the beam on the overlay and existing beams. The LVDTs are located 3.5 inches to the left of the applied load.

Shakedown testing for reflective cracking was performed using a specimen with the 15 oz/yd^2 nonwoven fabric, and the bottom of the beam was fully supported with two layers of Fabcel 25. Three specimens were tested, and a reflective crack could not be generated. The overlay cracked from the top-down – as opposed to bottom-up, as would be expected. This indicates that the failure was due to the stress concentration and crushing under the loading head and not due to a crack reflecting up from the underlying cracked beam.

In order to overcome this problem, a gap was created under the central 10 inches of the beam by removing the Fabcel so there was no support in this area. This gap under the center of the beam is intended to simulate a void under the joint of an existing pavement. Figure 31 shows the gap in the

Fabcel measured with plywood and centered with a plumb bob. With the gap under the beam, subsequent shakedown tests generated reflective cracking which propagated from the bottom-up.

Figure 31: 10-inch Gap in Fabcel with Plumb Bob to Center the Gap

Table 11 summarizes information relating to each specimen tested using the reflective cracking test setup. This includes the ultimate load and modulus of rupture (MOR) of the overlay beam.

Force vs displacement plots for each reflective cracking specimen are provided in Appendix A.

Table 11: Summary Information for Reflective Cracking Specimens

Specimen	Break Load (lbs)	Test Date (Time)	MOR of the Overlay Beam (psi)	Temp and Rel Humidity @ Test Time
0406F15EB 0429F15OB	6,218	5/4/15 (9:20 AM)	610	71.8°F (50%)
0406F15EC 0429F15OC	6,605	5/4/15 (10:00 AM)	644	71.9°F (51%)
0302F15EB 0701F15OD	7,508	7/6/15 (1:10 PM)	682	72.4°F (61%)
0316F10EC 0402F10OA	6,565	4/7/15 (2:40 PM)	628	71.7°F (57%)
0409F10EA 0501F10OA	6,984	5/6/15 (11:15 AM)	641	70.8°F (56%)
0316F10EB 0709F10OC	7,517 *	7/14/15 (11:35 AM)	701	72.3°F (60%)
0417MNDAUA	5,562	4/22/15 (11:20 AM)	590	71.7°F (46%)
0507MNDAUA	6,345	5/12/15 (3:00 PM)	738	70.7°F (51%)
0701MNDAUA	6,052	7/6/15 (12:00 PM)	658	70.3°F (62%)

Specimen	Break Load (lbs)	Test Date (Time)	MOR of the Overlay Beam (psi)	Temp and Rel Humidity @ Test Time
0422MNDAMC	5,923	4/27/15 (12:40 PM)	623	71.1°F (44%)
0507MNDAMB	6,638	5/12/15 (4:00 PM)	690	72.1°F (49%)
0709MNDAMB	5,912	7/14/15 (11:10 AM)	649	72.2°F (60%)
0507MNONUC	6,414	5/12/15 (5:00 PM)	694	71.9°F (47%)
0522MNONUC	6,678	5/27/15 (9:30 AM)	724	72.1°F (58%)
0701MNONUB	6,460	7/6/15 (12:30 PM)	636	72.1°F (61%)
0424MIDAUC	5,777	4/29/15 (11:10 AM)	652	72.4°F (42%)
0515MIDAUB	6,438	5/20/15 (11:15 AM)	717	72.2°F (35%)
0701MIDAUC	5,896	7/6/15 (1:10 PM)	663	72.4°F (59%)
0513MIOAUC	6,957	5/18/15 (12:20 PM)	697	70.1°F (60%)
0520MIOAUC	7,129	5/25/15 (10:35 AM)	711	72.2°F (48%)
0709MIOAUA	6,471	7/14/15 (10:40 AM)	698	72.3°F (60%)

4.4.3 Summary of Reflective Cracking Test Results

Reflective cracking is cracking which occurs in the overlay directly over a joint or cracking in the existing pavement. It is also possible to have reflective distress over a region of reduced support. This could occur over a severely deteriorated joint or crack where the stiffness is smaller in a short region where the distress in the existing pavement is located. As discussed in the section on Mechanism 3 setup, it is important to note that reflective cracking could not be generated from the bottom up when the specimen is fully supported. This suggests that the potential for reflective cracking in the concrete overlay is extremely low unless a void is present in the vicinity of the crack or joint. A summary of the results from Mechanism 3 testing is provided in Table 12, where the "Load Ratio" refers to the Reflective Crack Load normalized by the Failure Load for the Overlay MOR Beam.

Table 12: Reflective Cracking Beam Summary

UBOL Specimen	Reflective Crack Load (lbs)	MOR for the Overlay Mixture (psi)	Failure Load for Overlay MOR Beam (lbs)	Load Ratio	Average Load Ratio for Each Interlayer
F15	6218	610	7417	0.838	0.842
	6605	644	7980	0.828	
	7508	682	8730	0.860	
F10	6565	628	7707	0.852	0.869
	6984	641	7920	0.882	

	7517	701	8620	0.872	
MNDAU	5562	590	7480	0.744	
	6345	738	9217	0.688	0.725
	6052	658	8155	0.742	
MNDAM	5923	623	7767	0.763	
	6638	690	8730	0.760	0.753
	5912	649	8020	0.737	
MNONU	6414	694	8594	0.746	
	6678	724	8925	0.748	0.767
	6460	636	8015	0.806	
MIDAU	5777	652	8140	0.710	
	6438	717	8874	0.725	0.711
	5896	663	8460	0.697	
MIOAU	6957	697	8675	0.802	
	7129	711	8798	0.810	0.787
	6471	698	8637	0.749	

The load required to induce a reflective crack into the overlay beam is provided in the second column. The load required to fail a modulus of rupture beam cast with the same mixture as the overlay is provide in column 4. The reflective crack load (column 2) is divided by the failure load for the overlay modulus of rupture beam (column 4) to obtain the load ratio (column 6). The failure load of the overlay modulus of rupture beam is the maximum load sustained by the modulus of rupture beam according to ASTM C78. These load ratios were then averaged for each interlayer type.

The average load ratio has a range of 0.73 to 0.87. The fabric specimens are at the upper end this range, which may indicate that they are more resistant to the development of reflective cracking as compared to the specimens with an HMA interlayer. All of the HMA interlayer specimens performed roughly comparable to one another. The open graded HMA interlayer from Michigan yielding the highest average load ratio of 0.79. This is similar to that achieved by the F15 interlayer specimens.

4.5 BOND STRENGTH CHARACTERIZATION

4.5.1 Test Setup

Bond strength of interlayers was evaluated by measuring the vertical force-displacement relationship as the concrete layers of the unbonded overlay structure are loaded in direct tension, as shown in Figure 32. This test is intended to provide insight into how debonding between the existing and overlay concrete layers develops in the field and to determine if curling can result in debonding between the interlayer and the concrete layers.
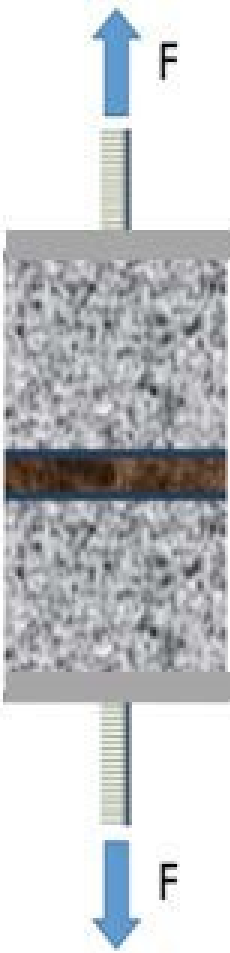
Figure 32: Schematic of direct tension test; at right, laboratory direct tension test on specimen with HMA interlayer

4.5.2 Notes on Extraction of Specimens from Beams

Each direct tension specimen was either cut from one of the already tested Mechanism 3 specimens (asphalt interlayers) or cast in cylindrical molds (fabric interlayers). It was assumed that little to no damage was experienced where the direct tension specimens were sawn from the Mechanism 3 specimens and would therefore not affect the results of the direct tension test. The direct tension specimens required very precise preparation. The location of the specimens in the direct tension beams is provided in Figure 33.
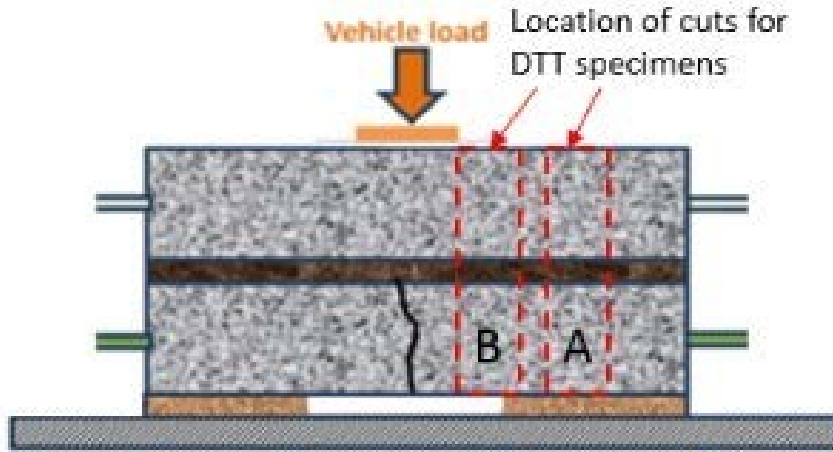
Figure 33: Location of asphalt direct tension specimens

A rig was used to provide compression while metal blocks were epoxied to the top and bottom of the specimens to ensure that the steel rods used in the testing apparatus were perfectly straight and in line with one another.

4.5.3 Test Specimens and Loading Conditions

The asphalt interlayer specimens were 4-inches on each side and approximately 12 inches tall (an asphalt interlayer direct tension specimen is shown in Figure 32). The fabric interlayer specimens were 4-inch diameter and approximately 8 inches tall cylinders. The fabric specimens were made in two steps. First, the bottom of the specimen was cast using a 0.36 w/cm. Next, the fabric was glued to the top of the specimen bottom and the top of the specimen was cast using a 0.42 w/cm overlay mixture.

An Instron loading machine was used to apply a direct tensile load. A photo of the test setup is shown in Figure 32. The test is run in displacement control mode at a rate of 1 mil/sec and the force is recorded by the load machine. Displacement is also recorded with two LVDTs attached to opposite sides of the specimen. The relative displacement between the concrete above and below the fabric is measured, which can be seen in Figure 32. Table 13 summarizes the specimens tested and the peak load and displacement at the peak load. Force vs displacement for each direct tension specimens is plotted in Appendix A.

Table 13: Summary of Specimens Tested for Bond Strength

Code	Replicate	Location	Peak Load (#)	Displacement at Peak Load (mils)	Location of Break
F15	1	N/A	18	64	Glued Interface
F15	2	N/A	16	61	Glued Interface
F10	1	N/A	31	139	Glued Interface
F10	2	N/A	38	120	Glued Interface
MNDAU	1	A	255	33	Middle of HMA

Code	Replicate	Location	Peak Load (#)	Displacement at Peak Load (mils)	Location of Break
MNDAU	2	B	251	42	Middle of HMA
MNDAM	1	A	262	10	Bond w/ Existing Concrete (into HMA)
MNDAM	2	B	392	13	Both interfaces and into HMA
MNONU	1	A	169	12	Middle of HMA
MNONU	2	B	208	12	Bond w/ Existing Concrete (into HMA)
MIDAU	1	A	586	22	Bond w/ Overlay Concrete
MIDAU	2	B	411	13	Bond w/ Overlay Concrete
MIOAU	1	A	206	4	Bond w/ Existing Concrete (into HMA)
MIOAU	2	B	142	6	Bond w/ Existing Concrete

4.5.4 Summary of Bond Strength Test Results

As shown in Table 13, both fabrics tested had comparable values of peak force and displacement at peak force. The F10 specimens resulted in a peak load of 30 – 40 lbs at a displacement ranging between 120 mils to 140 mils and the F15 specimens maintained a peak load of 15 to 20 pounds at a displacement of approximately 60 mils. The variation observed between fabric specimens can be partly attributed to the quality and quantity of geotextile adhesive placed at the glued interface. Overall, these results indicate that the fabrics would provide insignificant resistance to upward curl of the concrete overlay. Greater variability was observed with the HMA interlayers than the fabric interlayer specimens. Additionally, higher strength and smaller displacements at the peak load for the HMA specimens was observed as compared to the fabric specimens as one would expect. The magnitude of the peak load varied with the location of the failure within the inter layer system. Both the Minnesota and Michigan open graded asphalts produced the smallest peak loads, followed by Minnesota dense unmilled, Minnesota dense milled, and Michigan dense unmilled which had the greatest peak load.

CHAPTER 5: DEVELOPMENT OF INTERLAYER MODEL

In this study, the Totski model (Totski 1981, Khazanovich 1994, Khazanovich and Ioannides 1994) was adapted for structural modeling of unbonded overlays. This model, shown in Figure 34, simulates an UBOL and a slab resting on a spring interlayer supported by a slab resting on the Winkler subgrade. The advantage of this model is that it is capable of explicitly modeling the "cushioning" property of the interlayer. This model was developed specifically for modeling of unbonded concrete overlays but has not been widely used due to lack of data needed to verify the procedure for selection of the spring interlayer stiffness parameter.
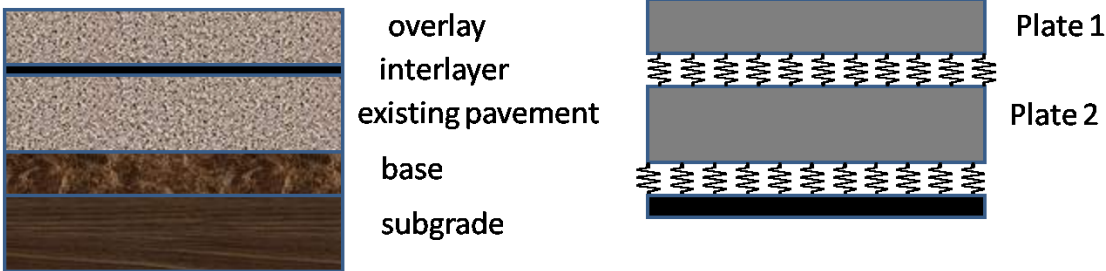
Figure 34: UBOL system (at left) and Totski model for layer interface (at right)

To accurately model the UBOL structure within ISLAB, the value of the Totsky interlayer k-value must be established for different interlayers. The laboratory research conducted, and field testing gathered during this study provided the information needed to fill this gap. This section details the use of expanded data from the reflective cracking laboratory testing as well as Falling Weight Deflectometer (FWD) data, to establish guidelines for the value of the interlayer Totsky k-value for UBOL design.

5.1 FINITE ELEMENT INTERPRETATION OF THE LABORATORY TEST DATA

The reflective cracking test described in the previous chapter was modeled in ISLAB2005 and the results from the LVDTs during the test were used to determine the corresponding value of the Totsky interlayer k-value.

Figure 35 provides a representation of the model used to determine the Totsky k-value for the different interlayers. Note that the simulated load is applied as a 0.25-in wide line-load along the beam depth of 6 in (indicated in blue in Figure 35a). Thus, the load contact area is 1.5 in^2. As the finite element model is static, a single load of 1 kip is applied to determine a response of the beam model to loading.
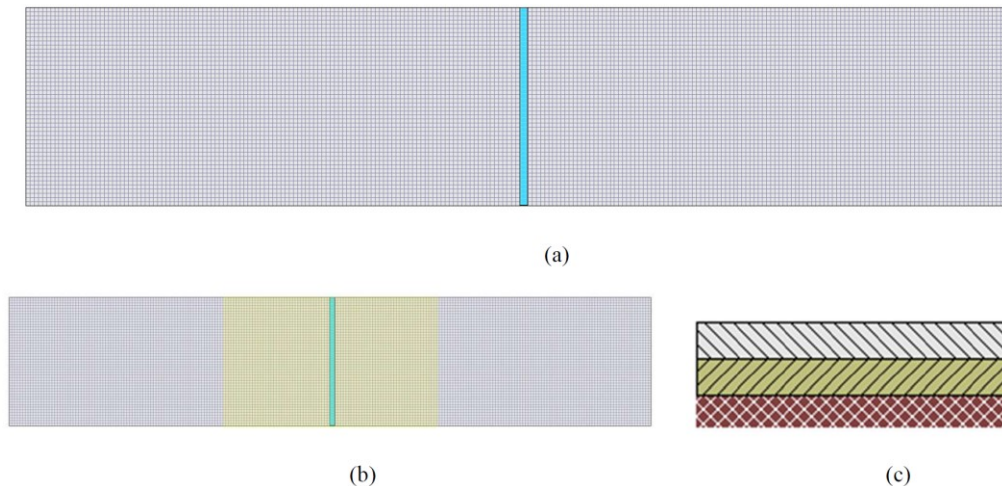
Figure 35: ISLAB two-dimensional model of Reflective Cracking test, where (a) shows the mesh and load area (plan view), (b) highlights the unsupported area in yellow (plan view), and (c) the structure profile view

In ISLAB2005, the notch at mid-span in the existing concrete is modeled by inserting a joint at mid-span. In the upper layer (the overlay), this joint fully transfers load (the load-transfer efficiency is 100% treated as a rigid joint). However, in the lower layer (the existing concrete), the joint does not transfer the load at all (load transfer efficiency is near-zero). This allows for the test setup to be modeled the same as the laboratory test setup.

With the beam model, a factorial of cases is modeled to observe the response utilizing interlayers of different properties. In each case, only the Totsky interlayer k-value (k_{totsky}) assumed is varied, otherwise the modeled beam has the following properties:

- Layer 1: h_{OL} = 6 in, E_{OL} = 4,255,000 psi (average of all Reflective Cracking beam overlay elastic moduli), Poisson ratio v = 0.15, unit weight γ = 0.087 lb/in^3
- Interlayer: k_{IL} varied from 100 to 50,000 psi/in
- Layer 2: h_{EX} = 6 in, E_{EX} = 4,790,000 psi (average of PCC elastic moduli for the "existing" beam of the reflective cracking laboratory specimens), Poisson ratio v = 0.15, unit weight γ = 0.087 lb/in^3
- Mesh details: Mesh elements are square (0.125 in to a side) for the entire model, as illustrated in Figure 35a.
- A static load of 1-kip is applied to determine a linear beam response associated with interlayer properties.

Figure 36 illustrates the final relationship determined for the modeled beam response and the Totsky interlayer stiffness. Also included in the figure is an exponential relationship determined by transforming the variables and finding a linear least-squares fit. As shown in the figure, the R-squared valued for the fitness of the exponential relationship is 0.99, thus the model adequately describes the relationship between model response and the Totsky k-value for this range of values. With the relationship

developed in ISLAB, interlayer Totsky k-values can be established for each beam specimen tested and therefore each type of interlayer system included in the laboratory study.
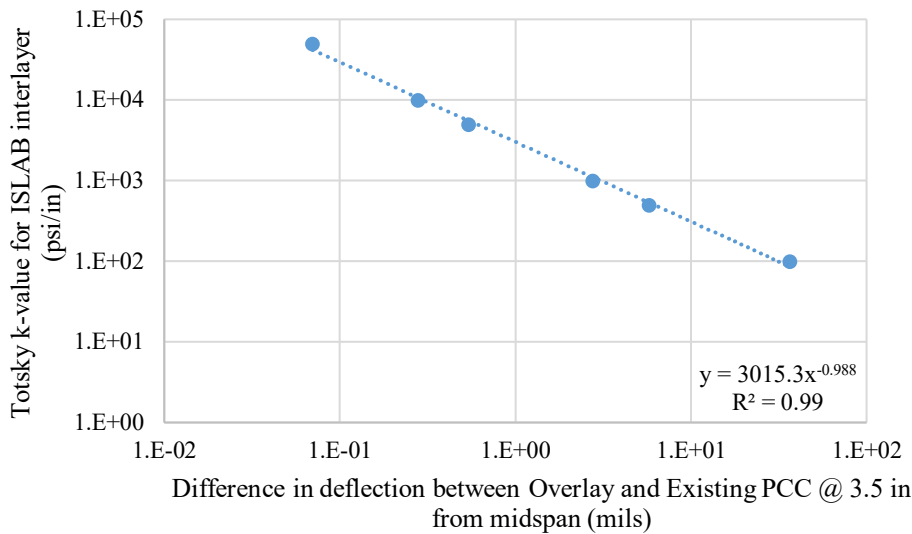
Figure 36: Relationship between difference in layer deflection (in mils) and Totsky k-value for interlayer from ISLAB

Table 14 presents the reflective cracking beam specimens for each interlayer and the corresponding Totsky k-value. Given the response of the different interlayer beams under a 1-kip load in the lab, the modeled relationship was used to infer an associated Totsky interlayer stiffness. Average and standard deviation of the different interlayers tested in the laboratory are presented in Table 15.

Table 14: Established Totsky k-values for reflective cracking laboratory testing specimens

Interlayer type	Overlay PCC			Fabric Type	Diff in defl @ 1 kip (mils)	Totsky k-value (psi/in)
	Specimen	E (psi)	f'c (psi)			
15 oz/yd² geotetextile fabric (Propex Reflectex)	0429F15OB	4280000	5059	F15	8.27	411
	0429F15OC	4280000	5059	F15	10.41	325
	0701F15OD	4430000	4632	F15	12.33	274
10 oz/yd² geotetextile fabric (Propex)	0402F10OA	3880000	4512	F10	10.58	320
	0501F10OA	4170000	5069	F10	7.76	439
	0402F10OA	3880000	4512	F10	9.48	358
				Asphalt Thickness		
MnDOT Aged, Dense graded	0417MNDAUA	3880000	4590	2.9	0.93	3824
	0507MNDAUA	4480000	5106	2.8	2.32	1504

61

| Interlayer type | Overlay PCC | | | Fabric Type | Diff in defl @ 1 kip (mils) | Totsky k-value (psi/in) |
	Specimen	E (psi)	f'c (psi)			
Unmilled asphalt	0701MNDAUA	4430000	4632	2.8	0.76	4698
MnDOT Aged, Dense graded Milled asphalt	0422MNDAMC	4300000	4696	0.9	1.37	2581
	0507MNDAMB	4480000	5105.75	1	1.25	2828
	0709MNDAMB	4490000	4732	0.8	0.66	5431
MnDOT New, Open graded Unmilled asphalt	0507MNONUC	4480000	5106	1.7	1.52	2324
	0522MNONUC	4650000	5131	1.7	0.93	3824
	0701MNONUB	4430000	4632	1.8	2.3	1518
MDOT Aged, Dense graded Unmilled asphalt	0424MIDAUC	4230000	5106	1.1	0.65	5521
	0515MIDAUB	4790000	5131	1	0.99	3584
	0701MIDAUC	4430000	4632	1.3	1.17	3033
MDOT Aged, Open graded Unmilled asphalt	0513MIOAUC	4710000	5013	1.8	1.28	2760
	0520MIOAUC	4620000	5073	1.9	0.68	5263
	0709MIOAUA	4490000	4632	1.8	1.32	2675
MDOT New, Dense graded Unmilled asphalt	0806PADNUC	4630000	4966	1.5	1.98	1766
	0909PADNUA	4340000	4824	1.4	1.3	2717
	0909PADNUC	4340000	4824	1.5	0.63	5690

Table 15. Average and standard deviation of Totsky k-value for different the different interlayer types

Interlayer Description	Interlayer Type	Average Totsky k	Standard Deviation
15 oz/yd^2 geotetextile fabric (Propex Reflectex)	F15	336.7	63.4
10 oz/yd^2 geotetextile fabric (Propex)	F10	372.2	54.9
MnDOT Aged, Dense graded Unmilled asphalt	MNDAU	3342.3	1261.9
MnDOT Aged, Dense graded Milled asphalt	MNDAM	3613.4	1175.1
MnDOT New, Open graded Unmilled asphalt	MNONU	2555.1	900.8
MDOT Aged, Dense graded Unmilled asphalt	MIDAU	4046.1	965.9
MDOT Aged, Open graded Unmilled asphalt	MIOAU	3566.1	1095.2
MDOT New, Dense graded Unmilled asphalt	PADNU	3390.8	1533.4

Hypothesis testing was performed to evaluate the effects of the different interlayers and determine if there was any statistical difference between the interlayers. Tukey's range test is utilized to compare all possible pairs of means (Montgomery, 2012). The null hypothesis is that the means of the two

interlayers compared are equal, while the alternative hypothesis is that the mean of one of the two interlayers differs from the other. Table 16 presents all pair-wise comparisons between each interlayer. The difference in means is the result of the subtraction of the averages of the two compared interlayers. The 95 percent confidence intervals on the difference between interlayers are also presented. The two interlayers are statistically different at 95 percent, if the range of the confidence interval does not contain zero. As can be seen from Table 16, the means of the fabric interlayers are statistically different from each of the asphalts with the exception of the open graded asphalt from Minnesota. No statistical difference was detected between any of the asphalt interlayers or between the fabric interlayers.

Table 16: Pair-wise Interlayer Comparisons

Comparison	Difference of Mean Totsky Coeff. Between Interlayers	95% Confidence Interval of Difference
F10 - F15	35	(-2762, 2833)
MNDAU - F15	**3006**	**(208, 5803)**
MNDAM - F15	**3277**	**(479, 6074)**
MNONU - F15	2218	(-579, 5016)
MIDAU- F15	**3709**	**(912, 6507)**
MIOAU - F15	**3229**	**(432, 6027)**
PADNU - F15	**3054**	**(257, 5852)**
MNDAU - F10	**2970**	**(173, 5768)**
MNDAM - F10	**3241**	**(444, 6039)**
MNONU - F10	2183	(-615, 4980)
MIDAU- F10	**3674**	**(876, 6471)**
MIOAU - F10	**3194**	**(396, 5991)**
PADNU - F10	**3019**	**(221, 5816)**
MNDAM - MNDAU	271	(-2526, 3069)
MNONU - MNDAU	-787	(-3585, 2010)
MIDAU - MNDAU	704	(-2094, 3501)
MIOAU - MNDAU	224	(-2574, 3021)
PADNU - MNDAU	49	(-2749, 2846)
MNONU - MNDAM	-1058	(-3856, 1739)
MIDAU - MNDAM	433	(-2365, 3230)
MIOAU - MNDAM	-47	(-2845, 2750)
PADNU - MNDAM	-223	(-3020, 2575)
MIDAU - MNONU	1491	(-1306, 4289)
MIOAU - MNONU	1011	(-1786, 3809)
PADNU - MNONU	836	(-1962, 3633)
MIOAU - MIDAU	-480	(-3278, 2318)
PADNU - MIDAU	-655	(-3453, 2142)
PADNU - MIOAU	-175	(-2973, 2622)

*Bold font indicates statistically significant comparisons.

Note that there does not appear to be a relationship between interlayer asphalt thickness and the inferred Totsky k-value. In addition, no relationship appears to be present between asphalt stiffness and the Totsky k-value. Based on the model and the lab data, other factors, including interlayer bond and perhaps loading/support conditions, must be considered if the inferred Totsky k-value is to be considered beyond an average across all asphalt lab beams.

5.1.1 MnROAD Falling Weight Deflectometer Analysis

To supplement the use of the laboratory beam testing in establishing the Totsky interlayer k-value, an analysis was carried out using FWD data from MnROAD UBOLs to establish the interlayer k-values for comparison and validation of the lab interlayer k relationship. MnROAD Cells 105, 205, 304, 405, 505, and 605 are UBOLs constructed with either an open graded Permeable Asphalt Stabilized Stress Relief Course (PASSRC - denoted MNONU from the laboratory testing) or a non-woven geotextile fabric. The designs of these cells are summarized in Table 17 below. The existing concrete pavement in Cell 5 was constructed in 1993 and consisted of 7.1 in of PCC placed over 3 in of Class 4 aggregate base over 27 in of Class 3 aggregate subbase over a clay subgrade (Watson and Burnham, 2010). Cell 5 had 20-ft long by 13-ft (passing lane) or 14-ft (driving lane) wide panels and bituminous shoulders. FWD data was available for each cell except 105.

Table 17: UBOL MnROAD cells

Cell	Construction Date	Slab Size* (Length x Width) (ft x ft)	Dowels (in)	Overlay Concrete Thickness (in)	Interlayer Thickness (in)	Interlayer Type	Existing Concrete Thickness (in)
105	10/8/08	15 x 14	None	4	1	Permeable Asphalt (PASSRC)	7.5 (cracked joints)
205	10/8/08	15 x 14	None	4	1	Permeable Asphalt (PASSRC)	7.5
305	10/8/08	15 x 14	None	5	1	Permeable Asphalt (PASSRC)	7.5
405	10/8/08	15 x 14	None	5	1	Permeable Asphalt (PASSRC)	7.5 (cracked joints)
505	8/24/11	6 x 7	None	5	-	Fabric (15 oz)	7.5 (cracked joints)
605	8/24/11	6 x 7	None	5	-	Fabric (15 oz)	7.5

*NOTE: Sizes shown for driving lane. For sections 15 x 14, passing lane is 15 x 13. For sections 6 x 7, passing lane is 6 x 6.5. This matches the width of the underlying Cell 5 driving and passing lanes.

Thermocouple data was available for Cells 205, 305, and 605 and were also used for Cells 105, 405, and 505 respectively since the overlay thickness and design are the same. The temperature profile through the PCC overlay, as well as an approximate temperature of the interlayer at the time of FWD testing, was then established for each cell and testing time. FWD testing performed in the wheel path and adjacent to the transverse joint was used to establish the LTE to be used in the ISLAB finite element model. The slab stiffness was obtained either directly from an elastic modulus test for the existing PCC or through a correlation with strength for the overlay. The layers beneath the existing PCC are modeled as a Winkler foundation with a k-value of 250 psi/in established from backcalculation from Cell 5 FWD data.

ISLAB's Totsky formulation was then used to model the structure for FWD testing performed at center slab to establish what interlayer Totsky k-value produces the closest deflection response. Mesh convergence was achieved by examining the deflection and overlay slab stress beneath the center slab load. Three sensors were used to define the deflection, including one directly under the load plate, and the sensors at +/- 12 in from the applied FWD load. Slabs that exhibited cracking and had a corresponding center slab drop after the cracking had initiated were excluded from this analysis in an attempt to isolate the effect of the interlayer on the resulting response. A batch of runs were then generated for Totsky interlayer k-value in increments of 100 psi/in. The FWD deflections were then matched to the Totsky k-value which produced the same deflection using linear interpolation to obtain the interlayer stiffness. The results of the Totsky k-value determination are presented in Figure 37. For the cells with the PAASRC interlayer, the range of interlayer k-values is 1180 to 8770 psi/in with an average value of 3900 psi/in. For the nonwoven geotextile fabric interlayer cells, the range of interlayer k-values is 135 to 900 psi/in with an average value of 425 psi/in.

As can be seen in Figure 37, there is no apparent trend between interlayer k-value and asphalt temperature, which is consistent with the laboratory data in that there was no apparent trend between different asphalts with varying stiffness. Statistical testing was carried out to see if a statistical difference could be identified between the k-values obtained from the laboratory specimens and those found from the FWD testing at MnROAD. Student t-tests were carried out using the null hypothesis that the mean laboratory k-values are equal to the mean k-values obtained from the FWD testing. These results are summarized in Table 18 below. Additionally, it can be seen that the FWD results for both asphalt and fabric interlayers are different from one another statistically.
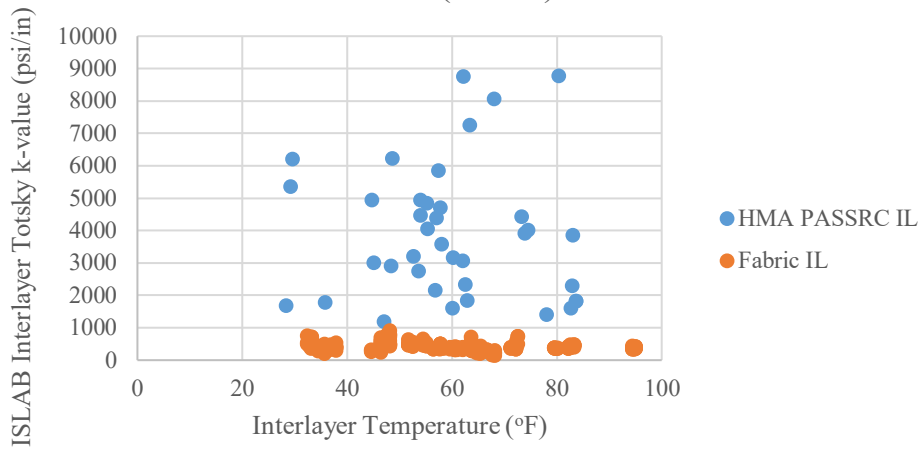
Figure 37: Interlayer Totsky k-value established from MnROAD FWD

Table 18: T-tests comparing FWD Totsky results

Comparison between means of established Totsky values	P-value of t-test for difference in means
Fabric LAB vs. MnROAD Fabric FWD	0.126
MNONU LAB vs. MnROAD Asphalt FWD	0.137
MnROAD Fabric FWD vs. MnROAD Asphalt FWD	<0.001

From the laboratory testing, the only significant comparisons were that all asphalt interlayers, except MNONU, were significantly different from the two fabric interlayers. Additionally, no apparent relationship exists between asphalt stiffness or thickness and Totsky k-values within the different asphalt interlayers tested. The k-values determined using FWD test data are not statistically different from the lab values for the same interlayer type, while the fabric and asphalt k-values established using FWD test data are statistically different from one another. Since there is not an apparent trend between different asphalt types or with temperature, one value is recommended as an average for all asphalt interlayer types and temperatures. Averaging the results from both the laboratory and FWD investigations produces an average Totsky value of approximately 3500 psi/in. This value is recommended for use in the development of a design procedure for UBOL with an asphalt interlayer. No discernable difference was detected between different weight fabrics; however, the fabric stiffness was shown to be statistically different from the asphalt stiffness. Therefore, one value is recommended as an average for all nonwoven geotextile fabrics. The average Totsky value of the laboratory and FWD results is 425 psi/in and this value should be used in the development of a design procedure for UBOL with a nonwoven geotextile fabric interlayer.

CHAPTER 6: DEVELOPMENT OF CRACKING MODEL

6.1 INTRODUCTION

Cracking is an important deterioration mechanism of UBOL (Unbonded Concrete Overlays of Existing Concrete Pavements) because it represents the principal structural deterioration mode of JPCP. In the past, various models were proposed for predicting cracking in UBOL. The AASHTO M-E cracking model is the most advanced and sophisticated model available today. Nevertheless, cracking analysis of UBOL has limitations that need to be addressed.

This document describes development of the modified cracking model for the UBOL. It includes the following:

- a summary of the current AASHTO M-E cracking model framework and its limitations
- an overview of the development of the alternative cracking model for unbonded concrete overlays, including development of the stress analysis and damage calculation procedure, modifications of the processing of temperature data, and built-in curl analysis
- an overview of cracking prediction process in the proposed cracking model
- implementation of the cracking model in the rudimentary software
- a modified reliability analysis.

6.2 AASHTO M-E TRANSVERSE CRACKING MODEL

The AASHTO M-E cracking analysis only considers transverse cracking in jointed UBOL. Two modes of transverse cracking development are considered:

- Bottom-up cracking
- Top-down cracking.

Both modes of cracking are assumed to have been caused by repeated application of excessive longitudinal stresses in the overlay, specifically, longitudinal stresses resulting from a combined effect of heavy axle loading and overlay curling.

When the truck axles are located near the longitudinal edge of the slab, midway between the transverse joints, a critical tensile bending stress occurs at the bottom of the slab, as shown in Figure 38 (Darter et al., 2001; NCHRP 2004), Positive temperature differences throughout the slab increase the tensile stress at the bottom of the slab. When the truck's steering axle is located near the transverse joint while the drive axle is within 10 to 20 feet away yet still on the same slab, a high tensile stress occurs at the top of the slab between the axles, some distance from the joint, as shown in Figure 39 (Darter et al., 2001; NCHRP 2004). Negative temperature differences throughout the slab increase the tensile stress at the top of the slab.

Repeated loadings of heavy axles cause fatigue damage along the edge of the slab, which eventually results in micro-crack propagation through the overlay thickness and transversely across the slab. These

cracks in unbonded overlays eventually deteriorate, cause roughness, and require repairs. The AASHTO M-E cracking model accumulates the amount of fatigue damage caused by every truck axle load in time increments (i.e. month by month) over the entire design period.
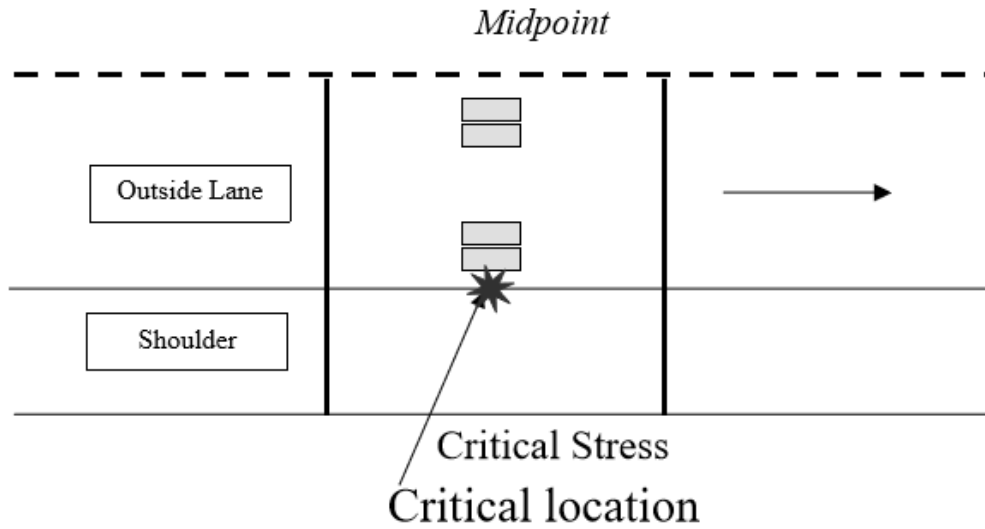
Figure 38: Critical loading and structural response location for unbonded JPCP overlay bottom-to-top transverse cracking.
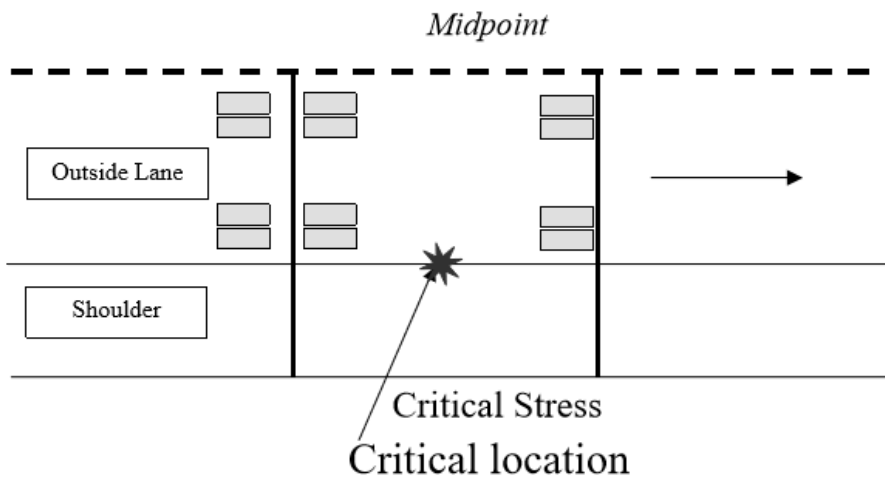
Figure 39: Critical loading and structural response location for unbonded JPCP overlay top-to-bottom transverse cracking

Under typical service conditions, the potential for either mode of cracking is present in all slabs. Although any slab may crack from the bottom up or from the top down, it cannot do both. The calculation required for the *MEPDG* unbonded overlay transverse cracking is listed below, see equation 11.

$$TRCRACK = (CRACK_{BU} + CRACK_{TD} - CRACK_{BU} CRACK_{TD})\ 100\%$$

where:

TCRACK = total cracking (percent)

$CRACK_{BU}$ =   predicted amount of bottom-up cracking (fraction)

$CRACK_{TD}$ = predicted amount of top-down cracking (fraction).

The following model is used to predict the amount of bottom up and transverse cracking:

$$CRACK_{BU\ or\ TD} = \frac{100\%}{1 + C_4 FD_{TD\ or\ BU}^{C3}}$$

where:

$CRACK_{BU\ or\ TD}$ = predicted amount of bottom-up or top-down cracking (fraction)

$FD_{TD\ or\ BU}$ = calculated fatigue damage (top-down or bottom-up)

C_3 and C_4 = calibration factors

Fatigue damage is calculated incrementally to account for the effects of changes in various factors of fatigue damage such as:

- PCC overlay modulus of rupture
- PCC overlay thickness and modulus of elasticity
- Existing pavement thickness and modulus of elasticity
- Axle weight and type
- Lateral truck wander
- Effective temperature difference
- Seasonal changes in base modulus, effective modulus of subgrade reaction, and moisture warping
- Axle type and load distribution.

The incremental damage approach is used to predict fatigue damage at the end of each month. The total bottom-up and top-down fatigue is calculated according to Miner's hypothesis in Equation 13:

$$FD = \sum \frac{n_{i,j,k,l,m,n,o}}{N_{i,j,k,l,m,n,o}}$$

(13)

where:

$n_{i,j,k,}$ = applied number of load applications at condition *i,j,k,…*

$N_{i,j,k,...,}$ = allowable number of load applications at condition $i,j,k,...$

i = age (accounts for change in PCC overlay modulus of rupture and modulus of elasticity)

j = season (accounts for change in base and effective modulus of subgrade reaction)

k = axle type (singles, tandems, and tridems)

l = load level (incremental load for each axle type)

m = temperature difference

p = traffic path

The allowable number of load applications is the number of load cycles at which fatigue failure is expected and is a function of the applied stress and PCC strength. The allowable number of load applications is determined using the following fatigue model:

$$Log\ N_{i,j,k,l,m} = C_1 \left(\frac{M_R}{\sigma_{i,j,k,l,m}} \right)^{C_2} + C_3 \tag{14}$$

where:

N = allowable number of load applications (cracking)

M_R = mean PCC modulus of rupture, psi

σ = critical stress calculated using axle combination k of load level l that passed through traffic path m under a given set of conditions (age i and temperature difference j)

C_1, C_2, and C_3 = calibration constants. The *MEPDG* default values for these constants are 1.22, 2, and 0.4371, respectively.

To predict the cracking in the unbonded overlay, maximum bending stress needs to be determined:

- at the bottom surface (JPCP bottom to top cracking)
- at the top surface (JPCP top to bottom cracking).

The unbonded overlay pavement structure is modeled in the *MEPDG* as a two-layered system consisting of slab and base with an unbonded interface. The magnitude of stresses in the concrete slab depends on axle weight, location, and the amount of temperature curling. The Enhanced Integrated Climatic Model (EICM) predicts the hourly pavement temperature profiles at eleven evenly spaced nodes throughout the slab thickness. The thermal profile is considered alongside differential shrinkage and built-in curling. For each combination of axle loading, axle location, and temperature profile, the following conceptual procedure is followed:

1. Parameters (thickness, radius of relative stiffness, and unit weight) are computed for the equivalent single layer slab that has the same flexural stiffness as the PCC slab and base system. These equivalent-slab parameters depend on the properties of the slab and base (thickness, modulus of elasticity, and unit weight).
2. The temperature distribution throughout the thickness of the PCC layer is split into three components: the constant strain-causing component, the linear (bending) strain-causing component, and the non-linear strain (self-equilibrating stress) causing component (Khazanovich, 1994).
3. Each hourly nonlinear temperature profile is converted to effective linear thermal difference for computational efficiency and more realistic stress predictions. For daytime conditions, the bottom-up cracking neural network is used to calculate the total stress corresponding to the nonlinear temperature distribution for 18,000 lb single axles, 36,000 lb tandem axles, and 54,000 lb tridem axles. This stress is compared with the total stress due to a linear temperature difference in the slab with the same support conditions (see Figure 40). The linear temperature difference that produces the same stress as the nonlinear temperature distribution is the effective linear temperature difference for that axle type. A similar procedure is followed for nighttime conditions.
4. Using rapid solutions, bending stress in the equivalent slab is calculated.
5. Using a closed-form relationship, bending stresses at the top and bottom of the slab are determined.
6. Self-equilibrating stresses at the top and bottom of the PCC slab are calculated.
7. Total stresses at the top and bottom PCC surfaces are computed by adding bending and self-equilibrating stresses.
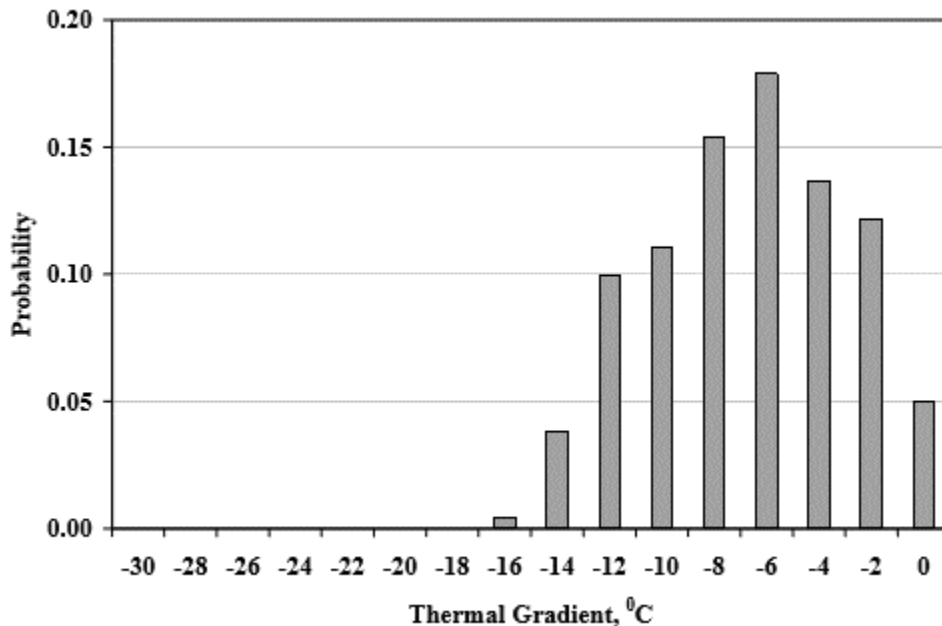

Figure 40: Example of nighttime effective thermal difference distribution plot.

The mechanistic-based cracking model for UBOL has many attractive features. Some of its most interesting characteristics are the following:

- The structural model has the capabilities to account for the key design features, such as UBOL thickness, flexural strength, elastic modulus, existing pavement thickness and stiffness, etc. as well as traffic loadings, climatic conditions, and subgrade support.
- The incremental damage approach makes the design procedure flexible and robust since material properties, traffic levels, seasonal climatic conditions, and joint load transfer can vary throughout the life of the pavement.
- It accounts for both top-down and bottom-up transverse cracking mechanisms.
- The model was calibrated using the LTPP performance data.

Nevertheless, the model has the following limitations:

- Only transverse cracking is considered.
- The effect of the interlayer properties on the UBOL behavior is ignored.
- The effect of temperature variation throughout the existing concrete slab thickness is ignored.
- The UBOL and the existing slab are assumed to have the same deflections profile. The effect of separation of the UBOL from the existing pavement is ignored.

The *MEPDG* cracking model for unbonded concrete overlay may exhibit counterintuitive trends. Figure 41 shows predicted results of cracking analysis performed using the AASHTO Pavement ME Design software. The following site conditions were considered:

- Location: Rochester, MN
- Design life: 20 years
- Traffic:
    - Two-way initial AADTT: 8,000
    - Linear yearly increase: 3.0%
    - Axle spectrum: Pavement ME default
- Existing pavement:
    - Thickness: 8 in
    - Modulus of elasticity: 4,000,000 psi
- Interlayer thickness: 1 in
- Overlay joint spacing: 15 ft
- Untied PCC shoulder
- Unbonded overlay flexural strength: 650 psi.

It can be observed from Figure 41 that Pavement ME predicts unrealistically low cracking for a 6-in thick overlay. An increase in overlay thickness from 6 in to 8 in leads to an increase in cracking from 3% to 27% and further increase in overlay thickness to 10 in leads to a decrease in predicted cracking to 0.22%. As a result, the overlays with thicknesses of 6 and 10 in meet cracking performance requirement of 15%

cracking at 90 percent reliability, while the 8-in thick overlay fails this performance requirement. This example illustrates the need for revisiting of the *MEPDG* cracking model for unbonded overlays.
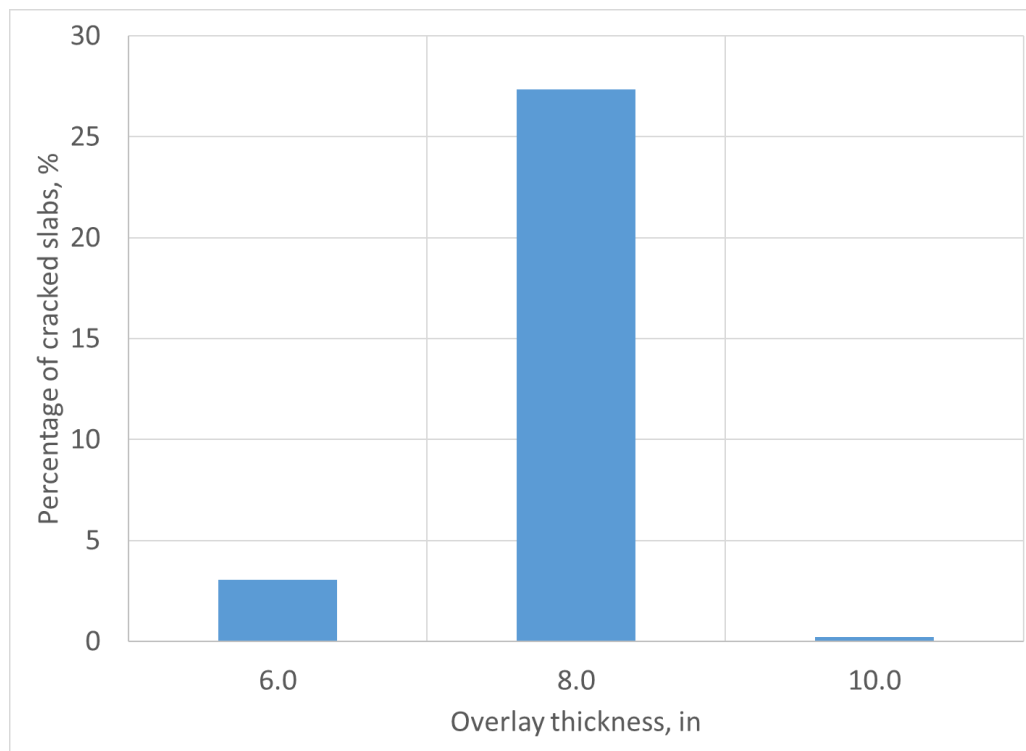
Figure 41: Predicted Pavement ME cracking for various thicknesses of unbonded concrete overlays.

6.3 DEVELOPMENT OF ALTERNATIVE CRACKING MODEL FOR UBOL

The modified UBOL fatigue damage calculation and cracking performance prediction process is based on the AASHTO M-E cracking model framework with some enhancements. The modified procedure for UBOL cracking involved major revisions of the following main areas:

1. Cracking prediction
2. Thermal linearization
3. Built-in curling characterization
4. Stress analysis and damage calculation

6.3.1 Cracking Prediction

The modified cracking analysis of jointed UBOL considers four mechanisms of cracking:

- Bottom-up cracking initiated at the bottom overlay surface, mid-slab location near overlay edge (see Figure 38) and propagating upward and transversely.
- Top-down cracking initiated at the top overlay surface, mid-slab location near overlay/shoulder joint (see Figure 39) and propagating downward and transversely.

73

- Bottom-up cracking initiated at the bottom of the overlay transverse joint (see Figure 42) and propagating upward and longitudinally.
- Top-down cracking initiated at the top of the overlay transverse joint (see Figure 42) and propagating downward and longitudinally.

Similar to the *MEPDG* cracking model, the cracking analysis of the proposed model utilizes the incremental damage approach and Miner's linear damage accumulation hypothesis. While the *MEPDG* cracking model computes damages at two locations, the proposed model does so at four locations:

- FDEB = cumulative damage at the bottom of the overlay edge, mid-slab location
- FDET = cumulative damage at the top of the overlay edge. The maximum value from several locations.
- FDJB = cumulative damage at the bottom of the overlay joint. The maximum value from several locations
- FDJT = cumulative damage at the top of the overlay joint. The maximum value from several locations
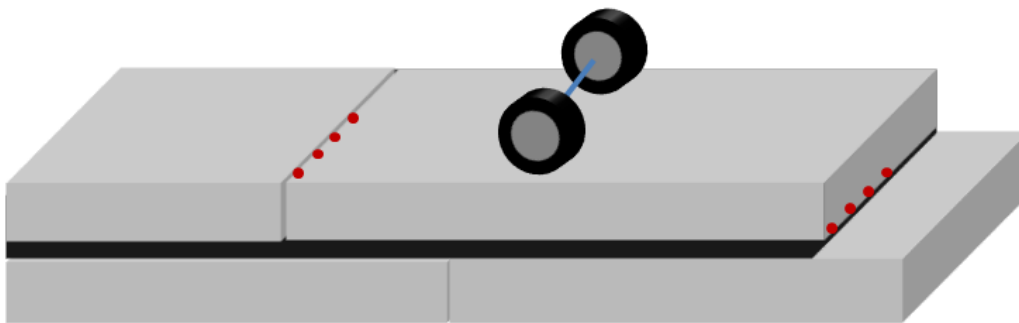
Figure 42: Proposed new locations for top and bottom stress calculation in UBOL

Each fatigue damage is computed using equations 113 and 114 where the stresses are computed at the corresponding critical locations. The details of the stress calculation process are provided below.

6.3.2 Stress Analysis and Damage Calculation

One of the main drawbacks of the *MEPDG* is its inability to adequately model interaction between the PCC slab and the underlying layer. The *MEPDG* analysis assumes that the unbonded overlay and the existing pavement have the same deflection profiles. The structural contribution of the interlayer is ignored. In reality, an interlayer may provide some "cushioning" to the overlay.

The following factors affect the magnitude of bending stresses in unbonded overlay slabs:

- Overlay slab thickness
- PCC modulus of elasticity
- PCC Poisson's ratio
- PCC unit weight

- PCC coefficient of thermal expansion
- Existing pavement thickness
- Existing pavement modulus of elasticity
- Interlayer stiffness
- Joint spacing
- Subgrade stiffness
- Lane-shoulder joint LTE
- Temperature distribution throughout the slab thickness
- Magnitude of effective permanent curl/warp
- Load configuration
- Axle weight
- Wheel tire pressure and wheel aspect ratio (length-to-width ratio)
- Axle position (distance from the critical slab edge)
- Transverse joint LTE
- Dowel bar stiffness and restraint.

Although ISLAB2005 is capable of analyzing all these factors, a direct inclusion of this proprietary finite element analysis program into the design software is not practical. To address this issue, rapid solutions were developed for determining critical stresses required for computing each type of fatigue damage.

To reduce the number of cases required for development of the rapid solutions, the principle of similarity was adapted in this study. The similar structure concept permits the computation of stresses in a multi-layer system (a concrete slab with a base on a subgrade) from those in a similar system. This concept has been used in the *MEPDG* for both the JPCP and continuously reinforced concrete pavement (CRCP) cracking models (Khazanovich et al., 2001). The two systems can be considered equivalent as long as their deflection basins are scalable, meaning that:

(15)

$$w_I(x_1, y_1) = \lambda_{def} w_{II}(a\, x_2, b y_2),$$

where:

w = deflections

a and b = coordinate scaling factors

x and y = horizontal coordinates s

λ_{def}, = scaling factor for deflections (dependent only on properties of the pavement structure)

Note: the subscripts *I* and *II* denote pavement systems *I* and *II*, respectively.

If system *2* is subjected to axle loading and a linear temperature strain causing temperature distribution throughout the slabs thickness, then if equation (15) is satisfied, the stresses in system *2* can be found from those in system *1* using the following relationship:

$$\sigma_{I,total}(x_1, y_1, z_1) = \lambda_{stress}\sigma_{II,linear}(a\,x_2, b\,y_2, z_2) + \sigma_{1,non-linear}(z_1) \tag{16}$$

where:

σ_{total} = the total stress at the surface of the slab

σ_{linear} = bending stress due to traffic and thermal loading at the surface of the slab independent of coordinates

$\lambda_{stress,}$ = the scaling factor for stress (only dependent on properties of the pavement structures)

$\sigma_{non-linear}$ = non-linear component of stress due to thermal loading solely at the surface of the slab, independent of in-plane coordinates (Ioannides and Khazanovich 1998).

Two pavement structures described by the Totski model were found to be similar if the following conditions are satisfied:

- The in-plane positions of the axles and the tire footprints are the same.
- The ratios of flexural stiffness of the pavement layers are equal i.e.

$$\frac{D_{OL,I}}{D_{EX,I}} = \frac{D_{OL,II}}{D_{EX,II}} \tag{17}$$

where:

$D_{OL,I}$ and $D_{OL,II}$ = overlay flexural stiffness for system *I* and *II*, respectively.

$D_{EX,I}$ and $D_{EX,II}$ = existing pavement flexural stiffness for system *I* and *II*, respectively.

A flexural stiffness of a layer is defined in Equation 18, as follows:

$$D = \frac{E\,h^3}{12\,(1-\nu^2)} \tag{18}$$

where:

E = the modulus of elasticity

h = thickness of the layer

ν = Poisson's ratio of the layer

- The ratios of the Totski-to-subgrade spring stiffnesses are equal, i.e.

$$\frac{k_{Tot,I}}{k_{subgr,I}} = \frac{k_{Tot,II}}{k_{subgr,II}}$$

where:

$k_{Tot,I}$ and $k_{Tot,II}$ = Totski interlayer spring stiffness for system *I* and *II*, respectively.

$k_{subgr,I}$ and $k_{subgr,II}$ = subgrade spring stiffness for system *I* and *II*, respectively.

- The radii of relative stiffness of the overlays are equal, i.e

$$\ell_{OL,I} = \ell_{OL,II}$$

(20)

where:

$$\ell_{OL,I} = \sqrt[4]{\frac{D_{OL,I}}{k_{Tot,I}}}$$

(21)

And

$$\ell_{OL,II} = \sqrt[4]{\frac{D_{OL,II}}{k_{Tot,II}}}$$

(22)

are radii of relative stiffness for the systems *I* and *II*, respectively.

- Load transfer efficiencies of the transverse joints are equal:

$$LTE_{tr,I} = LTE_{tr,II}$$

(23)

where:

$LTE_{tr,I}$ and $LTE_{tr,II}$ = load transfer efficiencies of the transverse joints in System I and *II*, respectively.

- Load transfer efficiencies of the longitudinal joints are equal.

$$LTE_{long,I} = LTE_{long,II} \tag{24}$$

where:

$LTE_{long,I}$ and $LTE_{long,II}$ = load transfer efficiencies of the transverse joints in System I and *II*, respectively.

- The ratios of the axle weight to the overlay self-weight are equal

$$\frac{P_I}{h_{OL,I}\,\gamma_{OL,I}} = \frac{P_{II}}{h_{OL,II}\,\gamma_{OL,II}} \tag{25}$$

- Korenev's non-dimensional temperature gradients are equal:

$$\varphi_{OL,I} = \varphi_{OL,II} \tag{26}$$

where:

$$\varphi_{OL,I} = \frac{2\alpha_{OL,I}(1+\nu_{OL,I})\,\ell_{OL,I}^2\,k_{Tot,I}}{h_{OL,I}^2\gamma_{OL,I}}\left(T_{OL,I}^{top} - T_{OL,I}^{bot}\right) \tag{27}$$

$$\varphi_{OL,II} = \frac{2\alpha_{OL,II}(1+\nu_{OL,II})\,\ell_{OL,II}^2\,k_{Tot,I}}{h_{OL,II}^2\gamma_{OL,II}}\left(T_{OL,II}^{top} - T_{OL,II}^{bot}\right) \tag{28}$$

where:

$\varphi_{OL,I}$ and $\varphi_{OL,II}$ = Korenev's temperature gradients (Korenev and Chernigovskaya 1962) in the overlay of systems *I* and *II*, respectively

$T_{OL,I}^{top}$ and $T_{OL,II}^{top}$ = temperature of the top overlay surfaces for systems *I* and *II*, respectively

$T_{OL,I}^{bot}$ and $T_{OL,II}^{bot}$ = temperature of the bottom overlay surfaces for systems *I* and *II*, respectively

$\gamma_{OL,I}$ and $\gamma_{OL,II}$ = unit weights of the overlays for systems *I* and *II*, respectively.

Two types of unbonded overlay structures were considered in this study:

- Conventional width overlays, i.e. overlay slab width is equal to lane width (usually 12 ft)

- Short slabs, i.e. overlays with an additional longitudinal joint in the middle of the lane. In this study, the slab size of 6 ft by 6 ft is assumed.

For both types of unbonded overlay structures, the critical stresses should be determined at the top and bottom overlay surfaces at the shoulder/lane and transverse joints. The similarity concept introduced above was adopted for development of the critical stress calculation procedures. The details of these procedures are provided below.

6.3.2.1 Determination of Critical Stresses for Conventional Width Overlays at the Bottom of the Overlay Edge

Critical stresses at the bottom of the overlay/shoulder edge occur in the middle of the overlay when the truck axles are located near the longitudinal edge of the overlay midway between the transverse joints, as shown in Figure 38. These stresses greatly increase when there is a high positive temperature gradient through the slab (the top of the slab is warmer than the bottom of the slab).

To develop a rapid solution for stress calculation, the following ISLAB2005 finite element model of a six-slab system was adopted. The slab widths were set to 8 ft and 12 ft for the unloaded and loaded slabs, respectively. The narrower slabs modeled the effect of shoulder, while the wider slabs modeled the driving lane. The slab length, i.e. transverse joint spacing, was set to 15 ft or 12 ft.

Two types of loading were considered:

- Single axle loading (see Figure 43)
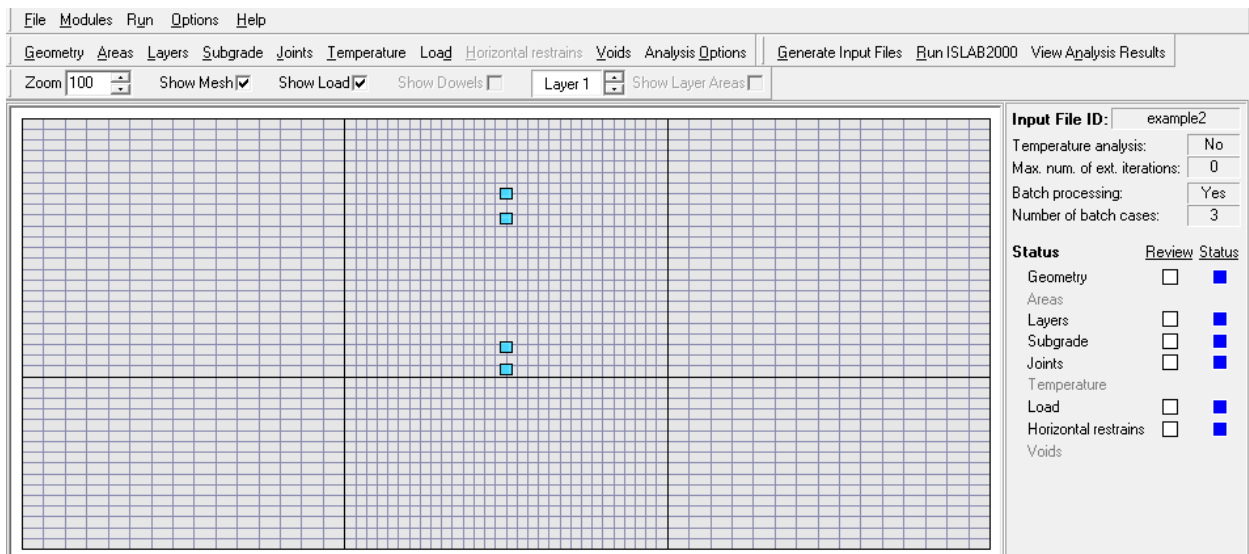- Tandem axle loading (see Figure 44)

Figure 43: ISLAB2000 model for determination of critical stresses at the bottom of the for conventional width overlays edge due to single axle loading
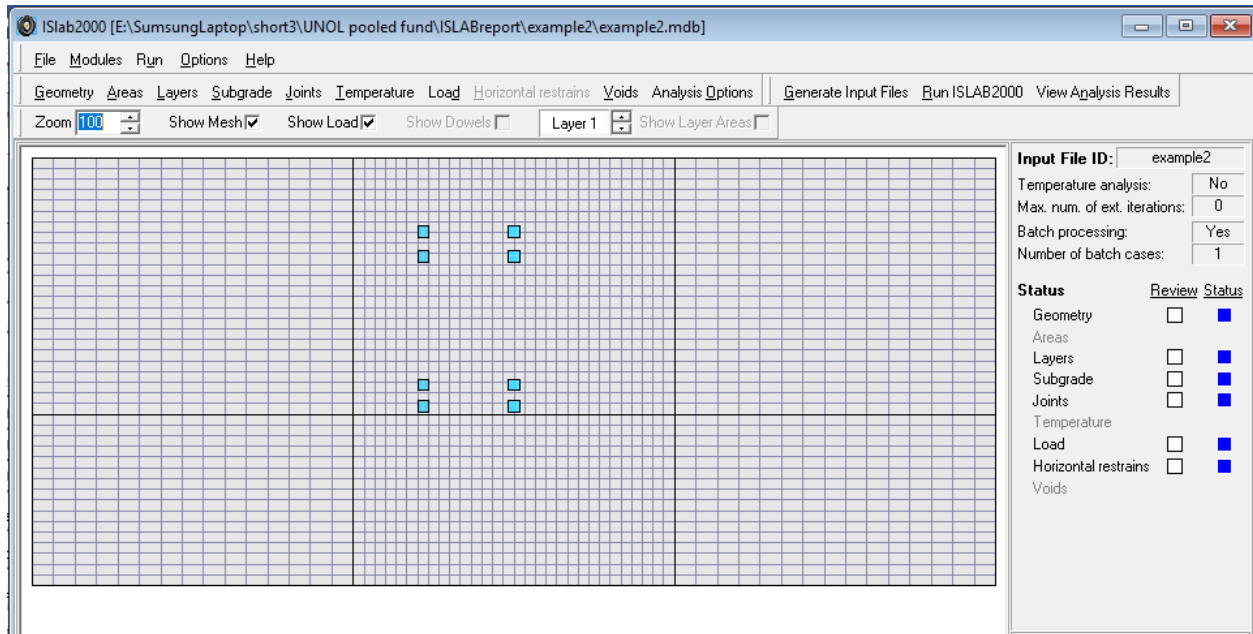
79

Figure 44: ISLAB2000 model for determination of critical stresses at the bottom of the for conventional width overlays edge due to tandem axle loading

A factorial of 76,800 ISLAB2005 runs was performed. The overlay Poisson's ratio, unit weight, and coefficient of thermal expansion for both layers were set to 0.15, 0.087 lb/in^3, and 6.0*10^{-6} 1/°F, respectively. The existing pavement thickness was set to 6 in. The steering axle weight was set to 12,000 lb. The tire pressure was set to 100 psi. The transverse joints in the existing pavements were considered rigid. The following parameters were varied:

- The overlay thickness: 6, 8, and 10 in
- The overlay modulus of elasticity: 2.0x10^6, 4.0x10^6, 6.0x10^6, and 8.0x10^6 psi
- The existing pavement modulus of elasticity: 5.0x10^5, 2.0x10^6, 1.0x10^7, and 4.0x10^7 psi
- The Totski interlayer stiffness: 400, 425, 3500, and 4000 psi/in
- The coefficient of subgrade reaction: 250 psi
- Transverse joint spacing: 12 and 15 ft
- Slab/shoulder deflection LTE: 20 and 50 percent
- Overlay transverse joint LTE: 70 percent
- Wheel offset from the longitudinal joint: 0.555 and 12 in
- Single axle load: 0, 10000, 20000, 30000, and 40000 lb.
- Tandem axle load: 0, 20000, 40000, 60000, and 80000 lb.
- Temperature difference between overlay top and bottom surface temperatures: 0, 10, 20, 30, and 40 °F.

The maximum bending stress at the bottom of the overlay slab was determined for each ISLAB2005 run and the rapid solutions were developed using modified MS-HARP neural network architecture (Banan and Hjelmstad 1994; Khazanovich and Roesler 1997). The developed rapid solutions were constrained to

80

ensure an increase in predicted stresses with an increase in transverse joint spacing or decrease in stiffness of the existing pavement.

The following procedure was used to calculate the top surface edge stresses:

Step 1. Select a similar system with the overlay thickness equal to the top layer thickness and the bottom layer thickness equal to 6 in.

Step 2. Calculate the moduli of elasticity of the overlay and existing pavement, as well as the Tostki interlayer stiffness, $E_{OL,S}$, $E_{EX,S}$, and $k_{Tot,S}$, respectively, for the similar system using the following equations:

$$k_{Tot,S} = \frac{250}{k_{subgr}} k_{Tot} \qquad (29)$$

$$E_{OL,S} = \frac{k_{Tot,S}}{k_{Tot}} \frac{1 - 0.15^2}{1 - v_{OL}^2} E_{OL} \qquad (30)$$

$$E_{EX,S} = \frac{E_{EX} h_{EX}^3}{1 - v_{EX}^2} \frac{1 - 0.15^2}{(6\,in)^3} \qquad (31)$$

Step 3. Compute the magnitude of the tandem axle load, P_{TS}, for the similar system satisfying the similarity condition Eqn. 15 using the following equation:

$$P_{TS} = \frac{P}{h_{OL}\gamma_{OL}} \times 6 \times 0.087 \qquad (32)$$

Step 4. Compute the temperature difference between the top and bottom surfaces, ΔT_S, for the similar system satisfying the similarity condition Eqn. **16**:

$$\Delta T_S = \frac{\alpha_{OL}(1+v_{OL})\,k_{Tot,OL}}{\gamma_{OL}} \frac{0.087}{6\times10^{-6} \times (1+0.15) \times k_{Tot,S}}, \qquad (33)$$

Step 5. Using the rapid solution, determine the critical stress in the similar system, $\sigma_{S,R}(P_{TS}, \Delta T_S)$

Step 6. Determine the total stress in the overlay, σ_{OL}, using the following equation:

$$\sigma_{Edge,T} = \frac{6}{h_{OL}} \frac{\gamma_{OL}}{0.087} \sigma_{S,R}(P_{TS}, \Delta T_S) \qquad (34)$$

To illustrate this approach, consider a concrete overlay with thickness, modulus of elasticity, Poisson's ratio, and the coefficient of thermal expansion equal to 8 in, 3,900,000 psi, 0.18, and 5.5 10^{-6} 1/°F, respectively. The joint spacing is 15 ft, the Totski interlayer stiffness is 3,500 psi/in, the existing pavement thickness, modulus of elasticity, and Poisson's ratio are equal to 10 in, 4,000,000 psi, and 0.15, respectively. The coefficient of the subgrade reaction is 250 psi/in. The pavement has an asphalt shoulder with a joint load transfer efficiency equal to 20%. A 20,000-lb single axle load is placed at the mid-slab 0.555 in away from the lane-shoulder joint, as shown in Figure 43, and the temperature difference between the top and the bottom surfaces equal to 20 °F. Compute stresses due to a combined effect of the axle loading and slab curling.

Step 1. Select a similar system with the overlay thickness equal to 8 in, the bottom layer thickness equal to 6 in, and the coefficient of subgrade reaction equal to 250 psi/in.

Step 2. Calculate the moduli of elasticity of the overlay and existing pavement, as well as the Tostki interlayer stiffness, $E_{OL,S}$, $E_{EX,S}$, and $k_{Tot,S}$, respectively, for the similar system using the following equations:

$$k_{Tot,S} = \frac{250}{250} 3500 = 3500 \; psi/in \qquad (35)$$

$$E_{OL,S} = \frac{3500}{3500} \frac{1 - 0.15^2}{1 - 0.18^2} 3,900,000 = 3,860,510 \; psi \qquad (36)$$

$$E_{EX,S} = \frac{4,000,000 \times 10^3}{1 - 0.15^2} \frac{1 - 0.15^2}{(6 \; in)^3} = 1.87 \times 10^3 \; psi \qquad (37)$$

Step 3. Compute the magnitude of the axle load, P_S, for the similar system satisfying the similarity condition 15 using the following equation:

$$P_{TS} = \frac{P}{h_{OL} \gamma_{OL}} \times 6 \times 0.087 = \frac{20,000}{8 \times 0.087} \times 8 \times 0.087 = 20,000 \; lb, \qquad (38)$$

Step 4. Compute the temperature difference between the top and bottom surfaces, ΔT_S, for the similar system satisfying the similarity condition **16**:

$$\Delta T_S = \frac{\alpha_{OL}(1+\nu_{OL})\, k_{Tot,OL}}{\gamma_{OL}} \frac{0.087}{6\times10^{-6}\times(1+0.15)\times k_{Tot,S}}\Delta T = \qquad (39)$$

$$\frac{5.5\times10^{-6}(1+0.18)\,3500}{0.087} \frac{0.087}{6\times10^{-6}\times(1+0.15)\times k_{Tot,S}}20 = 18.81\ °F$$

Step 5. Using the rapid solution, determine the critical stress in the similar system, $\sigma_{S,R}(P_{TS}, \Delta T_S) = 460.111\ psi$

Step 6. Since the thickness and unit weight of the similar system are equal to the thickness and unit weight of the unbonded overlay, the critical stress in the overlay is equal to 460.111 psi.

Using the model shown in Figure 43, ISLAB2005 analysis resulted in the maximum longitudinal stress at the bottom of the overlay slab of 453.98 psi (see Figure 45). Therefore, the relative difference between the approximate solution obtained using the rapid solutions and ISLAB2005 stress is (460.11-453.98)/453.98 = 1.3 %. One can conclude that the agreement between the stresses calculated using the rapid solutions and the ISLAB2005 stresses is very good.
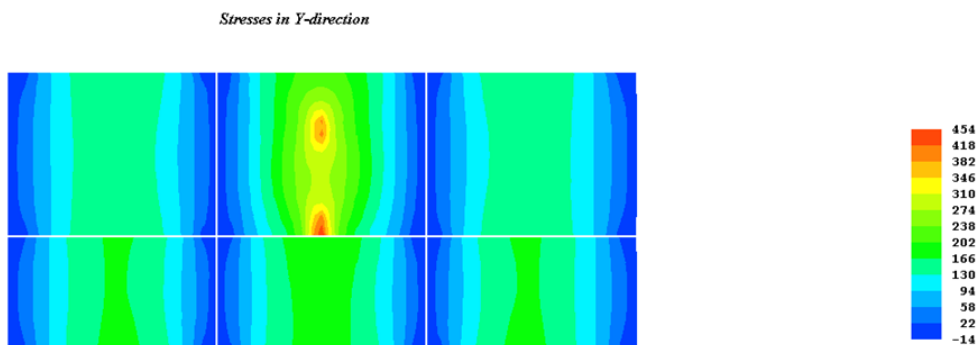

Figure 45: Longitudinal stresses due to 20,000 single axle loading and daytime curling

To further validate the developed rapid solutions for single axle loading, an additional factorial of 288 ISLAB2005 runs was performed using the finite element model shown in Figure 43. The modulus of elasticity for the overlay was set to $4.0\text{x}10^6$ psi. Poisson's ratio, unit weight, and coefficient of thermal expansion for both layers were set to 0.15, 0.087 lb/in³, and $5.5*10^{-6}$ 1/°F, respectively. The existing pavement thickness was equal to 8 in. The following parameters varied:

- Overlay thicknesses: 8 in.
- The overlay modulus of elasticity: $3.0\text{x}10^6$, $5.0\text{x}10^6$, and $7.0\text{x}10^6$ psi
- The existing pavement modulus of elasticity: $3.0\text{x}10^6$ psi
- The existing pavement thickness: 7, 8, an 9 in
- Totski interlayer stiffness: 425 psi/in
- Lane/shoulder load transfer efficiency: 20 and 50%.
- Coefficient of subgrade reaction: 250 psi/in
- Single axle load: 15, 25, and 35 kip

- Temperature difference between the top and bottom overlay surfaces: 5, 15, 25, and 35 °F.

Figure 46 shows a comparison of the stresses predicted using the rapid solutions and obtained from ISLAB2005. A very good agreement between these stresses is observed, but the rapid solutions predict the stresses at a fraction of time required to compute stresses using ISLAB2005.
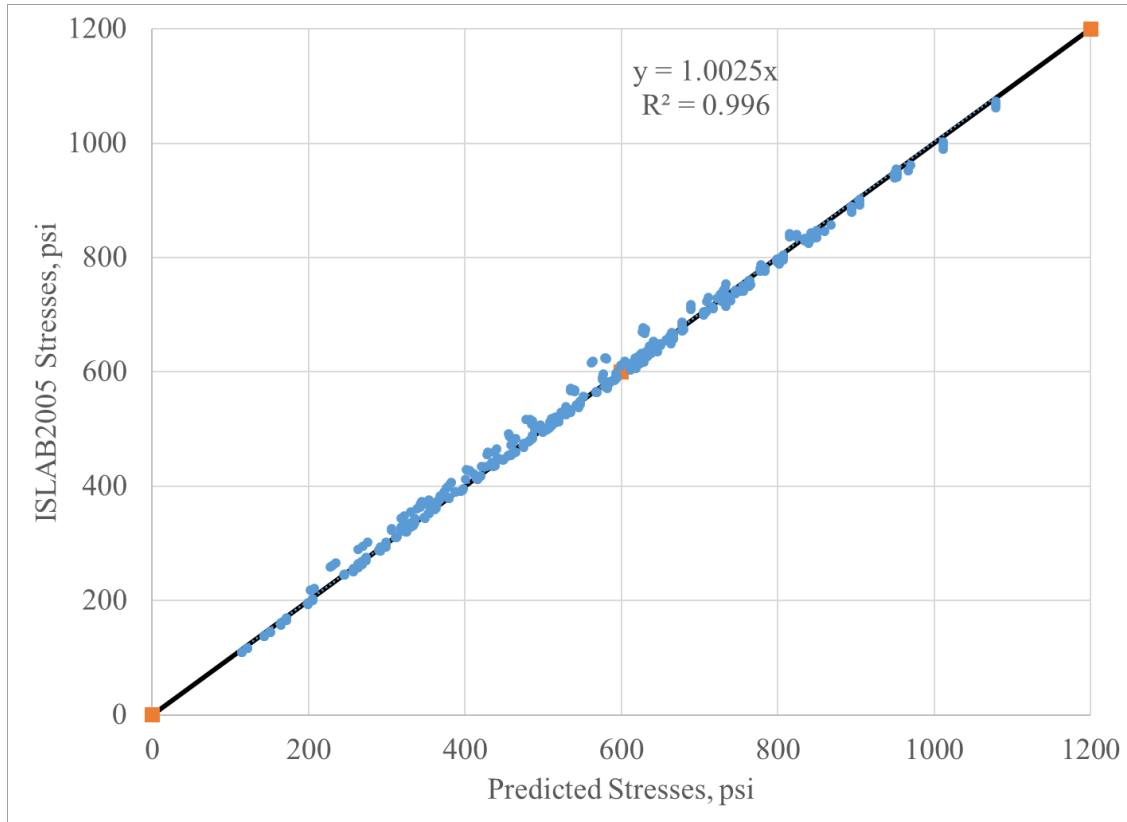

Figure 46: Critical bending stresses at the bottom of unbonded overlay predicted by ISLAB2005 and rapid solutions for single axle loads

Another factorial of 288 ISLAB2005 runs was performed for a tandem axle loading using the structural model shown in Figure 44. The same model parameters as in the verification factorial for the single axle loading were used, but the tandem axle loads were equal to 10, 30, 40 and 80 kip. Figure 47 shows a comparison of the stresses predicted using the rapid solutions and obtained from ISLAB2005. Similar to the single axle loading, a very good agreement between these stresses is observed.
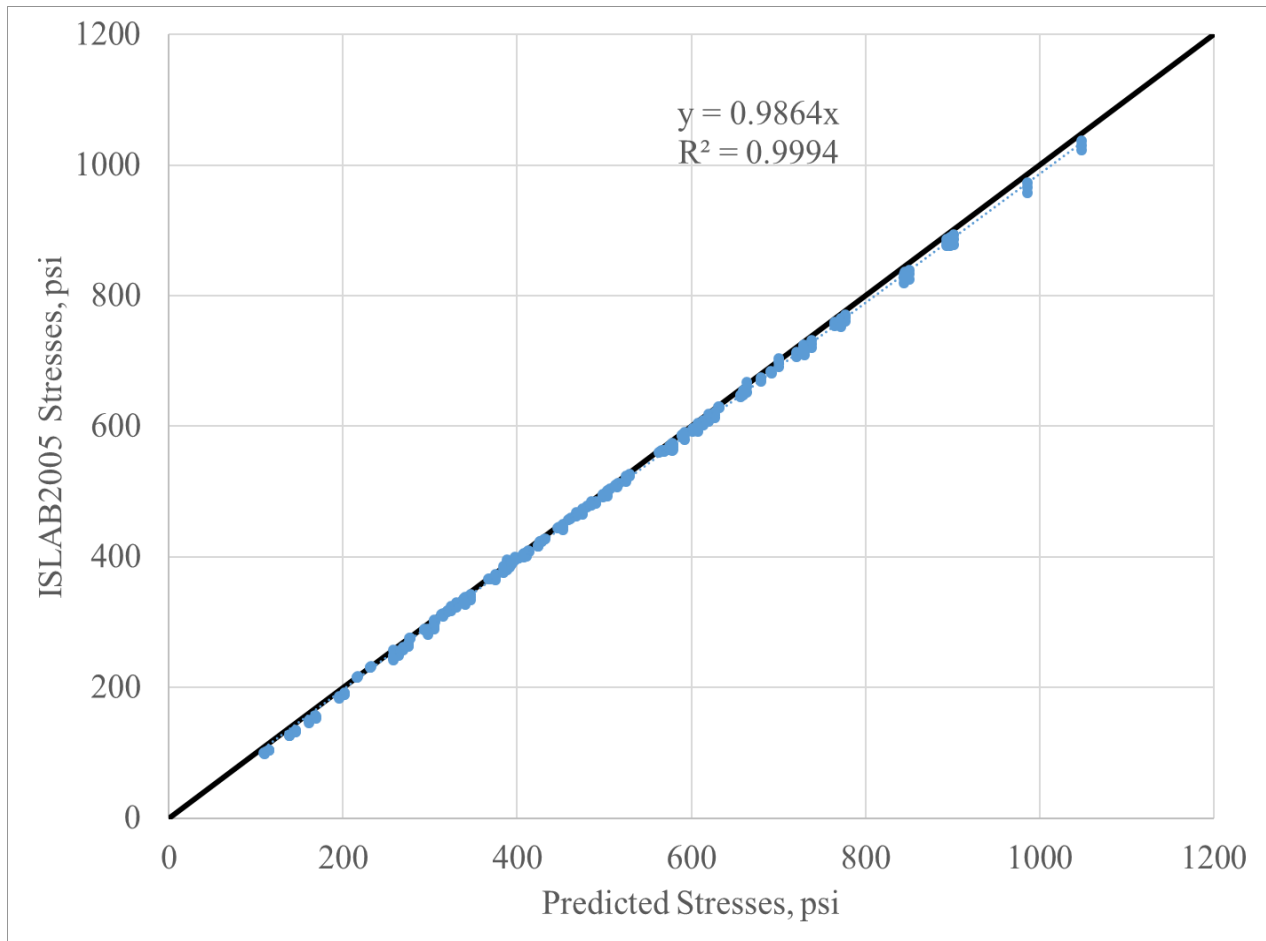
Figure 47: Critical bending stresses at the bottom of unbonded overlay predicted by ISLAB2005 and rapid solutions for tandem axle loads

6.3.2.2 Determination of Critical Stresses at the Top of the Overlay Edge for the Conventional Width Overlays

Critical stresses at the top of the overlay/shoulder edge occur near the middle of the overlay when the drive axle is near the transverse joint, as shown in Figure 38. These stresses increase greatly when there is a high negative temperature gradient throughout the slab (the top of the slab is colder than its bottom).

To develop a rapid solution for stress calculation, the following ISLAB2005 finite element model of a six-slab system loaded by a tandem drive axle and a single steel axle was developed (see Figure 48). The slab widths were set to 8 ft and 12 ft for the unloaded and loaded slabs, respectively. The narrower slabs modeled the effect of shoulder, while the wider slabs modeled the driving lane. The slab length, i.e. transverse joint spacing, was set to 15 ft.

A combined effect of nighttime temperature curling and truck loading was analyzed. The truck loading consisted of a tandem axle load applied at the transverse joint at the middle slab of the driving lane and

a steering axle load applied at the leave side of the other joint of this slab. The Totski model (see Figure 34) was used to model the pavement cross-section. A negative linear temperature distribution throughout the overlay thickness and the constant temperature distribution throughout the existing slab thickness were assumed.
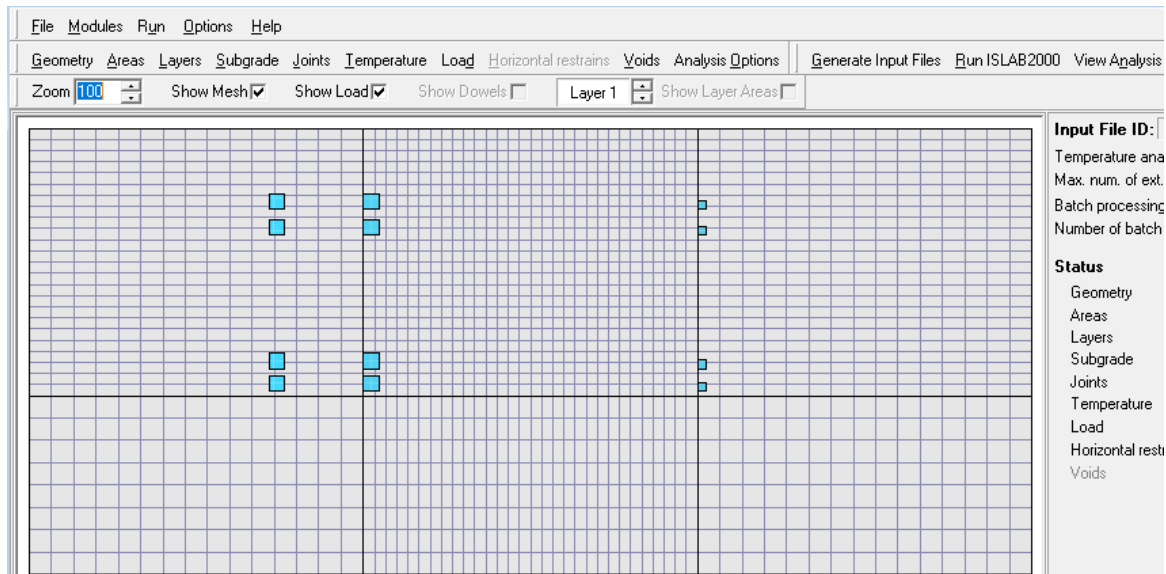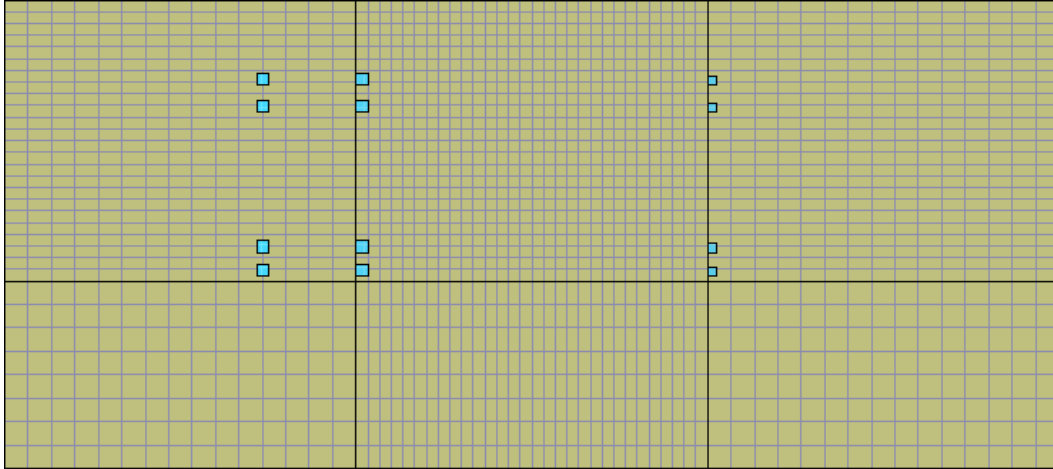

Figure 48: ISLAB2005 model for computing top surface edge stresses

The Totski interlayer model for the nighttime condition was assumed to be working in compression only, i.e. the overlay was allowed to separate from the interlayer. In addition, two cases of the interlayer conditions were considered:

- No deterioration of the interlayer. The Totski interlayer stiffness is the same for the entire layer.
- A void under the transverse joint extends throughout the entire lane width in transverse direction, 6 inches on the approach side of the joint and 24 inches on the leave side of the joint in the longitudinal direction. The Totski interlayer stiffness is set to 1 psi/in for this part of the model.

Figure 49 shows the top view of the interlayer surface for the models with and without interlayer deterioration.

ISLAB2005 model without voids under the overlay
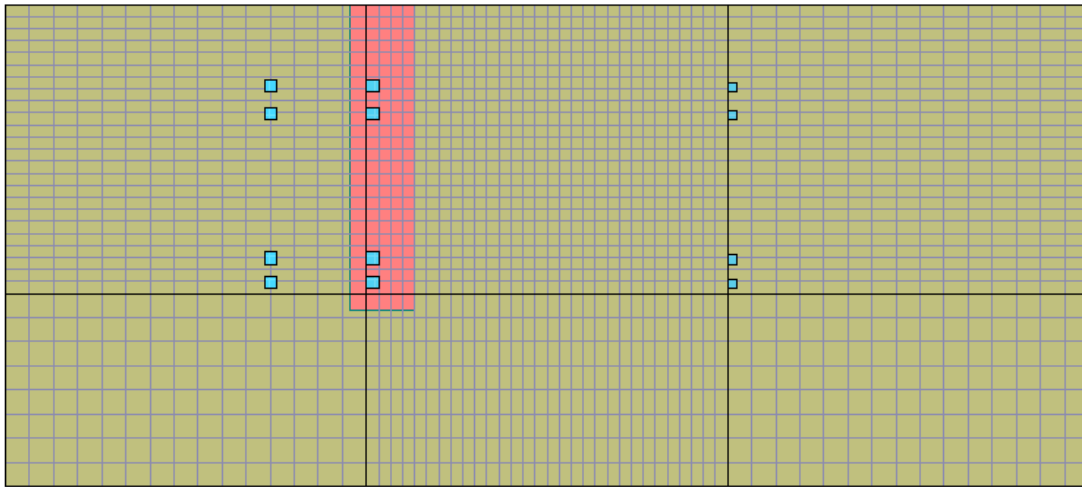
ISLAB2005 model with a void under the overlay

Figure 49: ISLAB2005 model for computing top surface edge stresses with and without voids under the overlay

A factorial of 18,432 ISLAB2005 runs was performed for both the interlayer with and without voids each. The overlay Poisson's ratio, unit weight, and coefficient of thermal expansion for both layers were set to 0.15, 0.087 lb/in^3, and 6.0*10^{-6} 1/°F, respectively. The existing pavement thickness was set to 6 in. The steering axle weight was set to 12,000 lb. The tire pressure was set to 100 psi. The transverse joints in the existing pavements were considered rigid. The following parameters were varied:

- The overlay thickness: 6, 8, and 10 in
- The overlay modulus of elasticity: 2.0x10^6, 4.0x10^6, 6.0x10^6, and 8.0x10^6 psi
- The existing pavement modulus of elasticity: 5.0x10^5, 2.0x10^6, 1.0x10^7, and 4.0x10^7 psi
- The Totski interlayer stiffness: 400, 425, 3500, and 4000 psi/in
- The coefficient of subgrade reaction: 250 psi
- Slab/shoulder deflection LTE: 20 and 50 percent

- Overlay transverse joint LTE: 20, 70, and 95 percent
- Wheel offset from the longitudinal joint: 1.666 in, and 12 in
- Tandem axle load: 10000, 20000, 30000, and 40000 lb.
- Temperature difference between overlay top and bottom surface temperatures: -40, -30, -20, -10, 0, 15, 30, and 40 $^{\circ}$F.

The bending stresses at the top surface of the truck lane/shoulder longitudinal edge of the overlay slab were determined for each ISLAB2005 run between 42 in from the tandem axle loaded transverse edge and the mid-slab and with an interval of 6 in. The rapid solutions were developed using modified MS-HARP neural network architecture (Banan and Hjelmstad 1994; Khazanovich and Roesler 1997). The developed rapid solutions were constrained to ensure an increase in predicted stresses with an increase in transverse joint spacing or decrease in stiffness of the existing pavement.

A similar approach that was used for calculation of the critical bottom surface overlay edge stresses is used for prediction of the critical top surface edge stresses. The only difference is in the rapid solution that was used for the prediction of the critical stresses in the similar system.

To illustrate this approach, consider a concrete overlay with thickness, modulus of elasticity, Poisson's ratio and the coefficient of thermal expansion equal to 8 in, 3,900,000 psi, 0.18, and 5.5× 10^{-6} 1/$^{\circ}$F, respectively. The joint spacing is 15 ft, the Totski interlayer thickness is 3,500 psi/in, the existing pavement thickness, modulus of elasticity, and Poisson's ratio are equal to 10 in, 4,000,000 psi, and 0.15, respectively. The coefficient of the subgrade reaction is 250 psi/in. The pavement has a tied shoulder with a joint load transfer efficiency equal to 50%. The load transfer efficiency of the overlay transverse joints is 20%. A 34,000-lb tandem axle load is placed at the longitudinal joint 1.6 in away from the lane-shoulder joint, as shown in Figure 49. The temperature difference between the top and bottom surfaces is -24°F. Figure 50 shows ISLAB2005-computed longitudinal stresses at the bottom of the overlay surface. The maximum tensile stress predicted by ISLAB2005 is 301 psi.
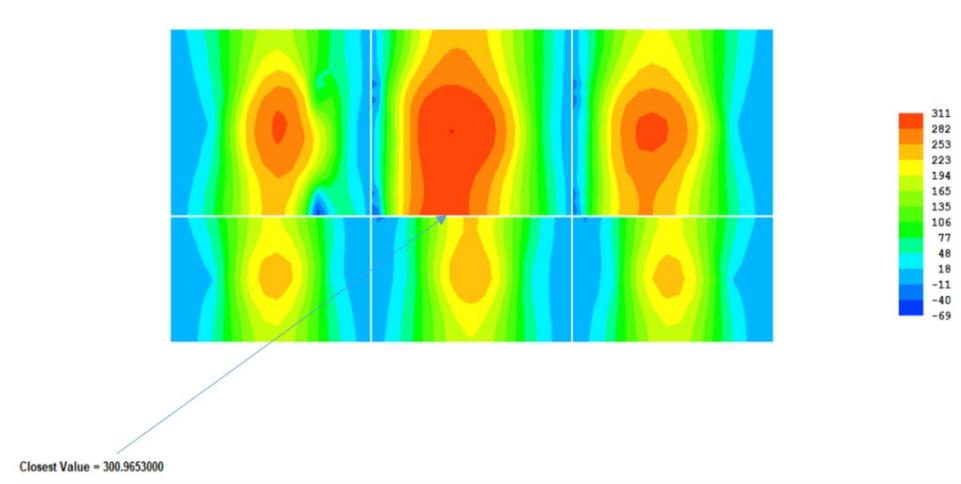

Closest Value = 300.9653000

Figure 50: Longitudinal stress distribution at the top surface of the unbonded concrete overlay

Below we will show the step-by-step calculation of the edge bending stress using the similarity concept approach.

Step 1. Select a similar system with an 8-in thick overlay, 6-in thick existing pavement and the coefficient of subgrade reaction equal to 250 psi/in.

Step 2. Calculate the moduli of elasticity of the overlay and existing pavement, as well as the Tostki interlayer stiffness:

$$k_{Tot,S} = \frac{250 \; psi/in}{250 \; psi/in} \; 3500 psi/in = 3500 \; psi/in \tag{40}$$

$$E_{OL,S} = \frac{3500 psi/in}{3500 \; psi/in} \frac{1 - 0.15^2}{1 - 0.15^2} 3.9 \times 10^6 psi = 3.9 \times 10^6 psi \tag{41}$$

$$E_{EX,S} = \frac{4 \times 10^6 psi \times (10 \; in)^3}{1 - 0.15^2} \frac{1 - 0.15^2}{(6 \; in)^3} = 1.85 \times 10^7 psi \tag{42}$$

Step 3. Compute the magnitude of the tandem axle load, P_{TS}, for the similar system satisfying the similarity condition 15 using the following equation:

$$P_{TS} = \frac{P}{0.087} \times 0.087 = 34,000 \; LB \tag{43}$$

Step 4. Compute the temperature difference between the top and bottom surfaces, ΔT_S, for the similar system satisfying the similarity condition 16:

$$\Delta T_S = \frac{6 \times 10^{-6} (1 + 0.18) \; 3500}{0.087} \frac{0.087}{6 \times 10^{-6} \times (1 + 0.15) \times k_{Tot,S}} = 22.57 \; °F \tag{44}$$

Step 5. Using the rapid solution, determine the stresses in the similar system, $\sigma_{S,Rl}(P_{TS}, \Delta T_S) = 296.94 \; psi$

Step 6. Determine the maximum stress at the overlay top surface for the shoulder/lane joint,
$\sigma_{S,R}(P_{TS}, \Delta T_S) = 296.94$ psi

Comparison with Figure 50 shows a good correspondence between stresses computed with ISLAB2005 and from this procedure.

Similar steps are required to compute the stresses if the void near joint is present. Steps 1 through 6 would result in the maximum stress in the similar system equal to $\sigma_{S,R}(P_{TS}, \Delta T_S)$ = 341.1 psi. Figure 51 shows the longitudinal stress distribution computed with ISLAB2005. The maximum stress at the slab edge is 332 psi.
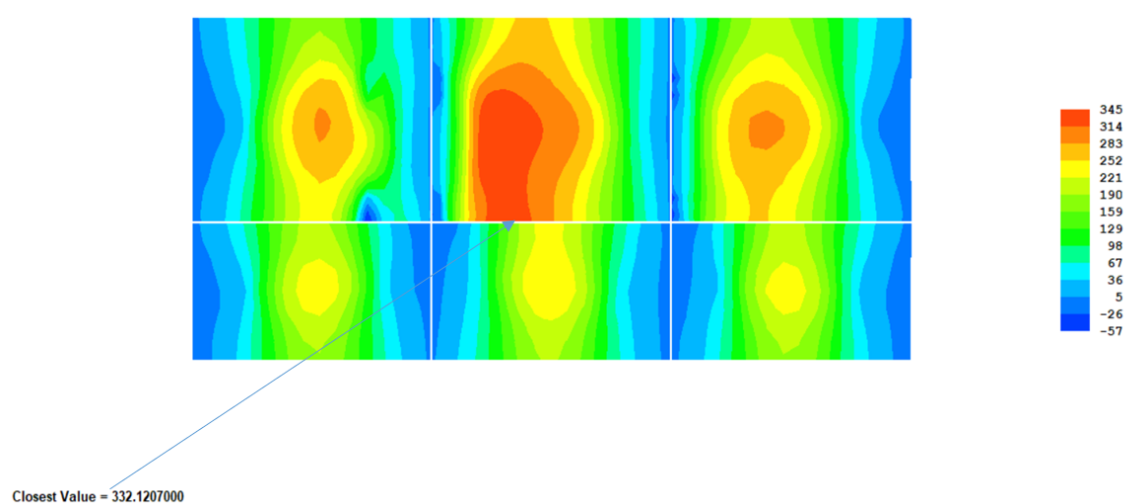

Closest Value = 332.1207000

Figure 51: Longitudinal stress distribution at the top surface of the unbonded concrete overlay with a void under the overlay

To further verify this procedure, a factorial of 2,916 ISLAB2005 finite element runs was performed. The structural model shown in Figure 48 was used with the following parameters:

- The overlay thickness: 6, 8, and 10 in
- The existing pavement thickness: 8 in
- The overlay modulus of elasticity: 3.0×10^6, 5.0×10^6, and 7.0×10^6 psi
- The existing pavement modulus of elasticity: 1.0×10^6, 6.0×10^6, 2.0×10^7 psi
- The Totski interlayer stiffness: 425 and 3,500 psi/in
- The coefficient of subgrade reaction: 250 psi
- Slab/shoulder deflection LTE: 20 and 50 percent
- Overlay transverse joint LTE: 20, 70, and 95 percent
- Wheel offset from the longitudinal joint: 1.666 in
- Tandem axle load: 15,000, 25,000, and 35,000 lb.
- Temperature difference between overlay top and bottom surface temperatures: -10, -20, and -35, °F.

Figure 52 shows a comparison of the maximum stresses at the top surface of the overlay lane/shoulder edge predicted using the procedure described above and the stresses obtained directly from ISLAB2005. A good agreement between these stresses is observed.
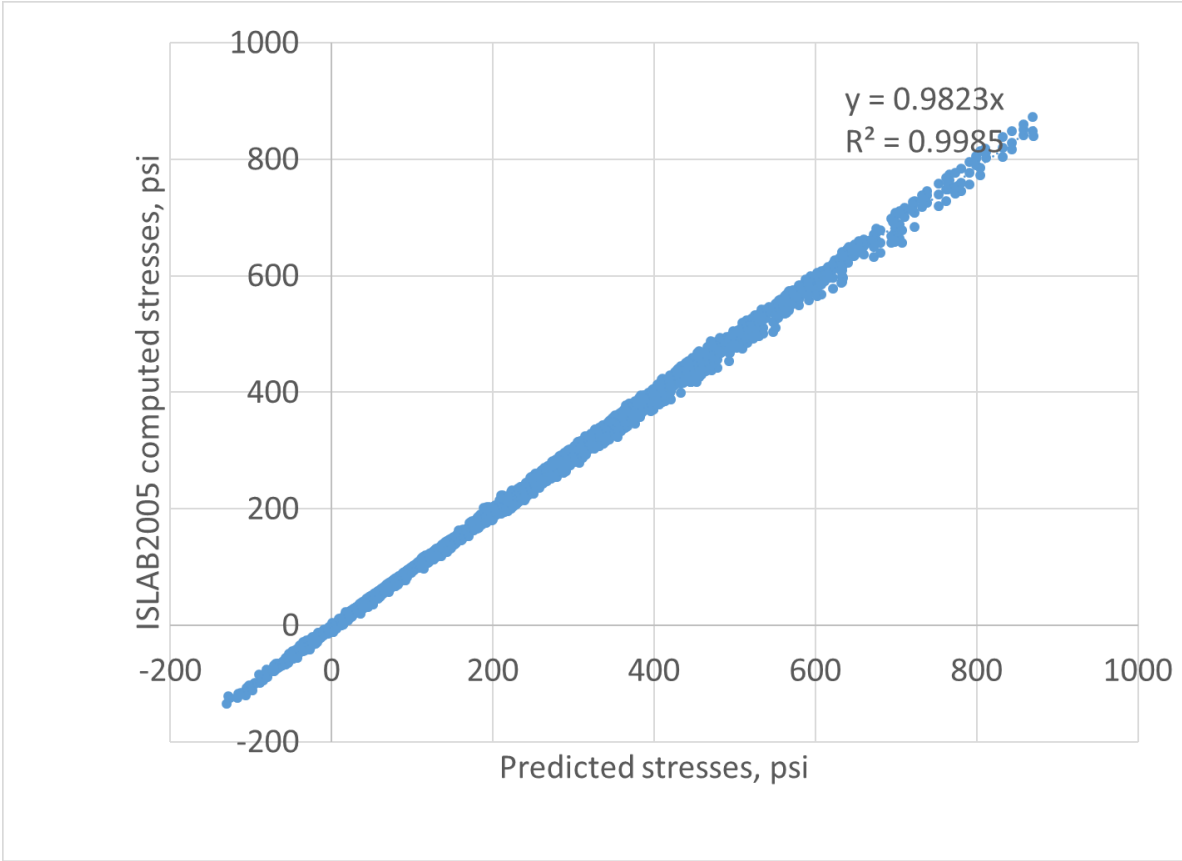

Figure 52: Comparison of stresses predicted using the developed procedure and ISLAB2005-computed stresses at the top surface of the slab/shoulder joint.

To demonstrate that the procedure predicts reasonable trends, a sensitivity study was conducted. The following baseline case was considered:

- The overlay thickness: 8 in.
- The existing pavement thickness: 9 in
- The overlay modulus of elasticity: 5.0×10^6 psi
- The existing pavement modulus of elasticity: 1.78×10^6 psi
- The Totski interlayer stiffness: 425 and 3,500 psi/in
- The coefficient of subgrade reaction: 250 psi
- Slab/shoulder deflection LTE: 50 percent
- Overlay transverse joint LTE: 70 percent

Wheel offset from the longitudinal joint: 1.666 in Figure 53 shows the predicted overlay top surface stresses for the temperature differences between the top and bottom overlay surfaces varied between -40 and 0°F and the axle load of 25,000 lb. Figure 54 shows the predicted overlay top surface stresses for temperature difference equal to -10°F and the axle load varied between 10,000 and 40,000 lb. Figure 55 shows variation of the predicted stresses for the axle load of 25,000 lb and the temperature difference of -35 °F with the overlay modulus of elasticity varied between 2 and 8 million psi. All these figures exhibited reasonable trends for both interlayer stiffnesses used in this analysis.

a. Interlayer stiffness 425 psi/in   b. Interlayer stiffness 3500 psi/in
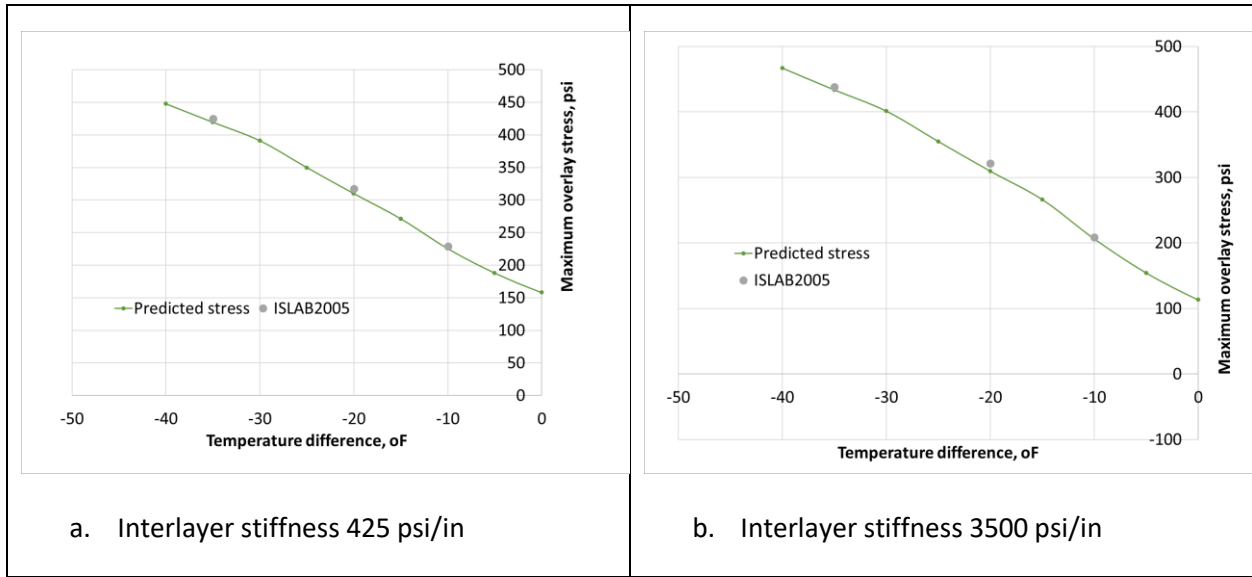
Figure 53: Effect of the temperature difference on predicted top surface maximum stresses

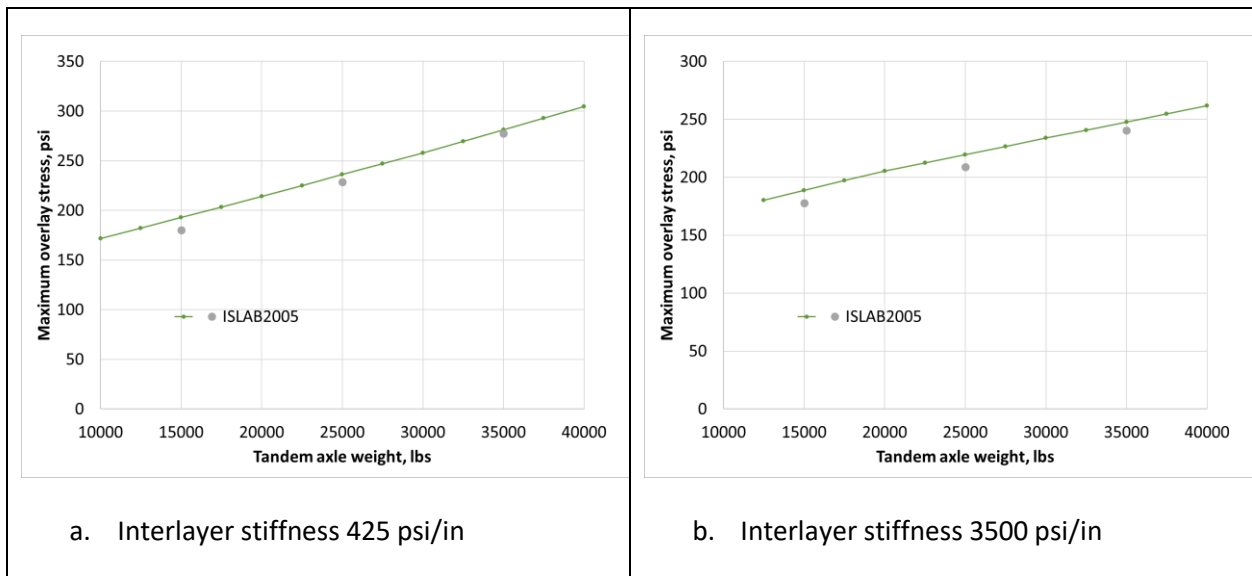a. Interlayer stiffness 425 psi/in   b. Interlayer stiffness 3500 psi/in

Figure 54: Effect of the axle weight on predicted top surface maximum stresses

92

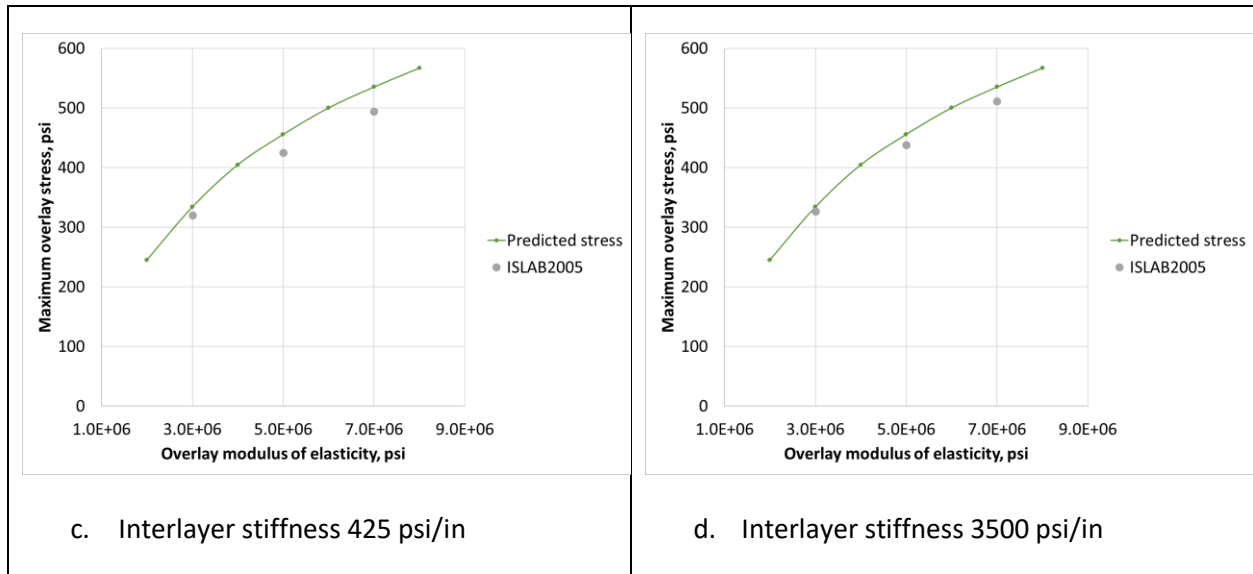| c. | Interlayer stiffness 425 psi/in | d. | Interlayer stiffness 3500 psi/in |

Figure 55: Effect of the overlay modulus of elasticity on predicted top surface maximum stresses

6.3.2.3 Determination of Critical Stresses at the Top and Bottom of the Transverse Joint for the Conventional Width Overlays

The results of the factorial of ISLAB2005 runs used for development of the prediction procedure for the critical stresses at the top surface of the slab/shoulder joint were used for the development of the procedure for prediction of the critical stresses at the top and bottom surfaces of the transverse joint of the overlay. The bending stresses were determined for each ISLAB2005 run at 16 locations along the loaded side of the transverse joint with an interval of 6 in starting 12 in away from the shoulder. The same procedure that was used for prediction of the critical stresses at the top surface of the slab/shoulder edge was adapted for prediction of the critical stresses at the transverse joint.

The procedure for predicting top surface stresses was verified using the results of the ISLAB2005 analysis for the cases used for verification of the procedure for prediction of the stresses at the top surface of the slab/shoulder joint, as described in the previous section. Figure 56 presents a comparison of the maximum stresses at the top surface of the overlay transverse joint predicted using the procedure described above and the stresses obtained directly from ISLAB2005.
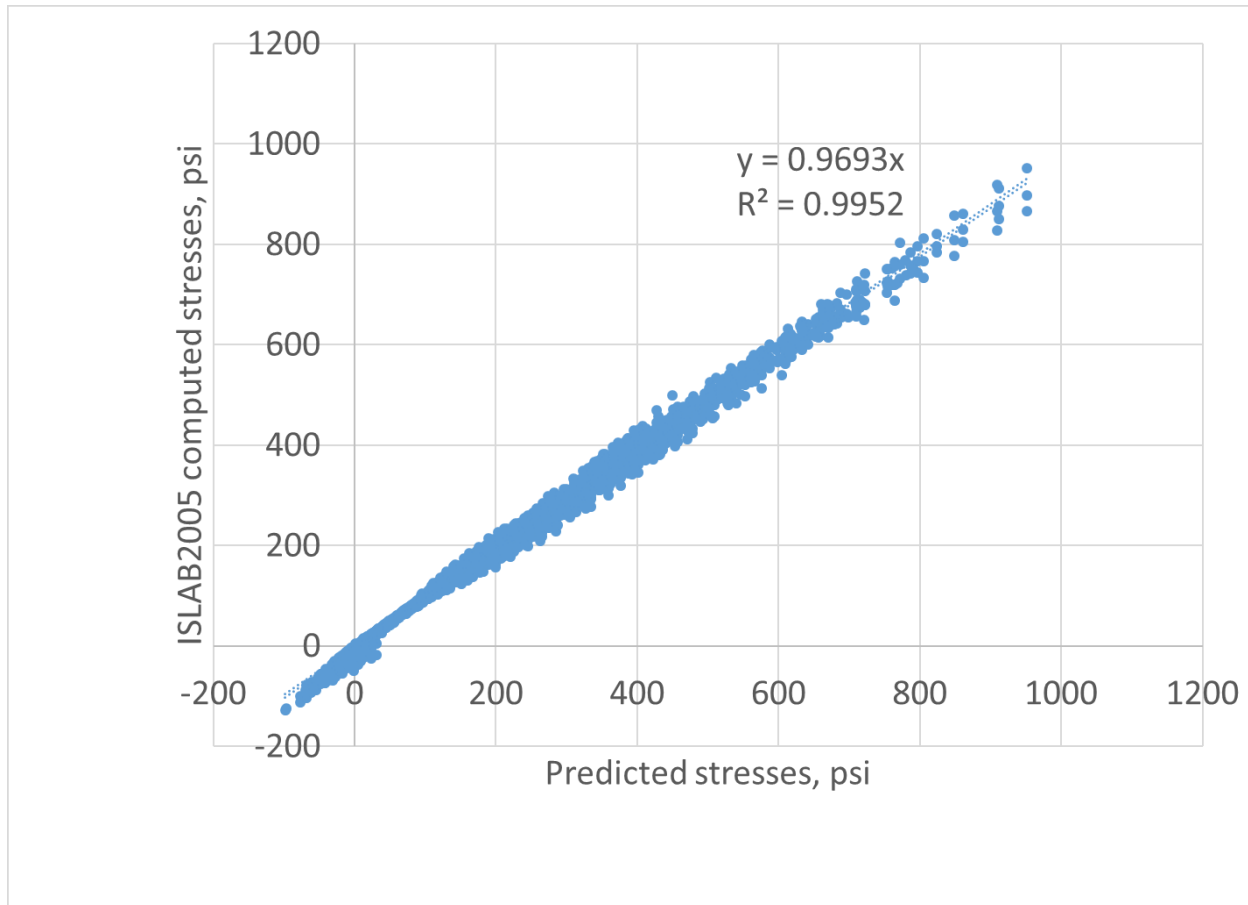
Figure 56: Comparison of stresses predicted using the developed procedure and ISLAB2005-computed stresses at the top surface of the transverse joint

To demonstrate that the procedure predicts reasonable trends, a sensitivity study was conducted. The following baseline case was considered:

- The overlay thickness: 8 in.
- The existing pavement thickness: 9 in
- The overlay modulus of elasticity: 5.0×10^6 psi
- The existing pavement modulus of elasticity: 1.78×10^6 psi
- The Totski interlayer stiffness: 425 and 3500 psi/in
- The coefficient of subgrade reaction: 250 psi
- Slab/shoulder deflection LTE: 50 percent
- Overlay transverse joint LTE: 70 percent
- Wheel offset from the longitudinal joint: 1.666 in

All these figures exhibited reasonable trends for both interlayer stiffness used in this analysis.
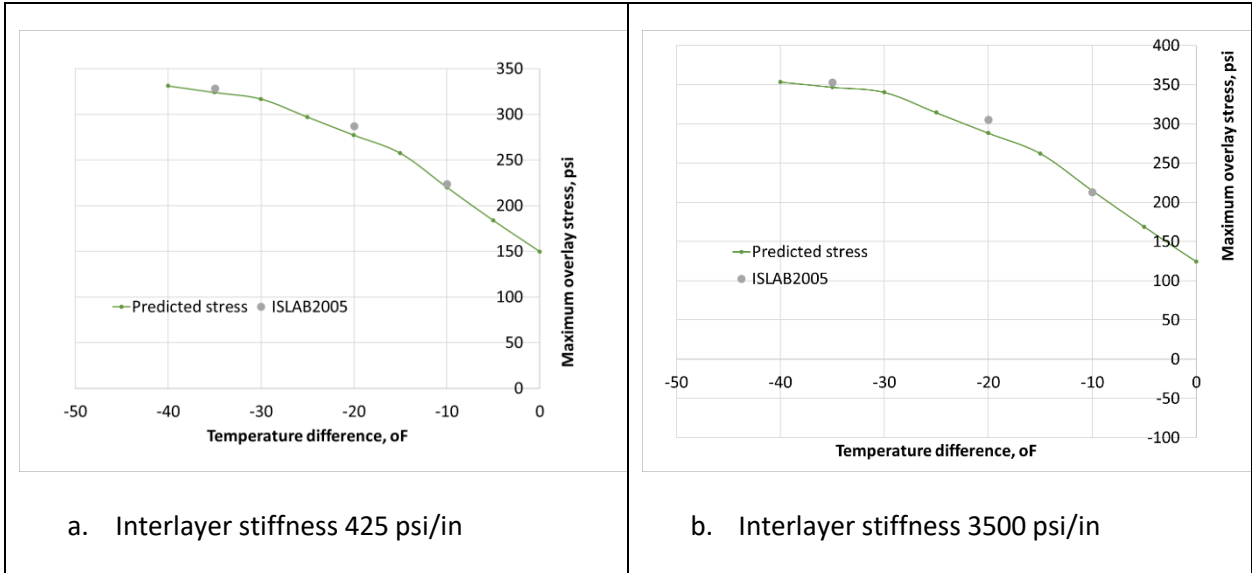
a. Interlayer stiffness 425 psi/in b. Interlayer stiffness 3500 psi/in

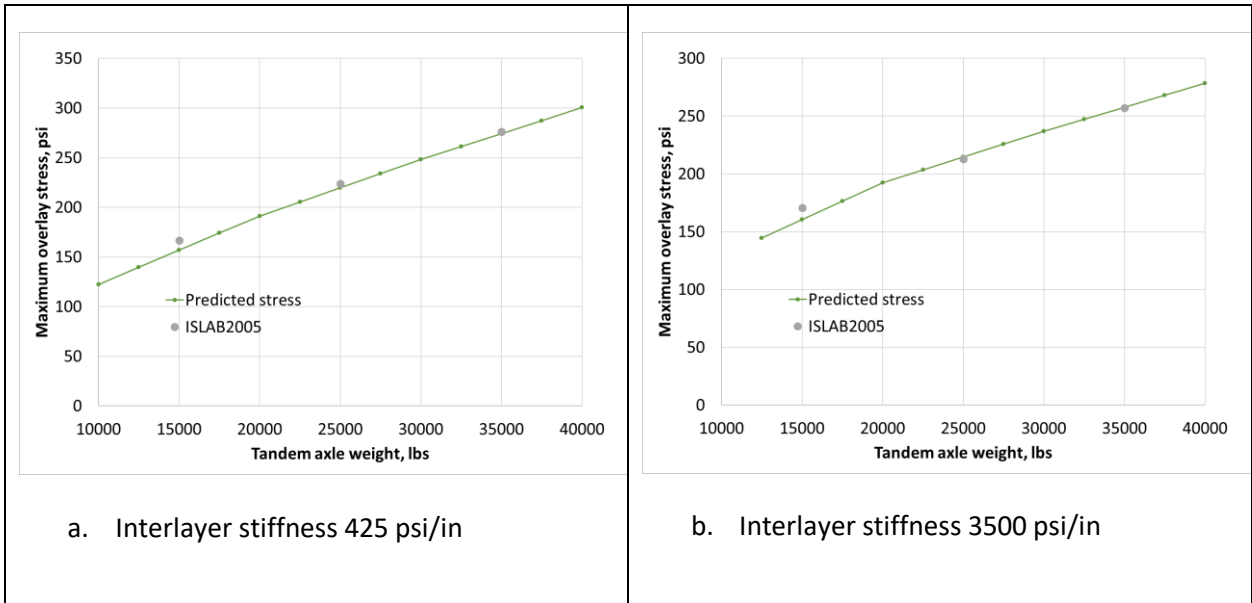**Figure 57: Effect of the temperature difference on the predicted top surface transverse joint maximum stresses**

a. Interlayer stiffness 425 psi/in b. Interlayer stiffness 3500 psi/in

Figure 58: Effect of the axle weight on the predicted top surface transverse joint maximum stresses

a. Interlayer stiffness 425 psi/in
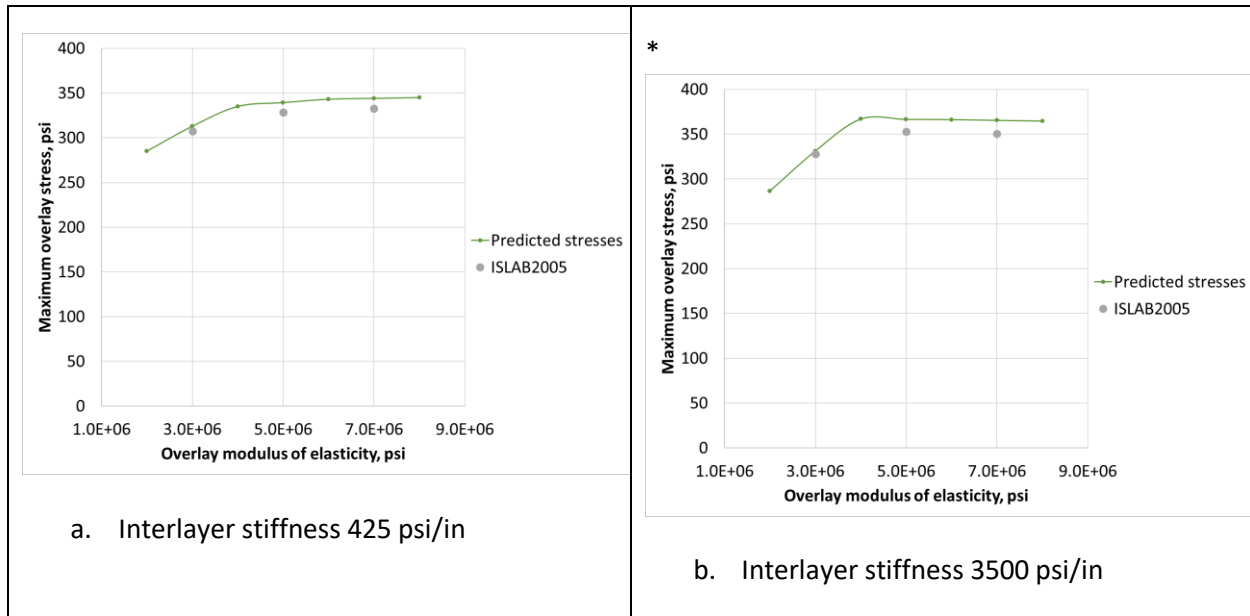
b. Interlayer stiffness 3500 psi/in

Figure 59: Effect of the overlay modulus of elasticity on the predicted top surface transverse joint maximum stresses

To verify the procedure for computing critical stresses at the bottom surface of a transverse joint, a factorial of 1,944 ISLAB2005 finite element runs was performed. The structural model shown in Figure 48 was used and most of the parameters were the same as were used for verification of the procedures for computing critical stresses at the top of the overlay surface at the slab/shoulder and transverse joint locations:

- The overlay thickness: 6, 8, and 10 in.
- The existing pavement thickness: 8 in
- The overlay modulus of elasticity: 3.0×10^6, 5.0×10^6, and 7.0×10^6 psi
- The existing pavement modulus of elasticity: 1.0×10^6, 6.0×10^6, 2.0×10^7 psi
- The Totski interlayer stiffness: 425 and 3,500 psi/in
- The coefficient of subgrade reaction: 250 psi
- Slab/shoulder deflection LTE: 20 and 50 percent
- Overlay transverse joint LTE: 20, 70, and 95 percent
- Wheel offset from the longitudinal joint: 1.666 in
- Tandem axle load: 15,000, 25,000, and 35,000 lb.
- Temperature difference between overlay top and bottom surfaces: 15 and 25 °F.

The difference between this factorial and the factorial for verification of the procedures for prediction of the critical stresses for the top overlay surface is the sign of temperature gradients. The top surface stresses have the highest values and cause most damage when a heavy axle loading is combined with a nighttime (negative) temperature gradient. The bottom edge stresses create most of the damage when the heavy axle loading is combined with a positive (daytime) temperature gradient. This justifies the selection of values for the differences between the top and bottom overlay surfaces.

Figure 60 compares the maximum stresses at the bottom surface of the overlay transverse joint predicted using the procedure described above and the stresses obtained directly from ISLAB2005. A very good agreement between the predicted and computed stresses is observed.
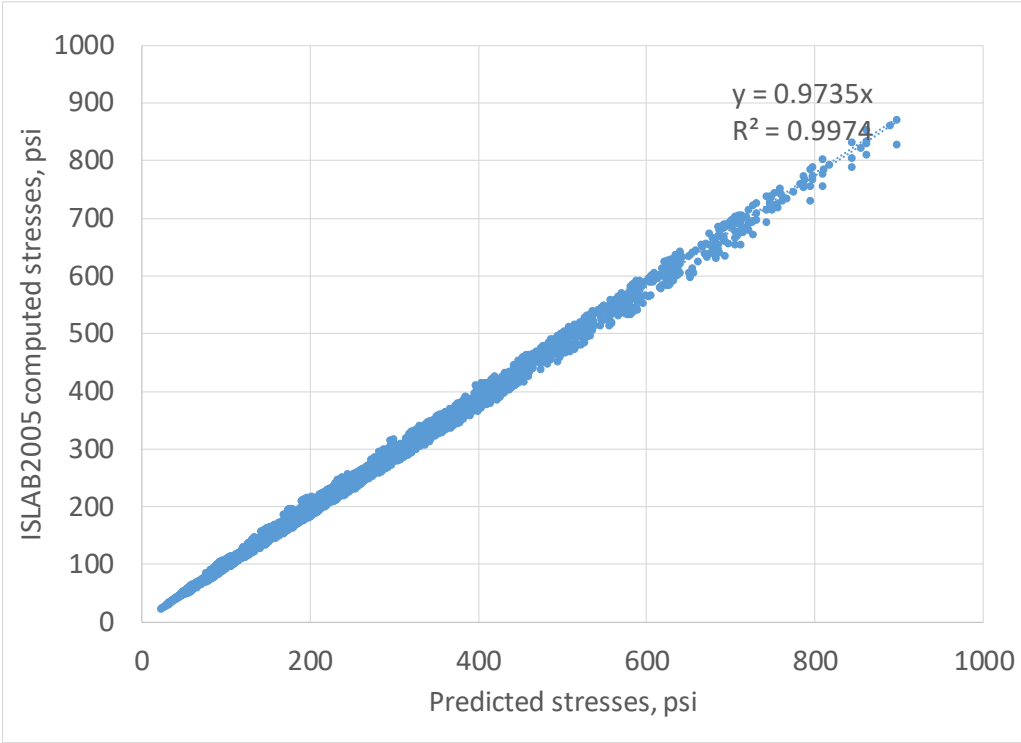

Figure 60: Comparison of stresses predicted using the developed procedure and ISLAB2005-computed stresses at the bottom surface of the transverse joint

To demonstrate that the procedure predicts reasonable trends, a sensitivity study was conducted. The following baseline case was considered:

- The overlay thickness: 6 in.
- The existing pavement thickness: 10 in
- The overlay modulus of elasticity: 5.0×10^6 psi
- The existing pavement modulus of elasticity: 4.32×10^6 psi
- The Totski interlayer stiffness: 425 and 3500 psi/in
- The coefficient of subgrade reaction: 250 psi
- Slab/shoulder deflection LTE: 20 percent
- Overlay transverse joint LTE: 20 percent
- Wheel offset from the longitudinal joint: 1.666 in

All these figures exhibited reasonable trends for both interlayer stiffness used in this analysis.
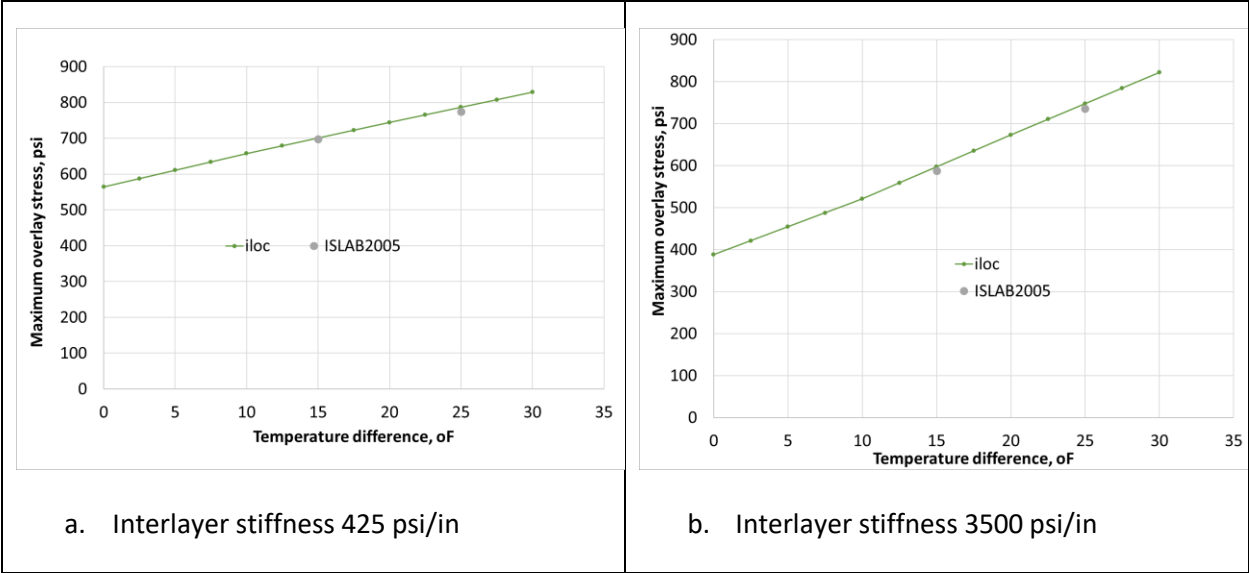
a. Interlayer stiffness 425 psi/in
b. Interlayer stiffness 3500 psi/in

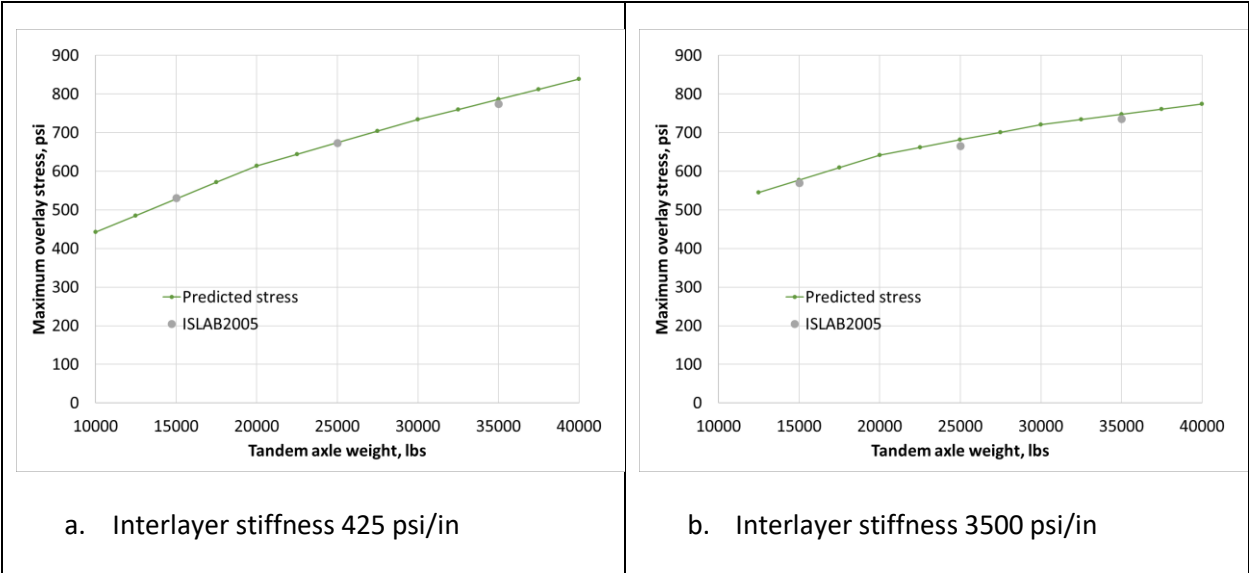**Figure 61: Effect of the temperature difference on the predicted bottom surface transverse joint maximum stresses**

a. Interlayer stiffness 425 psi/in
b. Interlayer stiffness 3500 psi/in

Figure 62: Effect of the axle weight on the predicted bottom surface transverse joint maximum stresses

| a.   Interlayer stiffness 425 psi/in | b.   Interlayer stiffness 3500 psi/in |
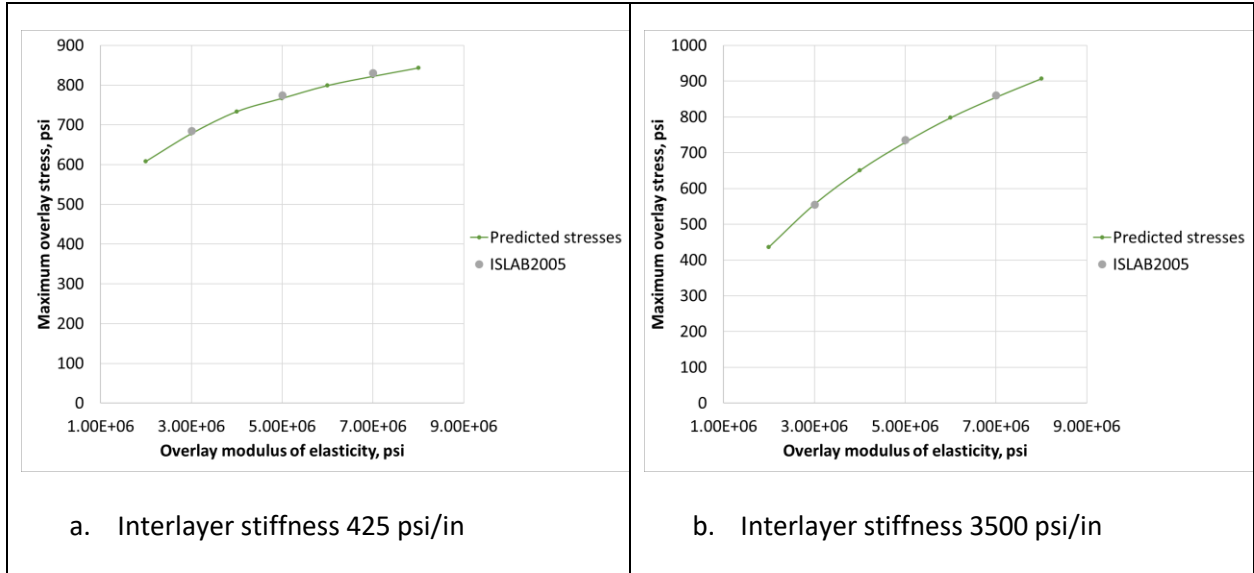
Figure 63: Effect of the overlay modulus of elasticity on the predicted bottom surface transverse joint maximum stresses

6.3.2.4 Determination of Critical Stresses for Short Slab Overlays at the Bottom of the Overlay Edge

The structural model used for prediction stresses for the short slab overlays is shown in Figure 64. The slab widths were set to 8 ft, 6 ft, and 6 ft for shoulder and two overlay slabs, respectively. The slab length, i.e. transverse joint spacing, was set to 6 ft.

Figure 64: ISLAB2005 model for computing bottom surface edge stresses for short slabs overlays

99

For the short slab, the tandem axle load was considered as two applications of the single axle load. Analogous to the conventional width slabs, a similarity concept was used to develop a procedure for the critical stress prediction. Two pav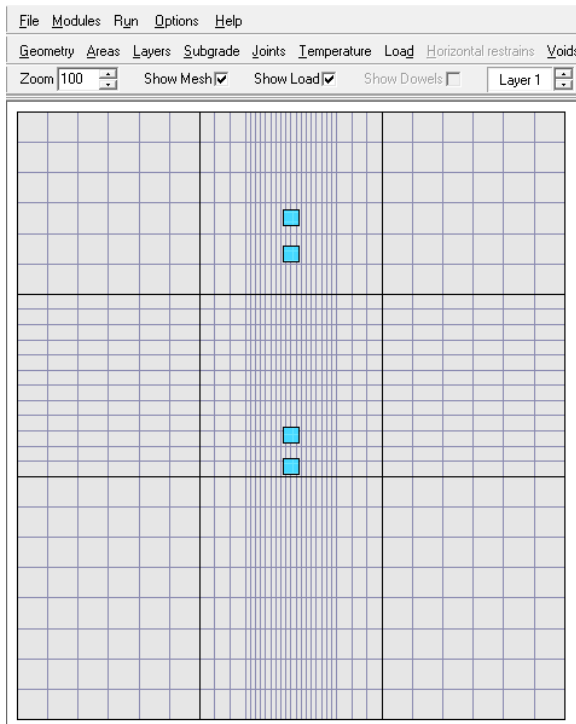ement structures described by the finite element models were found to be similar if the following conditions are satisfied:

- The in-plane positions of the axles are the same.
- The ratios of flexural stiffnesses of the pavement layers are equal (see Eq. (17)).
- The ratios of the Totski-to-subgrade spring stiffnesses are equal (see Eq. (119)).
- The ratios of overlays radii of relative stiffnesses are equal (see Eq. (10)).
- Load transfer efficiencies of the longitudinal joints are equal.
- The ratios of the axle weight to the overlay self-weight are equal (see Eq. (15)).
- Korenev's non-dimensional temperature gradients are equal (see Eq. (16)).

A factorial of 13,830 ISLAB2005 runs was performed for each of the cases with and without voids under overlay. The existing pavement thickness, Poisson's ratio, unit weight, and coefficient of thermal expansion for both layers were set to 6 in, 0.15, 0.087 lb/in^3, and $5.5*10^{-6}$ 1/$^\circ$F, respectively. The coefficient of subgrade reaction was set to 250 psi/in. The load transfer efficiency of the overlay transverse joints was set to 70%. The tire pressure was set to 100 psi. The transverse joints and the longitudinal joint under the overlay slabs in the driving lane of the existing pavements were considered to be rigid. The following parameters were varied:

- The overlay thickness: 4, 6, and 8 in
- The overlay modulus of elasticity: 2.0×10^6, 4.0×10^6, 6.0×10^6, and 8.0×10^6 psi
- The existing pavement modulus of elasticity: 5.0×10^5, 2.0×10^6, 1.0×10^7, and 4.0×10^7 psi
- The Totski interlayer spring stiffness: 400, 425, 3500, and 4000 psi/in
- Slab/shoulder deflection LTE: 20 and 50 percent
- Single axle load: 10000, 20000, 30000, and 40,000 lb
- Temperature difference between overlay top and bottom surface temperatures: 0, 10, 30, and 40 $^\circ$F.

The bending stresses at the bottom surface of the truck lane/shoulder longitudinal edge of the overlay slab were determined for each ISLAB2005 run at the mid-slab location. The procedure developed for determination of the critical stresses at the top surface of conventional width overlays was adapted for determining critical stresses at the bottom surface of the short slab overlay/shoulder joint. It involves the following steps:

Step 1. Select a similar system with the overlay thickness equal to the top layer thickness and the bottom layer thickness equal to 6 in.

Step 2. Calculate the moduli of elasticity of the overlay and existing pavement, as well as the Tostki interlayer stiffness, $E_{OL,S}$, $E_{EX,S}$, and $k_{Tot,S}$, respectively, for the similar system using the following equations 37 – 39.

Step 3. Compute the magnitude of the tandem axle load, P_{TS}, for the similar system satisfying the similarity condition Eqn. 15 using the equation 40.

Step 4. Compute the temperature difference between the top and bottom surfaces, ΔT_S, for the similar system satisfying the similarity condition Eqn. 16 using equation 41.

Step 5. Using the rapid solution, determine the critical stress in the similar system, $\sigma_{S,Rl}(P_{TS}, \Delta T_S)$.

Step 6. Determine the total stress in the overlay, σ_{OL}, using equation 42:

To verify this procedure, a factorial of 366 ISLAB2005 finite element runs was performed. The structural model shown in Figure 64 was used with the following parameters:

- The overlay thickness: 4, 6, and 8 in
- The existing pavement thickness: 8 in
- The overlay modulus of elasticity: 3.0×10^6, 5.0×10^6, and 7.0×10^6 psi
- The existing pavement modulus of elasticity: 1.0×10^6, 6.0×10^6, 2.0×10^7 psi
- The Totski interlayer stiffness: 425 and 3500 psi/in
- The coefficient of subgrade reaction: 250 psi
- Slab/shoulder deflection LTE: 20 percent
- Overlay transverse joint LTE: 70 percent
- Wheel offset from the longitudinal joint: 0.565 in
- Tandem axle load: 15,000, 25,000, and 35,000 lb.
- Temperature difference between overlay top and bottom surface temperatures: 10, 20, and 35 °F.

Figure 65 shows a comparison of the maximum stresses at the top surface of the overlay lane/shoulder edge predicted using the procedure described above and the stresses obtained directly from ISLAB2005. A very good agreement between these stresses is observed.
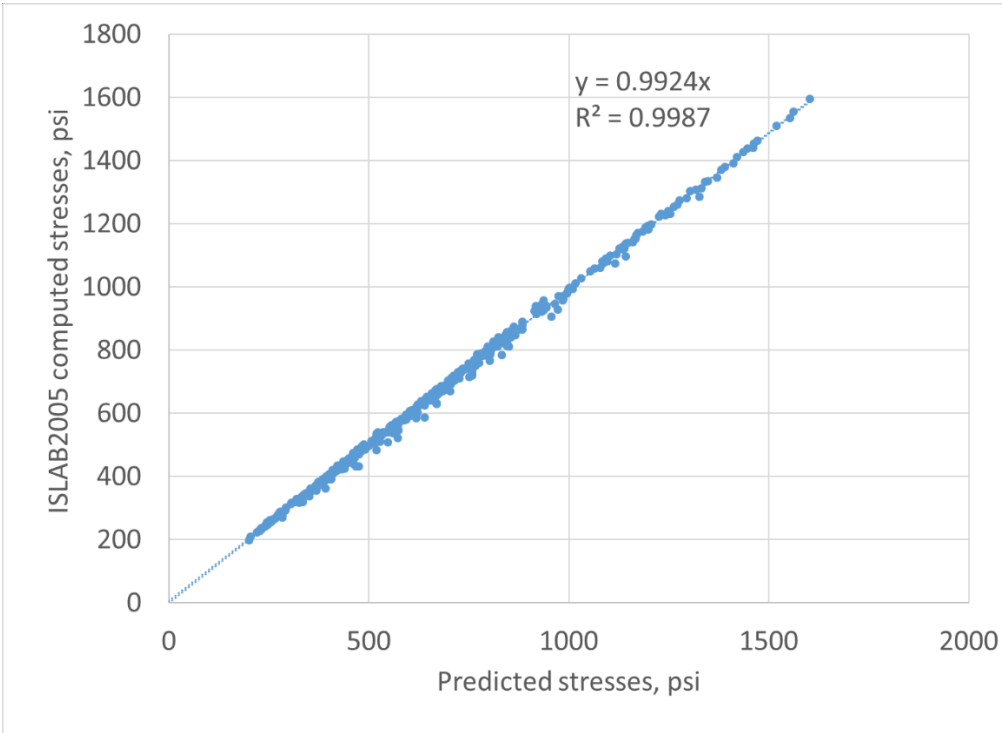
Figure 65: Comparison of stresses predicted using the developed procedure and ISLAB2005-computed stresses at the bottom surface of the short slab/shoulder joint.

6.3.2.5 Determination of Critical Stresses at the Top of the Overlay Edge for the Short Slab Overlays

Critical stresses at the top of the short slab overlay/shoulder edge occur near the middle of the overlay when the drive axle is near the transverse joint and there is a high negative temperature gradient throughout the slab. The following ISLAB2005 finite element model of a six-slab system loaded by a tandem axle load was developed (see Figure 66). The slab geometry was the same as for determination of the critical stresses at the bottom surface. A combined effect of nighttime temperature curling and truck loading was analyzed.
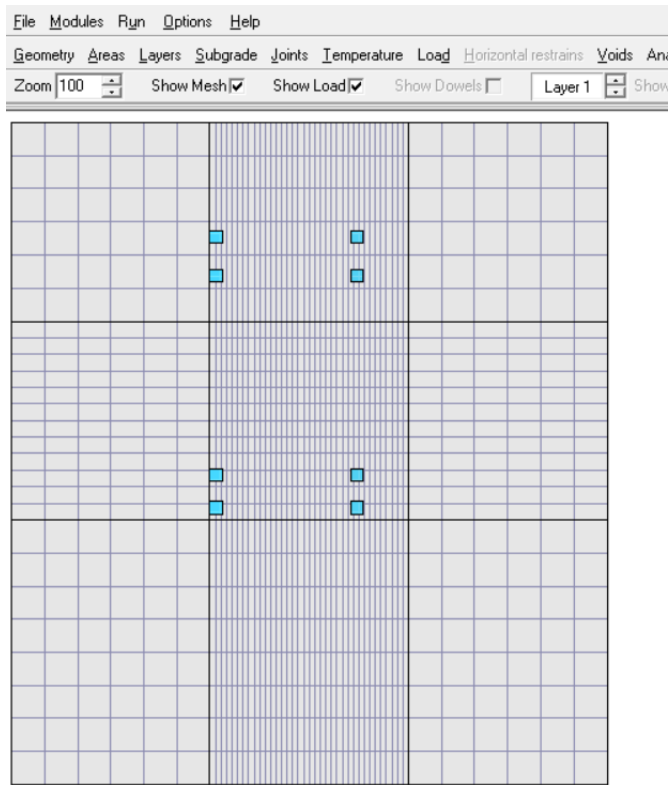
Figure 66: ISLAB2005 model for computing top surface edge stresses for short slabs overlays

The Totski model was used to model the pavement cross-section. The negative linear temperature distribution throughout the overlay thickness and the constant temperature distribution throughout the existing slab thickness were assumed. The Totski interlayer model was assumed to be working in compression only, i.e. the overlay was allowed to separate from the interlayer. Two cases of the interlayer conditions were considered:

- No deterioration of the interlayer. The Totski interlayer stiffness is the same for the entire layer.
- A void under the transverse joint extends throughout the entire lane width in transverse direction 6 inches on the approach side of the joint and 12 inches on the leave side of the joint in the direction of traffic (see Figure 67). The Totski interlayer stiffness is set to 1 psi/in for this part of the model.
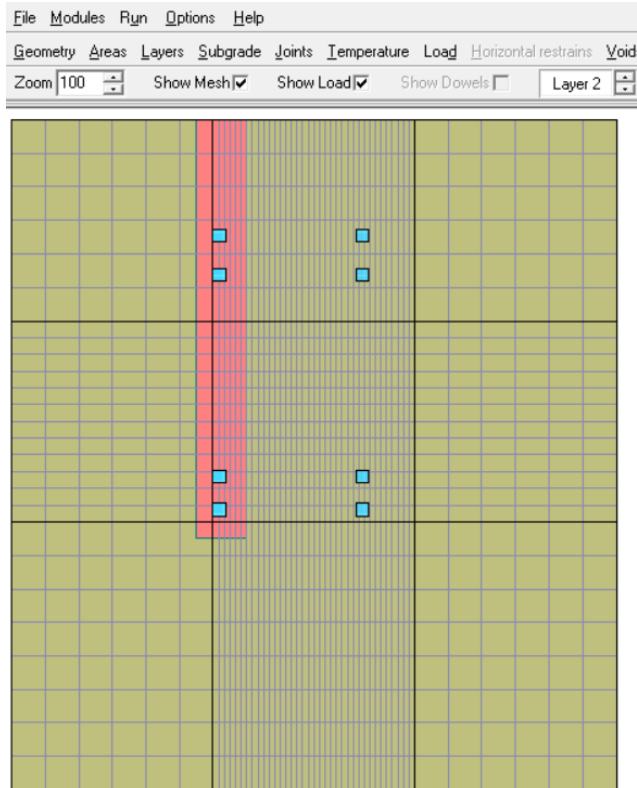
Figure 67: ISLAB2005 model for computing bottom edge stresses for short slab overlays with a void under the overlay

The procedure that was used for prediction of the critical stresses at the top surface of the top/shoulder edge was adapted to calculate the top surface edge stresses in the short overlay. The only difference is the neural networks were developed to predict stresses in the similar, short slab overlay system. To develop such neural networks, a factorial of 12,288 ISLAB2005 runs was performed for both the interlayer with and without voids each. The overlay Poisson's ratio, unit weight, and coefficient of thermal expansion for both layers were set to 0.15, 0.087 lb/in^3, and 6.0*10^{-6} 1/$^{\circ}$F, respectively. The existing pavement thickness was set to 6 in. The tire pressure was set to 100 psi. The transverse joints and the longitudinal joint under the overlay slabs in the driving lane of the existing pavements were considered to be rigid. The following parameters were varied:

- The overlay thickness: 4, 6, and 8 in
- The overlay modulus of elasticity: 2.0x10^6, 4.0x10^6, 6.0x10^6, and 8.0x10^6 psi
- The existing pavement modulus of elasticity: 5.0x10^5, 2.0x10^6, 1.0x10^7, and 4.0x10^7 psi
- The Totski interlayer spring stiffness: 400, 425, 3500, and 4000 psi/in
- Slab/shoulder deflection LTE: 20 and 50 percent
- Overlay transverse joints deflection LTE: 30 and 80 percent
- Single axle load: 10000, 20000, 30000, and 40,000 lb
- Temperature difference between overlay top and bottom surface temperatures: 0, -10, -30, and -40 $^{\circ}$F.

The bending stresses at the top surface of the truck lane/shoulder longitudinal edge of the overlay slab were determined for each ISLAB2005 run at 11 locations between the mid-slab and the tandem axle loaded transverse edge with an interval of 2 in. The rapid solutions were developed using modified MS-HARP neural network architecture (Banan and Hjelmstad 1994; Khazanovich and Roesler 1997).

To verify this procedure, a factorial of 1944 ISLAB2005 finite element runs was performed. The structural model shown in Figure 66 was used with the following parameters:

- The overlay thickness: 4, 6, and 8 in
- The existing pavement thickness: 8 in
- The overlay modulus of elasticity: 3.0×10^6, 5.0×10^6, and 7.0×10^6 psi
- The existing pavement modulus of elasticity: 1.0×10^6, 6.0×10^6, 2.0×10^7 psi
- The Totski interlayer stiffness: 425 and 3500 psi/in
- The coefficient of subgrade reaction: 250 psi
- Slab/shoulder deflection LTE: 20 and 50 percent
- Overlay transverse joint LTE: 20 and 80 percent
- Wheel offset from the longitudinal joint: 1.666 in
- Tandem axle load: 15,000, 25,000, and 35,000 lb.
- Temperature difference between overlay top and bottom surface temperatures: -10, -20, and -35 °F.

Figure 68 shows a comparison of the maximum stresses at the top surface of the overlay lane/shoulder edge predicted using the procedure described above and the stresses obtained directly from ISLAB2005. A very good agreement between these stresses is observed.
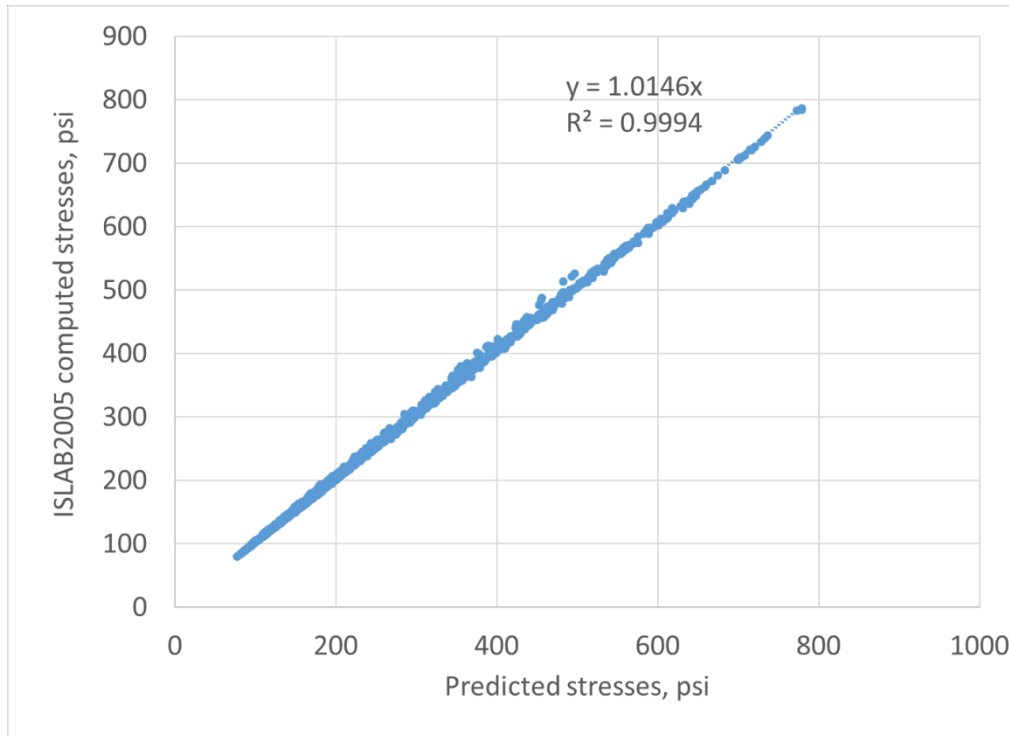
Figure 68: Comparison of stresses predicted using the developed procedure and ISLAB2005-computed stresses at the top surface of the short slab/shoulder joint.

6.3.2.6 Determination of Critical Stresses at the Top and Bottom of the Transverse Joint for Short Slab Width Overlays

The results of the factorial of ISLAB2005 runs used for development of the prediction procedure for the critical stresses at the top surface of the slab/shoulder joint in short slab overlays were used for the development of the procedure for prediction of the critical stresses at the top and bottom surfaces of the transverse joint of the short slab overlay. The bending stresses were determined for each ISLAB2005 run at 10 locations along the loaded side of the transverse joint. Seven points were selected in the short slab adjacent to the shoulder and located 12, 18, 24, 30, 36, 42, and 48 in from the slab/shoulder joint. Three points were located in the adjacent slab and located 12, 24, and 36 in from the longitudinal joint in the middle of the lane. The same procedure that was used for prediction of the critical stresses at the top surface of the slab/shoulder edge was adapted for prediction of the critical stresses at the transverse joint.

The procedure for predicting top surface stresses was verified using the results of the ISLAB2005 analysis for the cases used for verification of the procedure for prediction of the stresses at the top surface of the slab/shoulder joint, as described in the previous section. Figure 69 presents a comparison of the maximum stresses at the top surface of the overlay transverse joint predicted using the procedure described above and the stresses obtained directly from ISLAB2005.
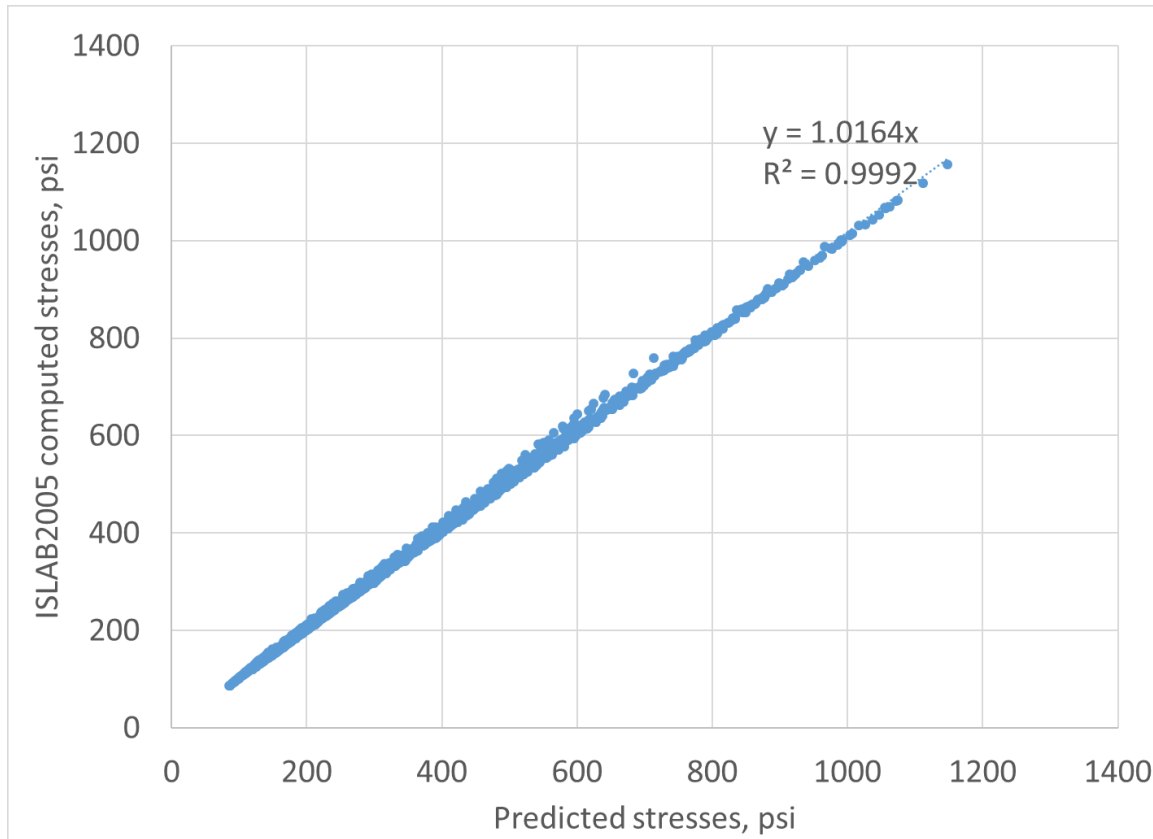
Figure 69: Comparison of stresses predicted using the developed procedure and ISLAB2005-computed stresses at the top surface of the transverse joint

To verify the procedure for computing critical stresses at the bottom surface of a transverse joint, a factorial of 1,944 ISLAB2005 finite element runs was performed. The structural model shown in Figure 66 was used and most of the parameters were the same as were used for verification of the procedures for computing critical stresses at the top of the overlay surface at the slab/shoulder and transverse joint locations:

- The overlay thickness: 4, 6, and 8 in
- The existing pavement thickness: 8 in
- The overlay modulus of elasticity: 3.0×10^6, 5.0×10^6, and 7.0×10^6 psi
- The existing pavement modulus of elasticity: 1.0×10^6, 6.0×10^6, 2.0×10^7 psi
- The Totski interlayer stiffness: 425 and 3500 psi/in
- The coefficient of subgrade reaction: 250 psi
- Slab/shoulder deflection LTE: 20 and 50 percent
- Overlay transverse joint LTE: 20 and 80 percent
- Wheel offset from the longitudinal joint: 1.666 in
- Tandem axle load: 15,000, 25,000, and 35,000 lb.
- Temperature difference between overlay top and bottom surface temperatures: 5, 15, and 25 °F.

The difference between this factorial and the factorial for verification of the procedures for prediction of the critical stresses for the top overlay surface is the sign of temperature gradients. The top surface stresses have the highest values and cause most damage when a heavy axle loading is combined with a nighttime (negative) temperature gradient. The bottom edge stresses create most of the damage when the heavy axle loading is combined with a positive (daytime) temperature gradient. This justifies the selection of values for the differences between the top and bottom overlay surfaces.

Figure 70 compares the maximum stresses at the bottom surface of the overlay transverse joint predicted using the procedure described above and the stresses obtained directly from ISLAB2005. An excellent agreement between the predicted and computed stresses is observed.
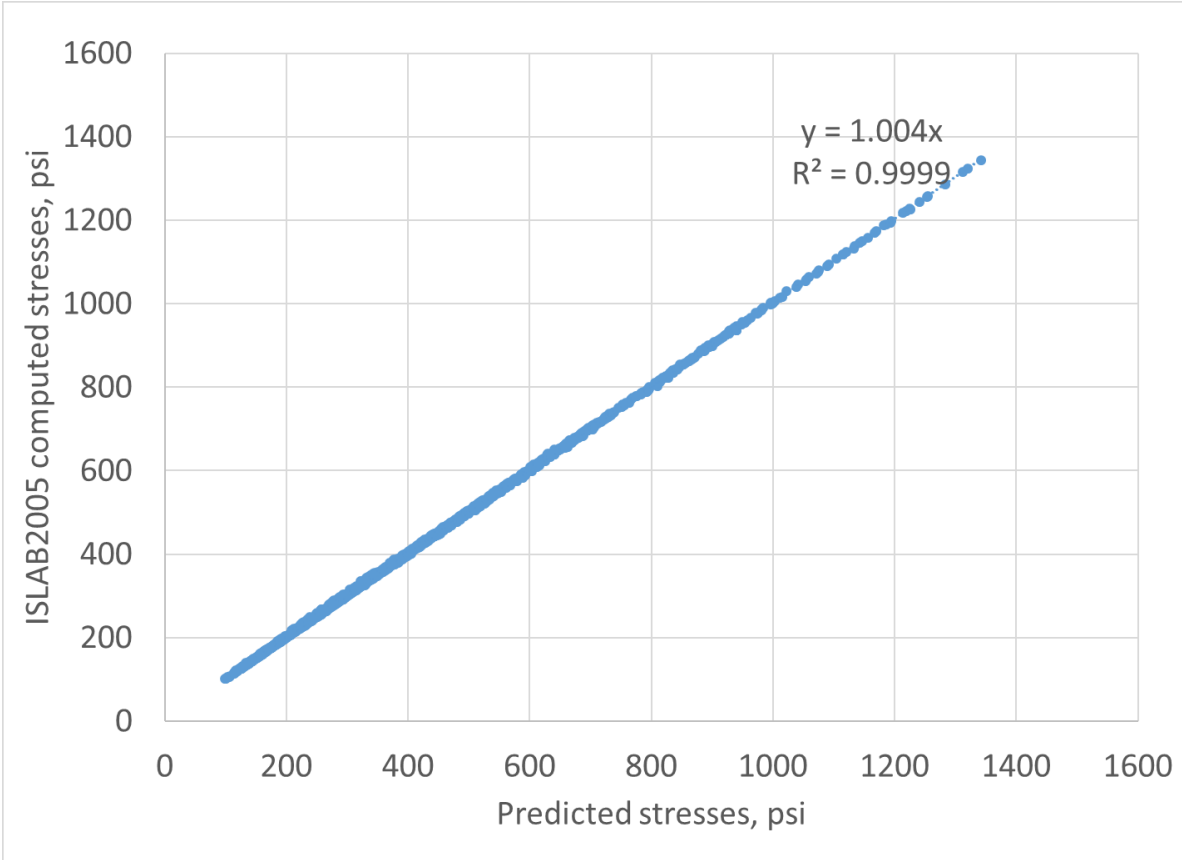

Figure 70: Comparison of stresses predicted using the developed procedure and ISLAB2005-computed stresses at the bottom surface of the transverse joint

6.3.3 Major Modifications to the Processing of EICM Temperature Data for the Modified UBOL Cracking Model

Thermal gradients throughout the unbonded concrete overlay affect greatly the critical stresses in the slab that contribute to cracking. Distributions of thermal gradients are required over each month throughout the year (both day and night). The EICM (Enhanced Integrated Climatic Model) module of

Pavement ME generates the thermal profiles throughout concrete slab thickness for every hour of pavement life.

To improve computation efficiency, the AASHTO M-E procedure converts those hourly predictions into monthly distributions of probability of combinations of traffic and temperature (known as the thermal linearization process). The AASHTO M-E linearization process eliminates the need to compute the number of loads as a function of both linear and nonlinear temperature differences by equating stresses due to nonlinear temperature distribution with those due to linear gradients (ARA 2004; Yu et al., 2004).

The equivalent temperature distribution concept was introduced by Thomlinson (1940) and further developed by other researchers (Choubane and Tia 1992). The concept, later generalized for non-uniform slabs (Khazanovich 1994, Ioannides and Khazanovich 1998), states that if two slabs have the same plane-view geometry, flexural stiffness, self-weight, boundary conditions, and applied pressure, and rest on the same foundation, then these slabs have the same deflections and bending moment distribution if the throughout-the-thickness temperature distributions satisfy the following condition:

$$\int_{h_a} E_a(z)\alpha_a(z)(T_a(z)-T_{0,a})zdz = \int_{h_b} E_b(z)\alpha_b(z)(T_b(z)-T_{0,b})zdz$$

where:

a, b = subscripts denoting two slabs

z = distance from the neutral axis

T_0 = the temperatures at which theses slabs are assumed to be flat

α = coefficient of thermal expansion

E = modulus of elasticity

h, , = slab thickness.

The temperature distribution throughout the slab thickness can be split into its three components:

- the part that causes constant strain throughout-the-slab-thickness,
- the part that causes linear throughout-the-slab-thickness strains, and
- the part that causes nonlinear strains.

The first step in the AASHTO M-E linearization process is to compute the monthly PCC stress frequency distribution in the pavement at critical locations for linear temperature difference, ΔT_L, non-linear temperature, T_{NL}, and standard axle loading. For bottom-up damage accumulation, an 18-kip single axle load is placed on the mid-slab edge, where it will produce the maximum stress, as shown in Figure 37. For top-down damage accumulation, a 12-kip single axle load and a 34-kip tandem axle load with a medium wheelbase is placed at the critical loading location, as shown in Figure 38.

The second step in the linearization process involves finding the frequency distribution of linear temperature gradients, in increments of 2°F, which produces the PCC bending stress frequency distribution (without non-linear temperature stresses) that is the same as the stress distribution from the previous step. The temperature frequency distribution for each month developed for the standard load and wheel offset conditions only, is used in the fatigue analysis for all axle loads and offsets conditions.

This thermal linearization process significantly reduces the amount of computing required to estimate stresses. Nevertheless, it has the following drawbacks:

- It is still computationally expensive and needs to be performed for each combination of concrete overlay properties.
- It assumes that the stress due to the interaction between nonlinear temperature and traffic is constant for all traffic loads.
- Piecewise integration may be oversensitive to error in the EICM predictions.

In this study, an alternative approach was developed. It is an adaptation of approaches proposed by Hiller and Roesler (2010) and Khazanovich and Tompkins (2017), involving the following steps:

- EICM analysis is conducted to predict hourly distributions of the temperature throughout the UBOL pavement system.
- Each hourly temperature profile is approximated by a quadratic temperature distribution:

$$T(z) = A + B\,z + C\,z^2 \tag{46}$$

where

z = the distance from the mid-depth (inches)
- The frequency distribution of linear and quadratic coefficients is created.

In this study, the increment of the linear term B was selected to ensure 2°F for the linear temperature difference between the top and bottom PCC surfaces. The frequency distribution for the quadratic term, C, is in increments of $0.1°F/in^2$. The following procedure was used for the frequency calculation:

- For each hourly pair of B and C, the nearest tabulated values for these coefficients were identified, i.e. values of B_i and B_{i+1}, so $B_i \leq B \leq B_{i+1}$, and C_j and C_{j+1}, so $C_j \leq C \leq C_{j+1}$
- The values of the frequency table, f_{ij}, were updated as follows:

$$f_{i,j} = f_{ij} + \frac{B_{i+1}-B}{B_{i+1}-B_i} \frac{C_{j+1}-C}{C_{j+1}-C_j},$$

$$f_{i,j+1} = f_{ij} + \frac{B_{i+1}-B}{B_{i+1}-B_i} \frac{C-C_j}{C_{j+1}-C_j},$$

$$f_{i+1,j} = f_{ij} + \frac{B-B_i}{B_{i+1}-B_i} \frac{C_{j+1}-C}{C_{j+1}-C_j},$$

$$f_{i+1,j+1} = f_{ij} + \frac{B-B_i}{B_{i+1}-B_i} \frac{C-C_j}{C_{j+1}-C_j},$$

- o Each value from the frequency table is divided by the total number of the hours in the EICM analysis.

Table 19 presents an example of the frequency distribution table of a 6-in thick UBOL. It can be observed that for this example the probability of the temperature profile with the coefficients B and C equal to 2 and 0.3, respectively, is equal to 0.00587.

If a concrete slab-on-grade has a temperature distribution throughout the slab thickness described by Equation 47 then the equivalent difference, i.e. the difference between the top and bottom slab surfaces for a linear temperature variation throughout the slab thickness that causes the same slab deflections has the following form (Choubane and Tia 1992, Khazanovich 1994):

$$\Delta T_{Linear} = B\, h_{slab} \qquad\qquad (47)$$

where:

ΔT_{Linear} is equivalent temperature differences throughout the slab thickness,

h_{slab} is the slab thickness

B is the equivalent linear temperature gradient

Table 19: Example of frequency distribution of probability of a given combination B and C

Coefficient B	Coefficient C											
	-0.5	-0.4	-0.3	-0.2	-0.1	0	0.1	0.2	0.3	0.4	0.5	0.6
-3	0	0	0	0	0	0	0	0	0	0	0	0
-2.6667	0	0	0	0	0.00176	0	0	0	0	0	0	0
-2.3333	0	0	0.00352	0.01174	0.02136	0.00012	0	0	0	0	0	0
-2	0	0.00188	0.0108	0.03087	0.08815	0.00047	0	0	0	0	0	0
-1.6667	0	0.00704	0.00798	0.01772	0.075	0.00857	0	0	0	0	0	0
-1.3333	0	0.00305	0.00575	0.01279	0.06455	0.01772	0.00434	0	0	0	0	0
-1	0	0.00211	0.00646	0.01009	0.03216	0.02676	0.00669	0.00387	0	0	0	0
-0.6667	0	0.00129	0.00798	0.00575	0.01455	0.02019	0.00458	0.00481	0	0	0	0
-0.3333	0	0.00129	0.00739	0.00446	0.00646	0.00528	0.00352	0.00716	0	0	0	0
0	0	0	0.00528	0.00376	0.00434	0.00258	0.00387	0.00692	0.00317	0	0	0
0.3333	0	0	0.00258	0.00599	0.00411	0.00423	0.00352	0.00399	0.00692	0	0	0
0.6667	0	0	0.00188	0.00692	0.00481	0.00481	0.00387	0.00293	0.00692	0.00176	0	0
1	0	0	0	0.00493	0.00575	0.00376	0.00434	0.00317	0.00692	0.00246	0	0
1.3333	0	0	0	0.00387	0.00822	0.00516	0.00258	0.00329	0.00646	0.00446	0	0
1.6667	0	0	0	0.00223	0.00634	0.00657	0.00387	0.00376	0.00411	0.00646	0	0
2	0	0	0	0	0.00575	0.00669	0.00552	0.00364	0.00587	0.00751	0	0
2.3333	0	0	0	0	0.00246	0.00716	0.00657	0.00575	0.00563	0.00669	0.00164	0
2.6667	0	0	0	0	0.00188	0.00528	0.00798	0.00716	0.00516	0.0081	0.00129	0
3	0	0	0	0	0	0.00469	0.00728	0.00751	0.00587	0.00528	0.00188	0
3.3333	0	0	0	0	0	0.00164	0.00516	0.00857	0.00728	0.00716	0.00188	0
3.6667	0	0	0	0	0	0.00059	0.00282	0.00599	0.00669	0.00387	0.00176	0
4	0	0	0	0	0	0.00035	0.00153	0.00282	0.00364	0.00364	0.002	0
4.3333	0	0	0	0	0	0.00082	0	0.00176	0.00246	0.00235	0.00153	0
4.6667	0	0	0	0	0	0	0.00129	0	0.00211	0.00141	0.00106	0
5	0	0	0	0	0	0.00012	0	0.00117	0	0	0.00117	0
5.3333	0	0	0	0	0	0.00023	0	0	0.00141	0	0	0
5.6667	0	0	0	0	0	0.00035	0	0	0	0.00117	0	0
6	0	0	0	0	0	0	0	0	0	0	0	0

The self-equilibrating stresses on the top and bottom overlay surfaces can be found using the Equation 40

$$\sigma_{NL} = \frac{C_j E}{1 - \nu_{OL}} \alpha_{OL} \frac{h_{OL}^2}{6} \qquad (48)$$

where:

α_{OL} = the coefficient of thermal expansion (of the overlay)

6.3.4 Built-in Curl Analysis

A recently completed NCHRP 1-51 study (Khazanovich and Tompkins, 2017) suggested that built-in curl modeling for pavement performance models should not be limited to a single parameter/value. The following observations were used to support this claim:

- Theories of slab behavior discussed in the literature review treat built-in curl as a property that depends on the paving conditions and varies throughout the service life (Eisenmann and Leykauf, 1990).
- Built-in curl depends on the time of concrete placement, i.e. morning versus afternoon (Springenschmid and Fleischer, 2001).
- The empirical mode decomposition (EMD) analysis of the LTPP profilometer data indicated that the slab profiles of in-situ pavements vary by base material. Furthermore, the analysis found high variance in slab profile within a given project.

The NCHRP 1-51 study proposed to modify the built-in curl factor in pavement performance modeling by dividing the default AASHTO parameter into two different built-in curl temperature gradients for daytime and nighttime conditions (ΔT_{bot} and ΔT_{top}, respectively). Furthermore, it proposed that the developed model for built-in curl consider the properties of the concrete slabs' thickness and stiffness in the slab and base layers; this model thus ensures that projects with stiffer bases will have more exaggerated levels of built-in curl.

The existing pavement provides a much stiffer foundation to an unbonded overlay than a base layer provides to a new concrete pavement. Therefore, it was hypothesized that the amount of built-in curling depends on the stiffness of the overlay and the existing pavement, overlay joint spacing, and stiffness of the interlayer. The following representation for $\Delta T_{built\text{-}in}$ was proposed and implemented in the cracking model:

$$
\Delta T_{built-in} = \Delta T_{input} \left(1 \pm \left(1 - \exp\left(-0.001 \left(\frac{\ell_{OL}}{L} \right)^4 \right) \right) \left(1 - \exp\left(-10^{-6} \left(\frac{\ell_{eff}}{L} \right)^4 \right) \right) \right)
$$

(49)

where:

ΔT_{input} is the default value of the built-in curl (independent from the UBOLDesign design parameters), ℉

L is the overlay joint spacing, ft,

ℓ_{OL} is the overlay radius of relative stiffness in the Totski model defined as:

$$\ell_{OL} = \sqrt[4]{\frac{E_{OL}h_{OL}^3}{12(1-\nu_{OL}^2)\,k_{Tot}}} \qquad\qquad (50)$$

ℓ_{eff} is the effective overlay radius of relative stiffness defined as:

$$\ell_{eff} = \sqrt[4]{\frac{E_{OL}h_{eff}^3}{12(1-\nu_{OL}^2)k_{subgr}}} \qquad\qquad (51)$$

where h_{ol}, E_{ol}, and, ν_{OL} are overlay thickness, modulus of elasticity, and Poisson's ratio, respectively; k_{Tot} and k_{subgr} are the Totski interlayer stiffness and the coefficient of subgrade reaction, respectively; and h_{eff} is he effective pavement stiffness (Ioannides et al., 1992):

$$h_{eff} = \sqrt[3]{E_{OL}h_{OL}^3 + E_{ex}h_{ex}^3} \qquad\qquad (52)$$

where h_{ex} and E_{ex} are existing pavement thickness and modulus, respectively.

In this study, the same default value of ΔT_{input} = -10°F as used in the *MEPDG* procedure is selected. Once the calculation for $\Delta T_{built-in}$ is conducted, it is split into (A) $\Delta T_{built-in,day}$, a more positive component to simulate slab-base interaction during daytime loading, or (B) $\Delta T_{built-in,night}$, a more negative component to simulate the slab-base interaction during nighttime loading, i.e.

$$\Delta T_{built-in,day} = \Delta T_{input}\left(1 + \left(1 - \exp\left(-0.001\left(\tfrac{\ell_{OL}}{L}\right)^4\right)\right)\left(1 - \exp\left(-10^{-6}\left(\tfrac{\ell_{eff}}{L}\right)^4\right)\right)\right) \quad (53)$$

$$\Delta T_{built-in,night} = \Delta T_{input}\left(1 - \left(1 - \exp\left(-0.001\left(\tfrac{\ell_{OL}}{L}\right)^4\right)\right)\left(1 - \exp\left(-10^{-6}\left(\tfrac{\ell_{eff}}{L}\right)^4\right)\right)\right) \quad (54)$$

6.4 OVERVIEW OF CRACKING PREDICTION PROCESS

The overall unbonded overlay cracking prediction process developed in this study is a modification of the *MEPDG* cracking prediction process for rigid pavements. The main steps include the following:

1. Assemble design inputs for a specific site conditions, such as traffic, climate, existing concrete pavement properties, and foundation. Define the interlayer properties, as well as overlay PCC properties, and design features such as joint spacing, dowel diameter, and shoulder type.
2. Process input to obtain monthly values of traffic, material, and climatic inputs needed in the design evaluations for the entire design period.
3. Compute structural responses (stresses and deflections) using finite element based rapid solution models for each axle type and load, as well as for each damage-calculation increment throughout the design period.

4. Calculate accumulated top surface and bottom surface damages at the lane-shoulder joint and the transverse joint for each month of the entire design period.
5. Predict cracking at the end of the entire design period.

6.4.1 Design Inputs

Input data used for cracking prediction developed in this study are categorized as follows:

- Pavement location
- General information
    - expected pavement design life (years)
    - number of lanes (two-way)
- Traffic
    - Two-Way Annual Average Daily Truck Traffic (AADTT) for the base year – the total number of heavy vehicles (classes 4 to 13) in the traffic stream passing a point or segment of a road facility to be designed in both directions during a 24-hour period
    - Linear traffic volume growth factor
- Pavement Structure
    - Unbonded concrete overlay
        - Thickness
        - Modulus of rupture (flexural strength), MR, at 28 days
    - Interlayer type (asphalt or fabric). If an asphalt interlayer is used, then the following properties should be provided:
        - Effective binder content, percent
        - Percent passing #200 sieve in the interlayer
        - Percent of air voids in the interlayer
    - Existing pavement
        - Thickness
        - Modulus of elasticity
- Design Features
    - Joint spacing in the unbonded overlay
    - Dowel diameter
    - Shoulder type

6.4.2 Input Data Processing

6.4.2.1 Pavement location

Environmental conditions have a significant effect on the performance of unbonded overlays. The cracking model developed in this study requires the user to provide hourly temperature distribution throughout the overlay thickness for the entire design period. Similar to the *MEPDG* cracking analysis for rigid pavements, this information can be obtained by executing the Enhanced Integrated Climatic Model

(EICM) using the trial design before performing damage computation. The EICM database includes historical weather data for hundreds of weather stations across the U.S. The designer can select a nearby weather station or can create a virtual weather station by combining one or more weather stations that are in the vicinity of the project.

Since an objective of this study was to develop a standalone tool, the EICM analysis was performed for 68 weather stations located throughout the United States and the results of this analysis were used to develop a database to be used by the designer. For each location, the analysis was performed assuming the overlay thickness of 4, 6, 8, and 10 in. The existing pavement thickness was kept equal to 10 in. The output of the EICM executions are temperature file that predicts hourly temperature profile in the PCC overlay system with a 1-inch interval for the entire design period.

For each EICM result, each hourly nonlinear temperature profile was converted to a sum of the effective linear thermal gradient and quadratic temperature distribution component. For computational efficiency and more realistic stress predictions, the hourly temperature component data are converted to a frequency distribution table as discussed in Section 6.3.3.

6.4.2.2 Traffic

Traffic data is one of the key data elements required for the analysis and design of unbonded concrete overlays. Similar to the *MEPDG*, the procedure developed in this study considers truck traffic loadings in terms of axle load spectra:

Single axles – 3,000 to 40,000 lb in 1,000 lb increment.

Tandem axles – 6,000 to 80,000 lb in 2,000 lb increment.

Tridem axles – 12,000 to 99,000 lb in 3,000 lb increment.

The *MEPDG* procedure requires prediction of the number of axle load applications for each hour of pavement life. The procedure for cracking analysis developed is this study uses a simplified approach where the axle spectrum is predicted on a yearly basis. The user is asked to provide the Annual Average Daily Truck Traffic (AADTT) for base year and the linear growth factor. The following steps are performed next to obtain the required axle loading spectrum:

Step 1. Determine the daily number of trucks in the design lane.

The daily number of heavy trucks in the design lane is determined using the following equation:

$$AADTT_d = AADTT \ \times LDF \times DDF \tag{55}$$

where:

DDF is the directional distribution factor: percent of trucks in the design direction assumed to be equal to 50 percent.

LDF is the lane distribution factor, i.e. percent of trucks in design lane from trucks in one direction. The following values for LDF are assumed in this procedure:

- Single-lane roadways in one direction, LDF = 1.00.
- Two-lane roadways in one direction, LDF = 0.90.
- Three-lane roadways in one direction, LDF = 0.60.
- Four-lane roadways in one direction, LDF = 0.45.

Step 2. Determine axle spectrum for the base year.

The procedure uses the default normalized axle load distribution and converts it to the axle spectrum for the design line using the following equation:

$$NA_{ij1} = DNA_{ij} \frac{AADTT_d}{1000} \tag{56}$$

where:

NA_{ij1}, is the number of axles of type I (single, tandem, or tridem) and weight j for the first year

DNA_{ij}, is default normalized axle load distribution, i.e. number of axles of type I (single, tandem, or tridem) and weight j if the number of trucks is 1000. The default normalized axle load distribution is provided in Table 20.

Table 20: Default normalized axle load distribution

Single		Tandem		Tridem	
Axle Weight	Number of axles	Axle Weight	Number of axles	Axle Weight	Number of axles
3000	19837.36	6000	9253.26	9000	3566.87
4000	15914.99	8000	8413.03	12000	1901.56
5000	21939.21	10000	13000.1	15000	1605.13
6000	18565.38	12000	14501.45	18000	1308.71
7000	19883.77	14000	14918.13	21000	1203.83
8000	24489.3	16000	13965.56	24000	1223.07
9000	28694.03	18000	12215.46	27000	1279.32
10000	32210.34	20000	11611.85	30000	1287.95
11000	29251.46	22000	12107.23	33000	1693.41
12000	23160.7	24000	10604.27	36000	1707.45
13000	15202.1	26000	10407.94	39000	1652.92
14000	10140.26	28000	11240.28	42000	1301.51
15000	7272.29	30000	12527.2	45000	1334.5
16000	5770.38	32000	11166.19	48000	971.78
17000	4066.03	34000	9972.46	51000	831.81
18000	3246.62	36000	7990.36	54000	690.56

Single		Tandem		Tridem	
Axle Weight	Number of axles	Axle Weight	Number of axles	Axle Weight	Number of axles
19000	2492.23	38000	6527.66	57000	404.7
20000	1892	40000	4752.48	60000	331.64
21000	1426.63	42000	3276.7	63000	351.16
22000	1044.86	44000	2353.85	66000	176.37
23000	840.26	46000	1751.09	69000	169.85
24000	550.85	48000	1139.27	72000	146.7
25000	413.34	50000	830.61	75000	134.72
26000	405.89	52000	548.14	78000	73.42
27000	346.71	54000	585.78	81000	76.85
28000	189.61	56000	324.98	84000	27.47
29000	185.19	58000	216.3	87000	27.43
30000	81.54	60000	141.59	90000	34.17
31000	86.15	62000	145.32	93000	11.28
32000	106.57	64000	90.22	96000	12.21
33000	72.44	66000	88.17	99000	13.66
34000	47.23	68000	59.42	102000	0
35000	31.44	70000	49.8	105000	0
36000	33.49	72000	45.99	108000	0
37000	22.27	74000	26.37	111000	0
38000	19.37	76000	25.89	114000	0
39000	12.32	78000	13.85	117000	0
40000	11.21	80000	45.25	120000	0

Step 3. Determine axle spectrum over time.

The traffic spectrum for any year is computed using the linear growth model.

$$NA_{ijk} = DNA_{ij1} \times (1 + \text{AGE} * \text{LGR}) \qquad (57)$$

where:

NA_{ijk} is the number of axles of type *i* (single, tandem, or tridem) and weight j for year k

LGR is the linear traffic volume growth factor

AGE is the, pavement age in years.

6.4.2.3 Pavement Structure Input

6.4.2.3.1 UNBONDED OVERLAY CONCRETE LAYER

To predict cracking, the user provides the unbonded overlay thickness and 28-day concrete flexural strength, MR. The concrete coefficient of thermal expansion, Poisson's ratio, and unit weight are assumed to be equal to 5.5×10^{-6} 1/°F, 0.18, and 0.087 lb/in³, respectively. The concrete strength parameter is used to predict both concrete modulus of rupture and modulus of elasticity every year of the pavement life. The flexural strength for the *k-th* year of the pavement life is predicted using the following model adapted from the model proposed by Rao et al. (2012):

$$MR\,(Age) = \; MR_{28\,days} + (88.3 + 35.4Ln\left(Age - 1 + \frac{1}{12}\right)) \qquad (58)$$

where:

MR(Age) is concrete flexural strength, psi;

     Age is concrete age in years,

$MR_{28\,days,}$ is concrete flexural strength at 28 days, psi.

The concrete overlay modulus of elasticity is predicted using the *MEPDG* default relationship between the concrete modulus of elasticity and flexural strength:

$$E_k = 6000\,MR_k \qquad (59)$$

6.4.2.3.2 INTERLAYER

The user has an option to select an asphalt or fabric interlayer. Depending on the interlayer type, the following Totski interlayer stiffnesses are used in the cracking analysis:

- Asphalt interlayer: $k_{Tot} = 3500$ psi/in
- Fabric interlayer: $k_{Tot} = 425$ psi/in

The interlayer type also affects the erosion factor use for nighttime condition damage. For the asphalt interlayer, the erosion factor, ER, is determined as follows:

$$ER = C_{E1}\,L\,e^{C_{E2}EROSION} \qquad (60)$$

where C_{E1} and C_{E2} are calibration parameters equal to 0.0000002 and 140, respectively, L is joint spacing, and $EROSION$ is the erosion parameter from the faulting model for unbonded overlay:

$$EROSION = \begin{cases} (1.8483 * \alpha^2 - 0.8179 * \alpha + 0.1123) & Asphalt\ Interlayer \\ 0.02 & Non\ woven\ geotextile\ fabric\ \text{Interlayer} \end{cases}$$

where α is the erodibility index:

$$\alpha = \log(1 + a * (5 - \%Binder) + b * (10 - \%AV) + c * P_{200}) \qquad (61)$$

$\%Binder$ is the binder content of the interlayer (%), $\%AV$ is the air voids percentage for the interlayer, P_{200} is percent aggregate passing No. 200 sieve in interlayer, and a, b, c = calibration coefficients are equal to 0.14, 0.15, and 0.04, respectively.

6.4.2.3.3 DESIGN FEATURES

For cracking prediction, the user should provide joint spacing in the unbonded overlay, dowel diameter, and shoulder type.

Joints Spacing

If a joint spacing is equal or greater than 12 ft, then the slab width is assumed to be equal to 12 ft and the rapid solution for conventional width slabs is used. If the joint spacing is assigned to be less 12 ft, then the 6 ft by 6ft slab size is assumed and the corresponding rapid solutions are used.

Dowel Diameter

Based on the dowel diameter, the transverse joint load transfer efficiency is selected to be used in the stress analysis according to Table 21:

Table 21: Assumed transverse joint LTE in the cracking model stress analysis

Dowel Diameter, in	LTE, %		
	$h_{OL} < 7\ in$	$7\ in \leq h_{OL} < 9\ in$	$h_{OL} \geq 9\ in$
Undoweled	20%	20%	20%
1 in	95%	70%	20%
1.25 in	95%	95%	70%
1.5 in	95%	95%	95%

Shoulder type

Depending on the shoulder type selected by the user, the following load transfer efficiency of the overlay lane and shoulder are selected:

- Tied PCC shoulder: 50%
- Asphalt shoulder on non-tied PCC shoulder: 20%.

6.4.2.4 Cracking Prediction Procedure

This section presents the step-by-step procedure for predicting unbonded overlay cracking. The steps involved include the following:

1. Tabulate input data – summarize all inputs needed for predicting JPCP cracking.
2. Process traffic– the processed traffic data needs to be further processed to determine equivalent number of single, tandem, and tridem axles produced by each passing of tandem or tridem, axle.
3. Process pavement temperature profile data – the hourly pavement temperature profiles generated using EICM (nonlinear distribution) need to be converted to distribution of equivalent linear temperature differences by calendar month.
4. Calculate stress – calculate stress corresponding to each load configuration (axle type for bottom-up and axle spacing for top-down), load level, load position, and temperature difference for each month within the design period.
5. Calculate fatigue damage – calculate damage for each damage increment and sum up to determine total bottom-up and top-down damage at the overlay/shoulder joint and transverse joint.
6. Determine the amount of slab cracking.

Step 1: Tabulate input data

The procedure begins with tabulation of all inputs required for UBOLDesign cracking prediction. The required parameters are summarized in Table 22. In addition to the inputs listed in this table, the processed inputs from Steps 2, 3, and 4 below are needed for the fatigue analysis of UBOLDesign.

Table 22: Summary of input parameters for unbonded overlay cracking prediction

Input	Variation*	Source
Design life (yr)	Fixed	Direct design input
Axle spectrum	Design year	Result of traffic volume and growth factor input processing
PCC overlay temperature frequency distribution	Design year	Result of pavement location input processing
PCC overlay strength for year	Design year	Result of overlay PCC strength input processing
PCC overlay modulus for each year (psi)	Design year	
Joint Spacing (ft)	Fixed	Direct design input
Dowel diameter (in)	Fixed	Direct design input
Lane-shoulder deflection LTE (%)	Fixed	Direct design input
Interlayer type	Fixed	Direct design input
Existing pavement thickness	Fixed	Direct design input

Input	Variation*	Source
Existing pavement modulus (psi)	Fixed	Direct design input
Slab width (ft)	Fixed	Results of joint spacing processing

Step 2: Process traffic data

The traffic inputs are first processed to determine the expected number of single, tandem, and tridem axles for each year. For bottom-up transverse cracking damage, each passing of an axle may cause one or more occurrences of critical loading. The *MEPDG* procedure for conversion of each passing of an axle to an equivalent number of single and tandem axles for bottom-up damage computation was adapted in this study.

For conventional width overlays, the conversion procedure for various axle types is illustrated in Figure 71:

- One actual single axle is effectively equal to one application of a single axle of the same load (Figure 71a).
- One actual tandem axle is effectively equal to two applications of a tandem axle of the same load at the positions shown in Figure 71b.
- One actual tridem axle is effectively equal to two tandem axles with two-thirds of the total load (Figure 71c).

Denote, $\overline{NA}_{ijk}$ is the adjusted number of applications of axles of type *i* (single or tandem) with weight *j* kips for year *k*. Then this quantity is computed as follows:

$$\overline{NA}_{1jk} = NA_{1jk},,,,,j = 3, 4, ..40$$

$$\overline{NA}_{2jk} = 2 \times (NA_{2jk} + NA_{3jk}),, j = 3, 4, ..40$$

(62)

For top-down cracking, the number of loadings was estimated by adding the number of tandem and single axles with a half-load of the tandem load.
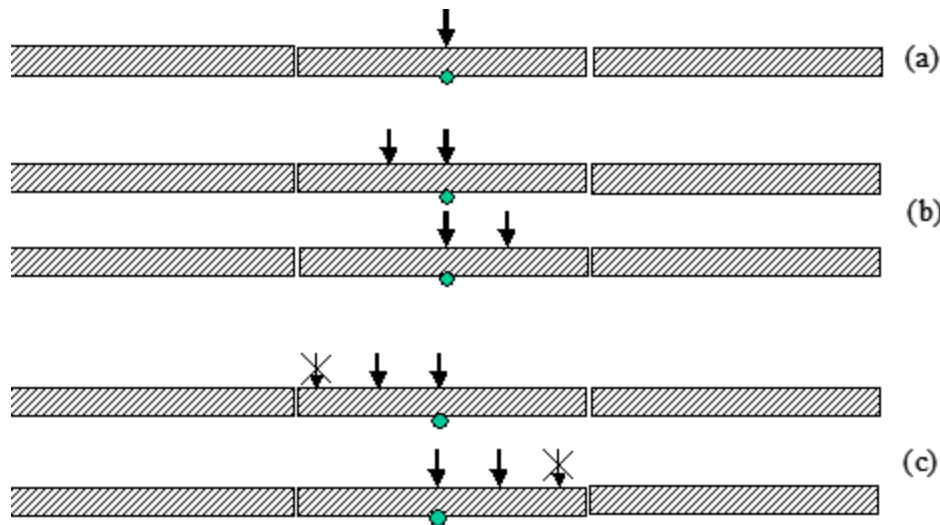
Figure 71: Accounting for different axle types in JPCP bottom-up cracking damage accumulation: (a) single, (b) tandem, and (c) tridem (NCHRP 2004).

Step 3: Process temperature profile data

The EICM produces temperatures at evenly spaced points throughout the thickness of the unbonded overlay with a 1-in interval. For calculation expediency, each temperature profile is converted to equivalent linear temperature gradient and a quadratic component. Then the frequency distribution of the combination of the equivalent linear temperature difference and quadratic components is determined as explained in Section 6.3.3.

The *MEPDG* procedure also splits the temperature distribution into a linear and non-linear component, but then it converts them into an equivalent temperature differences (top minus bottom) and adjusts them for built-in curling effect. In the proposed procedure, the linear temperature differences are also adjusted for built-in curling, but the non-linear (quadratic) temperature component is accounted for in the stress analysis explicitly and the adjustment for built-in curling is performed independently for the daytime and nighttime analysis. It results in the following expressions:

$$\Delta T_{Linear,day} = \left(Bh_{OL} + \Delta T_{built-in,day} \right) \tag{63}$$

$$\Delta T_{Linear,day} = \left(Bh_{OL} + \Delta T_{built-in,night} \right) \tag{64}$$

Step 4: Calculate stress

Calculate stresses for all cases that need to be analyzed:

- Pavement age – by year.
- Load configuration – axle type for bottom-up cracking.

- Load level – discrete load levels in 1,000 to 3,000 lb increments, depending on axle type.
- Temperature gradient – equivalent linear temperature difference from top to bottom with non-zero frequency.
- Lateral load position – 2 specific locations for both top-down and bottom-up cracking.
- Non-linear self-equilibrating stresses for all values of the quadratic components with non-zero frequency.

The procedures for calculation of the stresses due to combined action of the linear temperature gradients and axle loading as well as nonlinear temperature stresses are discussed in more detail in Section 6.3.3. The combined total stress for each combination of the nonlinear temperature distribution throughout the slab thickness and axle loading are determined as follows:

$$\sigma_{tot} = \sigma_{bend} + \beta \sigma_{nonlinear} \qquad (65)$$

where σ_{bend} is bending stress due to linear component of the temperature distribution and axle loading, $\sigma_{nonlinear}$ is the stress due to nonlinear component of the temperature distribution, and β is the coefficient accounting for the difference in the stress gradients throughout the slab thickness between the bending and non-linear temperature stresses. In this study, a value of $\beta = 0.5$ is used.

Step 5: Calculate fatigue damage

The following types of fatigue damage are calculated to predict cracking in the overlay:

- Overlay/shoulder joint, bottom-up
- Overlay/shoulder joint, top-down
- Transverse joint, bottom-up
- Transverse joint, top-down

Overlay/shoulder joint, bottom overlay surface

As discussed in Section 6.3.2, the critical stresses at the bottom surface of the lane/shoulder joint are computed in the mid-slab location. These stresses are used to compute bottom-up fatigue damage at the overlay/shoulder joint based on Miner's linear fatigue accumulation hypothesis:

$$FD_{Bot,OS} = \sum_{k=1}^{DLife} \sum_{j=1}^{2} \sum_{i=3}^{40} \sum_{wp=1}^{nWp} \sum_{nb=1}^{Nbp} \sum_{tn=1}^{tNp} \frac{n_{k,j,i,wp,nb,tn}}{N\left(\frac{\sigma_{k,j,i,wp,tg,tn}}{MR_k}\right)} \qquad (66)$$

where:

$FD_{Bot,OS}$ is the total overlay/shoulder joint fatigue damage (bottom-up).

$n_{k,j,i,wp,nb,tn}$ is the applied number of load applications in year *k*, of type *j* (single or tandem), axle weight *i*, linear temperature gradient *nb,* and quadratic component *tn*.

$N(\sigma/MR)$ is the allowable number of load applications at the stress level, $N\left(\frac{\sigma_{k,j,i,tg,tn}}{MR_k}\right)$.

$\sigma_{j,i,wp,tg,tn}$, is the mid-slab overlay stress at the bottom surface computed for the concrete properties predicted for year k, from the load of type j (single or tandem), axle weight i, wheel path wp, linear temperature gradient tg, and quadratic component tn.

Dlife is the design life, years.

nWp is the number of wheel paths.

Nbp is number of positive values of linear temperature gradients with non-zero frequencies.

Np   is the number of quadratic terms corresponding to positive values of linear temperature gradients with non-zero frequencies.

The number of load applications $n_{k,j,i,wp,nb,tn}$ is computed as follows:

$$n_{k,j,i,wp,nb,tn} = \overline{NA}_{ijk} \times \chi_{wp} \times \psi_{nb,tn} \qquad (67)$$

where:

$\overline{NA}_{ijk}$ is the adjusted number of applications of axles of type i (single or tandem) with weight j kip for year k.

χ_{wp} is the percentage of traffic assigned to a certain traffic wander position: 3% for the wheel path 1 (closest to the edge) and 17% for the wheel path 12 in away from the joint for the overlay with a ties shoulder and 2% and 18% for these wheel paths for other shoulder types.

$\psi_{nb,tn}$ is the frequency of the temperature gradient B_{nb} and the quadratic term, C_{tn}, as illustrated in Table 19.

The *MEPDG* model for the allowable number of the load repetitions along with the *MEPDG* default values were adopted for this procedure.

Overlay/shoulder joint, top overlay surface

As discussed in Section 6.3.2, the critical stresses at the top surface of the lane/shoulder joint and at the transverse joint are computed using two assumptions: (a) there are no permanent voids under the unbonded overlay and (b) there is a 2 ft-wide permanent void under the overlay on the leave side of the transverse joint. These stresses are used to compute bottom-up fatigue damage with the following approach:

$$FD_{Bot,OS} = \sum_{k=1}^{DLife} \sum_{j=1}^{2} \sum_{i=3}^{40} \sum_{wp=1}^{nWp} \sum_{nb=1}^{Nbp} \sum_{tn=1}^{tNp} \left[(1-\xi) \frac{n_{k,j,i,wp,nb,tn}}{N\left(\frac{\sigma'_{k,j,i,wp,tg,tn}}{MR_k}\right)} + \xi \frac{n_{k,j,i,wp,nb,tn}}{N\left(\frac{\sigma''_{k,j,i,wp,tg,tn}}{MR_k}\right)} \right]$$

$$(68)$$

125

where:

$FD_{Bot,OS}$ = total fatigue damage (bottom-up).

$n_{k,j,i,wp,nb,tn}$ = applied number of load applications in year k, of type j (single or tandem), axle weight i, wheel path wp, linear temperature gradient nb, and quadratic component tn.

$N(\sigma)$ = allowable number of load applications at the stress level, $N\left(\frac{\sigma_{k,j,i,tg,tn}}{MR_k}\right)$

$\sigma'_{j,i,wp,tg,tn}$, = mid-slab overlay stress at the top surface computed if there is no permanent void under the overlay with concrete properties predicted for year k, from the load of type j (single or tandem), axle weight i, wheel path wp, linear temperature gradient tg, and, quadratic component tn.

$\sigma''_{j,i,wp,tg,tn}$, = mid-slab overlay stress at the bottom surface computed if there is a, permanent void under a transverse joint of the overlay with concrete properties predicted for year k, from the load of type j (single or tandem), axle weight i, wheel path wp, linear temperature gradient tg, and, quadratic component tn.

ξ = interlayer erosion damage estimated as follows:

$$\xi = e^{-ER\,k} \tag{69}$$

where k is the overlay age.

Transverse joints fatigue damage

The process used for computing damage at the top surface of the overlay/shoulder joint, was used to determine damage at the top and bottom overlay surfaces of the transverse joint.

Step 6: Determine the amount of slab cracking

The percentage of cracked slabs is then computed using the following equations:

$$OLCRAK = \left(CRACK_{JC} + CRACK_{EC} - CRACK_{JC}CRACK_{EC}\right) \times 100\% \tag{70}$$

where:

$OLCRAK$ = percentage of cracked overlay slabs

$CRACK_{JC}$, and $CRACK_{TC}$ = predicted amount (fraction) of overlay cracking, initiated at transverse joints and slab edge, respectively, determined as follows:

$$CRACK_{JC} = \left(CRACK_{JB} + CRACK_{JT} - CRACK_{JB}CRACK_{JT}\right) \times 100\% \qquad (1)$$

$$CRACK_{EC} = \left(CRACK_{EB} + CRACK_{ET} - CRACK_{EB}CRACK_{ET}\right) \times 100\%$$

and

$$CRACK_{JB} = \frac{100\%}{1 + C_4 FD_{JB}^{C5}}$$

$$CRACK_{JT} = \frac{100\%}{1 + C_4 FD_{JT}^{C5}}$$

$$CRACK_{EB} = \frac{100\%}{1 + C_4 FD_{EB}^{C5}} \qquad (71)$$

$$CRACK_{ET} = \frac{100\%}{1 + C_4 FD_{WT}^{C3}}$$

where C_4 and C_5 are calibration coefficients.

This cracking calculation procedure is a generalization of the cracking calculation procedure proposed under the NCHRP 1-37A project and currently used in Pavement ME Design program. The procedure implies that a slab can be cracked due to accumulation of damage at four critical locations (top or bottom overlay surfaces, overlay/shoulder or transverse joints), but a slab cannot be counted as cracked more than once.

6.5 IMPLEMENTATION OF THE CRACKING MODEL IN THE RUDIMENTARY SOFTWARE

To facilitate implementation of the model, a rudimentary software was developed. The program incorporates the frequency tables of the coefficients of the quadratic temperature distributions throughout the overlay thickness for 68 locations throughout the United States. These tables were created based on the results of the EICM analysis for the overlay thicknesses of 4, 6, 8, and 10 in.

The following procedure for predicting cracking in an unbonded overlay was developed:

Step 1. For every design increment (i.e., 1 year) compute damages at four locations for PCC overlay thicknesses of 6, 8, and 10 in if the overlay joint spacing is greater than or equal to 12 ft or 4, 6, and 8 in if the overlay joint spacing is 6 ft.

Step 2. For each year, compute fatigue damages at the top and bottom of the overlay surface at the lane/shoulder and transverse joint locations. If the overlay joint spacing is not less than 12 ft and the

overlay thickness is less than 10 in or if the overlay joint spacing is equal to 6 ft and the overlay thickness is less than 8 in, the following equation is used:

$$Dam(h_{OL}) = \exp(L_{12}(h_{OL})\ln(Dam_{h1}) + L_{22}(h_{OL})\ln(Dam_{h2}) + L_{32}(h_{OL})\ln(Dam_{h3}))$$
$$(72)$$

where:

Dam_{h1}, Dam_{h2} and Dam_{h3} are fatigue damages for overlay thicknesses h_1, h_2, and h_3, respectively;

h_1, h_2, and h_3 are equal to 6, 8, and 10 in, respectively, if the overlay joint spacing is greater or equal to 12 ft and 4, 6, and 8 in, respectively, if the overlay joint spacing is equal to 6 ft,

L_{12}, L_{22}, and L_{32} are the Lagrange quadratic shape functions:

$$L_{12}(h_{OL}) = \frac{(h_{OL}-h_2)(h_{OL}-h_3)}{(h_1-h_2)(h_1-h_3)}$$

$$L_{22}(h_{OL}) = \frac{(h_{OL}-h_1)(h_{OL}-h_3)}{(h_2-h_1)(h_2-h_3)} \qquad (73)$$

$$L_{32}(h_{OL}) = \frac{(h_{OL}-h_1)(h_{OL}-h_2)}{(h_3-h_1)(h_3-h_2)}$$

If the overlay joint spacing is not less than 12 ft and the overlay thickness is greater than 10 in, or if the overlay joint spacing is equal to 6 ft and the overlay thickness is greater than 8 in, the following equation is used:

$$Dam(h_{OL}) = \exp((\ln(Dam_{h3}) - \ln(Dam_{h2}))/(h_3 - h_2) + \ln(Dam_{h3})) \qquad (74)$$

Step 3. Using the fatigue damages determined in step 2, compute cracking in the overlay using equations (55) through (57).

6.5.1 Cracking Model Calibration and Validation

The transverse cracking model described in the section above was calibrated using the LTPP projects in the AASHTO M-E calibration database (Sachs et al., 2014). Table 23 summarizes the design features for the sections used in the calibration.

Table 23: Calibration sections

LTPP Section ID	Age at the time of observation	Initial AADTT	Percent of cracked slabs	Overlay thickness, in	PCC overlay flexural strength, psi	Overlay joint spacing (in)	Dowel diameter (in)	Tied PCC Shoulder	Existing pavement thickness	Existing pavement PCC modulus of elasticity
069048	21.1	850	3.1	6.4	680	186	0	No, AC	8.1	4.00E+06
069048	26.3	850	28.6	6.4	680	186	0	No, AC	8.1	4.00E+06
069048	28.3	850	46.9	6.4	680	186	0	No, AC	8.1	4.00E+06
069049	23.6	400	61.3	7.5	700	186	0	No, AC	7.7	4.00E+06
069049	30.4	400	62.5	7.5	700	186	0	No, AC	7.7	4.00E+06
069107	3.77	2,000	0	8.8	530	162	none	No, AC	7.6	4.75E+06
069107	8.93	2,000	0	8.8	530	162	none	No, AC	7.6	4.75E+06
089019	12.5	1,500	13.9	9	480	156	none	No, PCC	7.9	3.50E+06
089020	11.9	1,500	8.2	8	480	240	none	Yes	7.7	3.68E+06
189020	7.57	3,500	3.1	10.2	541	186	0	No, AC	10.2	4.23E+06
189020	12.2	3,500	3.1	10.2	541	186	0	No, AC	10.2	4.23E+06
209037	16.4	480	42	5.8	750	180	0.5	No, Granular	8.8	4.88E+06
279075	18.4	103	3.1	5.9	714	186	none	No, AC	7.8	3.70E+06
287012	8.04	8,078	0	10	1022	252	1	No, AC	9.4	5.00E+06
287012	14.6	8,078	4.2	10	1022	252	1	No, AC	9.4	5.00E+06
316701	11.1	300	3.3	8	595	174	none	Yes	7.5	3.75E+06
489167	3.08	3,580	0	10.2	858	180	1.25	No	8.4	4.85E+06
489167	5.15	3,580	0	10.2	858	180	1.25	No	8.4	4.85E+06
489167	7.04	3,580	0	10.2	858	180	1.25	No	8.4	4.85E+06
489167	9.97	3,580	0	10.2	858	180	1.25	No	8.4	4.85E+06
489167	12.6	3,580	0	10.2	858	180	1.25	No	8.4	4.85E+06
899018	7.87	300	3.3	6.4	810	195.6	none	No, AC	8.9	2.80E+06
899018	10.8	300	6.5	6.4	810	195.6	none	No, AC	8.9	2.80E+06

The nonlinear optimization was conducted to minimize the sum of squared differences between the observed and predicted cracking. It involved conducting cracking predictions for the sections used in the calibration for a wide range of the calibration coefficients and selecting the set of the coefficients that would minimize the discrepancy between the predicted and measured values. The resulting cracking model has the following form:

$$CRACK_L = \frac{100\%}{1+1.375\ FD^{-2}} \tag{75}$$

Figure 72 presents a comparison of the calibrated cracking model predictions with the measured cracking. It can be observed that the model shows a reasonably good fit of the field data and does not exhibit a bias in predictions.
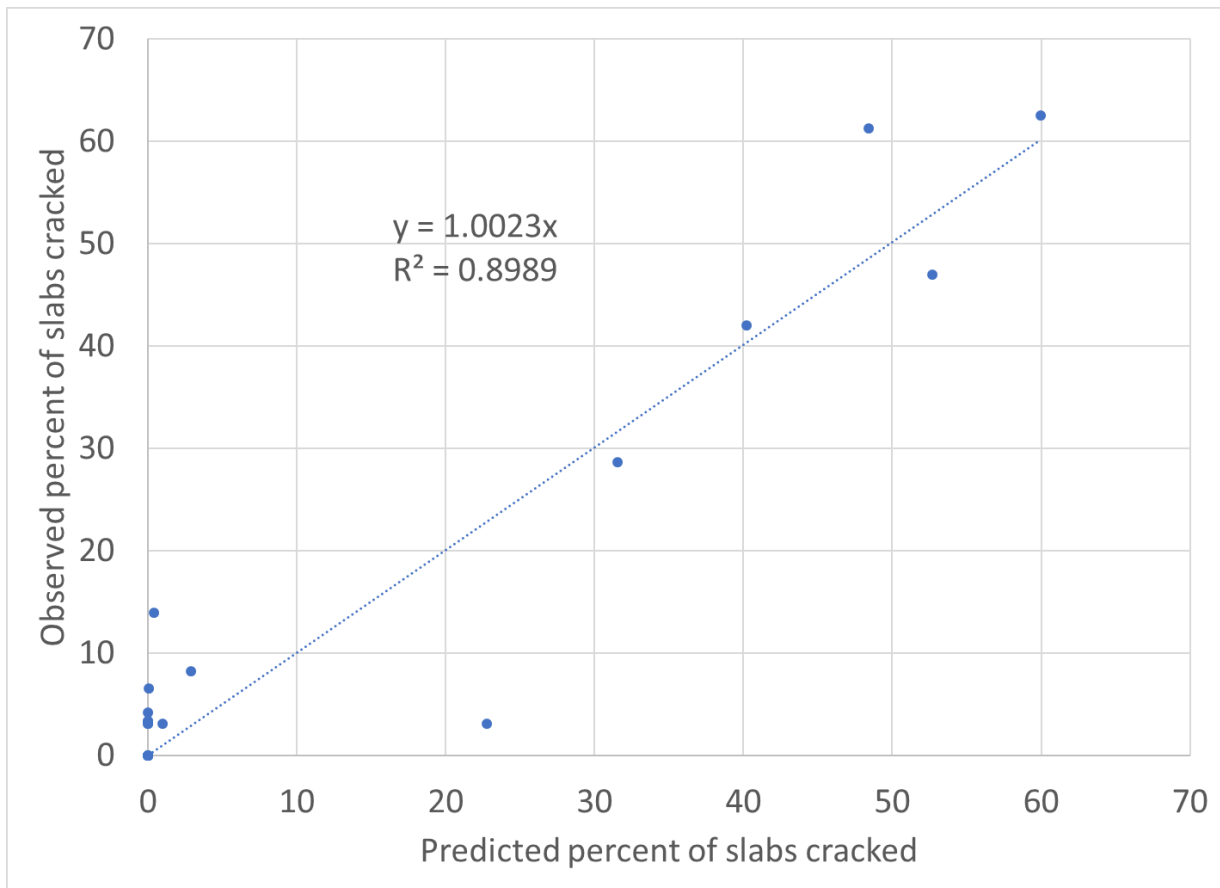
Figure 72: UBOL cracking model predictions compared to LTPP observations

A sensitivity analysis of the predicted cracking to various parameters of interest was conducted to further evaluate the model. The base design parameters in this study were selected the same as those used in the evaluation of the Pavement ME unbonded overlay cracking predictions in Section 2: 8-in thick undoweled PCC overlay with a modulus of rupture of 650 psi, 1-in dense graded asphalt interlayer, 8-in thick existing

PCC with an elastic modulus of $4*10^6$ psi,15-ft joint spacing, asphalt shoulder, and two-way initial AADTT of 8,000.

Figure 73 shows predicted cracking for the overlay thickness of 6, 8, and 10 in computed for undoweled overlays and the overlays with 1-in dowels. Unlike Pavement ME, the proposed procedure predicts that the use of dowels will reduce cracking, because dowels reduce potential of both longitudinal and corner cracking initiated at the transverse joint. While Pavement ME predicts non-monotonic relationship between the overlay thickness and cracking (see Figure 41), the proposed procedure predicts that an increase in overlay thickness will reduce cracking.
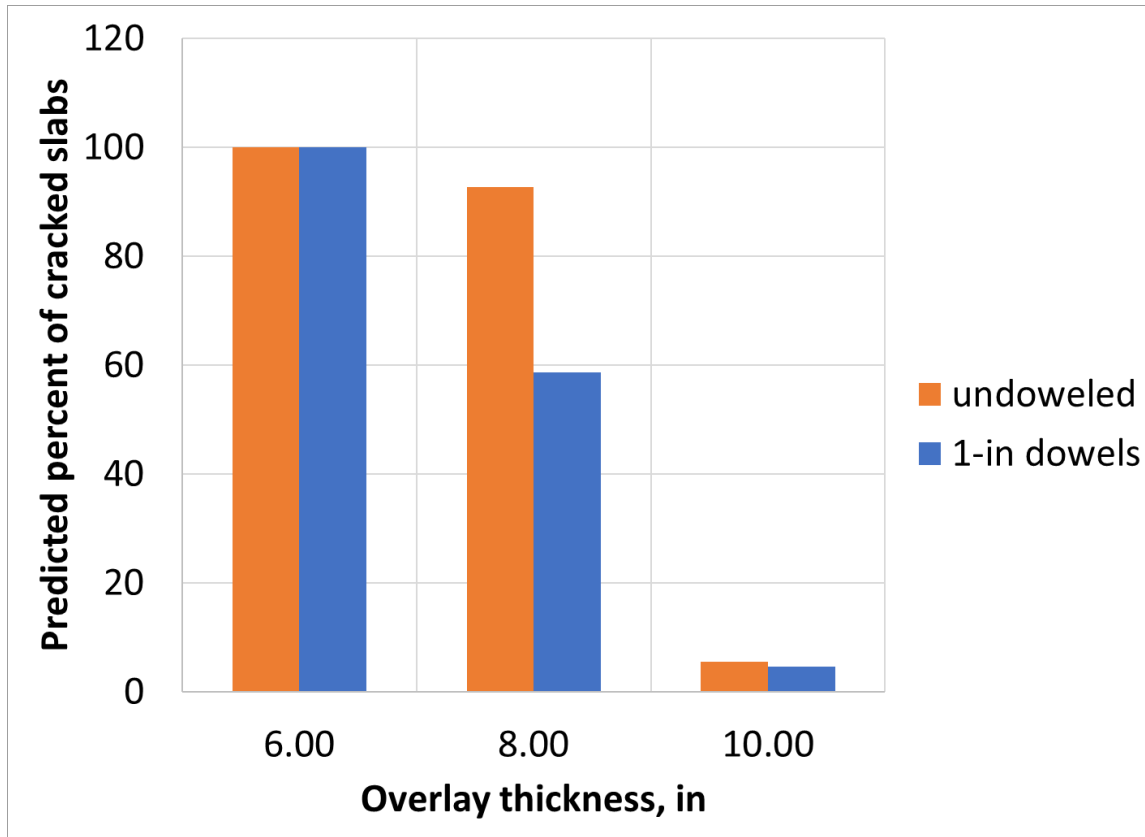
Figure 73: Effect of overlay thickness on predicted cracking

The effect of traffic volume and joint spacing on cracking is illustrated in Figure 74. It can be observed that an increase in traffic volume increased predicted cracking. For each traffic volume level, predictions for an overlay with 12-ft joint spacing resulted in a lower cracking than for the overlay with 15-ft joint spacing. Figure 75 compares predicted cracking for an HMA and fabric interlayer. The fabric interlayer resulted in a slightly lower cracking level. Figure 76 shows the effect of dowel diameter and shoulder type on the predicted cracking. It can be observed that an increase in dowel diameter and the presence of a tied PCC shoulder decrease cracking. Analysis of these sensitivity plots suggests that exhibited predictions have reasonable trends.
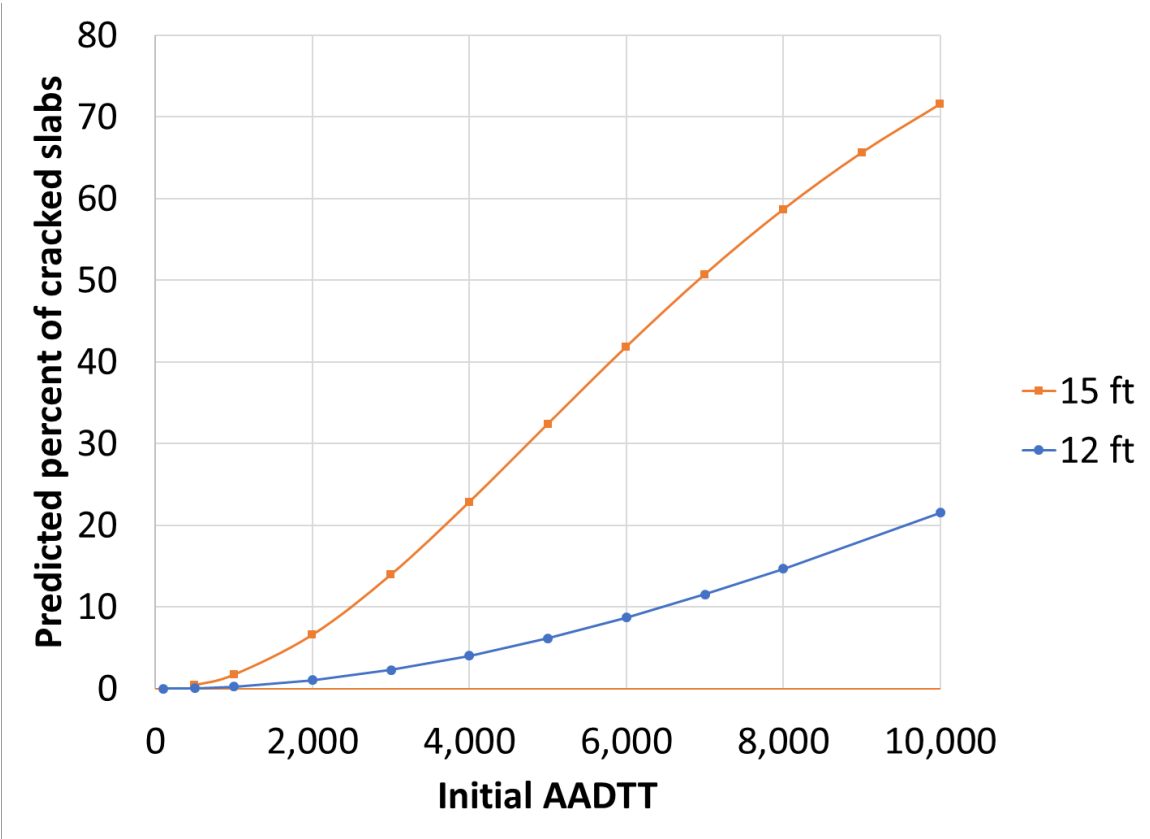
Figure 74: Effect of traffic volume and joint spacing on predicted cracking
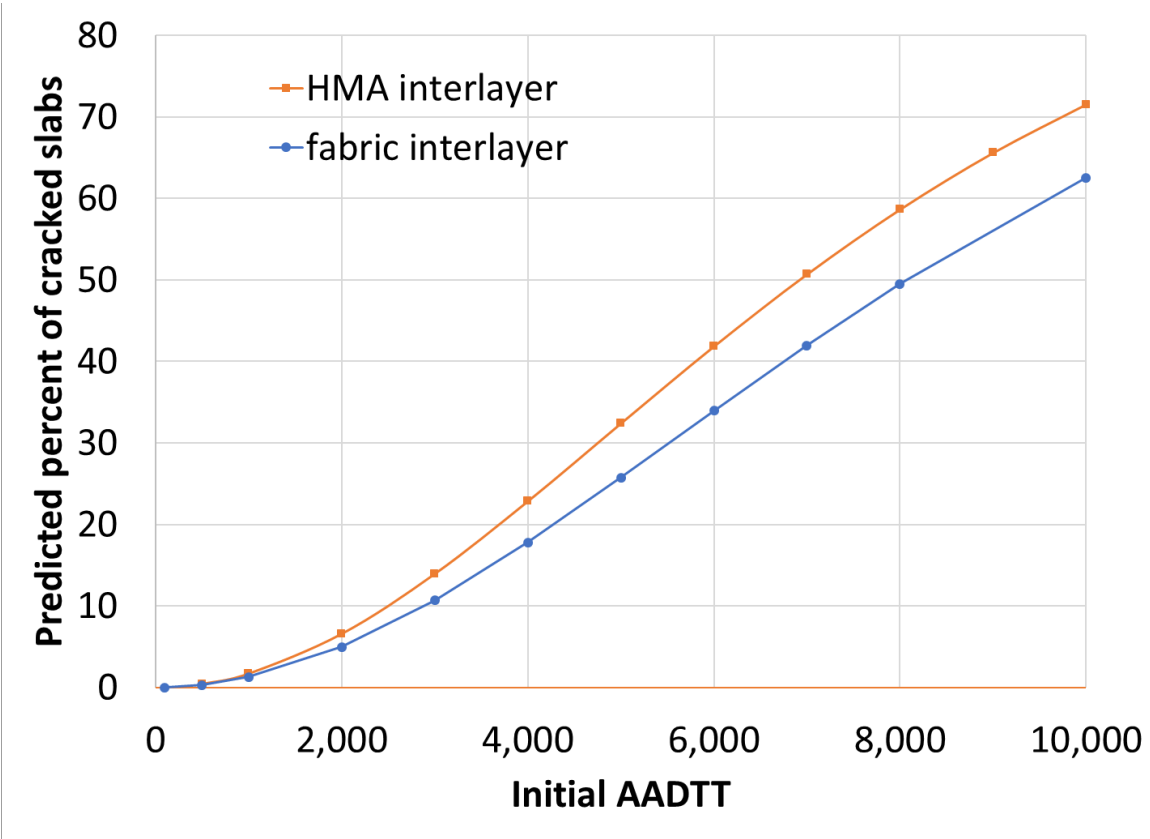
Figure 75: Effect of interlayer type on predicted cracking
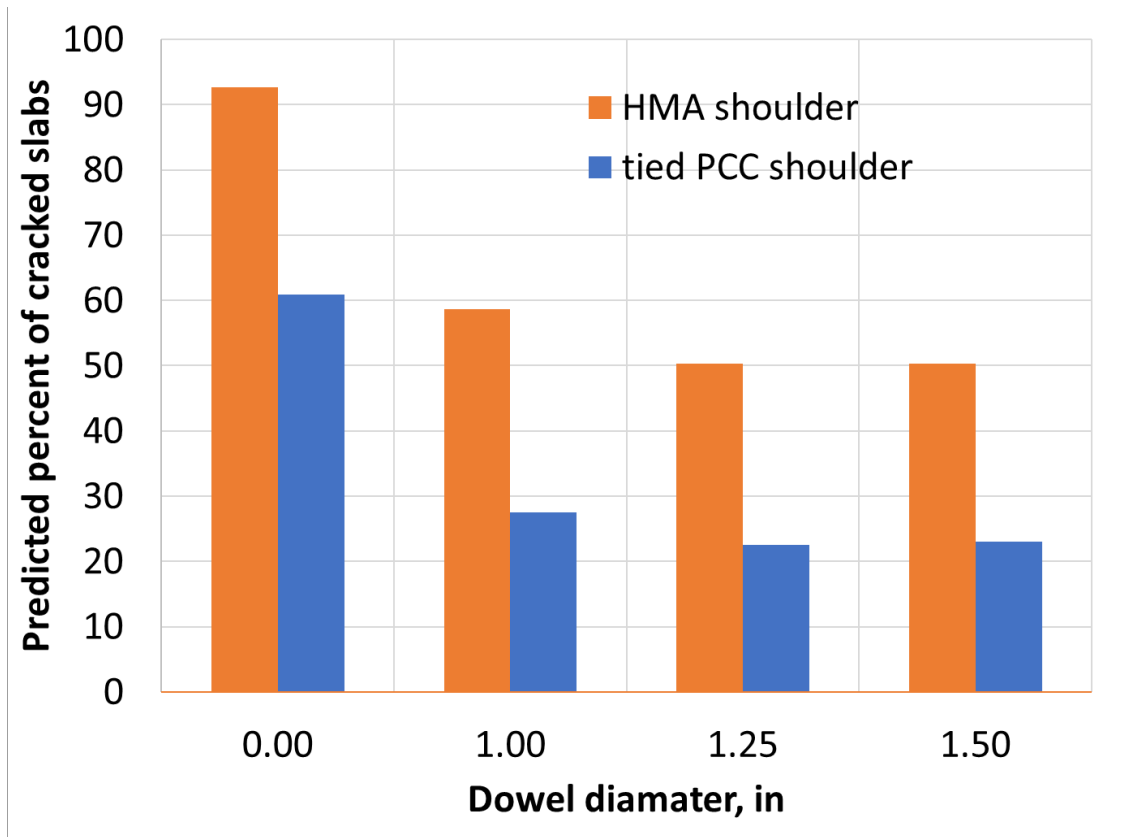
Figure 76: Effect of shoulder type and dowel diameter on predicted cracking

6.5.2 Reliability Analysis and As-Built Variation

The procedure described above allows the designer to predict cracking for a given set of the design parameters. However, it can be observed from Figure 72 that the actual data are scattered about the line representing the final calibrated–validated model. The calibration of the procedure ensured only the unbiased nature of the model, i.e., some of the observation points used in the calibration were above the equality line and some were below it. The *MEPDG* reliability design is obtained by determining the predicted cracking at the desired level of reliability *p* as follows (NCHRP 2004, Darter et al., 2005):

$$CRACK\_P = CRACK + STD_{CR} * Z_P \qquad (76)$$

where:

   CRACK = predicted cracking based on mean inputs (corresponding to 50% reliability), percent of slabs.

STD$_{CR}$ = standard deviation of cracking at the predicted level of mean cracking

Z_p =   standardized normal deviate (mean 0 and standard deviation 1) corresponding to reliability level *p*

A major deficiency in the *MEPDG* is that its reliability analysis does not relate the reliability level with variation in key design inputs (NCHRP 2004, AASHTO 2008). In addition, the expression for the standard deviation for the unbonded overlays is not definitive due to a small number of the sections used in the model calibration. For these reasons, a simple Monte Carlo simulation approach that resembles the reliability analysis used by MnPAVE Rigid (Khazanovich et al.,, 2015) was selected.

In the procedure implemented in this study, the controlling distress for reliability is the predicted transverse cracking and the varied parameters are concrete thickness and modulus of rupture.

The recommended design thickness is the thickness value that meets the performance criteria, i.e., percentage of cracking at the specified reliability level. In addition to the design inputs required to predict cracking (except the overlay thickness), the user needs to provide the standard deviations for the flexural strength and the overlay thickness. The following analysis is then performed:

1. Assume the minimum overlay thickness allowed by the procedure (6 in if the joint spacing is greater than 12 ft or 4 in if the joint spacing is equal to 6 ft).
2. Generate a set of 21 values of concrete overlay flexural strength normally distributed with the mean and standard deviation values provided by the user.
3. Generate a set of 21 values of concrete overlay thickness normally distributed with the mean value selected in Step 2 and the standard deviation values provided by the user.
4. For each pair of the concrete flexural strength and thickness from the sets generated in Steps 2 and 3, respectively, predict the overlay cracking at the end of the design life.
5. Determine the percentage of pairs of the concrete flexural strength and thickness resulting in the cracking level less than the specified by the user performance threshold. This percentage is the reliability of the design with the specified cracking threshold level.
6. If the reliability of the cracking determined in Step 5 is less than the user-specified reliability level, then the mean overlay thickness is increased by 0.1 in and Steps 3 through 5 are repeated. Otherwise, the mean PCC thickness is the recommended PCC thickness.

As an example, let's predict performance of a 7-in unbonded overlay over an 8-in existing concrete pavement located in Sioux City, IA. The system has the following parameters:

- Overlay flexural strength (modulus of rupture): 650 psi
- Overlay joint spacing: 12 ft
- Overlay joints load transfer devices: 1-in dowels
- Overlay shoulder type: asphalt
- Existing overlay thickness: 10 in
- Existing PCC modulus of elasticity: 4,000,000 psi
- Interlayer type: asphalt

- o Effective binder content by volume: 5%
- o Air voids: 5%
- o Percent passing #200 sieve: 3%
- AADTT in the design lane in the first year: 1,000
- Linear yearly growth of the traffic volume: 3%
- Coefficient of variation of the PCC overlay thickness: 3%
- Coefficient of variation of the PCC flexural strength: 8.7%

The cracking model prediction for this unbonded overlay is 10.29% of the cracked slabs after 20 years of performance. To evaluate the probability that this system will exhibit less than 15% of cracked slabs, the procedure developed in this study requires simulated pavement performance of the unbonded overlay with the following parameters:

- Overlay thickness: 6.5840, 6.6923, 6.7523, 6.7968, 6.8338, 6.8661, 6.8956, 6.9231, 6.9494, 6.9749, 7.0000, 7.0251, 7.0506, 7.0769, 7.1044, 7.1339, 7.1662, 7.2032, 7.2477, 7.3077, and 7.4160 in.
- Overlay flexural strength: 537.9885, 567.1411, 583.2845, 595.2923, 605.2328, 613.9503, 621.8833, 629.2967, 636.3691, 643.2339, 650.0000, 656.7661, 663.6309, 670.7033, 678.1167, 686.0497, 694.7672, 704.7077, 716.7155, 732.8590, and 762.0116 psi

The obtained frequency distribution of percentages of cracked slabs from these 441 simulations is shown in Figure 77 and the corresponding cumulative distribution is shown in Figure 78. It can be observed that some simulations resulted in the predicted cracking of less than 2.5 percent. These cracking levels were predicted for the combinations of the overlay thickness and strength greater than the corresponding mean values. At the same time, the combinations of the overlay thickness and strength lower than the corresponding mean values resulted in cracking as high as 50 percent. The median predicted cracking is 11.51%. This means that although the deterministic prediction of cracking for a 7-in thick overlay with the flexural strength of 650 psi is 9.64%, we can say with 50% confidence that the cracking will be less than 9.64%. At the same time, 127 observations resulted in the predicted cracking greater than the target value of 15%. This means that the predicted reliability of cracking of less than 15% is 71%.
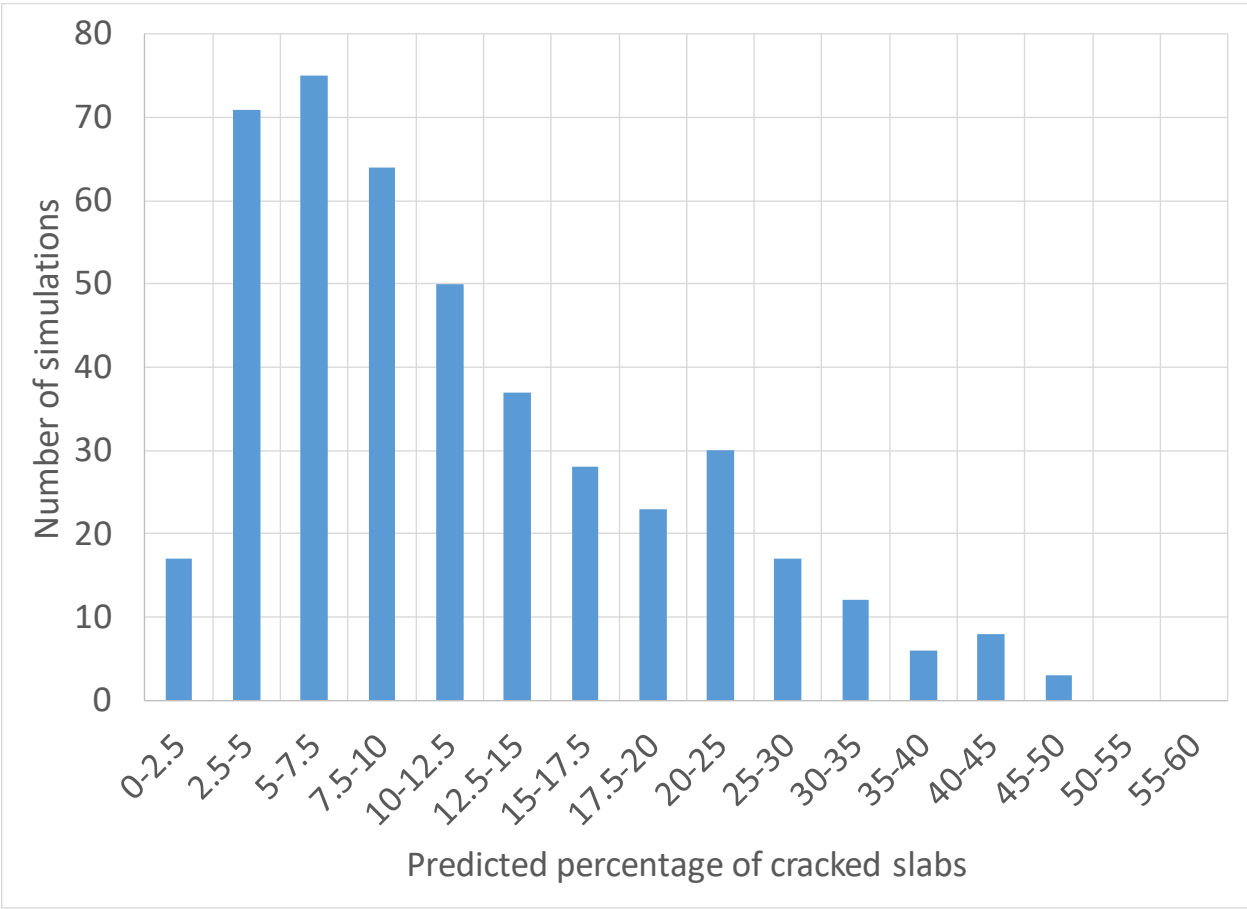
Figure 77: Predicted frequency of percentages of cracked slabs
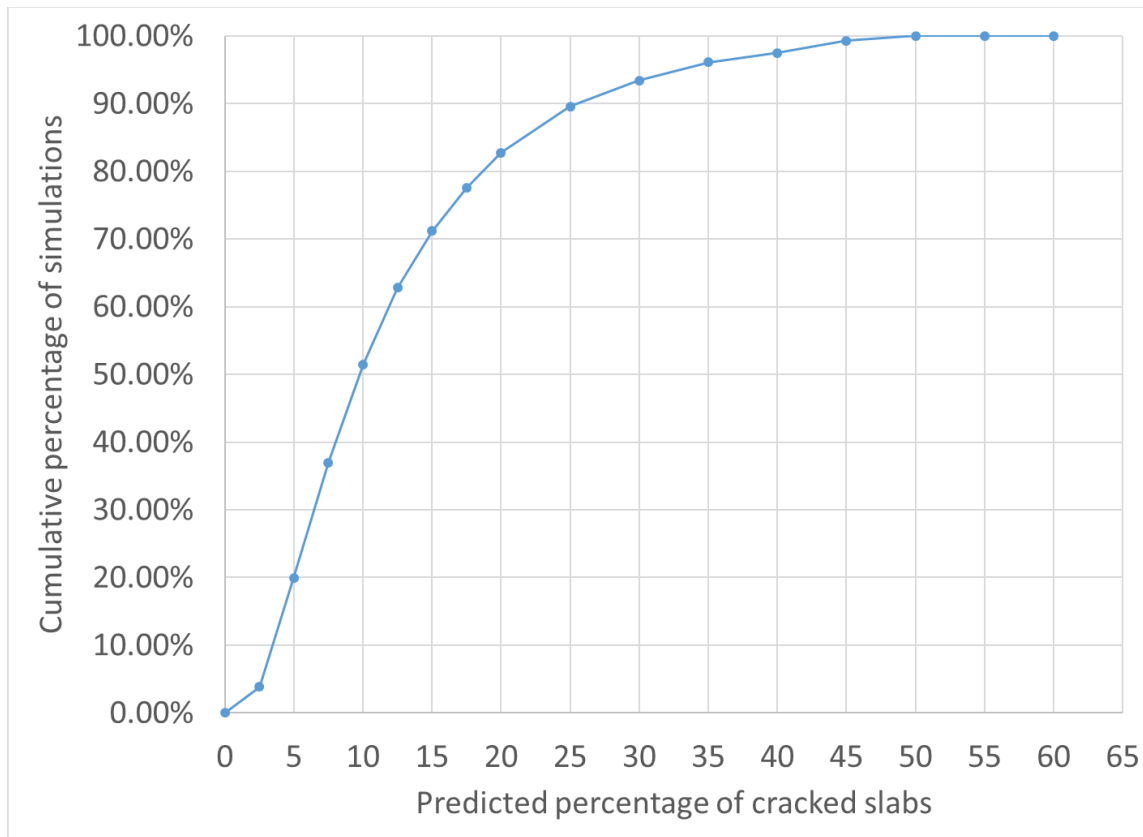
Figure 78: Predicted cumulative distribution of percentages of cracked slabs

To determine the overlay thickness required to ensure the predicted cracking at the end of the design life is less than 15% with the reliability level of 90%, the developed procedure requires the user to perform a similar analysis for each overlay thickness starting from 6 in and increasing it with increment of 0.1 in until less than 10% of the simulations predict cracking less than 15%.

Table 24 presents the results of this analysis for the overlay thickness from 6 to 7.6 in. It can be observed that if the overlay thickness is 6 in, then the predicted cracking with 90% reliability is 50.4%. To achieve the target 15% cracking with 90% reliability, a 7.5-in overlay should be used.

Table 24: Predicted cracking at 90% reliability

Overlay thickness, in	Cracking at 90% reliability
6	40.24
6.1	40.24
6.2	38.77
6.3	37.02
6.4	35.32
6.5	33.66

Overlay thickness, in	Cracking at 90% reliability
6.6	32.05
6.7	30.49
6.8	28.98
6.9	27.11
7	25.14
7.1	23.04
7.2	21.05
7.3	18.68
7.4	16.72
7.5	14.67

A sensitivity analysis of the required overlay thickness to various parameters of interest was conducted to further evaluate the procedure. The base design parameters in this study were selected similar to those used in the evaluation of the cracking predictions: PCC modulus of rupture of 650 psi, 1-in dense graded asphalt interlayer, 8-in thick existing PCC with an elastic modulus of $4*10^6$ psi, 15-ft joint spacing, 1-in dowels, asphalt shoulder, two-way initial AADTT of 8,000, and 90% reliability design to ensure predicted cracking is less than 15% at the end of the design period.

Figure 79 shows required overlay thickness for various traffic volumes and reliability levels. As expected, an increase in the traffic volume or reliability level leads to an increase in the required overlay thickness. Figure 80 presents the effect of joint spacing on the required overlay thickness. For each traffic volume level, a 12-ft joint spacing resulted in a lower required overlay thickness than the one for the overlay with a 15-ft joint spacing. Figure 81 compares required overlay thicknesses for HMA and fabric interlayers. The fabric interlayer resulted in slightly higher overlay thicknesses for low volume traffic, but in thinner overlays for high volume traffic. Figure 82 shows the effect of dowel diameter and shoulder type on the required thickness. It can be observed that an increase in dowel diameter or the presence of a tied PCC shoulder decreases the required overlay thickness.

Analysis of these sensitivity plots suggests that exhibited predictions have reasonable trends. The only exception is the reduction of the required overlay thickness for heavy volume traffic if a fabric interlayer is used instead of an HMA interlayer. Due to lack of long-term performance data for unbonded overlays with fabric interlayer under heavy traffic, this trend cannot be confirmed or disproved.
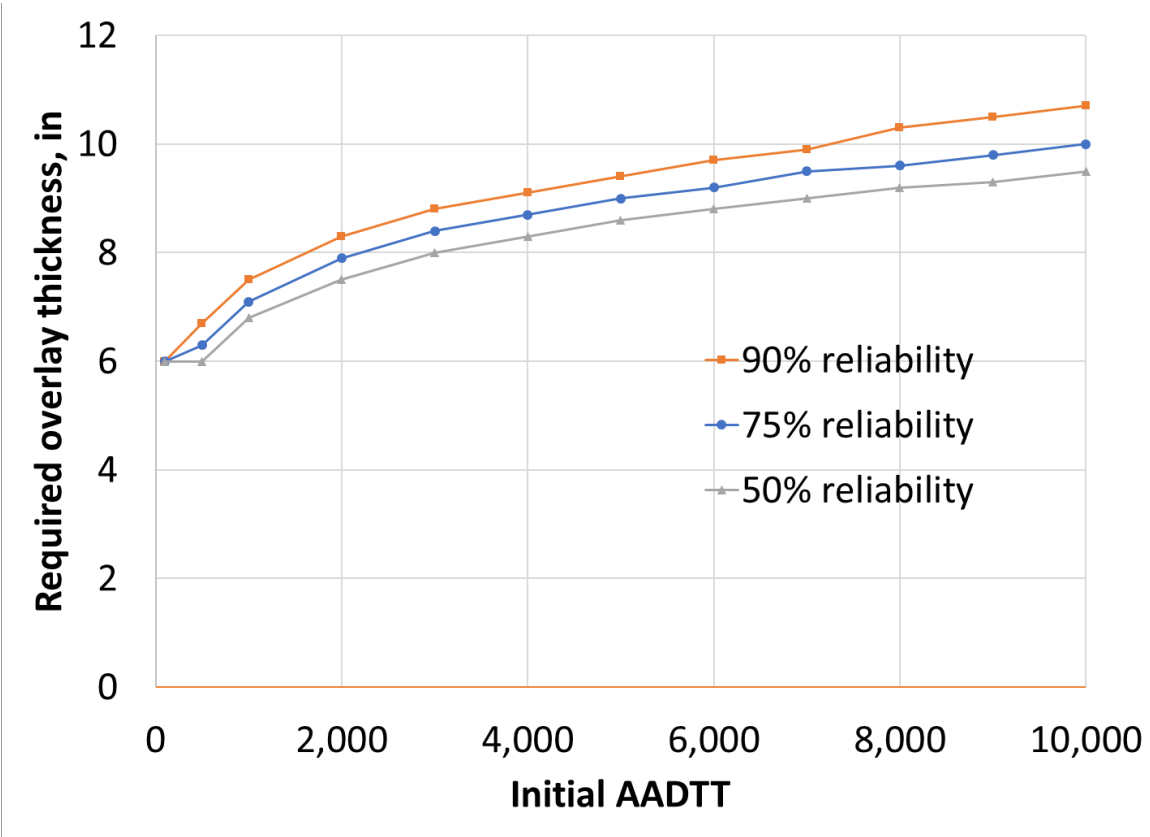
Figure 79: Effect of reliability revel on required overlay thickness
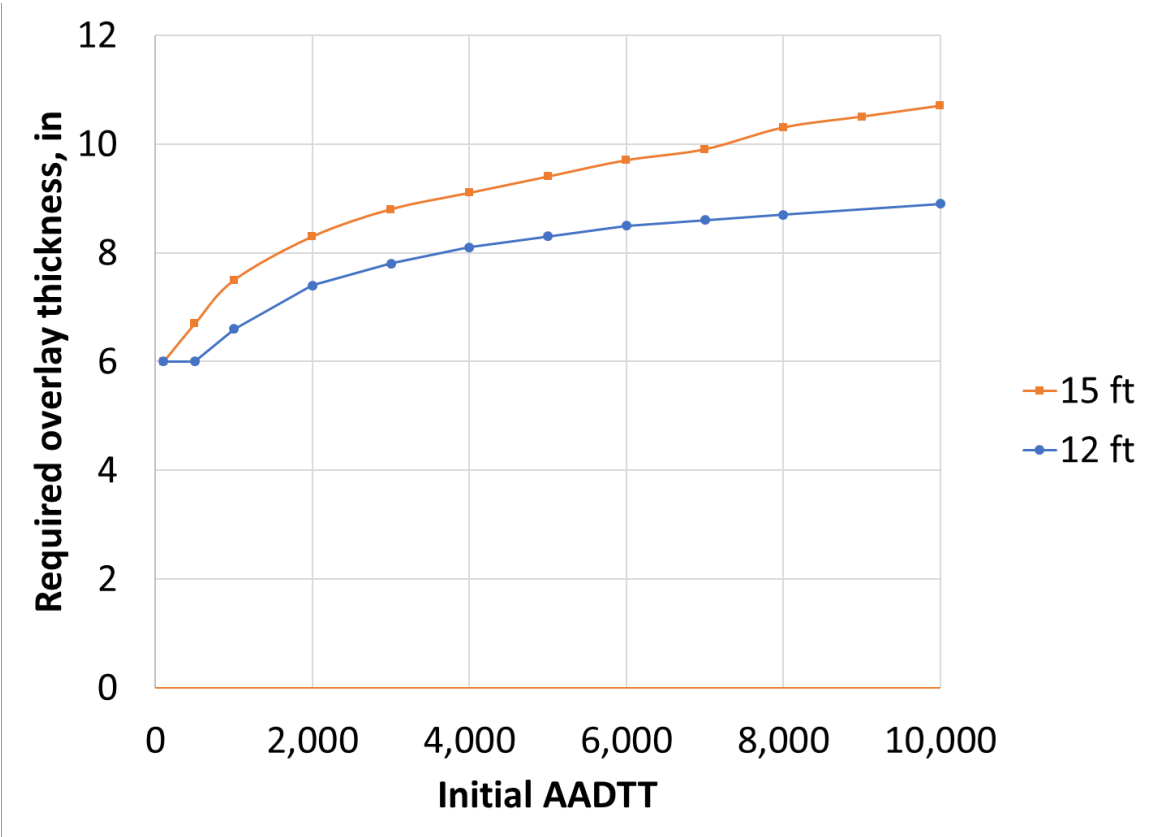
Figure 80: Effect of traffic volume and joint spacing on required overlay thickness
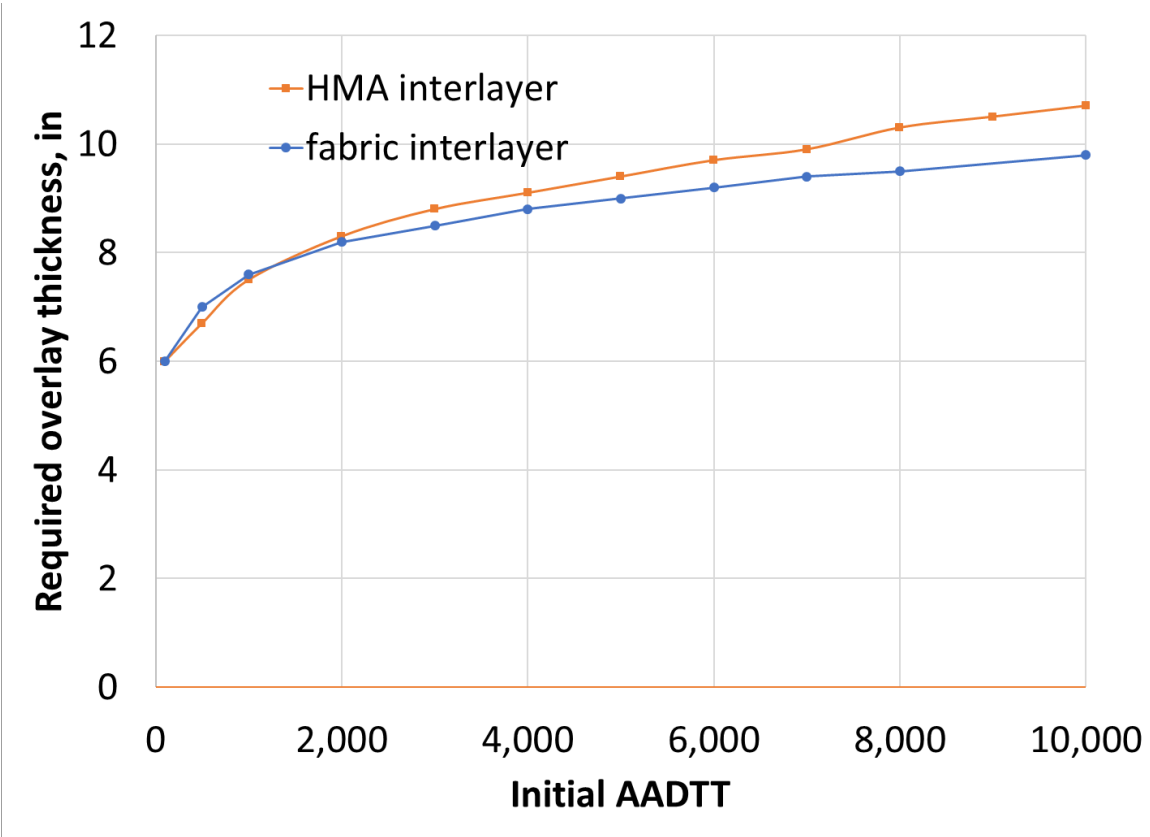
Figure 81: Effect of interlayer on required overlay thickness
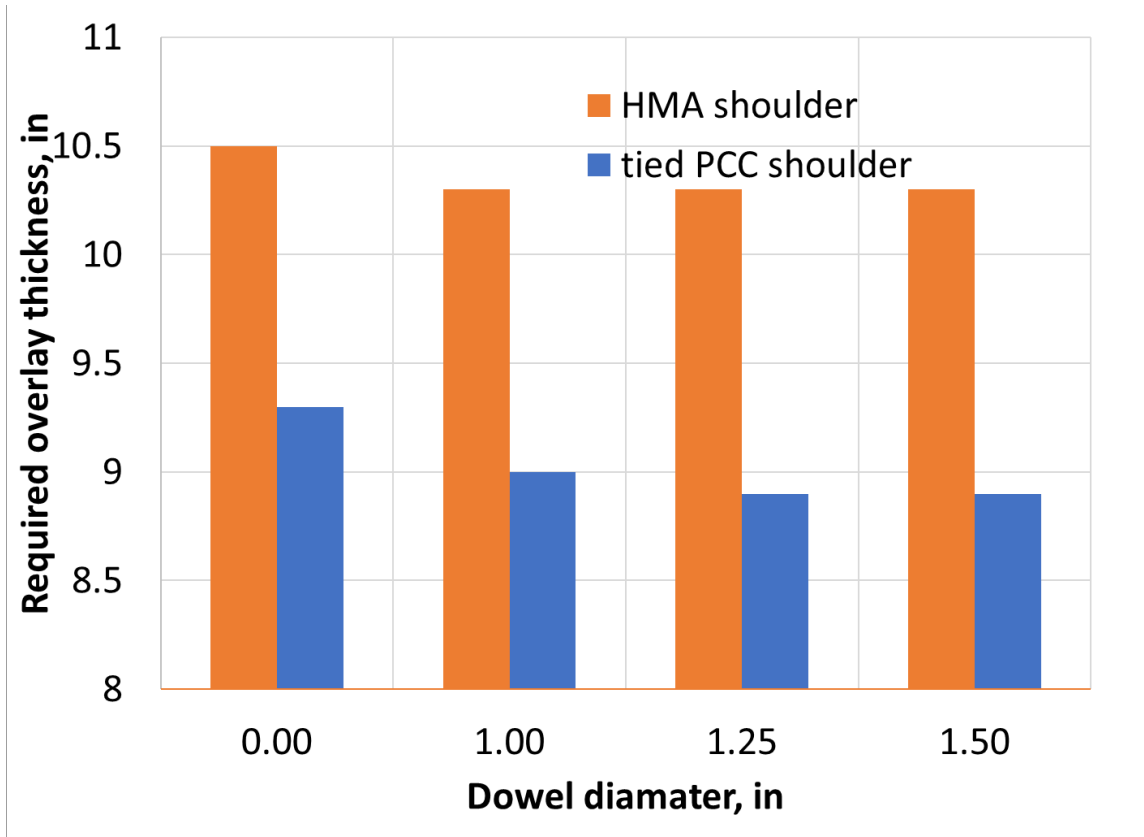
Figure 82: Effect of shoulder type and dowel diameter on required overlay thickness

CHAPTER 7: DEVELOPMENT OF FAULTING MODEL

This section details the UBOL faulting model development. First, previously developed faulting models are presented and outlined. Then, the framework that is established for UBOL joint faulting is presented, focusing on the steps which go into the monthly incremental analysis. Information regarding the calibration sections is then shown with detailed section information presented in Appendix B. Results of the initial model calibration are discussed including the calibrated model coefficients as well as a developed standard deviation model for reliability.

7.1 PREVIOUSLY DEVELOPED FAULTING MODELS

Many of the faulting models developed under previous research were reviewed. Specific attention to the variables chosen for inclusion in the models was made. The details of each of the faulting models reviewed under this study are described separately in the following sections. The faulting models presented are only for Jointed Plain Concrete Pavements (JPCP). Six different models will be presented.

7.1.1 ACPA JPCP Transverse Joint Faulting Model

The first model which is presented is a mechanistic-empirical faulting model for doweled and undoweled pavements developed for the American Concrete Paving Association (ACPA) by Wu et al. (1993). These models were expanded from models developed for the Portland Cement Association (PCA) by Packard (1977). The percent erosion damage is established using Miner's linear cumulative damage concept using Equation 77 (Wu et al., 1993). The allowable number of load applications is computed using Equation 78. The power of each axle pass at the corner of the slab is computed using Equation 79. The faulting for JPCP doweled and undoweled pavements can then be calculated using Equation 80 and 81, respectively.

$$EROSION = 100 \sum_i \frac{C_2 n_i}{N_i} \tag{77}$$

Where:

$EROSION$ is the percent erosion damage

n_i is the expected number of axle load repetitions for each axle group i

N_i is the allowable number of axle load repetitions for each axle group i

C_2 is a constant which takes into account the presence of a tied shoulder.

$$Log(N) = 14.524 - 6.777 * (C1 * P - 9.0)^{0.103} \tag{78}$$

Where:

N is the allowable number of axle load repetitions to end of design period

P is the power of each axle pass at the corner of the slab

$C1$ is equal to $1 - (\dfrac{k}{2000} * \dfrac{4}{h_{pcc}})^2$

k is the modulus of subgrade reaction (psi/in)

h_{pcc} is the slab thickness (in).

$$P = 268.7 * \frac{p^2}{h_{pcc}\, k^{0.73}} \tag{79}$$

Where:

P is the power of each axle pass at the corner of the slab

p is the pressure at slab-foundation interface (psi).

$$FAULTD = EROSION^{0.25} * \left[0.0038332 * \left(\frac{PRECIP}{10}\right)^{1.84121} + 0.0057763 \\ * JTSPACE^{0.38274}\right] \tag{80}$$

$$FAULTND = EROSION^{0.25} * \left[9.75873 * 10^{-4} * (PRECIP)^{0.91907} + 0.0060291 \\ * JTSPACE^{0.54428} - 0.016799 * DRAIN\right] \tag{81}$$

Where:

$FAULTD$ is the mean transverse doweled joint faulting (in)

$FAULTND$ is the mean transverse undoweled joint faulting (in)

$EROSION$ is the percent erosion damage

$PRECIP$ is the annual precipitation (in)

$JTSPACE$ is the transverse joint spacing (ft)

$DRAIN$ is equal to 1 (w/ edge drains) or equal to 0 (w/o edge drains).

7.1.2 SHRP P-020 JPCP Transverse Joint Faulting Model

Simpson et al. (1994) conducted a Strategic Highway Research Program (SHRP) project looking at early Long-Term Pavement Performance (LTPP) General Pavement Study data and developed both doweled and undoweled JPCP faulting models which are presented in Equation 82 and 83 respectively.

$$
\begin{aligned}
FAULTD = CESAL^{0.25} * [0.0238 + 0.0006 * \left(\frac{JTSPACE}{10}\right)^2 + 0.0037 * \left(\frac{100}{k_{static}}\right)^2 \\
+ 0.0039 * \left(\frac{AGE}{10}\right)^2 - 0.0037 * EDGESUP - 0.0218 * DOWELDIA]
\end{aligned}
\tag{82}
$$

$$
\begin{aligned}
FAULTND = CESAL^{0.25} * [-0.07575 + 0.0251 * \sqrt{AGE} + 0.0013 * \left(\frac{PRECIP}{10}\right)^2 \\
+ 0.0012 * \left(FI * \frac{PRECIP}{1000}\right) - 0.0378 * DRAIN]
\end{aligned}
\tag{83}
$$

Where:

$FAULTD$ is the mean transverse doweled joint faulting (in)

$FAULTND$ is the mean transverse undoweled joint faulting (in)

$CESAL$ is equal to the cumulative 18 kip ESALs in traffic lane (millions)

$JTSPACE$ is the transverse joint spacing (ft)

k_{static} is the mean backcalculated static k-value (psi/in)

AGE is the age since construction (yrs)

$EDGESUP$ is edge support (1 = tied PCC shoulder, 0 = any other shoulder type)

$DOWELDIA$ is the diameter of dowel in transverse joints (in)

$PRECIP$ is the annual precipitation (in)

FI is the mean freezing index (°F-days)

$DRAIN$ is equal to the drainage type (1 = longitudinal subdrainage, 0 = otherwise).

7.1.3 FHWA RPPR 1997 JPCP Transverse Joint Faulting Model

Yu et al. (1996) developed both doweled and undoweled faulting models as part of the Federal Highway Administration (FHWA) RPPR project. These models are presented as Equation 84 and 85 below.

$$FAULTD = CESAL^{0.25} * [0.0628 - 0.0628 * C_d * + 0.3673 * 10^{-8} * BSTRESS^2 \\ + 0.4116 * 10^{-5} * JTSPACE^2 + 0.7466 * 10^{-9} * FI^2 * PRECIP^{0.5} \\ - 0.009503 * BASE - 0.01917 * WIDENLANE + 0.0009217 \\ * AGE]$$

(84)

$$FAULTND = CESAL^{0.25} * [0.2347 - 0.1516 * C_d - 0.00025 * \frac{h_{pcc}^2}{JTSPACE} - 0.0115 \\ * BASE + 0.7784 * 10^{-7} * FI^{1.5} * PRECIP^{0.25} - 0.002478 \\ * DAYS90^{0.5} - 0.0415 * WIDENLANE]$$

(85)

Where:

$FAULTD$ is the mean transverse doweled joint faulting (in)

$FAULTND$ is the mean transverse undoweled joint faulting (in)

$CESAL$ is the cumulative 18-kip ESALs in traffic lane (millions)
C_d is the modified AASHTO drainage coefficient

$BSTRESS$ is the maximum dowel/concrete bearing stress (psi)
$JTSPACE$ is the transverse joint spacing (ft)

FI is the mean freezing index (°F-days)

$PRECIP$ is the mean annual precipitation (in)

$BASE$ is the base type (0 = nonstabilized base, 1 = stabilized base)

$WIDENLANE$ is the widened lane (0 = not widened, 1 = widened)

AGE is the age since construction (yrs)

$DRAIN$ is the drainage type (1 = longitudinal subdrainage, 0 = otherwise)
h_{pcc} is the slab thickness (in)

$DAYS90$ is the mean annual number of hot days (days with max temperature greater than 90 °F).

7.1.4 LTPP Data Analysis Study JPCP Transverse Joint Faulting Model

Titus-Glover et al. (1999) recalibrated the 1997 Nationwide Pavement Cost Model (NAPCOM) model (Owusu-Antwi et al., 1997) using only LTPP data. Equation 86 is the developed model for both doweled and undoweled pavements.

$$FAULT = DAMAGE^{0.3} * [0.05 + 0.00004 * WETDAYS - 0.0024 * DOWELDIA \\ - 0.025 * C_d * (0.5 + BASE)] \tag{86}$$

Where:

$FAULT$ is the mean transverse joint faulting (in)

$DAMAGE$ is equal to n/N

n is the cumulative 18-kip ESALs applied

N is the cumulative 18-kip ESALs allowable

Log(N) is equal to 4.27-1.6*Log(DE)

DE is the differential subgrade elastic energy density

$WETDAYS$ is the annual average number of wet days

$DOWELDIA$ is the diameter of dowel in transverse joints (in)

C_d is the AASHTO drainage coefficient

$BASE$ is the base type (0 = erodible base, 1 = nonerodible base).

7.1.5 NCHRP 1-34 Model

Yu et al. (1998) developed the model in (87) as part of the National Cooperative Highway Research Program (NCHRP) project 1-34.

$$FAULT = DAMAGE^{0.2475} * [0.2405 - 0.00118 * DAYS90 + 0.001216 * WETDAYS \\ - 0.04336 * BASETYPE - (0.004336 + 0.007059 * (1 - DOWEL)) \\ * LCB] \tag{87}$$

Where:

$FAULT$ =is the mean transverse joint faulting (in)

$DAMAGE$ is equal to n/N

n is the cumulative 18-kip ESALs applied

N is the cumulative 18-kip ESALs allowable

Log(N) is equal to 0.785983-0.92991*(1+0.4*PERM*(1-DOWEL)) *Log(DE)

PERM is the base permeability (0 = not permeable, 1 = permeable)

DE is the differential subgrade elastic energy density

$DAYS90$ is the number of days per year with the maximum temperature greater than 90°F

$WETDAYS$ is the annual average number of wet days

$BASETYPE$ is equal to 0 if not stabilized or 1 if stabilized

$DOWEL$ is the presence of dowels (1 = present, 0 = not present)

LCB is the presence of lean concrete base (1 if present, 0 if not present).

7.1.6 Pavement ME Model

The Pavement ME faulting model is a monthly incremental approach developed by ARA (2004). For each month of an analysis a faulting increment is determined which is dependent on the faulting level from the previous month. The faulting is then determined by summing up all of the previous months faulting increments. Equation 88 through 91 detail the faulting models iterative process (ARA, 2004).

$$FMAX_0 = (C_1 + C_2 * FR^{0.25}) * \delta_{curl}$$
$$* \left[Log(1 + C_5 * 5^{EROD}) * Log(\frac{P_{200} * WetDays}{p_s}) \right]^{C_6} \tag{88}$$

$$FMAX_i = FMAX_{i-1} + C_7 * DE_i * [Log(1 + C_5 * 5^{EROD})]^{C_6} \tag{89}$$

$$\Delta Fault_i = (C_3 + C_4 * FR^{0.25}) * (FMAX_{i-1} - Fault_{i-1})^2 * DE_i \tag{90}$$

$$Fault_i = Fault_{i-1} + \Delta Fault_i * \tag{91}$$

Where:

$FMAX_0$ is the initial maximum mean transverse joint faulting (in)

FR is the base freezing index defined at the percentage of the time that the top of the base is below freezing

δ_{curl} is the maximum mean monthly PCC upward slab corner deflection due to temperature curling and moisture warping

$EROD$ is the base/subbase erodibility index (Integer between 1 and 5)

P_{200} is the percent of the subgrade soil passing No. 200 sieve

$WetDays$ is the average number of annual wet days (> 0.1 in of rainfall)

p_s is equal to the overburden on the subgrade (lb)

$FMAX_i$ is the maximum mean transverse joint faulting for month i (in)

$FMAX_{i-1}$ is the maximum mean transverse joint faulting for month i-1 (in) (If i =1, $FMAX_{i-1} = FMAX_0$)

DE_i is the differential energy density of subgrade accumulated during month i

$\Delta Fault_i$ is the incremental monthly change in mean transverse joint faulting during month i (in)

FR is the base freezing index defined at the percentage of the time that the top of the base is below freezing (<32°F)

$Fault_{i-1}$ is the mean joint faulting at the beginning of month i (in) (0 if i = 1)

$C_1 \dots C_7$ are the calibration coefficients.

The one component of the faulting calculation, which changes from month to month, is the differential energy. The differential energy is computed using Equation 92. NNs are used to calculate the loaded and unloaded slab deflection for each axle and temperature loading condition, and then the differential energy is calculated for each axle crossing the pavement structure for each month of the analysis. This value of differential energy is then used in Equation 88 through 91.

$$DE_m = \sum_{A=1}^{3} \sum_{i=1}^{N_A} \frac{1}{2} n_{i,A} k_m \left(\delta_{L,i,A}^2 - \delta_{U,i,A}^2 \right) \tag{92}$$

Where:

DE_m is the differential energy density of subgrade deformation accumulated for month m

$n_{i,A}$ is the number of axle load applications for current month and load group i

k_m is the modulus of subgrade reaction for month m

$\delta_{L,i,A}$ is the corner deflections of the loaded slab caused by axle loading

$\delta_{L,i,A}$ is the corner deflections of the unloaded slab caused by axle loading.

Of the procedures which have been presented, important predictive parameters include the following: the differential energy between the loaded and unloaded slabs, an indication of the amount of precipitation, an estimate of the traffic, the presence of dowel bars, and an indication of the erodibility of the base material. The Pavement ME faulting model is the standard mechanistic-empirical framework currently available. Therefore, the framework for the UBOL faulting model will adopt a similar approach to calculate joint faulting.

7.2 STRUCTURAL RESPONSE PREDICTIONS

In order to predict joint faulting, the UBOL pavement deflections are needed from structural modeling. Incremental faulting calculations require many time-consuming finite element runs, so the creation of neural networks to predict the response greatly decreases run time. The range of parameters used to generate a factorial of finite element runs and the critical responses to be used in the faulting model were defined. Finally, the development of neural networks to predict the critical responses for the UBOL structure using MATLAB's Neural Network Toolbox is discussed (MATLAB, 2013).

7.2.1 Modeling Parameters

In performing the runs necessary to create a database of critical response parameters to train neural networks to predict the critical structural responses, the range of parameters for the UBOL structure had to be established. Additionally, the choice of the critical response parameter to be used as the predictor in the faulting model was made.

ISLAB2005 was chosen as the modeling software for UBOL joint faulting. A convergence analysis was conducted and showed that the element size of 6 inches is sufficient for the analysis. Example output for one of the mesh convergence checks performed is shown in Table 25. This mesh convergence analysis was carried out for a 12-ft joint spacing and a 6-in overlay on a 10-in existing concrete slab with a subgrade Winkler k-value of 150 psi/in. An 18-kip single axle load was applied at the joint. Additionally, validation checks were performed with FWD data from UBOLs in Michigan and Minnesota. An example validation with FWD data for two Michigan sections using interlayers tested in the lab study is shown in Table 26.

Table 25: Mesh convergence check in ISLAB

Mesh size (in)	Corner deflection (mils)	Maximum interlayer compressive stress (psi)
12	70.2	25.72
8	80.5	26.07
6	80.7	26.21
3	80.8	26.34

Table 26: ISLAB validation with FWD data

	US 131 Kalamazoo (MIOAU)			US 131 Rockford (MIDAU)	
FWD Location	FWD (mils)	ISLAB (mils)		FWD (mils)	ISLAB (mils)
-12	4.6	5		3.7	3.9
0	5.1	5.4		3.8	4.1
12	4.4	4.7		3.5	3.7

The axle dimensions used are shown in Figure 83. When considering tandem axles, the longitudinal spacing between tires is defined as 40 in. For each different structure, 3 slabs are modeled in the driving lane and the passing lane is not modeled. If there is a tied shoulder then there is a shoulder modeled on the edge of the pavement, but in the case of an asphalt shoulder, no shoulder is modeled.

a.) Single axle

b.) Tandem axle
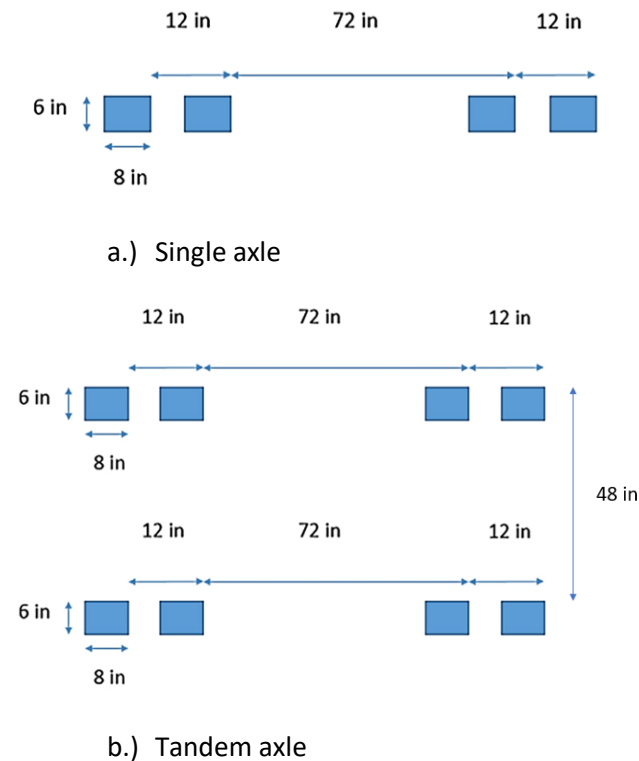
Figure 83: Axle dimensions for structural modeling

In the current faulting model in the Pavement ME, the critical response to determine differential energy (DE) for rigid pavement design are the deflections at the corners on the approach slab (loaded side of the joint) and leave slab (unloaded side of the joint) (ARA, 2004). The DE parameter is commonly used as a predictor of faulting (Larralde 1984, Khazanovich et al., 2004). The pavement ME design procedure estimates the DE using only two deflections, the deflection in the corner of the loaded and unloaded slab (ARA 2004). In a previous study, corner deflections, full lane width deflection basins, triangular deflection basins and 2 ft by 6 ft deflection basins were all considered for UBOL and BCOA (Sachs, 2017, DeSantis et al., 2018). The deflection basin was selected to characterize slab response instead of deflections at the corner, because the basin is able to more accurately represent the difference in energy density on both sides of the joint. The 2 ft by 6 ft basin size was selected because it characterizes the basin in the area most heavily influenced by the load and also accommodates the 6 ft by 6 ft slab size that is becoming more common in overlay design. The deflection basin selected to characterize slab response can be seen in Figure 84. The critical response is used in the following equation to determine differential energy:

$$DE = \frac{1}{2}k_{IL}(B_L^2 - B_{UL}^2) \qquad (93)$$

Where:

DE is the differential energy,

k_{IL} is the Totsky interlayer stiffness,

B_L is the deflection basin on the loaded slab, and

$B_{UL}$is the deflection basin on the unloaded slab.
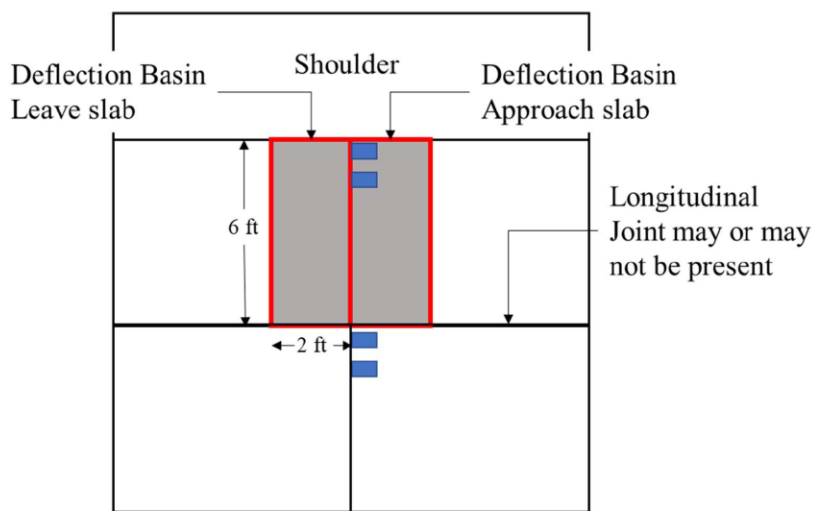
Figure 84: Deflection basin definition (DeSantis et al., 2018)

Critical responses from the structural model must be established for every combination of variables considered. The structural model considers a wide range of parameters for the overlay, interlayer, and existing concrete slab. In performing the database of runs to generate critical responses, a baseline case is established and one parameter at a time is allowed to vary. In order to decrease the number of finite element runs required, some parameters within the structure are combined with one another. This can be seen in Figure 85.

153
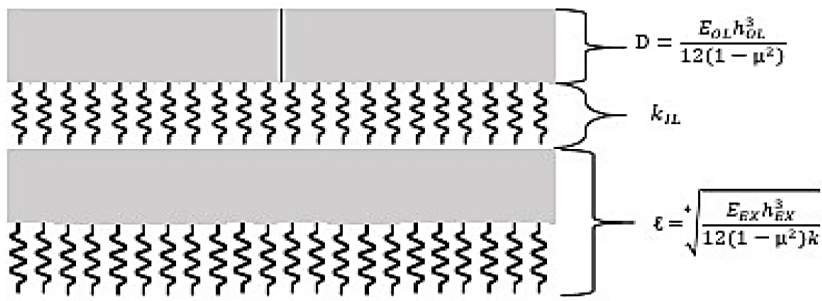
Figure 85: Consolidation of structural model for UBOL faulting model

To ensure the NNs encompass a sufficient inference space for the overlay, interlayer, and existing concrete pavement, a partial factorial design was developed. A sensitivity analysis was performed to ensure the NNs are able to predict accurate results in comparison to the results from ISLAB. The results indicated more levels were necessary for certain parameters. Therefore, a full factorial was used, and all parameters considered, along with their corresponding values, can be seen in Table 27.

When using ISLAB, decoupling temperature loading, and traffic loading cannot be performed in a single analysis. Therefore, three different analysis needed to be performed. The first analysis combines temperature and traffic loading conditions, which resulted in a total of 145,152 analyses. The second analysis only considers traffic loading conditions (temperature is not considered by setting the overlay temperature difference equal to 0°F), which resulted in a total of 20,736 analyses. The third analysis only considers temperature loading conditions (traffic loading is not considered), which resulted in a total of 12,096 analyses. In total, 177,984 analyses were performed to fulfill the full factorial. ISLAB is a very computationally efficient FEM software, which enabled this large factorial analysis to be conducted (Khazanovich et al., 2000).

A list of all variables and range of values considered are included in Table 28. This design matrix results in approximately 180,000 finite element runs to be conducted. The values of the existing thickness, stiffness, and k-value are combined into a radius of relative stiffness. The radius of relative stiffness is adjusted by leaving the stiffness of the existing concrete as 4,500,000 psi and the k-value as 100 psi/in and only adjusting the thickness. To further decrease the number of finite elements runs that need to be generated, only four different values of flexural stiffness for the PCC overlay are used. The overlay elastic modulus remains 4,000,000 psi and only the thickness of the overlay is increased.

Table 27: UBOL parameters for structural model

Parameter	Parameter values							
Overlay PCC thickness (in)	3.43	6.00	8.46	12.20				
PCC modulus of elasticity (psi)	4.0E+06							
PCC joint spacing (ft)	6	12	15					
Overlay temp. difference (°F)	-30	-20	-10	0	10	20	30	40
Interlayer Totsky K-value (psi/in)	425	2,000	6,000					
Existing PCC thickness (in)	3.06	6.50	10.39	19.44				
Existing E_{PCC} (psi)	4.5E+06							
Modulus of subgrade reaction, k-value (psi/in)	100							
Shoulder width (ft)	8							
Lane shoulder LTE (%)	0 (Asphalt)	90 (Tied PCC)						
Trans. joint AGG (psi)	100	1,000	10,000	50,000	100,000	1,000,000		
Wheel wander (in)	0	4	16					
Single axle (kip)	0	18	30					
Tandem axle (kip)	0	36	60					

7.2.2 Neural Network Development for Faulting

Neural networks are developed to predict the sum of the vertical nodal displacements within a distance of 2 ft from the joint on both the loaded and unloaded sides of the joint within 6 ft of the longitudinal joint. The neural network toolbox in MATLAB is used to train and test the ANNs (MATLAB, 2013). A total of 5 ANNs for each interlayer (10 total) were trained, 2 ANNs for the deflection basins, 2 ANNs for corner deflections, and 1 ANN for corner deflections based on temperature. These networks are developed based on a set number of inputs (predictors) to return an output. The output in this case is either the difference between the deflection basin on the loaded and unloaded side of the joint, the difference between the corner deflections on the loaded and unloaded side of the joint, or the corner deflection on the loaded side of the joint due to temperature only. Due to symmetry of the temperature loading condition, only one NN is developed for both the loaded and unloaded sides of the joint. The predictors for each of these ANNs

are presented along with pertinent network development information. Finally, the results of the training are presented.

Each of the NNs with each of their predictors are shown in Equation 94 through 96.

$$NN_{\Sigma B,A,IL}(JTSpace, s, LTE_{shoulder}, \ell_{OL}, \ell_{EX}, \Phi, \frac{AGG}{k_{IL}\ell_{OL}}, q_i^*) \qquad (94)$$

$$NN_{\Sigma C,A,IL}(JTSpace, s, LTE_{shoulder}, \ell_{OL}, \ell_{EX}, \Phi, \frac{AGG}{k_{IL}\ell_{OL}}, q_i^*) \qquad (95)$$

$$NN_{\Sigma T,IL}(JTSpace, 0, LTE_{shoulder}, \ell_{OL}, \ell_{EX}, \Phi, \frac{AGG}{k_{IL}\ell_{OL}}, 0) \qquad (96)$$

Where:

$NN_{\Sigma B,A,IL}$ is the neural network for the sum of the 2-ft by 6-ft deflection basin for the difference between the loaded and unloaded slab for axle type A (A=1 for single; A=2 for tandem) and interlayer type IL (IL=A for asphalt; IL=F for fabric).

$NN_{\Sigma C,A,IL}$ is the neural network for the corner deflection for the difference between the loaded and unloaded slab for axle type A (A=1 for single; A=2 for tandem) and interlayer type IL (IL=A for asphalt; IL=F for fabric).

$NN_{\Sigma T,IL}$ is the neural network for the corner deflection for the condition when only temperature is present for interlayer type IL (IL=A for asphalt; IL=F for fabric).

$JTSpace$ is the joint spacing of the overlay (in).

s is wheel wander offset from the lane/shoulder (L/S) joint (in).

$LTE_{shoulder}$ is the L/S LTE (%).

ℓ_{OL} is the radius of relative stiffness of the overlay (in) and can be seen in Equation 97.

$$\ell_{OL} = \sqrt[4]{\frac{E_{OL}h_{OL}^3}{12(1 - \mu_{PCC}^2)k_{IL}}} \qquad (97)$$

where:

E_{OL} is the modulus of elasticity of the PCC (psi),

h_{OL} is the overlay thickness (in),

156

μ_{PCC} is the Poisson's ratio of the overlay,

k_{IL} is the Totsky interlayer stiffness (psi/in).

ℓ_{EX} is the radius of relative stiffness of the existing pavement (in) and can be seen in Equation 98.

$$\ell_{EX} = \sqrt[4]{\frac{E_{EX}h_{EX}^3}{12\left(1 - \mu_{PCC}{}^2\right)k}}$$

(98)

where:

E_{EX} is the modulus of elasticity of the existing PCC (psi),

h_{EX} is the existing thickness (in),

μ_{PCC} is the Poisson's ratio of the existing PCC,

k is the modulus of subgrade reaction (psi/in).

Φ is Korenev's non-dimensional temperature gradient, which is shown in Equation 99.

$$\Phi = \frac{2\alpha_{pcc}(1 + \mu_{pcc})\ell_{OL}^2}{h_{OL}^2}\frac{k_{IL}}{\gamma_{PCC}} * \Delta T$$

(99)

where:

α_{pcc} is the coefficient of thermal expansion for the PCC overlay (in/in/°F),

γ_{PCC} is the unit weight of the overlay PCC (pci),

ΔT is the temperature difference in the overlay (°F).

The nondimensional joint stiffness can be seen in Equation 100.

$$\frac{AGG}{k_{IL}\ell_{OL}}$$

(100)

Where:

AGG is the joint load transfer stiffness (psi).

q_i^* is the adjusted load/pavement weight ratio and can be seen in Equation 101.

$$q_i^* = \frac{P_i}{A * \gamma_{PCC} * h_{OL}}$$

<div align="right">(101)</div>

Where:

P_i is the axle load (lbs),

A is the parameter for axle type (1 for single and 2 for tandem axles).

The ANN architecture was determined based on the predictors used in Pavement ME, as well as through trial and error to enhance prediction (ARA, 2004, Sachs, 2017). The training of ANNs can have relatively high variability due to the possibility of local minima in the objective function, therefore 10 NNs are trained for each predictive model to reduce this variability (Ripley, 1996). The five resulting predictive models take a robust average of the 10 ANNs and eliminate the two highest and lowest estimates, resulting in an average of six values. To prevent overfitting, the Bayesian Regularization training algorithm was used. This method was selected over early stopping algorithms, such as Levenberg-Marquardt optimization, since computational time for training was not a concern (Ripley, 1996). For each of the ANNs trained, the architecture consisted of three hidden layers with ten neurons each. Along with the architecture, the breakdown of the data is as follows, 70% of the data was used in the training set and the remaining 30% in the testing set. Figure 86 shows the results of the ANN test set for the difference between the loaded and unloaded deflection basins for a single axle.

Figure 87 shows the results of the ANN test set for the difference between the loaded and unloaded deflection basins for a tandem axle. Figure 88 shows the results of the ANN test set for the difference between the loaded and unloaded corner deflections for a single axle. Figure 89 shows the results of the ANN test set for the difference between the loaded and unloaded corner deflections for a tandem axle. Figure 90 shows the results of the ANN test set for corner deflections of the loaded side of the joint under temperature loading conditions only.
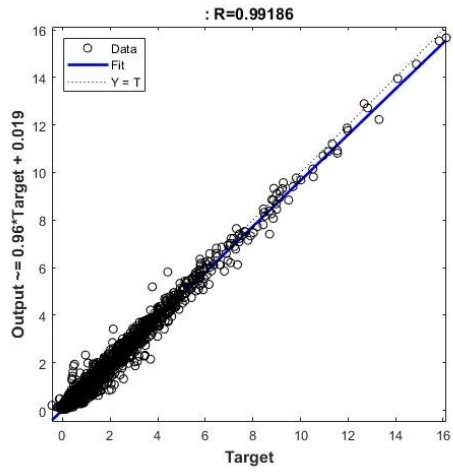
(a)
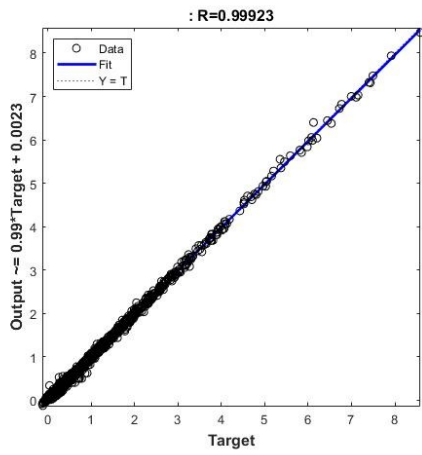
(b)

Figure 86: Comparison of the neural networks and ISLAB2005 computed differences between the loaded and unloaded deflection basins for a single axle loading (a) asphalt interlayer (b) fabric interlayer
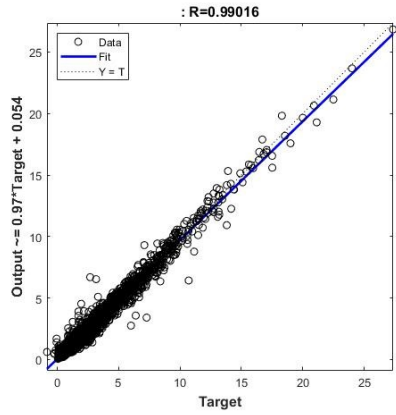
(a)
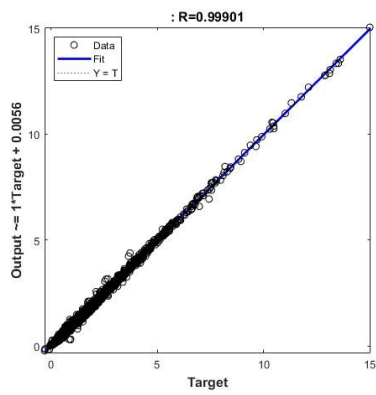
(b)

Figure 87: Comparison of the neural networks and ISLAB2005 computed differences between the loaded and unloaded deflection basins for a tandem axle loading (a) asphalt interlayer (b) fabric interlayer
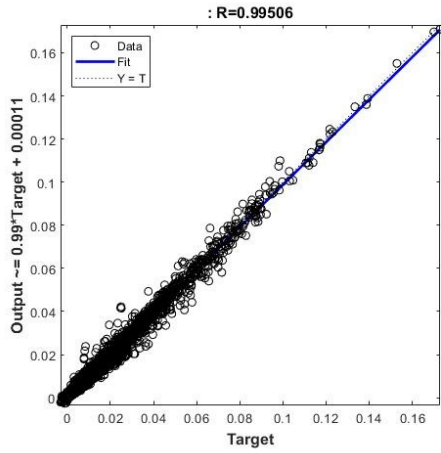
(a)
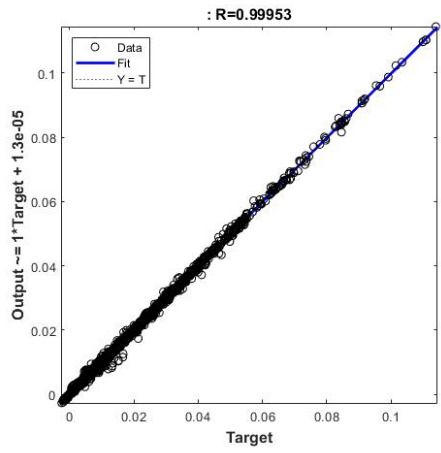
(b)

Figure 88: Comparison of the neural networks and ISLAB2005 computed differences between the loaded and unloaded corner deflections for a single axle (a) asphalt interlayer (b) fabric interlayer
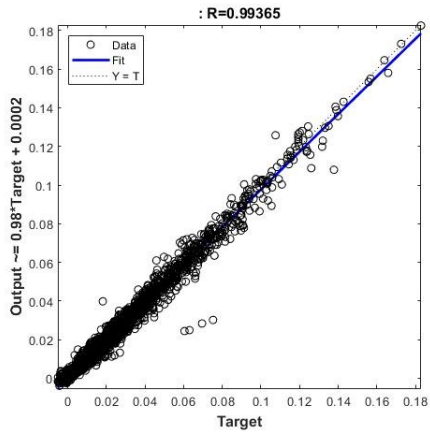
(a)
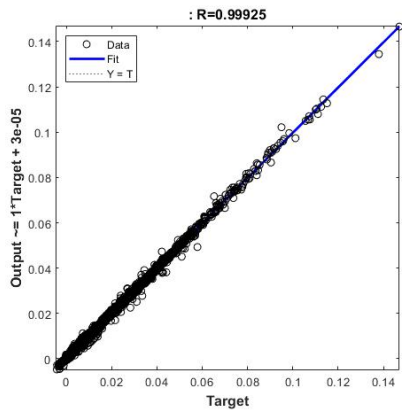
(b)

Figure 89: Comparison of the neural networks and ISLAB2005 computed differences between the loaded and unloaded corner deflections for a tandem axle (a) asphalt interlayer (b) fabric interlayer
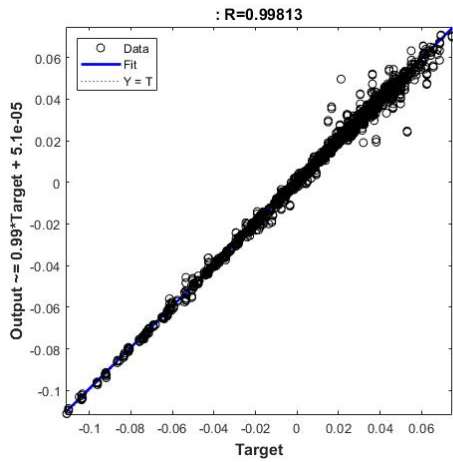
(a)
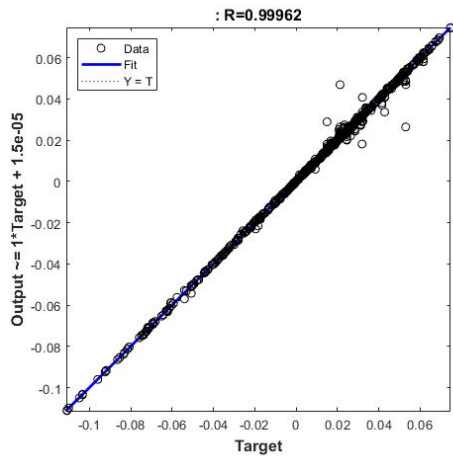
(b)

Figure 90: Comparison of the neural networks and ISLAB2005 computed corner deflections of the loaded side of the joint under temperature loading conditions only (a) asphalt interlayer (b) fabric interlayer

A validation was conducted and is included below summarizing the effects of wheel offset for a given structure using the deflection basin and corner deflection ANNs. The joint spacing, overlay PCC stiffness, Totsky interlayer stiffness, existing PCC stiffness, and k-value are 12 ft, 4.0E+06 psi, 3.5E+05 psi/in, 4.5E+06 psi, and 100 psi/in, respectively. The structure consists of a 6-in PCC overlay on a 10.5-in existing pavement with an asphalt interlayer and an asphalt shoulder. The AGG stiffness selected corresponds to an LTE of 85 percent. The comparisons can be seen in Figure 91.
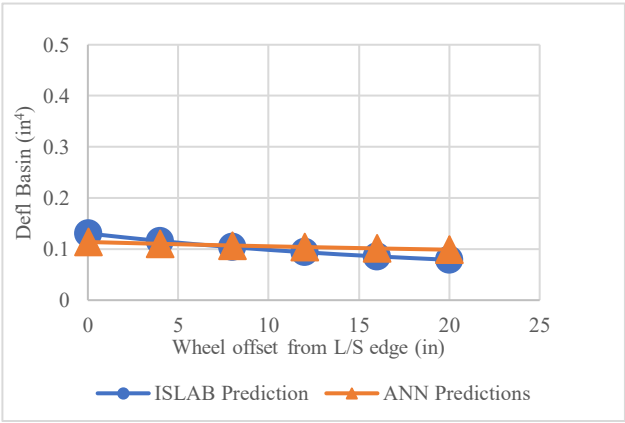
a) Single Axle: Deflection basin
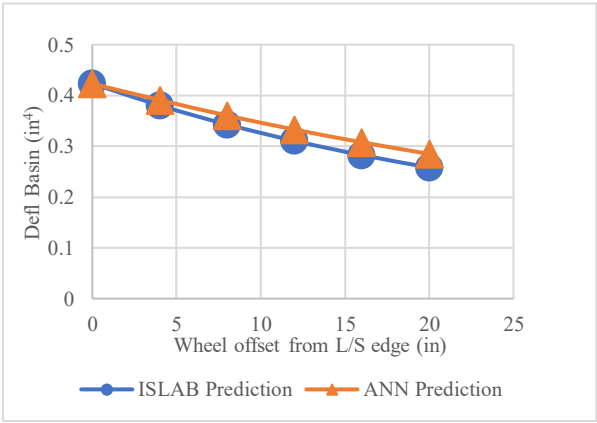
b) Tandem Axle: Deflection basin
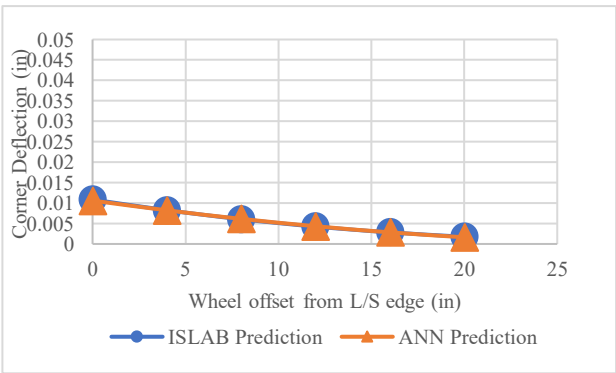
c) Single Axle: Corner deflection
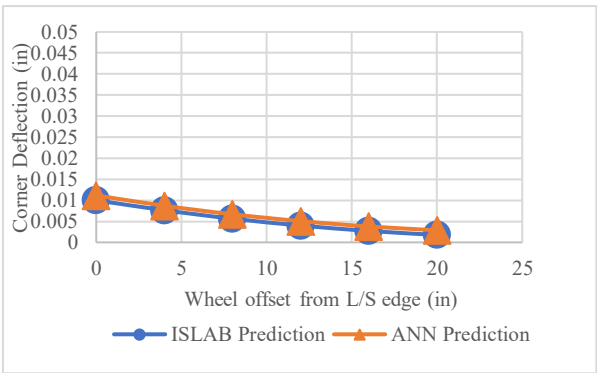
d) Tandem Axle: Corner deflection

Figure 91: Validation of ANNs

7.3 FAULTING MODEL FRAMEWORK

The framework to determine faulting will involve using the developed ANNs to determine the differential energy. For this model, an iterative monthly incremental analysis is performed. The treatment of climatic considerations as well as calculation of joint stiffness is outlined. This is then followed by a discussion on the calculation of differential energy and then the functional form of the methodology used to calculate faulting.

7.3.1 Climatic Considerations

This section focuses on incorporating the effects of temperature gradients in the overlay design process. It was established that there was no significant relationship between interlayer temperature and the resulting Totsky K-value so there is no need to consider these effects. Within the current framework, a separate analysis for each structure must be carried out within the EICM (Larson and Dempsey 2003). The

EICM performs an hourly incremental analysis that determines the temperature profile in the pavement structure at specified nodes. This is then used to help establish gradients for use in the design process. Therefore, for each calibration section, an EICM file is created. Within EICM, the structure must be defined including layer thickness, the number of nodes for each layer, thermal properties, and permeability, porosity, and water content to model moisture movement in granular layers. Within the overlay, nodes are placed at one-inch increments. Additionally, the nearest weather stations to the calibration sites are chosen to give hourly values of air temperature, precipitation, wind speed, and percent sunshine for several years that can be output as an .icm profile. The climatic analysis is then performed using the EICM so the hourly nodal temperature depths throughout the structure can be obtained in the form of an output file with a .tem extension. This information is then used to determine the mean monthly mid-depth overlay temperature, establish hourly equivalent strain gradients, and the freezing ratio (FR), which is the percentage of time that the interlayer is less than 32°F. The .icm file for used in the EICM analysis is used to establish mean monthly air temperature and the number of wet days in a year.

The equivalent strain gradients are calculated using the temperature-moment concept (Janssen and Snyder 2000) that converts the nonlinear temperature profile for a specific hour generated by the EICM into an equivalent linear temperature gradient (ELTG) based on Equation 102 through 104. This conversion was proposed by Janssen and Snyder (2000) to ensure that the resultant strains in the overlay under the ELTG and the nonlinear temperature gradient are the same which results in the same deflections profile of the slab under the two conditions.

$$T_{ave} = \sum_{i=1}^{n} \left[\frac{0.5(t_i + t_{i+1})(d_i - d_{i+1})}{(d_1 - d_n)} \right] \tag{102}$$

$$TM_0 = -0.25 \sum_{i=1}^{n} [(t_i + t_{i+1})(d_i^2 - d_{i+1}^2) - 2(d_1^2 - d_n^2)T_{ave}] \tag{103}$$

$$ELTG = -\frac{12 \cdot TM_0}{h^3} \tag{104}$$

Where:

ELTG is the equivalent linear temperature gradient (°F/in)

T_{ave} is the average temperature (°F)

TM_0 is the temperature moment (°F·in²)

d_i is the depth of the ith node (in)

t_i is the temperature at depth d_i (°F).

In order to perform a monthly analysis instead of an hourly incremental analysis, it is necessary to create an effective equivalent linear temperature gradient. For each month, the differential energy is summed with the hourly ELTGs for each calibration section. Then a, fmin search in MATLAB is used to find a single temperature gradient which causes the same value of differential energy calculated using the ANNs. For this analysis, 1 million ESALs are applied over the course of the year, hourly distributed according to the percentages established in Pavement ME based on LTPP traffic data and presented in Table 28 (ARA, 2004). Monthly joint stiffness is used in this analysis. The following section describes exactly how the inputs for the ANNs are established.

Table 28: Hourly truck traffic distributions from Pavement ME (ARA, 2004)

Time period	Distribution (percent)	Time period	Distribution (percent)
12:00 a.m. - 1:00 a.m.	2.3	12:00 p.m. - 1:00 p.m.	5.9
1:00 a.m. - 2:00 a.m.	2.3	1:00 p.m. - 2:00 p.m.	5.9
2:00 a.m. - 3:00 a.m.	2.3	2:00 p.m. - 3:00 p.m.	5.9
3:00 a.m. - 4:00 a.m.	2.3	3:00 p.m. - 4:00 p.m.	5.9
4:00 a.m. - 5:00 a.m.	2.3	4:00 p.m. - 5:00 p.m.	4.6
5:00 a.m. - 6:00 a.m.	2.3	5:00 p.m. - 6:00 p.m.	4.6
6:00 a.m. - 7:00 a.m.	5.0	6:00 p.m. - 7:00 p.m.	4.6
7:00 a.m. - 8:00 a.m.	5.0	7:00 p.m. - 8:00 p.m.	4.6
8:00 a.m. - 9:00 a.m.	5.0	8:00 p.m. - 9:00 p.m.	3.1
9:00 a.m. - 10:00 a.m.	5.0	9:00 p.m. - 10:00 p.m.	3.1
10:00 a.m. – 11:00 a.m.	5.9	10:00 p.m. – 11:00 p.m.	3.1
11:00 a.m. – 12:00 p.m.	5.9	11:00 p.m. – 12:00 a.m.	3.1

7.3.2 Traffic Considerations

Direct inputs for predicting joint faulting includes the one-way average daily traffic (ADT), percent of trucks (as a decimal), the number of lanes in each direction, the growth type and the growth rate. The growth type can either be no growth, linear growth, or compound growth and is computed as follows.

Table 29: Function used in computing/forecasting truck traffic over time (ARA 2004)

Growth Type	Model
No growth	1.0*AADTT
Linear growth	GR*Age+AADTT
Compound growth	$AADTT*GR^{Age}$

Where AADTT is the average annual daily truck traffic, GR is the growth rate, and Age is the age in years when traffic is to be computed (monthly increment). The number of lanes is used to determine the lane distribution factor (LDF) as a function of the defined one-way ADT. The LDFs are established from FHWA recommendations based upon the number of lanes and the one-way ADT. The LDFs can be seen below.

Table 30: Lane distribution factors for multiple-lane highways (ARA 2004)

One-Way ADT	2 Lanes (One Direction): % Outer Lane	3+ Lanes (One Direction): % Outer Lane
2,000	94	82
4,000	88	76
6,000	85	72
8,000	82	70
10,000	81	68
15,000	77	65
20,000	75	63
25,000	73	61
30,000	72	59
35,000	70	58
40,000	69	57
50,000	67	55
60,000	66	53
70,000	-	52

The axle load distribution factors are used to represent the total axle applications for each loading interval for single and tandem axles for vehicle classes 4 through 13. The load intervals for single axles is 3,000 lb to 41,000 lb at 1,000-lb intervals. The load intervals for tandem axles is 6,000 lb to 82,000 lb at 2,000-lb intervals. The Pavement ME default FHWA vehicle class distribution percentages (TTC 1) is adopted and can be seen in Table 31. The overall single and tandem axle load distributions used for each vehicle class can be seen in Table 32 and Table 33 (ARA 2004).

Table 31: FHWA vehicle class distribution percentages

Vehicle Class	Distribution
4	1.3
5	8.5
6	2.8
7	0.3
8	7.6
9	74
10	1.2
11	3.4
12	0.6
13	0.3

Table 32: Single axle load distribution (percentages) for each vehicle classification

Mean Axle Load (lbs)	Vehicle Classification									
	4	5	6	7	8	9	10	11	12	13
3000	1.8	10.03	2.47	2.14	11.62	1.74	3.64	3.55	6.68	8.88
4000	0.96	13.19	1.78	0.55	5.36	1.37	1.24	2.91	2.29	2.67
5000	2.91	16.4	3.45	2.42	7.82	2.84	2.36	5.19	4.87	3.81
6000	3.99	10.69	3.95	2.7	6.98	3.53	3.38	5.27	5.86	5.23
7000	6.8	9.21	6.7	3.21	7.98	4.93	5.18	6.32	5.97	6.03
8000	11.45	8.26	8.44	5.81	9.69	8.43	8.34	6.97	8.85	8.1
9000	11.28	7.11	11.93	5.26	9.98	13.66	13.84	8.07	9.57	8.35
10000	11.04	5.84	13.55	7.38	8.49	17.66	17.33	9.7	9.95	10.69
11000	9.86	4.53	12.12	6.85	6.46	16.69	16.19	8.54	8.59	10.69
12000	8.53	3.46	9.47	7.41	5.18	11.63	10.3	7.28	7.09	11.11
13000	7.32	2.56	6.81	8.99	4	6.09	6.52	7.16	5.86	7.34
14000	5.55	1.92	5.05	8.15	3.38	3.52	3.94	5.65	6.58	3.78
15000	4.23	1.54	2.74	7.77	2.73	1.91	2.33	4.77	4.55	3.1
16000	3.11	1.19	2.66	6.84	2.19	1.55	1.57	4.35	3.63	2.58
17000	2.54	0.9	1.92	5.67	1.83	1.1	1.07	3.56	2.56	1.52
18000	1.98	0.68	1.43	4.63	1.53	0.88	0.71	3.02	2	1.32
19000	1.53	0.52	1.07	3.5	1.16	0.73	0.53	2.06	1.54	1
20000	1.19	0.4	0.82	2.64	0.97	0.53	0.32	1.63	0.98	0.83
21000	1.16	0.31	0.64	1.9	0.61	0.38	0.29	1.27	0.71	0.64
22000	0.66	0.31	0.49	1.31	0.55	0.25	0.19	0.76	0.51	0.38
23000	0.56	0.18	0.38	0.97	0.36	0.17	0.15	0.59	0.29	0.52
24000	0.37	0.14	0.26	0.67	0.26	0.13	0.17	0.41	0.27	0.22
25000	0.31	0.15	0.24	0.43	0.19	0.08	0.09	0.25	0.19	0.13
26000	0.18	0.12	0.13	1.18	0.16	0.06	0.05	0.14	0.15	0.26
27000	0.18	0.08	0.13	0.26	0.11	0.04	0.03	0.21	0.12	0.28
28000	0.14	0.05	0.08	0.17	0.08	0.03	0.02	0.07	0.08	0.12
29000	0.08	0.05	0.08	0.17	0.05	0.02	0.03	0.09	0.09	0.13
30000	0.05	0.02	0.05	0.08	0.04	0.01	0.02	0.06	0.02	0.05
31000	0.04	0.02	0.03	0.72	0.04	0.01	0.03	0.03	0.03	0.05
32000	0.04	0.02	0.03	0.06	0.12	0.01	0.01	0.04	0.01	0.08
33000	0.04	0.02	0.03	0.03	0.01	0.01	0.02	0.01	0.01	0.06
34000	0.03	0.02	0.02	0.03	0.02	0.01	0.01	0.01	0.01	0.02
35000	0.02	0.02	0.01	0.02	0.02	0	0.01	0.01	0.01	0.01
36000	0.02	0.02	0.01	0.02	0.01	0.01	0.01	0.01	0.01	0.01
37000	0.01	0.01	0.01	0.01	0.01	0	0.01	0	0.01	0.01
38000	0.01	0.01	0.01	0.01	0	0	0.01	0.02	0.01	0.01
39000	0.01	0	0.01	0.01	0.01	0	0.01	0.01	0	0.01
40000	0.01	0	0.01	0.01	0	0	0.04	0.02	0	0
41000	0	0	0	0	0	0	0	0	0	0

Table 33: Tandem axle load distribution (percentages) for each vehicle classification

Mean Axle Load (lbs)	Vehicle Classification									
	4	5	6	7	8	9	10	11	12	13
6000	5.88	7.06	5.28	13.74	18.95	2.78	2.45	7.93	5.23	6.41
8000	1.44	35.42	8.42	6.71	8.05	3.92	2.19	3.15	1.75	3.85
10000	1.94	13.23	10.81	6.49	11.15	6.51	3.65	5.21	3.35	5.58
12000	2.73	6.32	8.99	3.46	11.92	7.61	5.4	8.24	5.89	5.66
14000	3.63	4.33	7.71	7.06	10.51	7.74	6.9	8.88	8.72	5.73
16000	4.96	5.09	7.5	4.83	8.25	7	7.51	8.45	8.37	5.53
18000	7.95	5.05	6.76	4.97	6.77	5.82	6.99	7.08	9.76	4.9
20000	11.58	4.39	6.06	4.58	5.32	5.59	6.61	5.49	10.85	4.54
22000	14.2	2.31	5.71	4.26	4.13	5.16	6.26	5.14	10.78	6.45
24000	13.14	2.28	5.17	3.85	3.12	5.05	5.95	5.99	7.24	4.77
26000	10.75	1.53	4.52	3.44	2.34	5.28	6.16	5.73	6.14	4.34
28000	7.47	1.96	3.96	6.06	1.82	5.53	6.54	4.37	4.93	5.63
30000	5.08	1.89	3.21	3.68	1.58	6.13	6.24	6.57	3.93	7.24
32000	3.12	2.19	3.91	2.98	1.2	6.34	5.92	4.61	3.09	4.69
34000	1.87	1.74	2.12	2.89	1.05	5.67	4.99	4.48	2.74	4.51
36000	1.3	1.78	1.74	2.54	0.94	4.46	3.63	2.91	1.73	3.93
38000	0.76	1.67	1.44	2.66	0.56	3.16	2.79	1.83	1.32	4.2
40000	0.53	0.38	1.26	2.5	0.64	2.13	2.24	1.12	1.07	3.22
42000	0.52	0.36	1.01	1.57	0.28	1.41	1.69	0.84	0.58	2.28
44000	0.3	0.19	0.83	1.53	0.28	0.91	1.26	0.68	0.51	1.77
46000	0.21	0.13	0.71	2.13	0.41	0.59	1.54	0.32	0.43	1.23
48000	0.18	0.13	0.63	1.89	0.2	0.39	0.73	0.21	0.22	0.85
50000	0.11	0.14	0.49	1.17	0.14	0.26	0.57	0.21	0.22	0.64
52000	0.06	0.2	0.39	1.07	0.11	0.17	0.4	0.07	0.23	0.39
54000	0.04	0.06	0.32	0.87	0.06	0.11	0.38	0.13	0.2	0.6
56000	0.08	0.06	0.26	0.81	0.05	0.08	0.25	0.15	0.12	0.26
58000	0.01	0.02	0.19	0.47	0.03	0.05	0.16	0.09	0.07	0.18
60000	0.02	0.02	0.17	0.49	0.02	0.03	0.15	0.03	0.19	0.08
62000	0.1	0.01	0.13	0.38	0.06	0.02	0.09	0.06	0.09	0.14
64000	0.01	0.01	0.08	0.24	0.02	0.02	0.08	0.01	0.04	0.07
66000	0.02	0.01	0.06	0.15	0.02	0.02	0.06	0.01	0.02	0.08
68000	0.01	0	0.07	0.16	0	0.02	0.05	0.01	0.04	0.03
70000	0.01	0.02	0.04	0.06	0	0.01	0.11	0	0.12	0.01
72000	0	0.01	0.04	0.13	0	0.01	0.04	0	0.01	0.04
74000	0	0	0.02	0.06	0	0.01	0.01	0	0.01	0.02
76000	0	0	0.01	0.06	0	0	0.01	0	0.01	0.04
78000	0	0	0	0.02	0	0	0.01	0	0.01	0.02
80000	0	0	0	0.02	0	0	0	0	0	0.08
82000	0	0	0	0	0	0	0	0	0	0

The number of axle types per truck class also uses the default values used in Pavement ME, that were based on the analysis of national databases, such as the LTPP database (ARA 2004). The number of axle

types per truck class can be seen in the following table. The effect of tridem axles is considered by calculating tridem axles with tandem axles. Tandem axles were calculated by summing the number of tandem and tridem axles per truck seen in the following table.

Table 34: Default values for the average number of single and tandem axles per truck class (ARA 2004)

Truck Classification	Number of Single Axles per Truck	Number of Tandem Axles per Truck	Number of Tridem Axles per Trucks[1]
4	1.62	0.39	0.00
5	2.00	0.00	0.00
6	1.02	0.99	0.00
7	1.00	0.26	0.83
8	2.38	0.67	0.00
9	1.13	1.93	0.00
10	1.19	1.09	0.89
11	4.29	0.26	0.06
12	3.52	1.14	0.06
13	2.15	2.13	0.35

[1]Tridem axles were calculated as tandem axles

In order to determine the load spectra for each month of the design period, the following steps are taken. First, the monthly AADTT is calculated based on the ADT, growth type, growth rate, and LDF. Next, the number of single and tandem axles (calculated separately) for each vehicle class for each month are determined using the AADTT, FHWA vehicle class distribution percentages (Table 31), and the number of single and tandem axles per truck (Table 32, Table 33). The last step is to combine the number of single and tandem axles per load level from each vehicle class (calculated in Table 34) into a single load distribution for each axle configuration

Another portion of the framework dealing with traffic considerations is wheel wander. The mean wheel location is assumed to be 18 in from the outer edge of the wheel to the edge of the lane. Also, a standard deviation of 10 in is assumed. Both values are national average (Level 3) values assumed in Pavement ME (ARA 2004).

7.3.3 Model Inputs

With the equivalent temperature gradients defined for each calibration section, the iterative faulting calculations can then be performed. The primary calculation for each month is to determine the differential energy which can be found using Equation 105 through 107. How each of the inputs to the neural network are defined is outlined next.

$$\Sigma\delta_{B,A,m} = NN_{\Sigma B,A}(JTSpace, s, LTE_{shoulder}, \ell_{OL}, \ell_{EX}, \Phi, \frac{AGG}{k_{IL}\ell_{OL}}, q_i^*) \tag{105}$$

$$\Sigma\delta_{C,A,m} = NN_{\Sigma C,A}\left(JTSpace, s, LTE_{shoulder}, \ell_{OL}, \ell_{EX}, \Phi, \frac{AGG}{k_{IL}\ell_{OL}}, q_i^*\right) \tag{106}$$

$$DE_m = \frac{1}{2}n_m k\left(\Sigma\delta_{B,A,m}\right) \tag{107}$$

Where:

DE_m is the differential energy density deformation accumulated for month m

n_m is the number of ESAL applications for current month

k is the Totsky interlayer coefficient (psi/in)

$\Sigma\delta_{B,A,m}$ is the basin sum deflection for the difference between the loaded and unloaded slab for axle type A (A=1 for single; A=2 for tandem) for month m (in)

$\Sigma\delta_{C,A,m}$ is the corner deflection for the difference between the loaded and unloaded slab for axle type A (A=1 for single; A=2 for tandem) for month m (in).

For each calibration section, three files are needed to perform the faulting calculation including input, traffic, .tem, and .icm files. The .tem and .icm EICM files have been previously discussed along with the climatic considerations. An example input text file is shown in Table 35. Twenty-seven different inputs are specified for each section.

Table 35: Example of an input text file

```
6        % Thickness of the PCC overlay (in)
4000000  % 28 day elastic modulus of PCC overlay (psi)
5000     % 28 day compressive strength of PCC overlay (psi)
600      % 28 day modulus of rupture of PCC overlay (psi)
1        % Thickness of the interlayer (in)
5.0      % Percent passing #200 sieve in interlayer
3.0      % Percent air voids in interlayer
5        % Effective % binder content in interlayer
3500     % Totsky k-value for the interlayer (psi/in)
10       % Thickness of the existing pavement (in)
5000000  % Elastic modulus of existing pavement (psi)
100      % k-value of all layers beneath the existing pavement (psi/in)
12       % Joint spacing (ft)
0        % Presence of dowels (O=none, 1=yes)
0        % Dowel diameter (in)
0        % Lane/shoulder LTE (%)
0.0000055 % Coefficient of thermal expansion of PCC overlay (in/in/oF)
360      % Analysis period (months)
-2.204   % EELTG established for each calibration section (oF/in)
5        % Numeric month of overlay construction
550      % Cement content for overlay concrete (lbs)
2        % Number of lanes in travel direction
10000    % One-way average daily traffic (ADT)
730      % Average daily truck traffic (ADTT)
0        % Growth type (none=0, linear=1, compound=2)
0        % Growth rate (decimal, not percentage)

1        % IL type (fabric=0, dense graded HMA=1, open graded HMA=2, other=3)
```

Looking at the inputs to the ANNs, the joint spacing and the radius of relative stiffness of the overlay and existing pavements can be easily calculated from the input file. Note that a default value of 0.18 is assumed for the Poisson's ratio of concrete. Additionally, $LTE_{shoulder}$ is binary depending on whether there is a tied concrete shoulder (90%) or an asphalt shoulder (0%). The normalized load-pavement weight ratio, $q_m^* = \frac{P_i}{A*\gamma_{pcc}*h_{OL}}$. P_i is each load level i (lbs) and γ_{pcc} is 150 lbs/ft³ for all calibration sections. The wheel wander, s, is a normally distributed in the wheel path with a standard deviation of 10 in. Korenev's nondimensional temperature gradient, Φ, is found according to the equation in the NN development section. All variables in this equation have been discussed previous with the exception of the temperature difference, ΔT. In this procedure, the temperature difference is calculated as the effective equivalent

linear temperature difference for differential energy plus the default value of the effective built-in temperature difference from Pavement ME of -10 °F (ARA, 2004). The final ANN input is $AGG/k_{IL}\ell_{OL}$ (J_{agg}). This variable is also referred to as the nondimensional joint stiffness. In order to calculate the nondimensional joint stiffness, the contribution of both aggregate interlock and dowels must be considered.

To establish the effects of aggregate interlock on joint stiffness, the joint width in the overlay must be estimated. The joint width for each month is calculated according to Equation 108. The two variables that still need to be determined to calculate the joint width are the PCC set temperature and the PCC overlay shrinkage strain. The concrete set temperature is estimated using Table 36, which requires the mean monthly temperature for the month of cast as well as the cement content. The concrete overlay shrinkage strain is established from tensile strength (correlated from compressive strength) using the recommendations in AASHTO 93. This recommendation is shown in Table 37. The nondimensional aggregate joint stiffness can then be calculated for each month using Equation 109 and 110 adopted from Zollinger et al. (1998). Note that is ΔS_{tot} equal to zero for the first month of the analysis and the individual monthly increments of loss in shear capacity can be calculated using (111).

$$JW(m) = max(12000 * c * JTSpace * (CTE * (T_c - T(m)) + \varepsilon_{sh}), 0) \qquad (108)$$

Where:

$JW(m)$ is the joint width for month m (mils)

c is the friction factor (0.65 for asphalt interlayers, 1.74 for fabric interlayers)

$JTSpace$ is the joint spacing in the overlay (ft)

CTE is the overlay PCC coefficient of thermal expansion (in/in/°F)

T_c is the concrete set temperature (°F)

$T(m)$ is the mean mid-depth PCC overlay temperature for month m (°F)

ε_{sh} is the PCC overlay shrinkage strain (in/in).

Table 36: PCC set temperature for cement content and mean temperature during month of cast (°F)

	Cement Content (lbs)			
Mean Monthly Air Temp (°F)	400	500	600	700
40	52	56	59	62
50	66	70	74	78
60	79	84	88	93
70	91	97	102	107
80	103	109	115	121

Mean Monthly Air Temp (°F)	Cement Content (lbs)			
	400	500	600	700
90	115	121	127	134
100	126	132	139	145

Table 1: PCC overlay shrinkage strain relationship

Tensile Strength (psi)	Shrinkage Strain (in/in)
400	0.0008
500	0.0006
600	0.00045
700	0.0003
800	0.0002

$$S = 0.5 * h_{pcc} * e^{-0.032*JW} - \Delta S_{tot} \tag{109}$$

$$\log(J_{AGG}) = -28.4 * e^{-e^{-\left(\frac{S-e}{f}\right)}} \tag{110}$$

Where:

S is the aggregate joint shear capacity

JW is the joint opening (mils)

$\Delta S_{tot} = \sum_{i=1}^{m} \Delta S_i$ which is the cumulative loss of shear capacity at the beginning of the current month

J_{AGG} is the nondimensional aggregate joint stiffness for current monthly increment

e is equal to 0.35

f is equal to 0.38.

$$\Delta S_i = \begin{cases} 0 & if\ JW < 0.001 h_{PCC} \\ n_{i,A} * \dfrac{0.005 * 10^{-6}}{1.0 + \left(\dfrac{JW}{h_{PCC}}\right)^{-5.7}} \left(\dfrac{\tau_i}{\tau_{ref}}\right) & if\ 0.001 \leq JW \leq 3.8 h_{PCC} \\ n_{i,A} * \dfrac{0.068 * 10^{-6}}{1.0 + 6.0 * \left(\dfrac{JW}{h_{PCC}} - 3\right)^{-1.98}} \left(\dfrac{\tau_i}{\tau_{ref}}\right) & if\ JW > 3.8 h_{PCC} \end{cases} \tag{111}$$

Where:

ΔS_i is the loss of shear capacity from all ESALs for current month i

$n_{i,A}$ = the number of axle A load applications for load level i

h_{PCC} is the overlay slab thickness (in)

JW = joint opening (mils)

$\tau_i = J_{AGG} * (\Sigma\delta_{C,A,i})$ which is the shear stress on the transverse joint surface from the response model

$\tau_{ref} = 111.1 * \exp(-\exp(0.9988 * \exp(-0.1089 * \log(J_{AGG}))))$ which is the reference shear stress derived from the PCA test results.

For a doweled pavement, the model adopted for the nondimensional dowel stiffness is that from ARA (2004). The initial nondimensional dowel joint stiffness is calculated using Equation 112 and the critical nondimensional dowel joint stiffness is calculated with Equation 113. The nondimensional dowel stiffness is then calculated using Equation 114 and the dowel damage parameter is presented in Equation 115.

$$J_0 = \frac{152.8 * A_d}{h_{pcc}} \tag{112}$$

$$J_d^* = \begin{cases} 118, if \dfrac{A_d}{h_{pcc}} > 0.656 \\[2mm] 210.0845\dfrac{A_d}{h_{pcc}} - 19.8, if 0.009615 \leq \dfrac{A_d}{h_{pcc}} \leq 0.656 \\[2mm] 0.4, if \dfrac{A_d}{h_{pcc}} < 0.009615 \end{cases} \tag{113}$$

$$J_d = J_d^* + (J_0 \text{-} J_d^*)exp(-DOWDAM) \tag{114}$$

$$\Delta DOWDAM = \frac{J_d * (\Sigma\delta_{C,A,m}) * DowelSpace * n_{i,A}}{d * f_c'} \tag{115}$$

Where:

A_d is the area of dowel bar (in^2)

h_{pcc} is the overlay PCC thickness (in)

J_0 is the initial nondimensional dowel stiffness

J_d^* is the critical nondimensional dowel stiffness

J_d is the nondimensional dowel stiffness for current month

$DOWDAM$ is the cumulative dowel damage for the current month

$DowelSpace$ is the dowel bar spacing (in)

$n_{i,A}$ = the number of axle A load applications for load level i

d is the dowel bar diameter (in)

f_c' is the PCC compressive stress estimated from the modulus of rupture.

With the differential energy calculated, the faulting can then be predicted using Equation 116 through 119.

$$F_0 = (C_1 + C_2 * FR^{0.25}) * \delta_{curl} * [C_5 * E]^{C_6} * log(WETDAYS * P_{200}) \tag{116}$$

$$F_i = F_{i-1} + C_7 * C_8 * DE_i * [C_5 * E]^{C_6} \tag{117}$$

$$\Delta Fault_i = (C_3 + C_4 * FR^{0.25}) * (F_{i-1} - Fault_{i-1})^2 * C_8 * DE_i \tag{118}$$

$$Fault_i = Fault_{i-1} + \Delta Fault_i \tag{119}$$

Where:

F_0 is the initial maximum mean transverse joint faulting (in)

FR is the base freezing index defined at the percentage of the time that the top of the base is below freezing (<32°F)

δ_{curl} is the maximum mean monthly PCC upward slab corner deflection due to temperature curling and moisture warping

E is the erosion potential of interlayer: f(% binder content, % air voids, P_{200})

P_{200} is the percent of interlayer aggregate passing No. 200 sieve

WETDAYS is the average number of annual wet days (> 0.1 in of rainfall)

F_i is the maximum mean transverse joint faulting for month i (in)

F_{i-1} is the maximum mean transverse joint faulting for month i-1 (in)(If i =1, $FMAX_{i-1} = FMAX_0$)

DE_i is equal to the differential energy density accumulated during month i

$\Delta Fault_i$ is the incremental monthly change in mean transverse joint faulting during month i (in)

$C_1 \dots C_8$ are the calibration coefficients

$Fault_{i-1}$ is the mean joint faulting at the beginning of month i (0 if i = 1)

$Fault_i$ is the mean joint faulting at the end of month i (in).

7.3.4 Calibration Sections

The calibration database used to calibrate the UBOL faulting model consists of 26 different sections from eight different states in the United States. The calibration sections are comprised of seven LTPP sections, six sections from the MnROAD, and eight MDOT pavement sections. Table 38 presents a range for some calibration section parameters. Of the sections, 9 are undoweled while the rest are doweled. The dowel diameter for the doweled sections ranged from 1 - 1.5 in. If the pavement section has a random joint spacing, the mean joint spacing was used in the analysis. Considering the number of time series observations available, a total of 129 data points is available for calibrating the model.

The age of the sections ranged from approximately 2.5 to 26.5 years with an average of 10.5 years of age. In terms of ESALs, the traffic ranged from approximately 0.99 million to 24.5 million with an average value of around 8 million ESALs. Over half of the sections had experienced over 6 million ESALs, while 20% of the sections had experienced over 10 million ESALs. Only one undoweled section was exposed to more than 10 million ESALs. Detailed information for each calibration section can be found in Appendix B.

Table 38: Range of parameters for calibration sections

Parameter	Minimum	Maximum	Average
Age, yrs	2.5	26.5	10.5
Estimated ESALs	8.56E+05	2.45E+07	8.27E+06
Avg. jt. spacing, ft	6	21	14.3
Interlayer thickness, in	0.5	8.6	2.2
Overlay thickness, in	4.5	10.3	7.3
Overlay EMOD, psi	3.09E+06	4.85E+06	3.97E+06
Overlay MOR, psi	530	1022	672
Existing thickness, in	7.1	10.2	8.5
Existing EMOD, psi	3.68E+06	5.00E+06	4.55E+06
Overlay cement content, lbs	354	594.5	536.9

7.4 RESULTS OF MODEL CALIBRATION

Calibration of the faulting model requires adjusting the calibration coefficients from Equation 116 through 119 to minimize the error function defined by Equation 120. Additionally, the shape of the erosion function had to be fit based upon the interlayer characteristics chosen to be important to faulting. The fitted erosion model can be seen in Equation 121 and 122. A macro driven excel spreadsheet was developed to calibrate the model and the following steps were taken to minimize the error. Several calibration parameters were fixed at a constant value while the remaining coefficients were varied to find the lowest values of the error function. Once the error is minimized for the varied coefficients, these values are kept constant while the coefficients that were previously held constant are allowed to vary until the lowest possible value of the error function is achieved. These two sets of coefficients are varied in this manner until the error can be minimized no further. These steps do not guarantee a global minimum error

but should provide a reasonable result. Minimization of the bias in the model with the calibration parameters must also be performed in addition to error minimization when selecting the final set of calibration coefficients. Predicted versus measured transverse joint faulting is presented in Figure 92. Table 39 summarizes all of the calibration coefficients that have been chosen.

$$\text{ERROR}(C_1, C_2, C_3, C_4, C_5, C_6, C_7, C_8, C_{\text{Dowel}})$$
$$= \sum_{i=1}^{N} (\text{FaultPredicted}_i - \text{FaultMeasured}_i)^2 \tag{120}$$

Where:

ERROR is the error function

$C_1, C_2, \dots, C_8$ are the calibration coefficients

$FaultPredicted_i$ is the predicted faulting for i$^\text{th}$ observation in dataset

$FaultMeasured_i$ is the measured faulting for i$^\text{th}$ observation in dataset

N is equal to the number of observations in the dataset.

$$\alpha = \log(1 + a * (5 - \%Binder) + b * (10 - \%AV) + c * P_{200}) \tag{121}$$

$$E = \begin{cases} (1.8483 * \alpha^2 - 0.8179 * \alpha + 0.1123) & Asphalt\ Interlayer \\ 0.02 & Non\ woven\ geotextile\ fabric\ \text{Interlayer} \end{cases} \tag{122}$$

Where:

α = is the erodibility index

a, b, c are the calibration coefficients, (0.15, 0.14, 0.04)

$\%Binder$ is the binder content of the interlayer (%)

$\%AV$ is the air voids percentage of interlayer

P_{200} is the percent aggregate passing No. 200 sieve in interlayer

E is the model erosion to be used in predictive equations.

178

$$y = 0.9836x + 0.0023$$
$$R^2 = 0.70$$
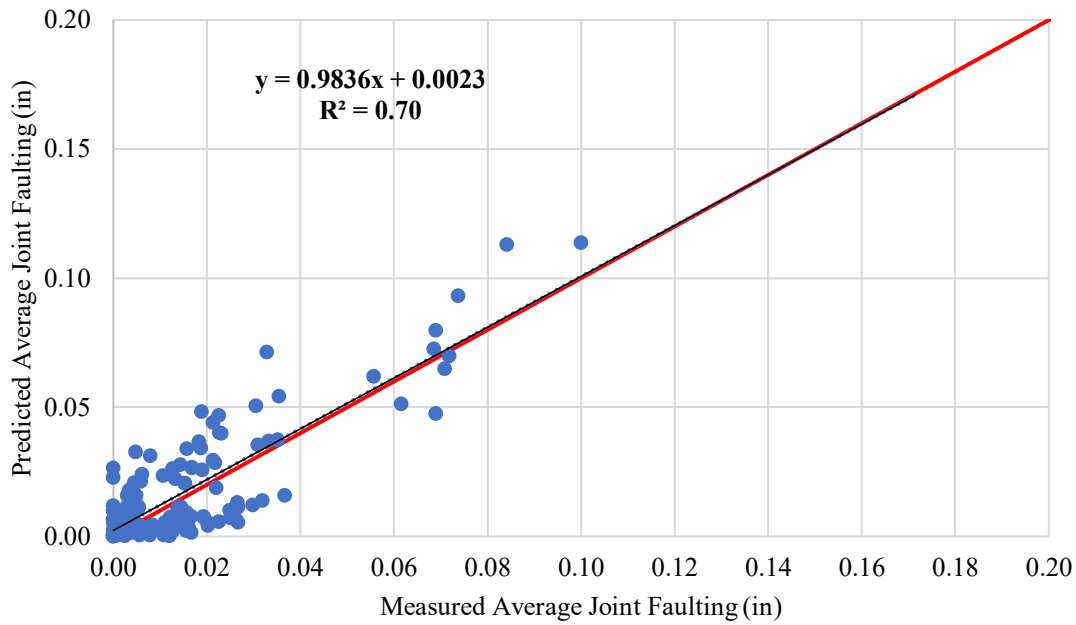
Figure 92: Measured vs. predicted UBOL transverse joint faulting

Table 39: UBOL transverse joint faulting calibration coefficients, [†]for joint spacing less than 12 feet, [‡]for joint spacing 12 feet or greater

Calibration Coefficient	Value
C_1	1.25
C_2	1.5
C_3	0.8
C_4	0.015
C_5	0.01
C_6	1.46
C_7	0.62
C_8	2.5×10^{-7} [†], $(-35 + JointSpacing \times 5) \times 10^{-8}$ [‡]

7.4.1 JPCP Transverse Joint Faulting Model Adequacy Checks

A series of model adequacy checks were performed to ensure the developed model coefficients provided reasonable values in terms of predictability and reasonableness. The tests outlined by Mallela et al. (2009) have been performed and are summarized below. For the model, an overall SEE of 0.013 in of faulting and a coefficient of determination, R^2, of 0.71 was deemed reasonable in comparison to values obtained from

179

Pavement ME JPCP transverse joint faulting model calibration efforts (Sachs et al., 2014). The model bias was checked by using the three hypothesis tests outlined in Table 40. The null and alternative hypothesis outlined in Table 41 were tested and the results summarized in Table 41. A significance level of 0.05 was assumed for hypothesis testing. From Table 41, none of the three null hypotheses are rejected indicating that model bias has been removed through the calibration.

Table 40: Null and Alternative hypothesis tested for JPCP faulting

Hypothesis 1	Null hypothesis H_o: Linear regression model intercept = 0
	Alternative hypothesis H_a: Linear regression model intercept ≠ 0
Hypothesis 2	Null hypothesis H_o: Linear regression model slope = 1.0
	Alternative hypothesis H_a: Linear regression model slope ≠ 1.0
Hypothesis 3	Null hypothesis H_o: Mean ME Design faulting = Mean LTPP measured faulting
	Alternative hypothesis H_a: Mean ME Design faulting ≠ Mean LTPP measured faulting

Table 41: Results from transverse joint faulting model hypothesis testing

Hypothesis Testing and t-Test			
Test Type	Value	95% CI	P-value
Hypothesis 1: Intercept = 0	0.0585	-0.0298 to 0.0344	0.89
Hypothesis 2: Slope = 1	-0.0252	-0.2926 to 2.260	0.98
Paired t-test	-	-	0.34

7.4.2 JPCP Transverse Joint Faulting Model Reliability

The JPCP transverse joint faulting model reliability (standard deviation) was determined in a similar way as was conducted for Pavement ME (ARA, 2004). The resulting standard deviation model developed from UBOL faulting for a design at a specified level of reliability is presented below as Equation 123 and Figure 93 using the data from Table 42, which was determined from the predicted faulting data.

$$Stdev(FLT) = 0.084 * (FLT^{0.5003})$$ (123)

Where:

Stdev(FLT) is the transverse joint faulting standard deviation (in)

FLT is the UBOL model predicted transverse joint faulting (in).
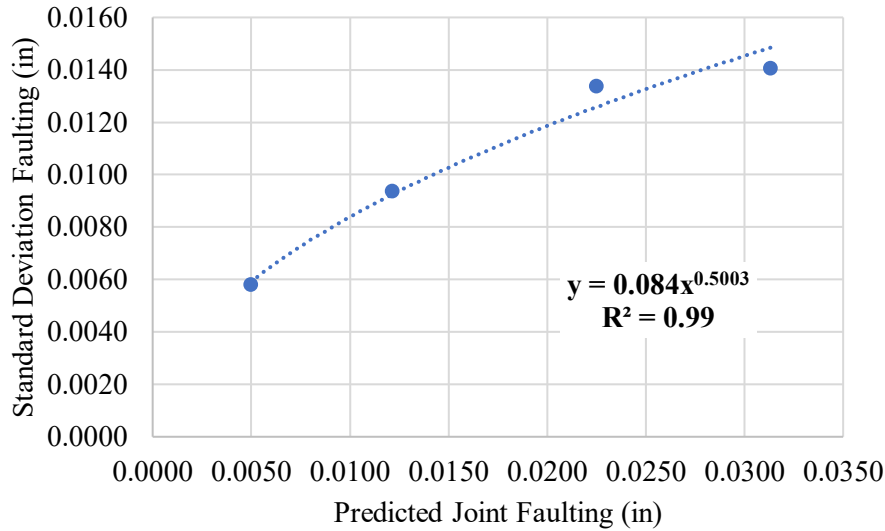
Figure 93: Predicted faulting versus faulting standard deviation

Table 42: Predicted faulting data used to develop faulting standard deviation model

Mean predicted faulting, in	Std. Dev. of predicted faulting, in
0.0225	0.0134
0.0313	0.0140
0.0121	0.0094
0.0050	0.0058

A sensitivity analysis of the predicted faulting to various parameters of interest is conducted to further evaluate the model. The base design parameters used in the sensitivity analysis are as follows: 6-in undoweled PCC overlay (elastic modulus of $4*10^6$ psi and modulus of rupture of 600 psi), 1-in dense graded asphalt, 10-in existing PCC (elastic modulus of $5*10^6$ psi), joint spacing is 12 ft, asphalt shoulder, and 20 million ESALs uniformly distributed over 30 years. The default climate was Pittsburgh, Pennsylvania (Wet-Freeze). The entire design parameters for the control section can be seen in Table 43.

Table 43: Sensitivity analysis control section design parameters

Parameter	Value
Overlay PCC thickness (in)	6
PCC modulus of elasticity (psi)	4,000,000
PCC modulus of rupture (psi)	600
Interlayer thickness (in)	1
% P200 in Interlayer	5
% Air voids in Interlayer	3
% Effective binder in Interlayer	5
Interlayer Totsky k-value (psi/in)	3,500
Existing PCC thickness (in)	10
Existing PCC modulus of elasticity (psi)	5,000,000
Modulus of subgrade reaction, k-value (psi/in)	100
PCC joint spacing (ft)	12
Dowel diameter (in)	0
Shoulder type (% LTE)	Asphalt (0%)
CTE-OL (°F/in/in)	5.50E-06
Design period (months)	360
EELTG (°F/in)	-2.94
ADT	10,000
ADTT	730
Growth type	No growth
Interlayer type	Dense graded asphalt

One parameter was allowed to vary at a time. The effect of the joint spacing on the resulting predicted faulting can be seen in Figure 94. As can been seen in Figure 94, as the joint spacing increases, the predicted faulting increases. It should be noted that as the joint spacing decreases the decrease in faulting may not result in the same level of roughness. As there are more joints with a smaller joint spacing, the amount of average faulting does not need to be as large to produce the same ride for a section with more faulting and a larger joint spacing (DeSantis et al., 2016). The significance of the presence and diameter of the dowels can be seen in Figure 95. The use of dowels, and the diameter of dowels greatly reduces the potential for faulting to develop.
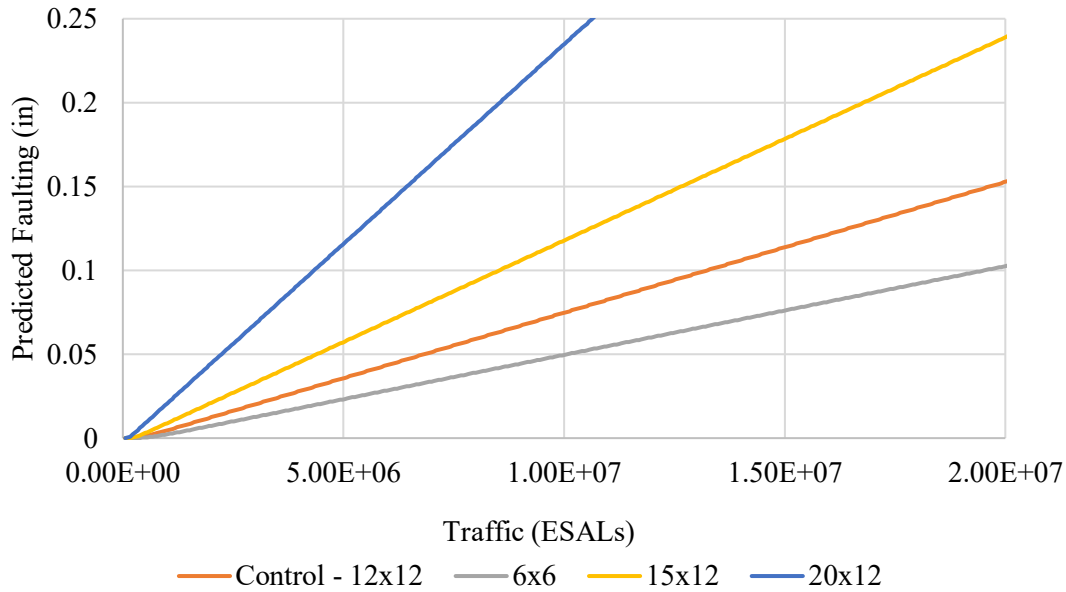
Figure 94: Sensitivity of joint spacing on predicted faulting (Width x Length)
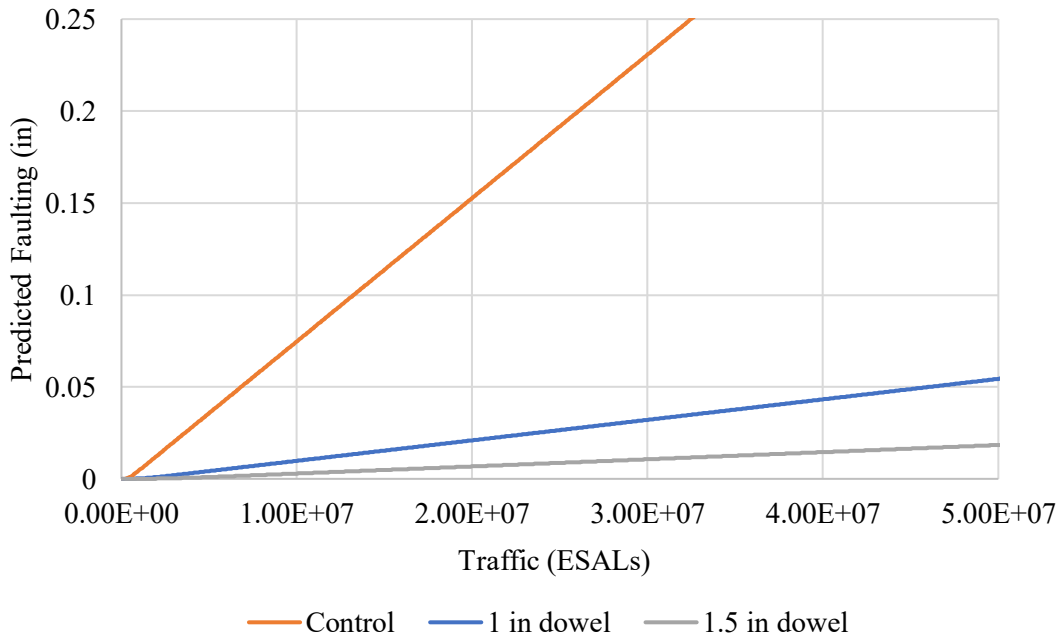
Figure 95: Sensitivity of dowels (dowel diameter) on predicted faulting

The effect of thickness on the predicted faulting can be seen in Figure 96. The trend observed is as expected, an increase in slab thickness results in a decrease in predicted joint faulting. Deflections at the corners and joints should decrease with increasing slab thickness and this is the case. Radius of relative stiffness for the existing PCC pavement and underlying layers was held constant in the faulting model, as the rigidity of the underlying structure has an effect on faulting up to a certain point at which there is no

additional support. The stiffnesses anticipated for existing pavements exceed the threshold. As can be seen from Figure 97, there is no change in faulting with variation in radius of relative stiffness of the existing PCC pavement and underlying layers.
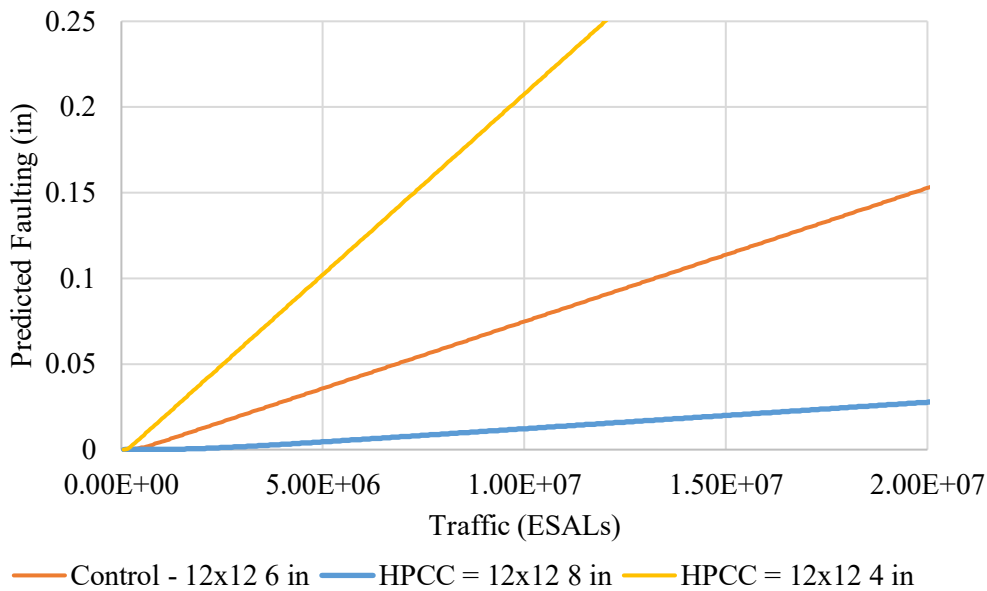
Figure 96: Sensitivity of thickness on predicted faulting
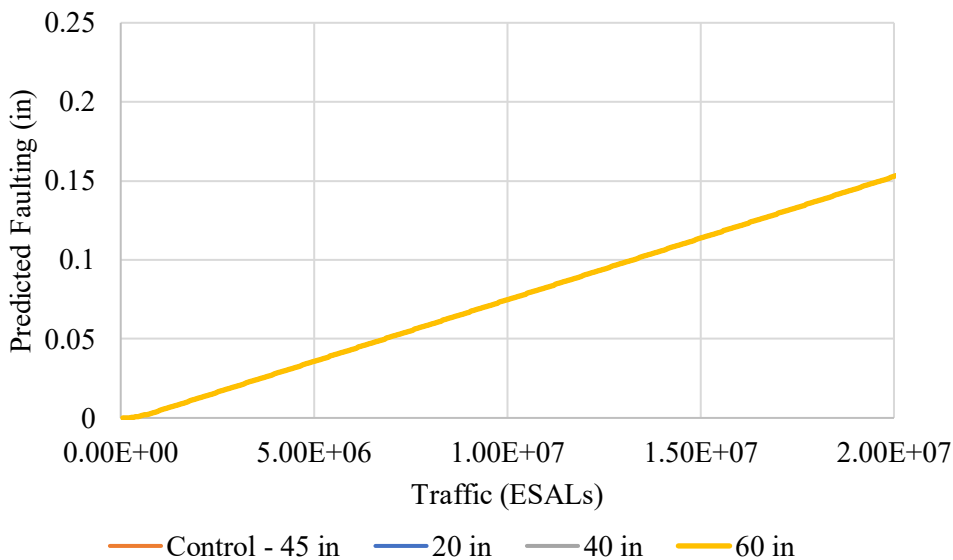
Figure 97: Sensitivity of radius of relative stiffness of existing PCC slab on predicted faulting

The effect of a concrete versus asphalt shoulder can be seen in Figure 98. The support condition at the shoulder reduces the deflections and stresses of the PCC slab. The greater the support, the greater the reduction in stress and deflections, which results in increased pavement performance.
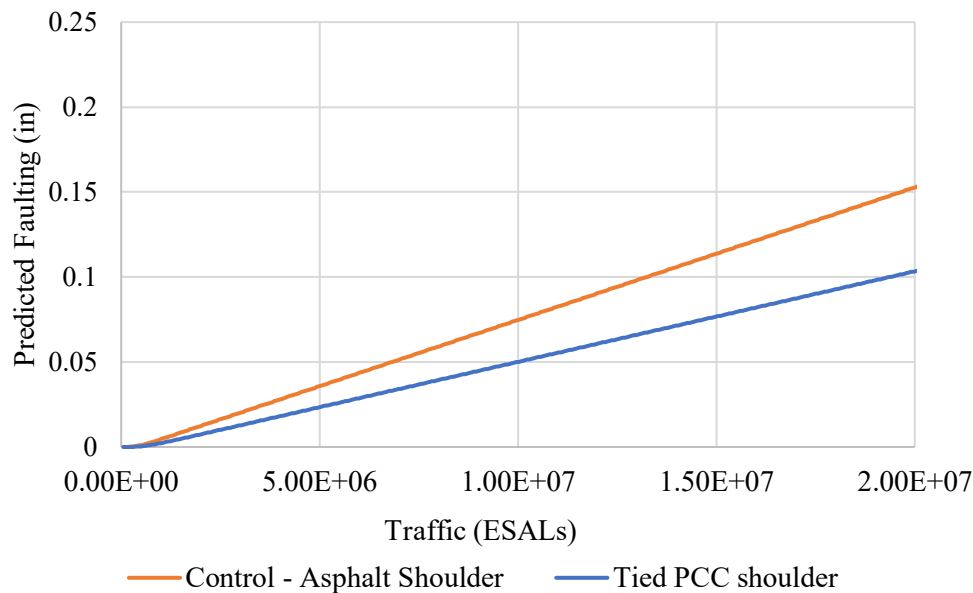
Figure 98: Sensitivity of shoulder support on predicted faulting

The interlayer was varied from a dense graded to an open graded (MIDAU) with the results shown in Figure 99 by modifying Equation 121 and 122 to change the calibrated erosion parameter. It should be noted that several calibration sections (MnROAD) had an asphalt interlayer with a much more open graded mix (PASSRC). These sections exhibited faulting due to insufficient strength in the interlayer. Because the model provides upper bounds on percent air voids and binder, it does not allow for such instable interlayers to be considered. Predicted faulting for a pavement with the PASSRC interlayer is not shown in Figure 99.
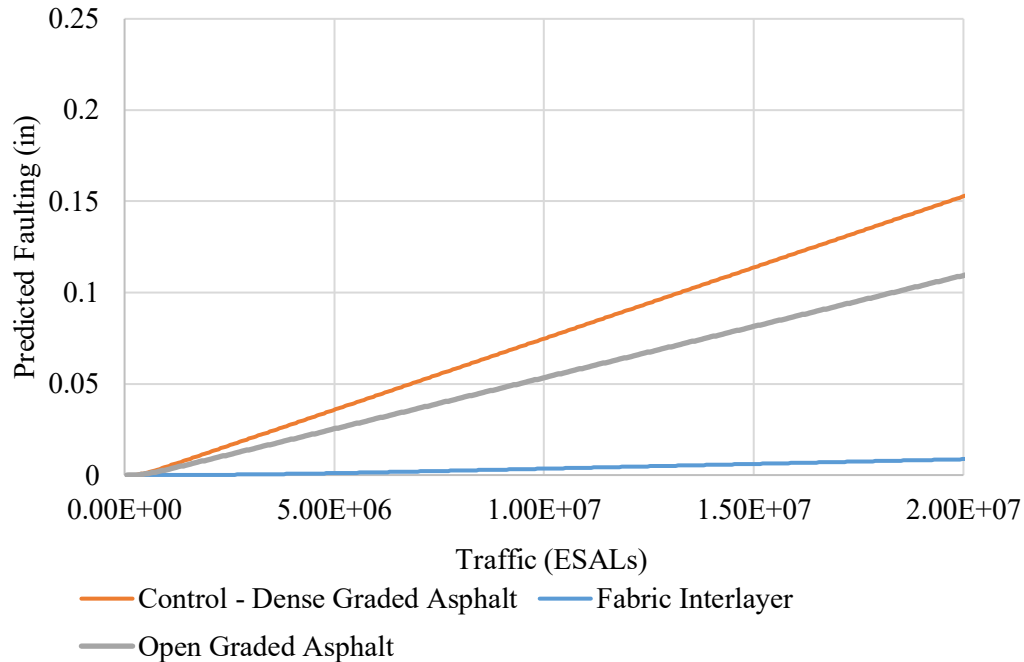
Figure 99: Sensitivity of interlayer type on predicted faulting

To better assess the erosion model, the sensitivity of each parameter was examined. Figure 100 shows the sensitivity of the percent passing the number 200 sieve for the asphalt interlayer. When a nonwoven geotextile fabric (NWGF) is used, this value is set to 0.01 (0%) because it is used in the incremental faulting equations. As the percent passing increases in the asphalt interlayer, the predicted faulting also increases. Figure 101 presents the sensitivity of percent air voids in the interlayer. When a nonwoven geotextile fabric is used, this value is set to 0%. As the percent air voids increases, the predicted faulting decreases. Percent air voids is not permitted to be greater than 6%, which is why the predicted faulting for 6% air voids is the same as 10% air voids in Figure 101. The last parameter to assess is the effective binder content in the interlayer, when an asphalt interlayer is present. Effective binder content is not permitted to be greater than 5%, as any incremental increase past this amount will have minimal effect on erosion. When a nonwoven geotextile fabric is used, this value is set to 0%. Figure 102 presents the sensitivity of effective binder content in the interlayer. It should be noted that each of these mixture parameters were varied one at a time for this analysis to show the effect of each. In reality they are all interdependent and in the development of the mixture design, changing one parameter would most likely result in the adjustment of one or both of the other parameters. This is why the composite effects of changes in the interlayer asphalt mixture have been provided in Figure 99.

186
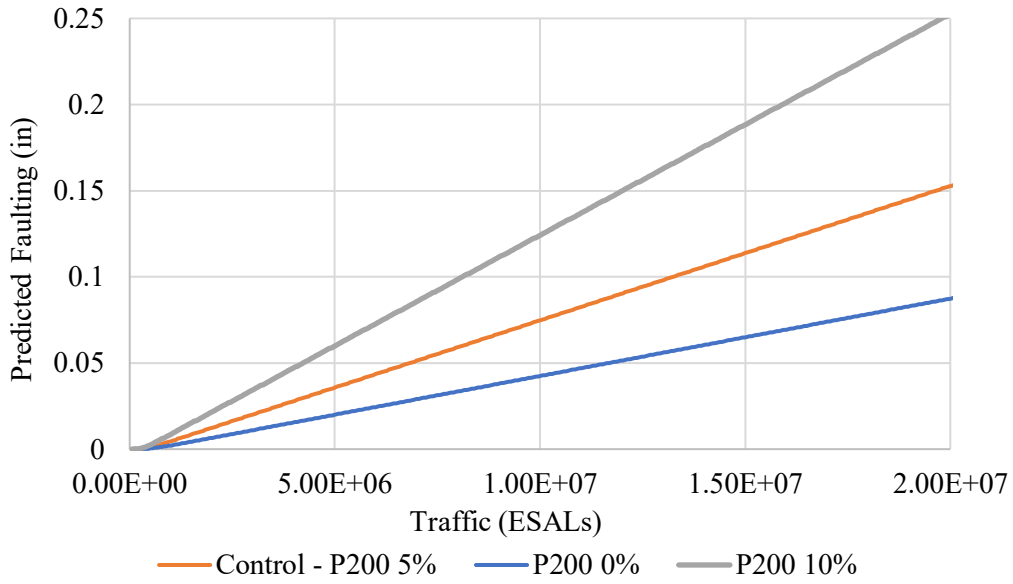
Figure 100: Sensitivity of P200 in the erosion model
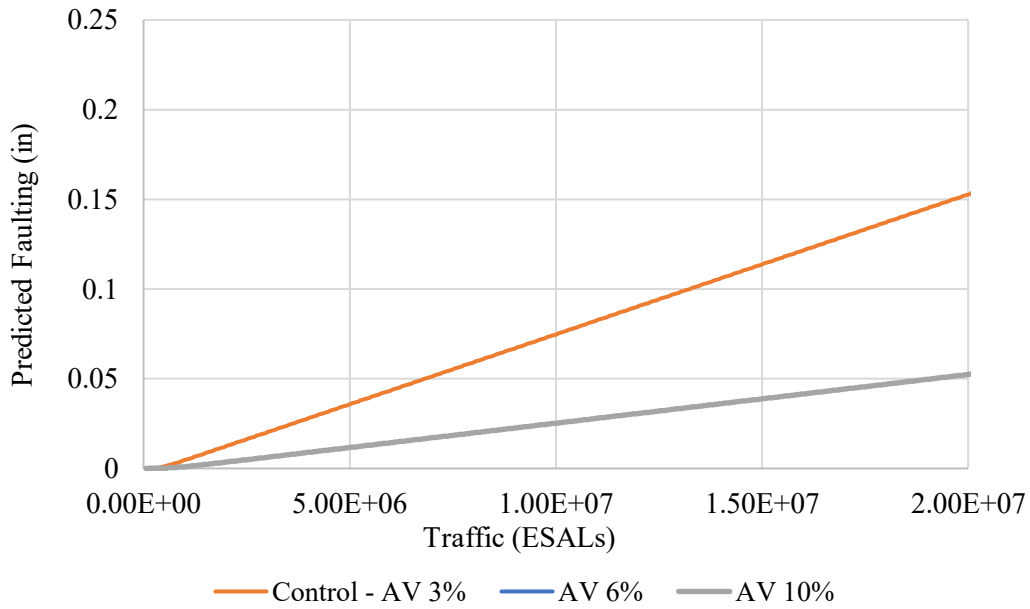
Figure 101: Sensitivity of percent air voids in the interlayer
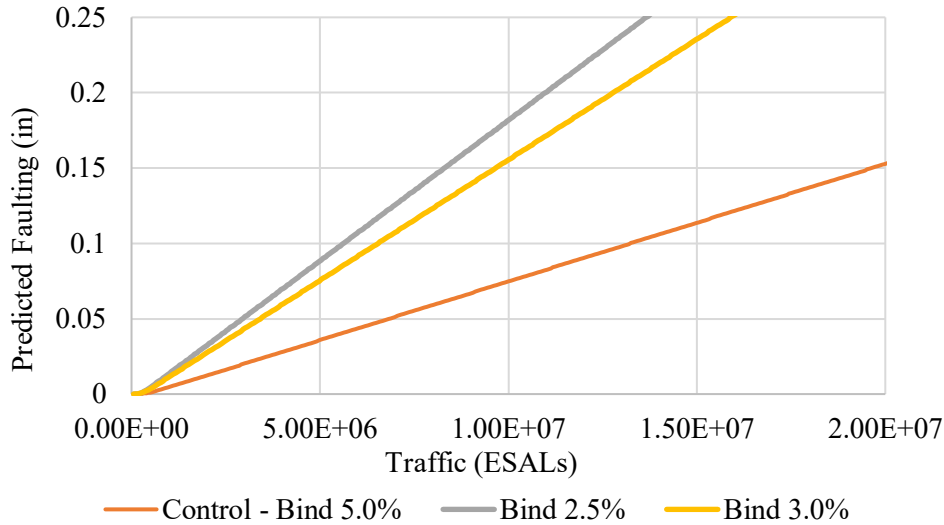
Figure 102: Sensitivity of effective binder content in the interlayer

It can be seen from Figure 103 that an increase in traffic over the 360 month analysis period results in an increase in joint faulting, as would be expected. Increased truck traffic will result in an increase in the differential energy for joint faulting as there is an increase in the number of load applications at the joints.
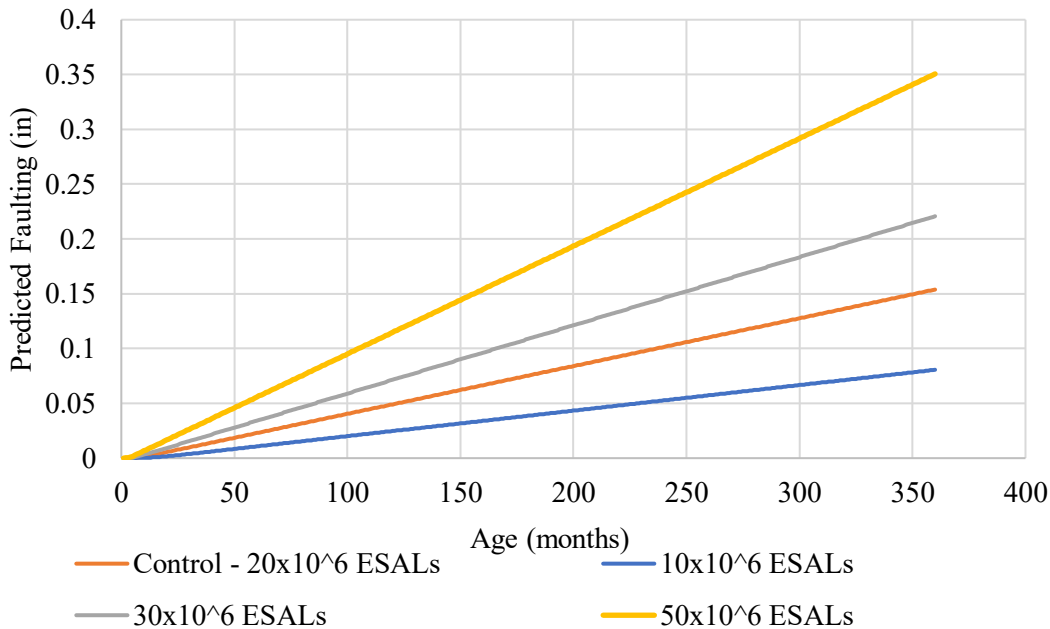
Figure 103: Sensitivity of traffic on predicted faulting

The elastic modulus of the overlay was varied along with the flexural strength since an increase in strength corresponds to an increase in stiffness. The effect of the increased strength on faulting can be seen in Figure 104.

188
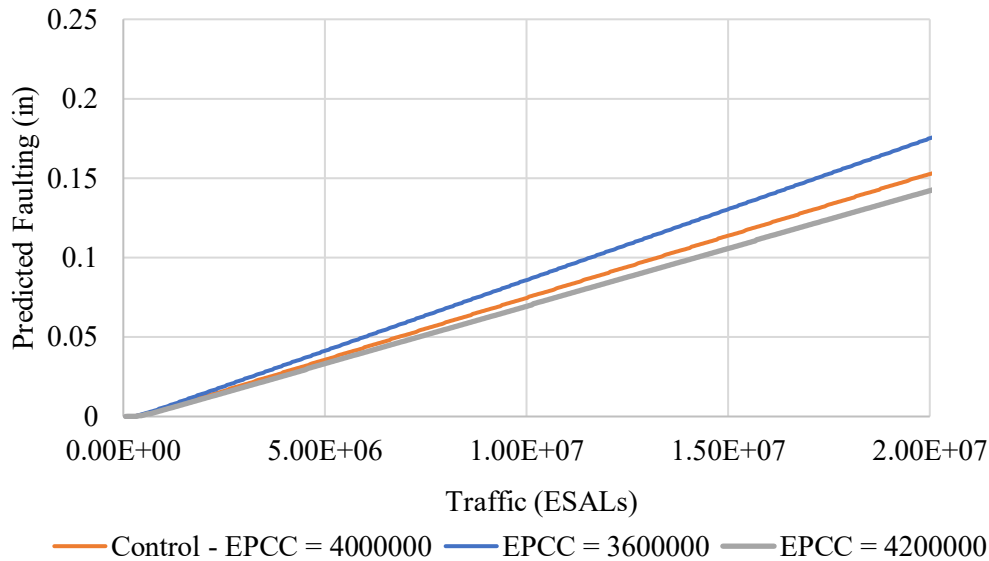
Figure 104: Sensitivity of overlay elastic modulus on predicted faulting

The effect of climate on predicted faulting can be seen in Figure 105. The predicted faulting due to climate is a function of three variables, the EELTG, Wetdays, and the freezing ratio. The EELTG has the largest influence on the predicted faulting because it is a direct input for predicting the differential energy (damage) in the ANNs. The EELTGs for Pittsburgh, PA; Miami, FL; Rapid City, SD; and Phoenix, AZ are as follows and correspond accordingly, -2.94, -3.09, -3.65, and -3.77 °F/in. This results in a higher predicted faulting in Phoenix, AZ than Pittsburgh, PA due to the larger magnitude of curvature, which causes a larger prediction of damage. It should be noted that the gradients provide above include a 10°F built-in gradient.

The effect of the reliability model is presented in Figure 106. It shows that higher amounts of faulting are predicted at higher levels of reliability.
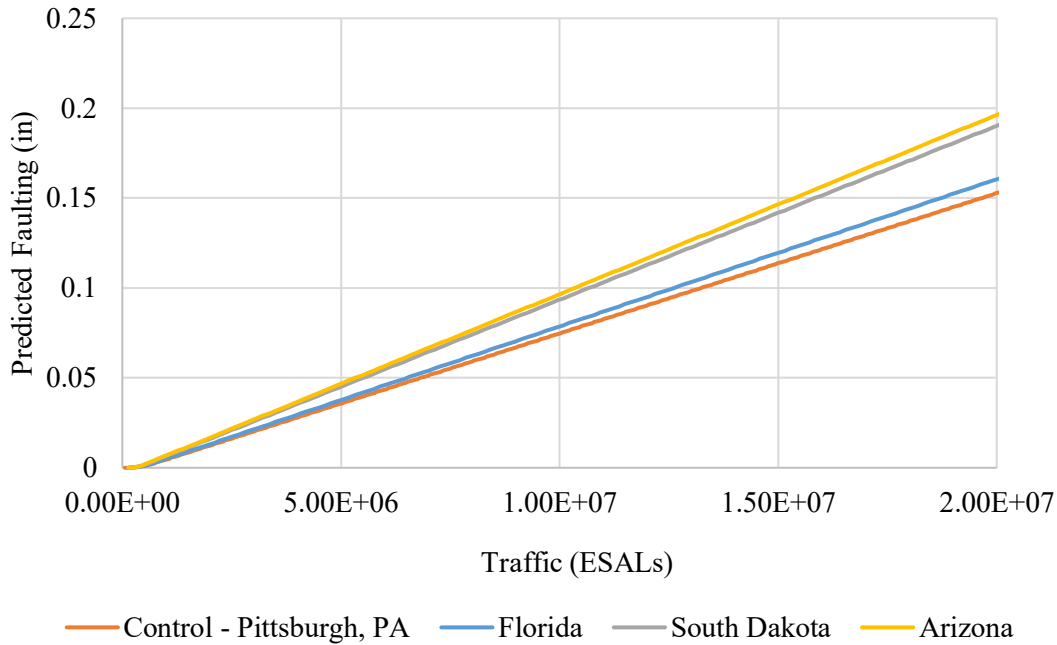
Figure 105: Sensitivity of climate type on predicted faulting
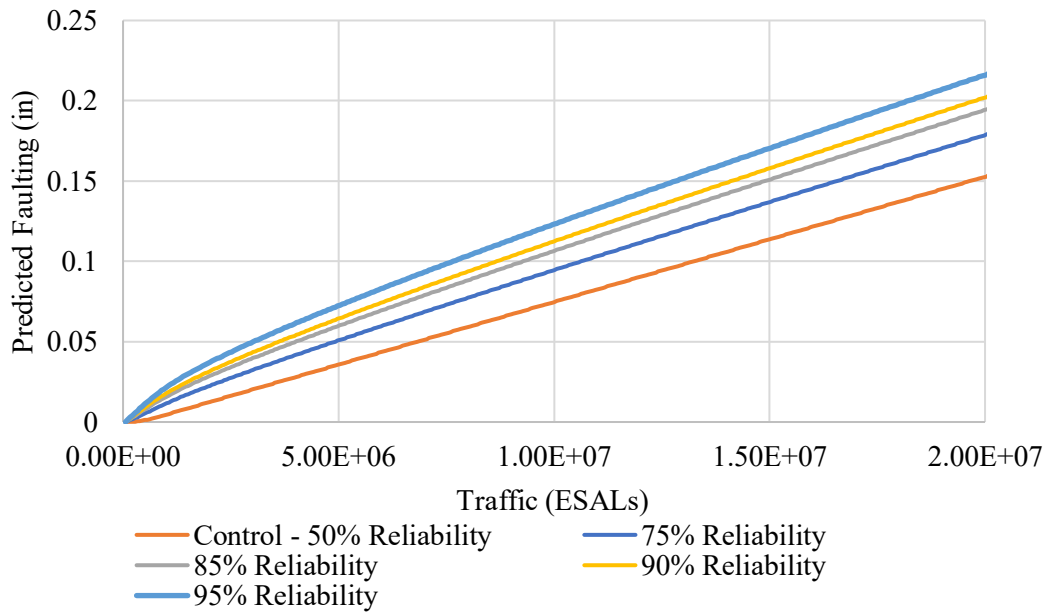
Figure 106: Sensitivity of reliability on predicted faulting

7.4.3 Model Implementation

In order to facilitate the implementation of the design procedure, an effective equivalent temperature gradient was used so that the procedure could be decoupled from the EICM. The effective equivalent

linear temperature gradient is the single gradient that, when applied for all traffic loads, would result in the same damage as would occur if hourly nonlinear temperature gradients were used. The effective equivalent temperature gradient was determined using the weather station data for each city incorporated into the design software. A total of 69 weather stations were chosen to represent the climatic conditions of the United States. For each weather station, a number of pavement structures and concrete mixture designs were considered. The effective equivalent linear temperature gradient was established for each weather station and each combination of design variables presented in Table 44. Interpolation is used to estimate the effective equivalent temperature gradient for design structures not included in Table 44.

Table 44: Design parameters used to generate framework of EELTG values

Parameter	Value
Existing layer thickness (in)	6 and 10
Overlay layer thickness (in)	4, 6, 8, and 10
Joint spacing (ft)	6 x 6, 12 x 12, 15 x 12, 20 x 12
Shoulder LTE (%)	0 and 90
PCC MOR (psi)	550
Overlay PCC modulus (10^6 psi)	3.5, 4.0, and 4.5
Dowel diameter (in)	0 and 1.25
Interlayer k-value (psi/in)	425 and 3500

7.5 SUMMARY FOR FAULTING MODEL

This chapter details the development of ANNs used to predict the critical responses for UBOL joint faulting using MATLAB's Neural Network Toolbox. Several previous faulting models were then examined looking at key predictive variables and frameworks used to determine faulting for JPCP pavements. The framework for the model to predict faulting for UBOL was then presented. This includes how climatic factors are treated, primarily the temperature gradient for the overlay. Then a discussion of how differential energy is calculated along with all the steps to establish the inputs for the ANNs. Finally, the incremental faulting equations are presented. With the framework to be used for predicting faulting defined, a discussion of the data available to calibrate the faulting model is made that includes the location of pavement sections and relevant design features. The model calibration is then presented.

CHAPTER 8: SUITABILITY OF EXISTING PROJECT TO RECEIVE UNBONDED CONCRETE OVERLAY

This chapter discusses suitability of an existing concrete or composite pavement to serve as a platform for an unbonded concrete overlay.

8.1 SUITABILITY FOR AN UNBONDED CONCRETE OVERLAY

Virtually any type and condition of existing concrete pavement can be overlaid with a well-designed unbonded JPCP overlay, but this treatment is especially attractive for concrete pavements nearing the end of their life yet still providing good, uniform support for the new overlay. Unbonded overlays can be used when existing concrete pavements present any level of material durability issues, such as spalling or popouts. However, the evaluations should confirm that future materials related expansion will not result in blow-ups (panel buckling) of the underlying pavement.

The evaluation of the existing pavement is the first step in determining if an unbonded concrete overlay is the correct rehabilitation alternative. The evaluation seeks to identify and characterize the existing pavement in terms of distresses (e.g. cracking and faulting), structural condition (i.e. ability to carry load), functional performance (e.g. roughness and noise), and material-related issues (e.g. ASR, D-cracking). Many available resources provide detailed procedures to evaluate a pavement prior to placing an overlay (e.g., Harrington and Fick 2014).

Typically, only severely distressed areas with major loss of structural integrity, or areas where voids are present, require pre-overlay repair for unbonded concrete overlays. Table 45 provides recommendations for the type of distresses requiring repair and suitable treatments.

Table 45: Pre-overlay Repair Recommendations for Unbonded Concrete Overlays (Harrington and Fick 2014, Harringtom et al. 2018)

Existing Pavement Condition	Possible Repairs to Consider
Faulting (0.25-0.38 in)	None
Faulting (>0.38 in)	Thicker separation layer
Significant tenting	Full-depth repair
Badly shattered slabs	Full-depth repair
Significant pumping	Full-depth spot repair and drainage improvements
Severe joint spalling	Clean

The presence of water at the interface between the overlay and underlying concrete can contribute to many distress mechanisms in UBOL systems. For example, moisture-driven materials-related distresses, such as freeze-thaw damage or alkali-aggregate reactions, often increase in severity and rate of development with increased presence of water. In addition, the build-up of hydraulic pressure under traffic can result in stripping and erosion of asphalt concrete interlayer materials. These pressures can even cause erosion in cement-based materials, as was found on the A5 in 1981 in Germany when pulverized fines and voids were found between the concrete pavement and cementitious base, which were constructed without using an interlayer, resulting in many cracked slabs. To provide drainage at the interface between concrete pavements and cement treated bases, German engineers proposed the use of nonwoven geotextile fabric interlayers (Rasmussen and Garber 2009).

Existing pavement drainage demand and capabilities should be evaluated at the initial stage of the overlay project design to determine the need for any steps required to ensure adequate drainage of the unbonded concrete overlay system (e.g., installation of retrofit edge drains, the need to "daylight" existing subbase materials, etc.). When existing underdrains are present, they should be inspected, cleaned, and repaired (if necessary) prior to construction of the overlay (Harrington and Fick 2014, Harrington et al. 2018).

Additional aspects of the pavement structure that should be considered in the design of the UBOL drainage system are the pavement geometrics (i.e., profile, cross-slope, and joint layout) and the details of the overlay joint system, which vary widely with state practices. For example, a change in profile and/or cross-slope can be designed in the overlay so that water is more readily shed from the pavement surface with less infiltration of joints. Overlay joints can be designed to resist excessive ingress of water by constructing them with a narrow, single saw cut and/or filling or sealing them appropriately (Harrington and Fick 2014).

8.2 INTERLAYER CONSIDERATIONS

The interlayer (also known as separation layer) is a layer of material that is placed, constructed or allowed to remain between the original pavement and the concrete overlay. The interlayer can serve many purposes, including:

1. Reducing (or eliminating) mechanical bond and interlock (due to faulting and other surface irregularities) between the overlay and underlying pavement, thereby reducing restraint stresses in the overlay.
2. Isolating the overlay from the underlying pavement so that cracks and other structural defects are less likely to reflect through the overlay.

The interlayer can have a major influence on the performance of unbonded concrete overlays. Insufficient attention is often given to interlayer design and construction. Several unbonded concrete overlays have failed prematurely because of insufficient interlayer thickness, poor interlayer quality or other interlayer-related issues.

The interlayer most commonly consists of hot-mixed asphalt (HMA) or a non-woven geotextile fabric (NWGF). HMA interlayers can be a newly placed layer, typically 1 to 2 inches thick. If the existing PCC pavement was previously overlaid with HMA to create a composite pavement, the existing aged HMA layer can serve as the interlayer. Surface defects in the existing HMA can be removed through milling, leaving 1 or more inches of HMA to serve as the interlayer. In addition to dense-graded HMA, open-graded HMA courses have been used to improve interlayer drainage characteristics and prevent future stripping of the newly laid asphalt interlayer.

Non-woven geotextile fabrics have recently become a popular interlayer option for unbonded concrete overlays. The use of fabrics is an adaptation of the German application of using fabrics to separate newly constructed PCC pavements from cement-stabilized bases (Rasmussen and Garber 2009). In the United States, non-woven fabric was first used as an interlayer in UBOLs in 2008.

Each interlayer type offers advantages and disadvantages:

- Dense-graded HMA is relatively resistant to internal breakdown and stripping because water does not flow through the interlayer. However, it is not drainable and trapped water can lead to erosion and stripping at the interfaces. In addition, hydraulic pressure from water trapped at the overlay-interlayer interface can cause joint sealant failure.
- Open-graded HMA allows water to drain, but the material is often more susceptible to degradation due to stripping and raveling. In addition, excessively porous open-graded HMA may have insufficient strength and stability to resist severe deformation or degradation.
- Non-woven geotextile fabric is not erodible and allows drainage through in-plane fabric permittivity. These fabrics are generally highly effective at reducing friction or bond between the overlay and underlying pavement. The use of tie bars or structural concrete fibers is sometimes required to prevent longitudinal joints from opening. Due to the lack of bond with the older concrete, thinner overlays may be free to curl up when placed on a fabric interlayer.

Interlayer type and design can affect the rates of development of overlay cracking and faulting, as described below.

8.2.1 Cracking

The interlayer can play a role in the development of both longitudinal and transverse overlay cracks. The development of UBOL longitudinal cracking is discussed below; the development of UBOL transverse cracking follows.

8.2.1.1 Longitudinal Cracking

Longitudinal cracking in UBOLs typically initiates at transverse joints and may develop in a wheel path or at random locations. These longitudinal cracks appear to be at least partially caused by the breakdown or consolidation of the interlayer (Alland, et al. 2016).

Longitudinal Cracking in Wheel Paths. A common location for the development of longitudinal cracks is the wheel path. Cracking may develop in either the outside and inside wheel path and can initiate on either the leave or approach side of the transverse joint or crack. Once these cracks initiate, they propagate longitudinally to the adjacent transverse joint, or may turn and propagate toward the adjacent longitudinal joint (lane-shoulder or centerline), appearing as a diagonal crack.

The high stress contributing to the initiation of this crack can be the result of a void or gap in the interlayer beneath the overlay. A void can form beneath the slab in the wheel path in several ways:

- HMA interlayer consolidation may occur in the wheel path at the joint, especially if the interlayer is placed just prior to overlay construction. It is imperative that that sufficient density be achieved during the placement of the interlayer prior to constructing the overlay to reduce the potential for consolidation of the interlayer under traffic.
- HMA interlayers that are susceptible to erosion can be pumped from beneath the joint, thereby resulting in faulting on the approach side of the joint and a void beneath the leave side of the joint.
- HMA with insufficient strength or stability, such as excessively open-graded asphalt or a dense-graded HMA where localized stripping has occurred, can breakdown in the wheel path due to fatigue after repeated loadings.

All of these mechanisms can lead to a loss of support in the wheel path at the transverse joint.

When a wheel load is applied over areas with reduced interlayer support, the overlay panel must bridge across the region with reduced support, resulting in high stress at the bottom of the slab and eventual bottom-up panel cracking. This mechanism is illustrated in Figure 107. Bonded concrete overlays of asphalt (BCOA) with 6 ft x 6 ft panels experience a similar distress mechanism (Li and Vandenbossche 2013).
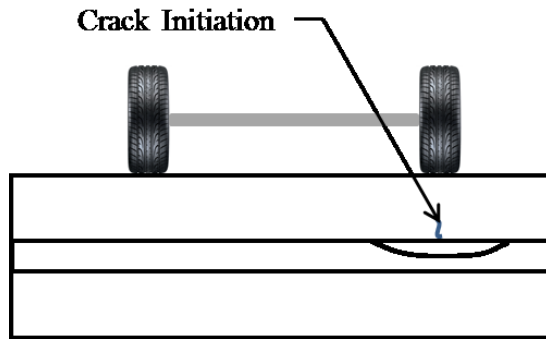
Figure 107: Illustration of condition and mechanism for UBOL longitudinal wheel path cracking.

Longitudinal cracking was the primary distress mechanism observed in the UBOLs included in the LTPP database and the overlays examined in Michigan. It was observed in 11 of the 13 JPCP LTPP sections, and in all of the Michigan sections investigated. The undoweled UBOL sections in the LTPP database experienced significant transverse joint faulting and developed more longitudinal cracks in the wheel path than did the doweled sections (where faulting did not develop). However, it is worth noting that the doweled sections were generally thicker than the undoweled sections, which would provide additional resistance to cracking.

There are several ways to mitigate the mechanisms of longitudinal cracking in UBOLs:
- Increase the thickness of the concrete overlay to decrease the contact stress on the interlayer, thereby decreasing the risk of degradation and/or consolidation.
- Reduce differential deflections and minimize potential for pumping by using load transfer devices.
- Use an interlayer system that is not prone to consolidation, stripping or breakdown due to fatigue.

a.

b.

c.

d.

Figure 108: Example photos of longitudinal wheel path and diagonal cracking in UBOLs

at: a) inside wheel path of LTPP Section 06-9049, CA (Photo from Infopave.com); b) outside wheel path of LTPP Section 48-9167, TX (Photo from Infopave.com); c) diagonal crack propagating from wheel path to adjacent longitudinal joint in LTPP Section 06-9049, CA (Photo from Infopave.com); and d) inside wheel path of I-96 near Walker, Michigan (Photo Courtesy of Andrew Bennett, Michigan Department of Transportation).

Random Longitudinal Cracking In traditional JPCPs, longitudinal cracking can develop as a result of loss of support beneath the slab due to erosion of the underlying layer along the roadway. It is often the result of consolidation or transport of base layer materials due to poor drainage. Similar distress is found in UBOLs when a portion of the interlayer becomes eroded. These cracks usually occur on the shoulder side of the pavement, not necessarily occurring in the wheel path. An illustration of this mechanism is presented in Figure 109.
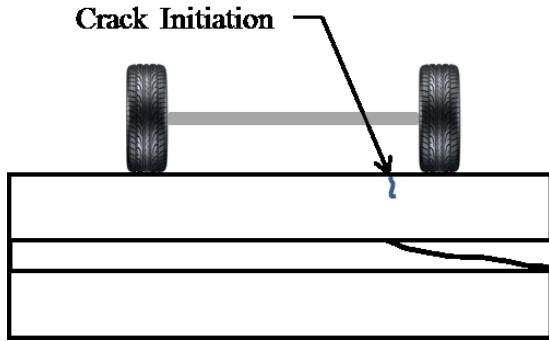
Figure 109: Illustration of condition and mechanism for UBOL longitudinal cracking due to loss of interlayer support along pavement edge.

A survey of Michigan UBOLs found that these cracks often occurred in clusters when proper drainage was not provided. Figure 110 shows a random longitudinal crack on I-75 near West Branch, Michigan. The Michigan DOT has identified proper drainage as being essential for good UBOL performance (Alland, et al. 2016). Without a means of escaping, water can become trapped along the interlayer.

Figure 110: Random longitudinal crack on I-75 near West Branch, Michigan.

Careful attention to pavement drainage details is important for preventing random longitudinal cracking. Any water that infiltrates the pavement joints must have a clear drainage path to exit the pavement structure. Proper maintenance of the drains and outlets is extremely important for these structures as well. The backup of water from a clogged drain can quickly strip and erode HMA interlayers. Drainable interlayers (such as open-graded asphalt or non-woven geotextile fabric) can only improve drainage characteristics if there is a suitable outlet for moving the water away from the pavement structure.

8.2.1.2 Transverse/Diagonal Cracking

Erosion-related transverse cracking. Transverse cracks in UBOLs caused by interlayer erosion typically form within 1.5 to 5 ft from the transverse joint, and most likely result from interlayer erosion due to the entry of water at the transverse joints. Water entering the transverse joints due to lack of sealant or damaged sealant often drains slowly from the pavement structure, even when an open-graded mixture is used. During periods of upward curling of the overlay, water may even pool in the gap between the interlayer and the existing slab. When subject to heavy and frequent vehicle loads, this water can cause an asphalt interlayer to strip and ravel, leading to a loss of support.

Longitudinal cracks often form between the transverse crack and the adjacent joint, producing a distress that appears similar a punchout in CRCP pavement. If water only enters on a portion of the lane, a corner break can develop. Images of this type of distress are shown in Figure 111. The distress in the right-hand side photo could by caused by curling/warping up of the leading edge of the leave slab (this thin overlay is undoweled), which cracks when subject to heavy loads transferred from the leave slab.
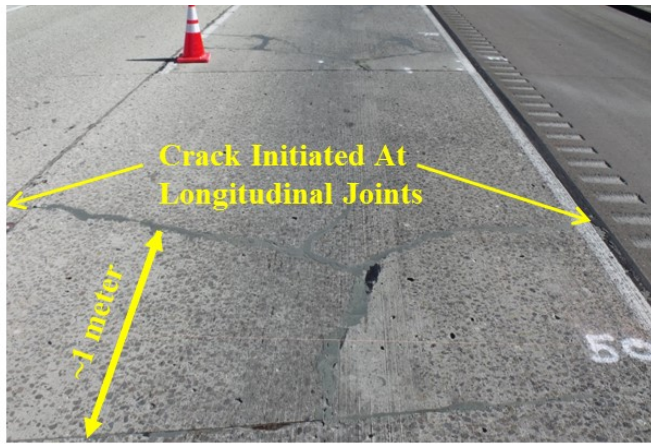
a.

b.

c.

Figure 111: Transverse cracking due to erosion at: a) LTPP Section 06-9048, California [www.datapave.com]; b) MnROAD Cell 305; and c) a corner break on a UBOL in Michigan.

To prevent cracks from forming on the leave side of the joint, it appears to be important to keep joints properly sealed. Using an interlayer which is less susceptible to erosion, such as a more stripping-resistant HMA mixture or a non-woven geotextile fabric, will also help in preventing the development of this distress.

Transverse Reflective Cracking. Based on a review of the performance of in-service overlays and an extensive laboratory study, the reflection of joints and cracks up into the overlay (reflective cracking) can be prevented using the following approach:

- The original (underlying) pavement must be fully supported. Slab stabilization and/or panel replacements should be performed prior to overlay construction if voids are present below the existing pavement.
- The interlayer must allow the overlay and underlying pavement to move independently of each other. Faulting and other surface irregularities can cause interlocking between the overlay and the distressed pavement.

- The use of a sufficiently thick interlayer (typically a minimum of about 1 inch of HMA or an appropriate geotextile) and leveling or filling of depressions in distressed regions prior to overlay placement will facilitate free, independent movements between the overlay and underlying pavement.

8.2.2 Faulting

Asphalt interlayers can break down through erosion caused by pumping. Pumping occurs as a result of poor drainage and poor load transfer across the joint. In this scenario, the interlayer is broken down, and fine materials are pumped from beneath the leave side of the transverse joint under the overlay to the approach side and/or are ejected out through the joints. This results in the development of faulting and the formation of a void beneath the overlay (on the leave side of the joint). Asphalt interlayers that are susceptible to stripping are more vulnerable to the development of a void due to erosion.

8.2.3 Optimizing Interlayer Performance

The following should be considered to optimize the performance of the interlayer:

1. *Use erosion resistant materials.*

The same characteristics that make conventional paving asphalt resistant to stripping and erosion are applicable to asphalt interlayers as well. Therefore, the same principles used in making asphalt more resistant to stripping should be applied to the asphalt mixture used as the interlayer (Roberts, et al. 1996; Lu and Harvey 2005; Tran, et al. 2016). The following additional factors should also be considered when selecting an asphalt interlayer mixture design:

- *Permeability.* A dense-graded asphalt interlayer can result in additional pressure buildup as the water beneath the overlay does not have sufficient voids in the interlayer system through which it can escape and thereby dissipate energy. An overly open-graded asphalt interlayer can also be more susceptible to erosion since these types of interlayers are more susceptible to stripping.
- *Strength.* The interlayer matrix can break down in the wheel path adjacent to the transverse joint. Extremely open-graded asphalt interlayers are vulnerable to this due to the lower strength/stiffness associated with these mixtures.

 Due to the limitations of mixtures with high air void contents, many DOTs specify asphalt mixtures with air void contents of 2 - 4 percent, with a maximum void content of 8 percent (VDOT 2011). The Pennsylvania DOT recommends 3 - 5 percent air voids, and the Arizona DOT recommends 3 - 6 percent, with anything exceeding 8 percent calling for removal (PennDOT 2016, AZMAG 2018). In general, every 1 percent of in-place air voids in excess of 8 percent generally results in a 10 percent or greater reduction in asphalt pavement life (Cornelison 2013, Linden et al. 1989).

The Michigan DOT developed the asphalt interlayer aggregate gradation shown in Table 1 to produce asphalt interlayer materials that balance permeability with strength/stability and resistance to erosion. This

specification requires an effective binder content of 5 percent by volume with 3 percent air void content and the aggregate gradation specified in Table 46.

Sieve Size	Percent Passing
½ in	100
3/8 in	85-100
No. 4	22-38
No. 8	19-32
No. 16	15-24
No. 30	11-18
No. 50	8-14
No 100	5-10
No. 200	4-7

2. Ensure density of asphalt interlayer is achieved.

It is easy to become complacent when compacting the interlayer knowing that a PCC overlay will be constructed above it. It is imperative that the target density is achieved when constructing the asphalt interlayer to avoid consolidation under traffic loadings. The resulting void at the intersection of the wheel path and transverse joint will often result in the development of a longitudinal crack in the wheel path.

3. Keep moisture out by keeping joints sealed/filled and providing a drainage path for water.

The potential for erosion of the interlayer can be reduced by preventing water from entering the system and providing a drainage path and outlet for water that does contact or enter the interlayer, as shown in Figure 112. In Figure 112a, the interlayer is not connected to a pathway for the water to exist from beneath the pavement. Figure 112b shows that by connecting the interlayer into a drainage system, the water is able to escape from beneath the pavement without developing hydraulic pressures that contribute to interlayer erosion and loss of overlay support.
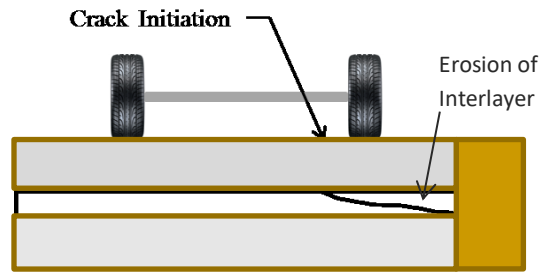
a. No drainage path is provided to remove water from the system, resulting in erosion.
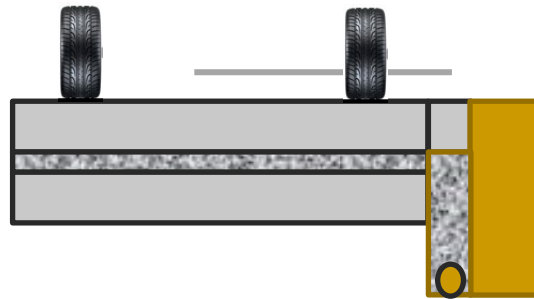
b. Interlayer is connected to a drainage system to prevent erosion.

Figure 112: Illustrations of interlayer drainage and trapped water on potential for erosion.

4. *Provide adequate interlayer thickness.*

An asphalt interlayer thickness of 1 inch is typically sufficiently thick to prevent reflective cracking. Guidance on selecting an appropriate thickness of a non-woven fabric can be found in Harrington and Fick (2014).

CHAPTER 9: RUDIMENTARY SOFTWARE

The user guide for the program is provided in Appendix C.

To facilitate implementation of the design procedure developed in this study, a standalone rudimentary software was developed. The software can perform two types of analyses: performance prediction and reliability. If performance prediction option is selected, the program predicts the percentage of cracked slabs and mean joint faulting at the end of the design life for a given overlay thickness. If the reliability analysis option is selected, then the program finds the overlay thickness meeting the specified cracking reliability level and predicted joint faulting for the specified faulting reliability level.

Using the Graphical User Interface of the software package, the user should provide the following information:

- Climate: choose from 68 locations throughout the United States;
- Traffic volume: expressed in heavy commercial two-way annual daily trucks, number of lanes, and linear yearly growth rate;
- Overlay slab size: 6 ft by 6 ft or slab width of 12 ft with joint spacing between 12 and 16 ft;
- Shoulder type: HMA or tied PCC;
- Concrete strength;
- Existing pavement thickness and stiffness;
- Interlayer type;
- Mix design if an HMA interlayer is used:
    - Effective binder content by volume
    - Percent passing #200 sieve
    - Percent of air voids
- Reliability level for overlay cracking and joint faulting predictions or overlay thickness.

The following ranges of the input values can be analyzed by the current version of the program:

- Reliability level: 40 to 99 %.

- Overlay thickness: from 6 to 12 in for conventional (12 ft) width overlays and 4 to 10 in for short slabs (6 ft by 6 ft) overlays

- Design life: from 1 to 100 years. Must be an integer value.

- Two-way annual average daily truck traffic (AADTT): from 0 to 10,000.

- Existing PCC thickness: from 6 to 16 in.

- Existing PCC elastic modulus: from 500,000 to 10,000,000 psi.

Upon opening, the program will display the Main tab, illustrated in Figure 113. The user will need to correct the input(s) and press the Run button.

Figure 113: Main input tab

If all the input values are acceptable, the MS DOS window will appear, and the cracking analysis will be performed. After the cracking analysis is completed, the faulting analysis is performed, and the results will be displayed on the screen. If the reliability checkbox is checked, the program will find the corresponding overlay thickness meeting the reliability level in terms of cracking and mean joint faulting prediction for this overlay thickness and specified faulting reliability level. If the reliability checkbox is unchecked, the program will predict the cracking level and mean joint faulting at the end of the pavement design life for the specified overlay thickness.

The tab corresponding to the default model parameters is shown in Figure 114.
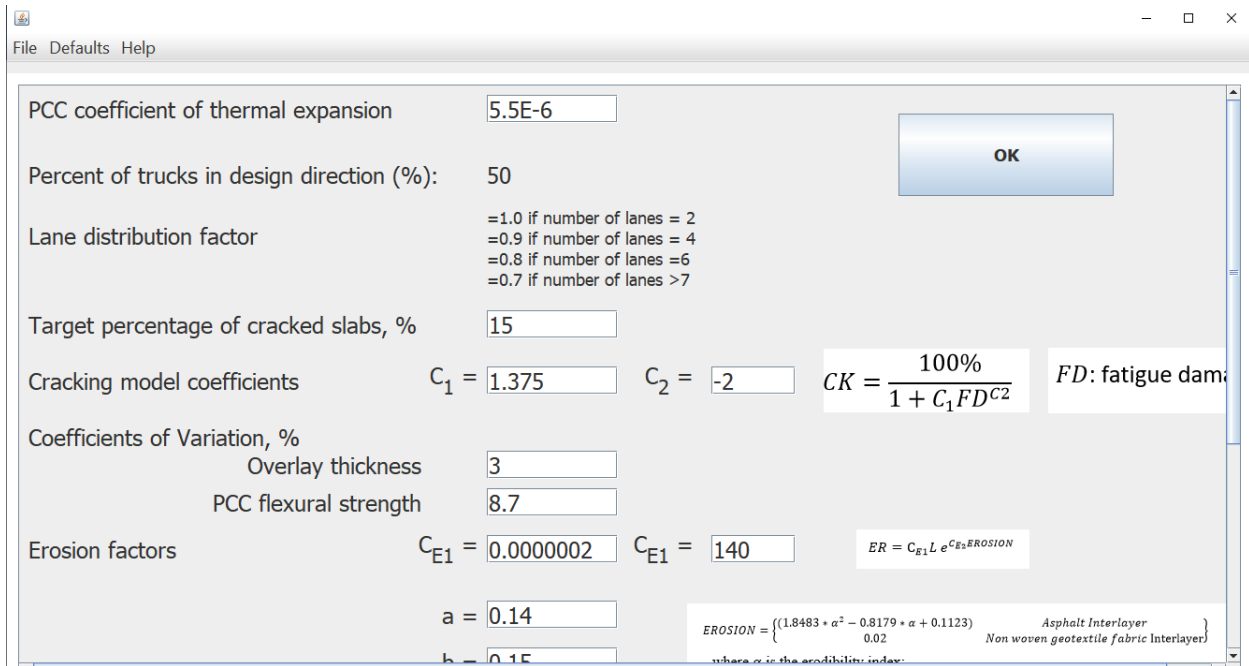
Figure 114: Default parameters tab

The user has an option to change the target percentage of cracked slabs, cracking model coefficients (see Equation 75), default coefficients of variation in reliability analysis, erosion model coefficients (see Equation 60), and other parameters.

It is recommended that only advanced users modify these parameters.

CHAPTER 10: CONCLUSIONS AND RECOMMENDATIONS FOR FUTURE RESEARCH

10.1 SUMMARY

Unbonded concrete overlays (UBOLs) have been used in the United States for more than a century, but there has been a need for a design procedure capable of quantifying the effect of key design features on the performance of the overlay. Developing such a procedure is essential to achieve the most cost-effective overlay design solutions. In the past 10 to 15 years, agencies have been experimenting with the use of different interlayer types. Most of the current design procedures are not able to capture the effect of this broad range of interlayer types on the performance of the overlay. The use of small slab sizes (partial lane widths) has also become more prevalent, and therefore the need to account for the effect of the smaller slab size on performance has become essential. These are two of the many challenges presented when using the design procedures that have been traditionally used by pavement engineers.

In this study, the research team reviewed literature pertaining to design and performance of unbonded concrete overlays, as well as conducted laboratory and field studies. Key observations from these activities are as follows:

10.2 GENERAL CONSIDERATIONS

- Many UBOLs exhibited very good performance for 20-plus years after construction showing this to be a sound rehabilitation alternative.
- The interlayer and drainage are two components of the UBOL that have a significant effect on performance.

10.3 DESIGN CONSIDERATIONS

- The failure modes that must be considered include transverse and longitudinal cracking (both at midslab and in the wheel path) and transverse joint faulting. To more accurately predict the occurrence of each of these distresses, the erodibility and compressibility of the interlayer must be considered.
- Longitudinal cracks that typically initiate at transverse joints and propagate in a wheel path or at random locations appear to be at least partially caused by the breakdown or consolidation of the interlayer and can be minimized through proper interlayer and drainage design, as well as the use of dowel bars.
- Traditional faulting models assume the source of the eroded material is below the existing slab, but the model developed under this study assumes it comes from the interlayer.
- Dowel bars improve the performance of unbonded overlays (thickness of 6 inches or more). Doweled joints provide more uniform slab deflections on both sides of transverse joints and are helpful in reducing pumping.

- It is preferable to avoid the use of widened slabs with UBOLs, because it can result in longitudinal cracking due to transverse curling and warping stresses.
- The effect of small slab sizes (less than full-lane width) on the overlay performance can be quantified in the design process developed under this study.

10.4 INTERLAYER CONSIDERATIONS

- The following should be considered to optimize the performance of the interlayer:
  - Use erosion resistant materials.
  - Provide adequate interlayer thickness (1-in or thicker HMA or an appropriate geotextile fabric).
- Material properties to consider for asphalt interlayers include:
  - *Permeability.* A dense-graded asphalt interlayer can result in additional pressure buildup as the water beneath the overlay does not have sufficient voids in the interlayer system through which it can escape and thereby dissipate energy. An overly open-graded asphalt interlayer can also be more susceptible to erosion since these types of interlayers are more susceptible to stripping.
  - *Strength.* The interlayer matrix can breakdown in the wheel path adjacent to the transverse joint. Extremely open-graded asphalt interlayers are vulnerable to this due to the lower strength/stiffness associated with these mixtures.
  - *Consolidation.* Ensure adequate density of the asphalt interlayer is achieved so that voids are not generated as the asphalt is consolidated under traffic in the wheel path adjacent to the transverse joints.
- Geotexile interlayers provide adequate drainage and appear to be working well, but only limited performance data is currently available. They also allow an overlay to freely curl/warp.

Drainage Considerations

- Providing clear drainage paths in design and drainage maintenance improves overlay performance.
- It is important to keep moisture out by sealing/filling joints and providing a drainage path for the water, so it does not become trapped in the interlayer.
- The interlayer should be sufficiently open graded to provide adequate drainage yet still maintain sufficient stability to resist breakdown due to wheel loads and erosion.

Construction Considerations

- The field investigation and laboratory study revealed that joints and cracks will not reflect up from the existing pavement into the overlay (reflective cracking) if the existing pavement is fully supported (no voids below existing pavement) and an adequate interlayer is used.
- A minimum of a 1-in or thicker HMA interlayer (or an appropriate geotextile fabric) should be used to prevent interlocking between the existing pavement and the overlay when faulting is present.

- Pre-overlay repairs are only necessary for severely distressed areas. This includes surface distresses in the existing pavement that will cause the two layers to interlock if the voids are not filled or when voids are present under the existing pavement and sub-sealing is needed.

Improved Design Procedure (UBOLDesign), a mechanistic-empirical design procedure for UBOLs, was developed in this study. The procedure computes structural responses in the UBOL using the Totski model incorporated into ISLAB2005. The structural model was calibrated using the deflection data from the laboratory testing and falling weight deflectometer (FWD) data collected on in-service pavements. The design procedure incorporates two performance prediction models, cracking and faulting, calibrated using LTPP test sections and the data collected at MnROAD and in Michigan.

The procedure is capable of analyzing the following design factors:

- Traffic volume
- Overlay joint spacing
- Overlay dowel diameter
- Shoulder type
- Concrete strength
- Existing pavement thickness and stiffness
- Interlayer type
- Mix design if an HMA interlayer is used
- Reliability level

To facilitate implementation of this procedure, a standalone rudimentary software named "UBOLDesign" was developed. The program incorporates the frequency tables of the coefficients of the quadratic temperature distributions throughout the overlay thickness for 68 locations throughout the United States. The software can perform two types of analyses: performance prediction or reliability. If the performance prediction option is selected, the program predicts the percentage of cracked slabs and mean transverse joint faulting at the end of the design life for a given overlay thickness. If the reliability analysis option is selected, then the program finds the overlay thickness meeting the specified cracking reliability level and predicted transverse joint faulting for the specified faulting reliability level.

10.5 RECOMMENDATIONS FOR FUTURE RESEARCH

The developed mechanistic-empirical design procedure has many improvements compared to the UBOL design procedure contained in the *AASHTO Pavement ME*. This includes an advanced structural (Totski) model to better capture the effects of the interlayer and separation between the overlay and the existing pavement, both transverse and longitudinal damage predictions, different values of built-in curling for day-time and night-time curling analyses, prediction of transverse joint faulting that develops due to erosion of the interlayer, interlayer erosion model, etc. Nevertheless, the developed procedure has many limitations that need to be addressed in future research:

- The procedure is not capable of designing overlays with the widened slabs.

- The current interlayer deterioration model for cracking depends on the overlay age only. A more advanced model incorporating a combined effect of axle loading, curling, and moisture would improve the procedure and permit quantifying the benefits of good drainage.
- At the time of the procedure development, no long-term performance data for the overlays with fabric interlayer were available. Collecting such performance data is recommended and, if necessary, model recalibration should be conducted.
- A more rigorous procedure is needed to predict built-in curl based on concrete materials, curing and construction techniques, site conditions at time of construction, etc. Meeting these research needs will not only improve pavement distress prediction but will also potentially lead to recommendations on controlling built-in curl parameters through construction techniques, construction timing, or materials.
- Partial friction between the interlayer and the overlay slab is neglected making the design more conservative.
- As more performance data becomes available for the more recently adopted interlayer types, the effects of the interlayer characteristics on the overlay performance can be better captured.
- The developed interlayer consolidation model could be incorporated into the distress prediction models at a later time.
- If local data is available, then local calibration could be beneficial.

REFERENCES

AASHTO. (1993). *Guide for Design of Pavement Structures* (ISBN 1560510552). American Association of State Highway and Transportation Officials, Washington D.C.

AASHTO. (1998). *Supplement to the Guide for Design of Pavement Structures* (ISBN 1560510781). American Association of State Highway and Transportation Officials, Washington D.C.

AASHTO. (2008). *Mechanistic-Empirical Pavement Design Guide, Interim Edition: A Manual of Practice*. American Association of State Highway and Transportation Officials Washington, D.C.

ACPA. (1990). *Guidelines for Unbonded Concrete Overlays* (Report TB005B). American Concrete Pavement Association, Rosemont, IL.

Alland, K.D., J.M. Vandenbossche, S. Sachs, J. W. DeSantis, L. Khazanovich, and T. Burnham. (2016), Failure Modes in Unbonded Concrete Overlays on Asphalt, *11th International Conference for Concrete Pavements Conference Proceedings*. San Antonio, TX.

Applied Research Associates (ARA), Inc., ERES Division. (2004). *Guide for Mechanistic-Empirical Design of New and Rehabilitated Pavement Structures* (Final Report NCHRP 1-37A). Transportation Research Board of the National Academies, Washington, D.C.

Arizona Maricopa Association of Governments (AZMAG). (2018). Uniform Standard Specifications and Details for Public Works Construction—2018 Revision to the 2015 Edition, Arizona, www.azmag.gov (accessed February 20, 2020).

Cornelison, D. (2013). In *Road Building Fundamentals: Volumetric Properties of Asphalt Mixes*. Arizona Pavements and Materials Conference, Phoenix, AZ, Nov. 14, 2013,

Army Corps of Engineers. (2001). *Pavement Design for Airfields* (Report No. UFC 3-260-02). U.S. Army Corps of Engineers, Transportation Systems Center, Omaha, NE.

Asbahan, R., and J.M. Vandenbossche. (2011). Effects of Temperature and Moisture Gradients on Slab Deformation for Jointed Plain Concrete Pavements. *Journal of Transportation Engineering, 137*(8), 563-570.

ASTM International. (2005). *Standard Test Method for Compressive Strength of Cylindrical Concrete Specimens* (ASTM Standard C 39). ASTM International, West Conshocken, PA.

ASTM International. (2009). Standard Test Method for Repetitive Static Plate Load Tests of Soils and Flexible Pavement Components, for Use in Evaluation and Design of Airport and Highway Pavements (ASTM Standard D1195/D1195M). ASTM International, West Conshocken, PA.

ASTM International. (2013). *Standard Practice for Making and Curing Concrete Test Specimens in the Laboratory* (ASTM Standard C 192). ASTM International, West Conshocken, PA.

ASTM International. (2014). *Standard Test Method for Static Modulus of Elasticity and Poisson's Ratio of Concrete in Compression* (ASTM Standard C 469). ASTM International, West Conshocken, PA.

ASTM International. (2015). *Standard Test Method for Flexural Strength of Concrete (Using Simple Beam with Third-Point Loading)* (ASTM Standard C 78). ASTM International, West Conshocken, PA.

ASTM International. (2015). *Standard Test Method for Measuring Pavement Macrotexture.* (ASTM Standard E 965) ASTM International, West Conshocken, PA

Chojnacki, T. (2000). *Evaluation of Fiber-Reinforced Unbonded Overlay* (Report No. RDT 00-015). Missouri Department of Transportation, Jefferson City, MO.

Choubane, B., & Tia, M. (1992). Nonlinear temperature gradient effect on maximum warping stresses in rigid pavements. *Transportation Research Record, 1370,* 11–19.

CP Tech Center. (2009.) *Use of Nonwoven Geotextiles as Interlayers in Concrete Pavements Systems* (MAP Brief 7-1). National Concrete Pavement Technology Center, Iowa State University, Ames, IA.

Darter, M.I., J. Mallela, & L. Titus-Glover (2009). Impact of Existing Pavement on Jointed Plain Concrete Overlay Design and Performance. *Proceedings of the National Conference on Preservation, Repair, and Rehabilitation of Concrete Pavements* (pp 15-30). St. Louis, Missouri, April 21-24. Federal Highway Administration.

Darter, M.I., L. Khazanovich, M. Snyder, S. Rao, & J. Hallin (2001). Development and Calibration of a Mechanistic Design Procedure for Jointed Plain Concrete Pavements, *Proceedings of the Seventh International Conference on Concrete Pavements* (p. 113–131). Lake Buena Vista, FL.

Darter, M.I., L. Khazanovich, H.T. Yu, & J. Mallela (2005). Reliability analysis of cracking and faulting prediction included in the new mechanistic-empirical pavement design procedure. *Transportation Research Record, 1936*, 150-160.

Departments of the Army and the Air Force (1979). Rigid Pavements for Airfields Other Than Army (Chapter 3). In *Army Technical Manual 5-824-3, Air Force Manual 88-6*.

DeSantis, J.W., J.M. Vandenbossche, K. Alland, S. Sachs, T. Burnham, & A. Montenegro. (2016). Joint Performance in Bonded Concrete Overlays of Asphalt. *11th International Conference for Concrete Pavements (ICCP).* San Antonio, TX.

DeSantis, J.W., J.M. Vandenbossche, K. Alland, & J. Harvey. (2018). Development of Artificial Neural Networks for Predicting the Response of Bonded Concrete Overlays of Asphalt for use in a Faulting Prediction Model. *Transportation Research Record*. DOI: 10.1177/0361198118758637

DeSantis, J.W., J.M. Vandenbossche, & S. Sachs. (2019) Artificial Neural Networks for Predicting the Response of Unbonded Concrete Overlays in a Faulting Prediction Model. Accepted for presentation at the 2019 Transportation Research Board Annual Meeting, Washington, D.C.

Eisenmann, J., & G. Leykauf (1990). Effect of Paving Temperatures on Pavement Performance. In *2nd International Workshop on Theoretical Design of Concrete Pavements* (pp. 419–428). Madrid, Spain.

ERES Consultants. (1999). *Evaluation of Unbonded Portland Cement Concrete Overlays* (NCHRP Report No. 415). Transportation Research Board. Washington, D.C.

FHWA. (2002). *Seperator Design for Unbonded PCC Overlays* (Report No. FHWA-IF-03-004). Federal Highway Administration, U.S. Department of Transportation, Washington, D.C.

FHWA. (2013). Long-Term Pavement Performance Database. Retrived from Infopave.org

FHWA. (2015). Long-Term Pavement Performance Database. Retrieved from http://www.infopave.com/ (Accessed September 17, 2015).

Garber, S., & R. Rasmussen (2010). Nonwoven Geotextile Interlayers in Concrete Pavements. *Transportation Research Record, 2152*(2), 11-15.

Hall, K.D., & N. Banihatti (1998). *Structural Design of Portland Cement Concrete Overlays for Pavements* (Report No. MBTC-1052). Mack-Blackwell Rural Transportation Center, University of Arkansas, Fayetteville, AK.

Hansen, W., & A. Liu. (2013). *Improved Performance of JPCP Overlays* (Report No. RC-1574). Michigan Department of Transportation, Lansing, MI.

Harrington, D. (2008). *Guide to Concrete Overlays: Sustainable Solutions for Resurfacing and Rehabilitating Existing Pavements*, Second edition (Report No. TB021.02P). American Concrete Pavement Association, Rosemont, IL.

Harrington, D., & G. Fick. (2014). *Guide to Concrete Overlays: Sustainable Solutions for Resurfacing and Rehabilitating Existing Pavements*, Third edition (ACPA Publication TB021.03P). National Concrete Pavement Technology Center, Iowa State University. Ames, IA.

Harrington, D. S., D. Degraaf, R. Riley, R. O. Rasmussen, J. Grove, & J. Mack. (2007). *Guide to Concrete Overlay Solutions.* National Concrete Pavement Technology Center at Iowa State University. Ames, IA.

Harrington, D.,. Ayers, M., Cackler, T., Fick, G., Schwartz, D., Smith, K., Snyder, M and Van Dam, T. (2018) *Guide for Concrete Pavement Distress Assessments and Solutions: Identification, Causes, Prevention, and Repair,* National Concrete Pavement Technology Center at Iowa State University. Ames, IA.

Heckel, L.B. (2002). *Performance of an Unbonded Concrete Overlay on I-74* (Report No. ILPRR-140). Illinois Department of Transportation, Springfield, IL.

Hiller J., & J. Roesler. (2010). Simplified nonlinear temperature curling analysis for jointed concrete pavements. *ASCE Journal of Transportation Engineering, 136*(10), 654-663

Huang, Y.H. (2004). *Pavement Analysis and Design*, Second edition (ISBN 0131424739). Pearson/Prentice Hall, Upper Saddle River, NJ.

Ioannides, A., L. Khazanovich, & J. Becque. (1992). Structural Evaluation of Base Layer in Concrete Pavement Systems, *Transportation Research Record, 1370,* 20–28.

Ioannides, A., & L. Khazanovich. (1998). Nonlinear Temperature Effects in Multi-Layered Concrete Pavements. *ASCE Journal of Transportation Engineering*, *124*(2),128–136.

Janisch, D. (2006). *An Overview of MnDOT's Pavement Condition Rating Procedures and Indices*, Internal report. MnDOT Office of Materials and Road Research, Minnesota Department of Transportation, Saint Paul, MN.

Janssen, D.J., & M. B. Snyder. (2000) The Temperature-Moment Concept for Evaluating Pavement Temperature Data. *Journal of Infrastructure Engineering, 6*(2), 81-83, 2000.

Khazanovich, L. (1994). Structural Analysis of Multi-Layered Concrete Pavement Systems. Ph.D. Thesis, University of Illinois, Urbana, IL.

Khazanovich, L., & A. Ioannides. (1994). Structural Analysis of Unbonded Concrete Overlays under Wheel and Environmental Loads. *Transportation Research Record,* 1449, 174–181.

Khazanovich, L., O. Selezneva, H.T. Yu, & M.I. Darter. (2001). Development of Rapid Solutions for Prediciton of Critical Continuoulsly Reinforced Concrete Pavement Stresses. *Transportation Research Record*, *1778,* 64–72.

Khazanovich, L., & A. Booshehrian. (2015). Dynamic visco-elastic analysis of falling weight deflectometer deflections for rigid and flexible pavements. Accepted for publication in *Transportation Research Record.*

Khazanovich, L., & D. Tompkins. (2017). Incorporating Slab/Underlying Layer Interaction into the Concrete Pavement Analysis Procedures. Washington, DC: The National Academies Press. https://doi.org/10.17226/24842.

Khazanovich, L., D. Tompkins, & L. Johanneck. (2015). State Design Procedure for Rigid Pavements Based on the AASHTO Mechanistic-Empirical Pavement Design Guide. *Transportation Research Record*, *2524,* 23–32.

Khazanovich, L., M. Darter, & H.T. Yu. (2004). Mechanistic-Empirical Model to Predict Transverse Joint Faulting. *Transportation Research Record, 1896*, 34-45.

Khazanovich, L., Yu, H.T., Rao, S., Galasova, K., Shats, E., & R. Jones. (2000). *ISLAB2000 - Finite Element Analysis Program for Rigid and Composite Pavements* (User's guide). ERES Consultants, Champaign, IL.

Korenev, B.G., & E.I. Chernigovskaya. (1962). *Analysis of Plates on Elastic Foundation*. Gosstroiizdat, Moscow (in Russian).

Larralde, J. (1984) Structural Analysis of Rigid Pavements with Pumping. Ph.D. Dissertation. Purdue University, West Lafayette, IN.

Larson, G., & B. Dempsey. (2003). *Enhanced integrated climatic model*. University of Illinois, Urbana, IL.

Lederle, R. E., K. Hoegh, T. Burnham, & L. Khazanovich (2013). Drainage Capabilities of a Nonwoven Fabric Interlayer in an Unbonded Concrete Overlay (Paper No. 13-4107). In *TRB 92nd Annual Meeting Compendium of Papers*, Transportation Research Board 92nd Annual Meeting, January 13-17, 2013, Transportation Research Board, Washington D.C.

Li. Z., & J.M. Vandenbossche. (2013). Redefining the Failure Mode for Thin and Ultra-thin Whitetopping with a 1.8- x 1.8-m (6- x 6ft) Joint Spacing. *Transportation Research Record, 2368,* 133-144.

Linden, R.N., J.P. Mahoney, & N.C. Jackson. (1989). *The Effect of Compaction on Ahalt Performance*. Annual Meeting of the Transportation Research Board. Washington, DC.

Mallela, J., L. Titus Glover, M. I. Darter, & E. Y. Chou. (2008). *Review of ODOT's Overlay Design Procedures, Volume 2: PCC Overlays of Existing Composite Pavements* (Report No. OH-2008/8). Ohio Department of Transportation, Columbus, OH.

MnDOT. (2011). *MnDOT Distress Identification Manual* (Internal report). MnDOT Office of Materials and Road Research, Minnesota Department of Transportation, Saint Paul, MN.

Mallela, J., Titus Glover, L., Darter, M.I., Von Quintus, H., Gotlif, A., Stanley, M., & S. Sadasivam. (2009). Guidelines for Implementing NCHRP 1-37A M-E Design Procedures. In *Ohio: Volume 1— Summary of Findings, Implementation Plan, and Next Steps*,FHWA Report No. FHWA/OH-2009/9, Ohio Department of Transportation., Columbus, OH.

Maitra, S. R., Reddy, K. S., & L.S. Ramachandra. (2009). Experimental Evaluation of Interface Friction and Study of Its Influence on Concrete Pavement Response. *Journal of Transportation Engineering*, *135*(8), 563–572.

MATLAB and Statistics Toolbox Release 2018b (2018). The MathWorks, Inc., Natick, Massachusetts, United States.

Minnesota Department of Transportation. (1993). *Unbonded Concrete Overlay Design,* Minnesota Department of Transportation, St. Paul, MN.

Montgomery, D. (2012). *Design and Analysis of Experiments* (Eighth edition). John Wiley & Sons, Inc., NY.

Moulton, L.K. (1980). Highway Subsurface Design (FHWA-TS-80-224). Federal Highway Administration, Washington, D.C.

Rasmussen, R., & S. Garber. (2009). *Nonwoven Geotextile Interlayers for Separating Cementitious Pavement Layers: German Practice and U.S. Field Trials.* Federal Highway Administration, Washington, D.C.

NCHRP. (2004). *Guide for Mechanistic-Empirical Design of New and Rehabilitated Pavement Structures* (Final report, Project 1-37A). National Cooperative Highway Research Program, Transportation Research Board, National Research Council, Washington, D.C.

Owusu-Antwi, E.B., Titus-Glover, L., Khazanovich, L., & J.R. Roesler. (1997, March). *Development and Calibration of Mechanistic-Empirical Distress Models for Cost Allocation*, Final Report. Federal Highway Administration, Washington, D.C.

Packard, R.G. (1997). *Design Considerations for Control of Joint Faulting of Undoweled Pavements.* Proceedings of the International Conference on Concrete Pavement Design. Purdue Univeristy, Lafayette, IN.

PennDOT. (2016). *Specifications* (Publication 408/2016). Pennsylvania Department of Transportation. Harrisburg, PA.

Rao, C., L. Titus-Glover, B. Bhattacharya, M.I. Darter, M. Stanley, & H. L. Von Quintus. (2012). *Estimation of Key PCC, Base, Subbase, and Pavement Engineering Properties from Routine Tests and Physical Characteristics* (Report No. FHWA-HRT-12-030). Federal Highway Administration, Washington DC.

Rasmussen, R. O., & D.K. Rozycki. (2001). Characterization and modeling of axial slabsupport restraint. *Transportation Research Record*, *1778*(1), 26–32.

Rasmussen, R.O., & S. I. Garber (2009). *Nonwoven Geotextile Interlayers for Separating Cementitious Pavement Layers: German Practice and US Field Trials*. International Technology Scanning Program, Federal Highway Administration, U.S. Department of Transportation, Washington D.C.

Ripley, B.D. (1996). *Pattern Recognition and Neural Networks.* Cambridge University Press, Cambridge, UK.

Roberts, F.L., P.S. Kandhal, E.R. Brown, D.Y. Lee, & T.W. Kennedy. (1996). *Hot Mix Asphalt Materials, Mixture Design, and Construction*. National Asphalt Paving Association Education Foundation, Lanham, MD.

Rollings, R.S. (1988). *Design of Overlays for Rigid Airport Pavements* (Report No. DOT/FAA/PM-87/19). Federal Aviation Administration, U.S. Department of Transportation, Washington D.C.

Ruiz, J. M., Kim, P. J., Schindler, A. K., & R.O. Rasmussen. (2000). Validation of HIPERPAV for Prediction of Early-Age Jointed Concrete Pavement. *Transportation Research Record, 1778*(1), 17–25.

Sachs, S.G., Vandenbossche, J.M., & M.B. Snyder. (2014). Calibration of National Rigid Pavement Performance Models for the Pavement Mechanistic-Empirical Design Guide. *Transportation Research Record, 2524,* 59-67.

Sachs, S. (2017). Development of a Joint Faulting Model for Unbonded Concrete Overlays of Existing Concrete Pavements Through a Laboratory and Numeric Analysis. Ph.D. Dissertation, University of Pittsburgh, Pittsburgh, PA.

Sachs, S., J.M. Vandenbossche, K.D. Alland, J.W. DeSantis, & L. Khazanovich. (2016). Effect of Different Interlayer Systems on Reflective Cracking in Unbonded Concrete Overlays of Existing Concrete Pavements (UBOLs). *Transportation Research Record, 2591(3),* 33-41.

Schnitter, O., W.R. Hudson, & B.F. McCullough. (1978). *A rigid pavement overlay design procedure for Texas* (Report No. TX79-177-13). Center for Highway Research, University of Texas, Austin, TX.

Simonsen, J.E., & A.W. Price. (1985). *Performance Evaluation of Concrete Pavement Overlays* (Construction report) (Report No R-1262). Michigan Department of Transportation, Lansing, MI.

Simonsen, J.E., & A.W. Price. (1989). *Performance Evaluation of Concrete Pavement Overlays* (Report No R-1303). Michigan Department of Transportation, Lansing, MI.

Simpson, A.L., J.B. Rauhut, P.R. Jordahl, E.B. Owusu-Antwi, M.I. Darter, & R. Ahmad. (1994). *Early Analysis of LTPP General Pavement Studies Data, Volume 3: Sensitivity Analyses for Selected Pavement Distresses* (Report SHRP-P-393). Strategic Highway Research Program, Washington, D.C.

Smith, K. D., H.T. Yu, & D.G. Peshkin. (2002). *Portland Cement Concrete Overlays: State of the Technology Synthesis* (Report No. FHWA-IF-02-045). Federal Highway Administration, U.S. Department of Transportation, Washington D.C.

Springenschmid, R., & W. Fleischer. (2001). Recent Developments in the Design and Construction of Concrete Pavements for German Expressways (Autobahns). In *7nd International Conference of Concrete Pavements.* Purdue University, Orlando, FL, September.

Tayabji, S.D., & P.A. Okamoto. (1985), Thickness Design of Concrete Resurfacing, In *3rd. Int. Conf. on Concrete Pavement Design and Rehabilitation* (pp. 367-379)., April 23-25, 1985, Purdue University, West Lafayette, Indiana, USA

Tayabji, S.D., P.J. Stephanos, & W.P. Davis. (1994). Evaluation and Rehabilitation Design of I495 in Delaware. *Transportation Research Record, 1449*, 159-168.

Taylor, P.C., S.H. Kosmatka, G.F. Voigt, M.E. Ayers, A. Davis, G. J. Fick, … B. Kerkhoff (2007). *Integrated Materials and Construction Practices for Concrete Pavement*. Federal Highway Administration, McLean, VA

Thomlinson, J. (1940). Temperature Variations and Consequent Stresses Produced by Daily and Seasonal Temperature Cycles in Concrete Slabs. Concrete and Construction Engineering, 1940, 36(6), 298-307.

Tighe, S., W. Chung, F. Leung, T. Ellerbusch, & R. Fung. (2005). A Pilot Study of Instrumented Unbonded Concrete Overlay in Toronto. *Proceedings of the Eighth International Conference on Concrete Pavements* (pp 857-882), International Society for Concrete Pavements, August 14-18, 2005, Colorado Springs, CO.

Titus-Glover, L., E.B. Owusu-Antwi, & M.I. Darter. (1999). *Design and Construction of PCC Pavements, Volume III: Improved PCC Performance* (Report No. FHWA-RD-98-113). Federal Highway Administration, Washington, D.C.

Torres, H., J. Roesler, R. Rasmussen, & D. Harrington. (2012). *Design of Concrete Overlays using Existing Methodologies* (Report DTFH61-06-H-00011). National Concrete Pavement Technology Center, Iowa State University, Ames, IA.

Totski, O. (1981). Behavior of Multi-Layered Plates and Beams on Winker Foundation. *Stroitel'naya Mechanika i Rasschet Sooruzheniy, 6*, 54-58 (in Russian).

Tran, N., L. Ga, P. Turner, & J. Shambley. (2016). *Enhanced Compaction to Improve Durability and Extend Pavement Service Life: A Literature Review* (NCAT Report 16-02R). Federal Highway Administration. Washington, D.C.

Vandenbossche, J.M. (2003). Interpreting Falling Weight Deflectometer Results for Curled and Warped Portland Cement Concrete Pavements, Ph.D. Dissertation. University of Minnesota, Minneapolis, MN.

VDOT. (2011). Testing of Asphalt Concrete Mixtures: Chapter 7. In *Asphalt Testing*. Virginia Department of Transportation, Charlottesville, VA.

Watson, M., & T. Burnham. (2010). *Construction Report for MnROAD Thin Unbonded Concrete overlay Test Cell 5 (Sub-Cells 105-405).* Minnesota Department of Transportation. St. Paul, MN.

Wu, C.L., J.W. Mack, P.A. Okamoto, & R.G. Packard. (1993, April). Prediction of Faulting of Joints in Concrete Pavements*. In *Proceedings, Fifth International Conference on Concrete Pavement Design and Rehabilitation*, Vol. 2. Purdue University, West Lafayette, IN.

Yu, H.T., M.I. Darter, K.D. Smith, J. Jiang, & L. Khazanovich.(1996). *Performance of Concrete Pavements Volume III - Improving Concrete Pavement Performance* (Final report, Contract DTFH61-91-C-00053). Federal Highway Administration, McLean, VA.

Yu, H.T., L. Khazanovich, M.I. Darter, & A. Ardani. (1998). Analysis of Concrete Pavement Responses to Temperature and Wheel Loads Measured from Instrumented Slabs. *Transportation Research Record*, *1639,* 94–101.

APPENDIX A: EXTENDED LABORATORY REPORTING

MATERIAL TEST DATA

The following tables contain all material test data from the study, including averages and standard deviations for each test date and concrete age at testing. Elastic modulus, compressive strength, and modulus of rupture tests were conducted according to ASTM C469, ASTM C39, and ASTM C78, respectively.

	Elastic Modulus			
	14 Day		28 Day	
Cast Date	Avg	Std Dev	Avg	Std Dev
Lower Beam Mixture				
2/11/2015	5.24E+06	90000	5.34E+06	47000
2/19/2015	4.53E+06	13000	4.92E+06	81000
3/2/2015			4.80E+06	63000
3/12/2015	4.77E+06	67000	4.83E+06	109000
3/16/2015			5.03E+06	149000
	29 Day		31 Day	
4/6/2015			4.64E+06	111000
4/9/2015	4.60E+06	171000		
	14 Day		28 Day	
4/13/2015			4.83E+06	171000
Upper Beam Mixture				
	14 Day		28 Day	
2/20/2015	2.81E+06	14000	3.11E+06	50000
2/22/2015	3.11E+06	69000	3.24E+06	64000
2/23/2015			3.28E+06	112000
2/26/2015			3.11E+06	251000

Cast Date	5 Day		7 Day	
3/3/2015			3.04E+06	49000
	5 Day		**7 Day**	
Cast Date	Avg	Std Dev	Avg	Std Dev
3/30/2015			3.81E+06	315000
4/2/2015			3.88E+06	187000
4/17/2015			3.88E+06	339000
4/22/2015			4.30E+06	142000
4/24/2015			4.23E+06	43000
	5 Day		**6 Day**	
4/29/2015			4.28E+06	155000
5/1/2015			4.17E+06	88000
5/6/2015	4.36E+06	258000		
5/7/2015	4.48E+06	218000		
5/13/2015			4.71E+06	47000
5/15/2015			4.79E+06	54000
5/20/2015			4.62E+06	88000
5/22/2015			4.65E+06	89000
7/1/2015	4.43E+06	165000		
7/9/2015	4.49E+06	112000		

	Compressive Strength			
	14 Day		**28 Day**	
Cast Date	Avg	Std Dev	Avg	Std Dev
	Lower Beam Mixture			

Cast Date	Avg	Std Dev	Avg	Std Dev
2/11/2015	7610	533	7411	271
2/19/2015	6232	61	6471	96
3/2/2015	6196	160	6991	129
3/12/2015	6325	170	7059	263
3/16/2015	6443	298	7093	459
	29 Day		31 Day	
4/6/2015			6982	170
4/9/2015	6806	303		
	14 Day		28 Day	
4/13/2015			6847	177

Upper Beam Mixture

	14 Day		28 Day	
2/20/2015	1977	199	2666	61
2/22/2015	2608	31	2905	242
2/23/2015	2352	129	2326	119
2/26/2015	2140	168	2237	32
3/3/2015	2242	24	2156	303
	5 Day		7 Day	
Cast Date	Avg	Std Dev	Avg	Std Dev
3/30/2015			3881	262
4/2/2015			4512	247
4/17/2015			4590	285
4/22/2015			4696	267
4/24/2015			4694	100

	5 Day		6 Day	
4/29/2015			5059	64
5/1/2015			5069	184
5/6/2015	5334	310		
5/7/2015	5106	225		
5/13/2015			5013	353
5/15/2015			5357	275
5/20/2015			5073	186
5/22/2015			5131	195
7/1/2015	4632	279		
7/9/2015	4732	235		

	Modulus of Rupture			
	14 Day		28 Day	
Cast Date	Avg	Std Dev	Avg	Std Dev
Lower Beam Mixture				
2/11/2015			932	86
2/19/2015			878	17.5
3/2/2015				
3/12/2015	838	20		
3/16/2015				
	29 Day		31 Day	
4/6/2015			884	3
4/9/2015	863	12		

	14 Day		28 Day	
4/13/2015			905	55

Upper Beam Mixture

	14 Day		28 Day	
2/20/2015			584	13
2/22/2015			573	-
2/23/2015				
2/26/2015				
3/3/2015			552	-

	5 Day		7 Day	
Cast Date	Avg	Std Dev	Avg	Std Dev
3/30/2015			688	58
4/2/2015	613	18		
4/17/2015	617	31		
4/22/2015	642	30		
4/24/2015	643	8		

	5 Day		6 Day	
4/29/2015	643	47		
5/1/2015	645	23		
5/6/2015	685	53		
5/7/2015	707	27		
5/13/2015	695	10		
5/15/2015	719	6		
5/20/2015	725	27		

5/22/2015	708	18
7/1/2015	660	19
7/9/2015	683	29

Cast Date	QC Data	
	Air	Avg. Slump
Lower Beam Mixture		
2/11/2015	*	2.5
2/19/2015	*	2.0
3/2/2015	*	1.3
3/12/2015	6.1	1.1
3/16/2015	6.1	1.1
4/6/2015	5.8	1.1
4/9/2015	5.5	1.3
4/13/2015	5.8	1.2
Upper Beam Mixture		
2/20/2015	*	4.0
2/23/2015	*	4.8
2/26/2015	*	4.2
3/3/2015	*	4.3
3/30/2015	6.3	3.5
4/2/2015	6.3	3.8
4/17/2015	6.5	2.5
4/22/2015	6.3	2.3
4/24/2015	6.3	2.1

4/29/2015	6.0	1.9
5/1/2015	5.9	1.9
5/6/2015	5.8	1.5
5/7/2015	6.0	1.6
5/13/2015	6.0	2.1
5/15/2015	6.2	1.7
5/20/2015	6.0	1.7
5/22/2015	6.4	2.1
7/1/2015	6.5	1.6
7/9/2015	6.3	1.5

*Not measured correctly due to air meter calibration issue

MECHANISM 1 DATA

This appendix contains two types of plots for each specimen discussed in Section 4.2.4. The first plots type shows measured deflection at each of the four locations versus the cycle number. All deflection values correspond to the dynamic load at the peak of 600 pounds. All abbreviations are described below. Refer to Figure 25, in the Section 4.2.2 on Mechanism 1 for the locations of the deflection measurements.

Note the following nomenclature:

OL = Overlay Loaded side

OU = Overlay Unloaded side

EL = Existing Loaded side

EU = Existing Unloaded side

The second plot type shows load transfer efficiency (LTE) and interlayer compression versus cycle number. Load Transfer Efficiency (LTE) is defined as the ratio of the deflection of the unloaded side to the loaded

side of the joint in the overlay and is reported as a percent. Interlayer compression is the overlay loaded deflection minus the existing beam loaded deflection.

Interlayer Compression = OL – EL

Interlayer LTE = (OU – EU)/(OL – EL)*100
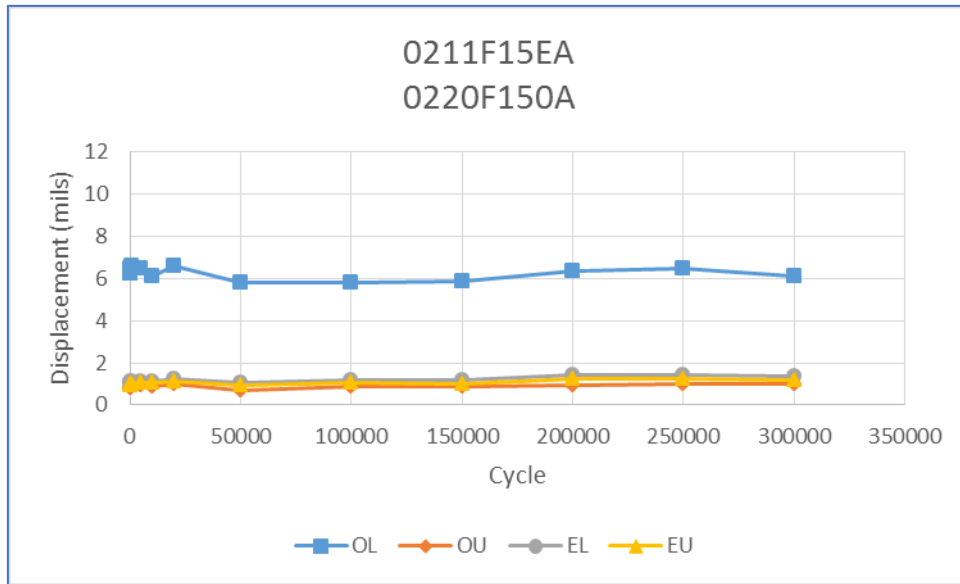
Figure A2.1. F15 Displacement vs. Load Cycle (Tested on 3/20/15)
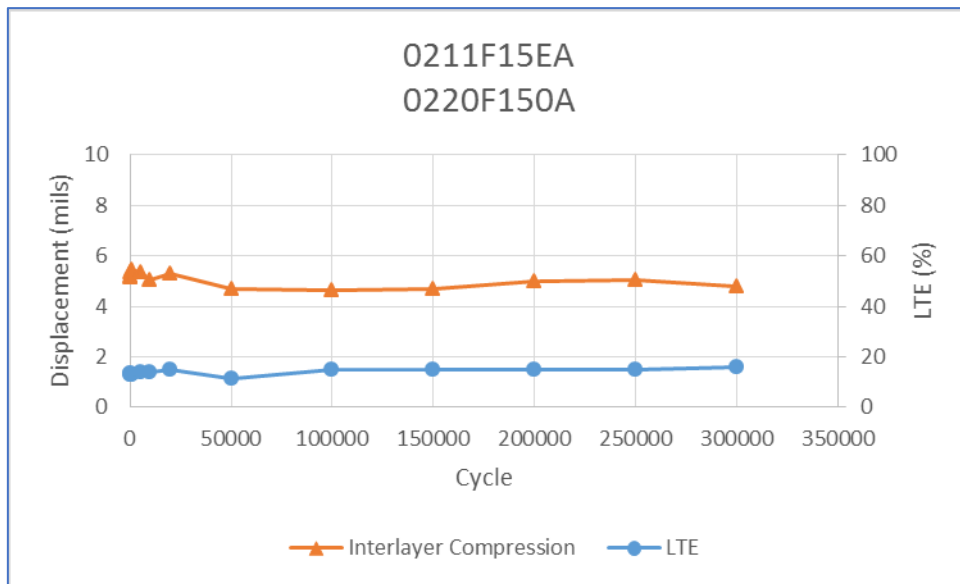
Figure A2.2. F15 Interlayer Compression and LTE vs. Load Cycle (Tested on 3/20/15)
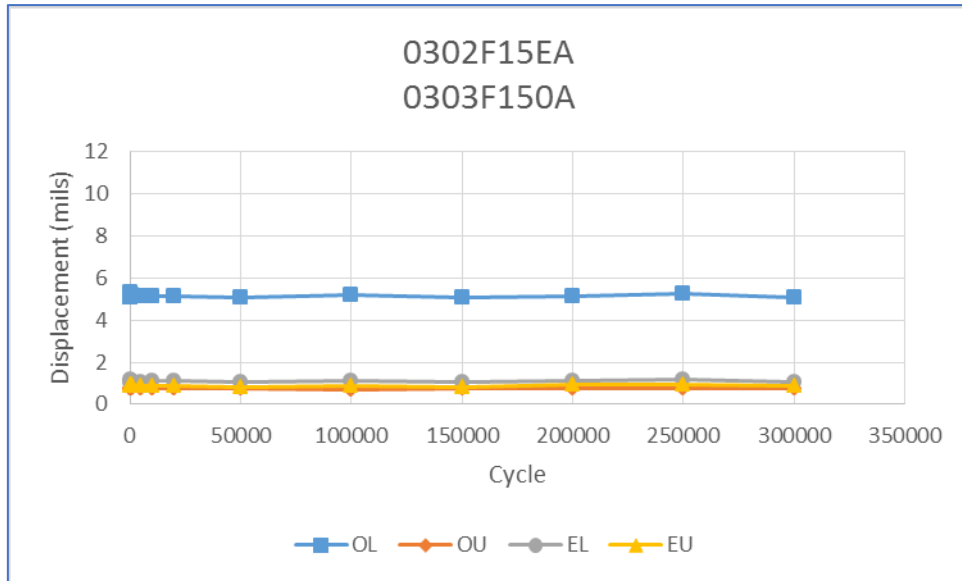
Figure A2.3. F15 Displacement vs. Load Cycle (Tested on 4/1/15)
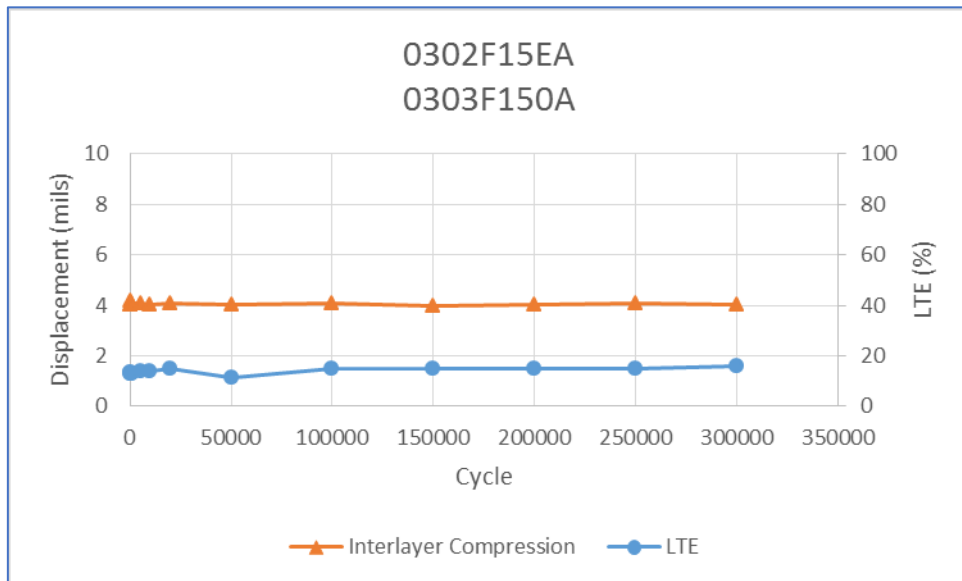
Figure A2.4. F15 Interlayer Compression and LTE vs. Load Cycle (Tested on 4/1/15)
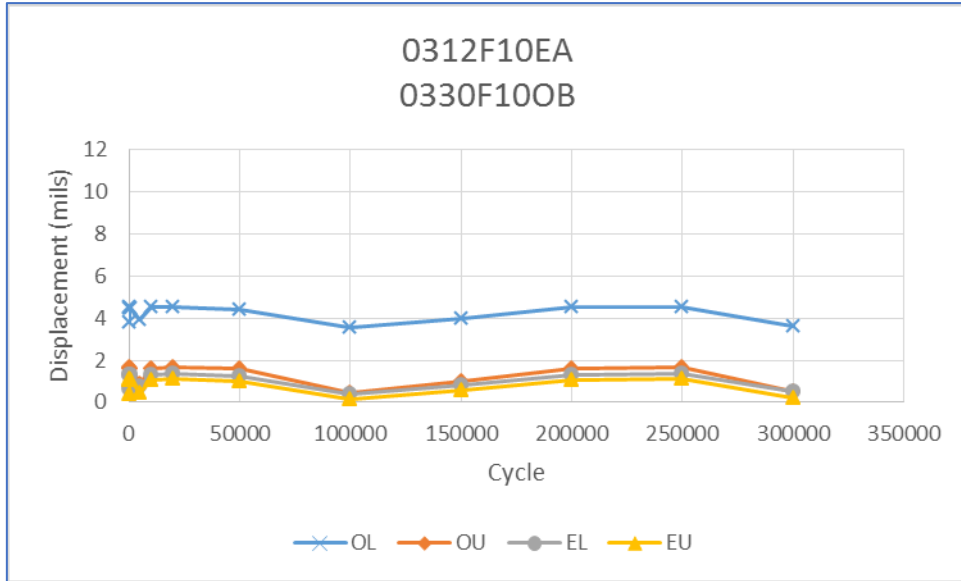
Figure A2.5. F10 Displacement vs. Load Cycle (Tested on 4/8/15)
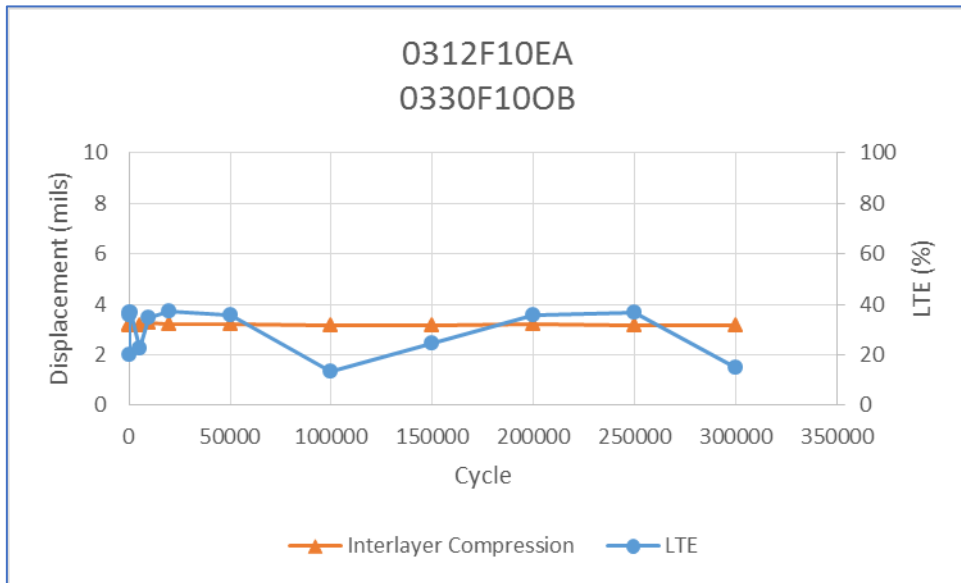
Figure A2.6. F10 Interlayer Compression and LTE vs. Load Cycle (Tested on 4/8/15)

A-11
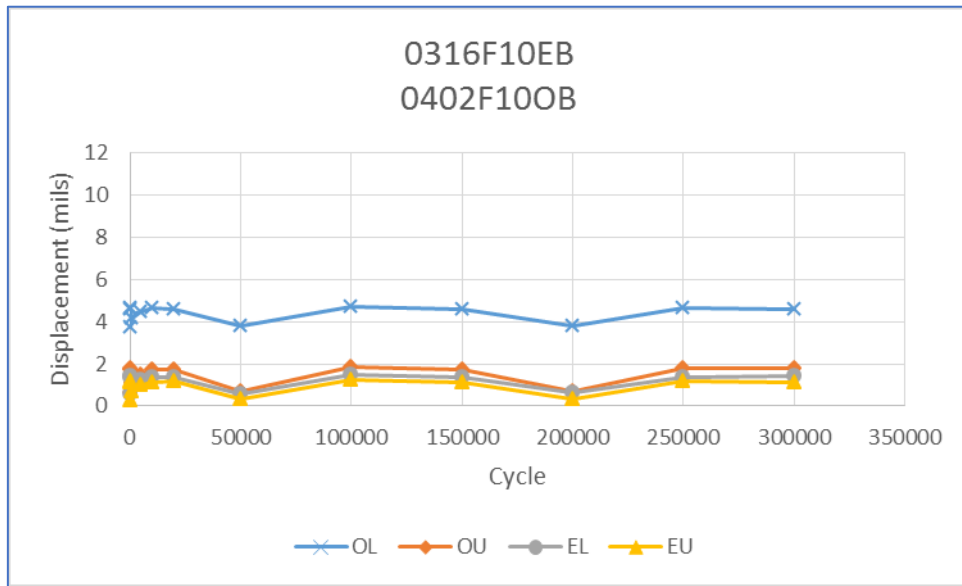
Figure A2.7. F10 Displacement vs. Load Cycle (Tested on 4/9/15)
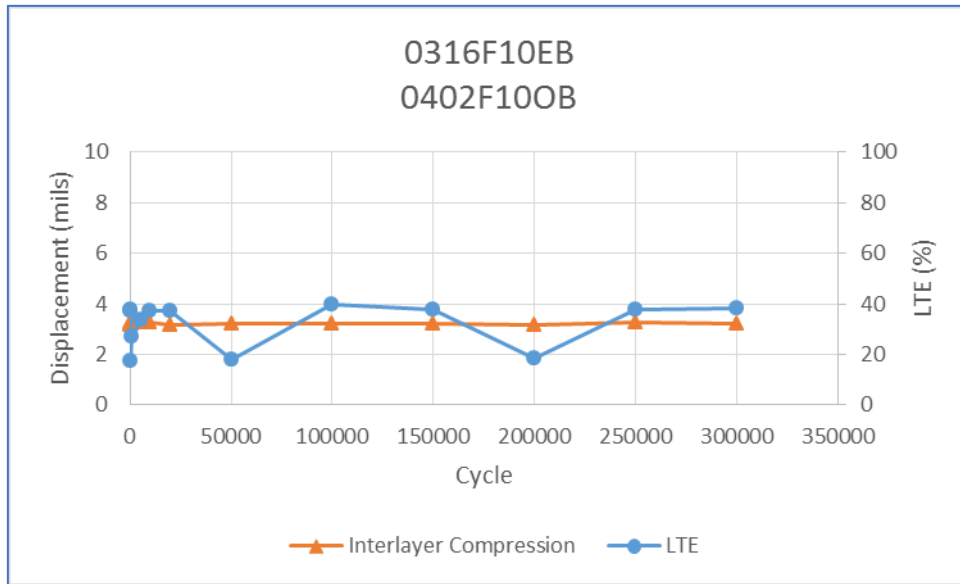
Figure A2.8. F10 Interlayer Compression and LTE vs. Load Cycle (Tested on 4/9/15)
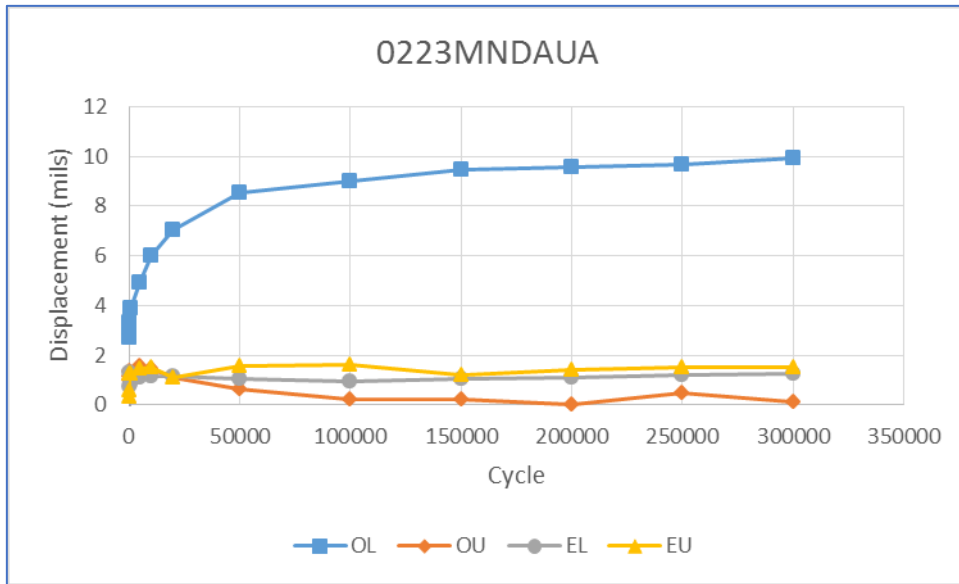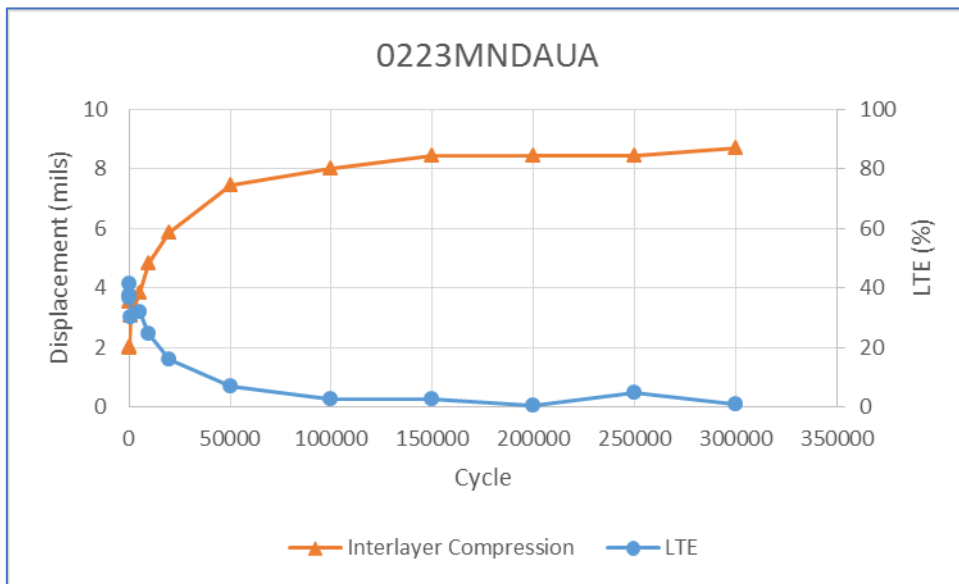
Figure A2.9. MNDAU Displacement vs. Load Cycle (Tested on 3/25/15)

Figure A2.10. MNDAU Interlayer Compression and LTE vs. Load Cycle (Tested on 3/25/15)

A-14
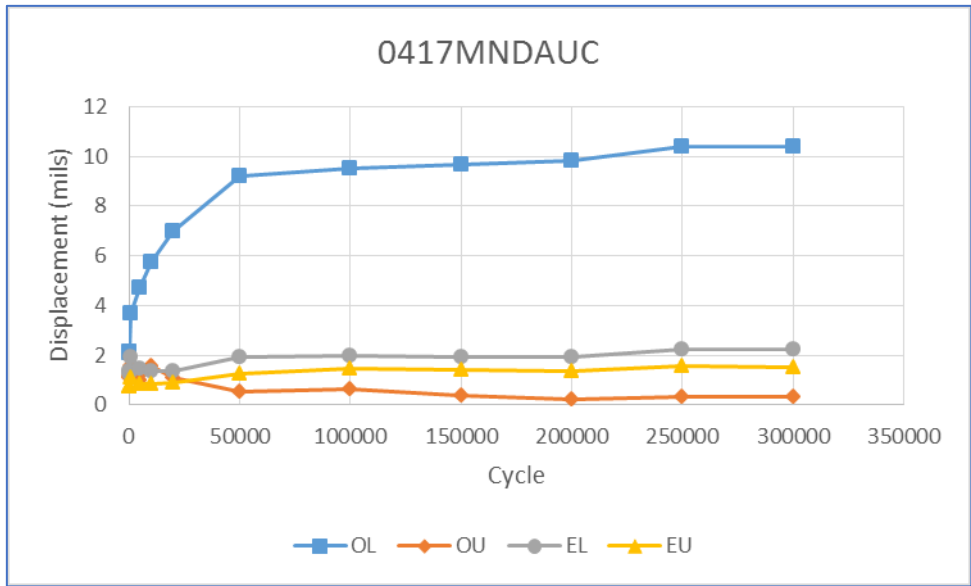
Figure A2.11. MNDAU Displacement vs. Load Cycle (Tested on 4/23/15)
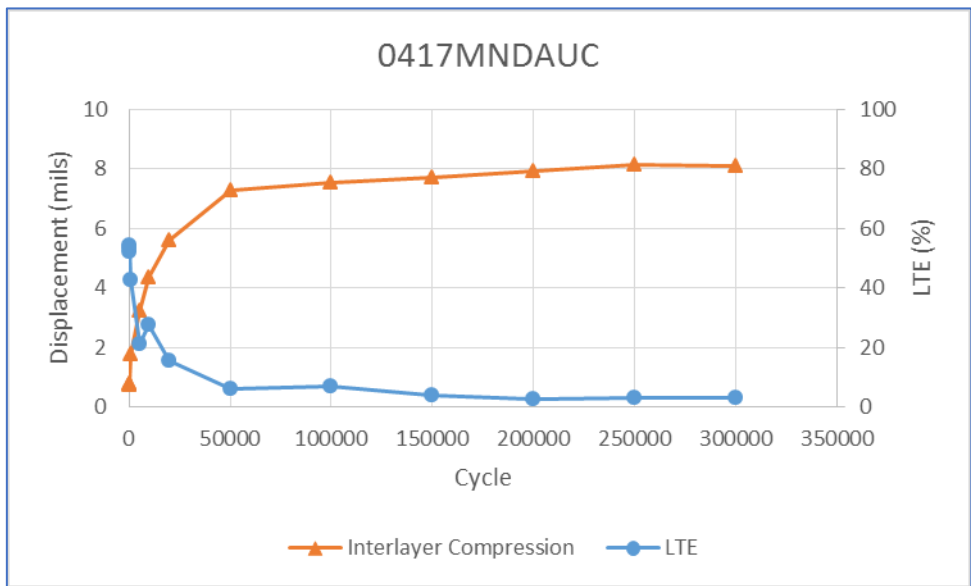
Figure A2.12. MNDAU Interlayer Compression and LTE vs. Load Cycle (Tested on 4/23/15)

A-15
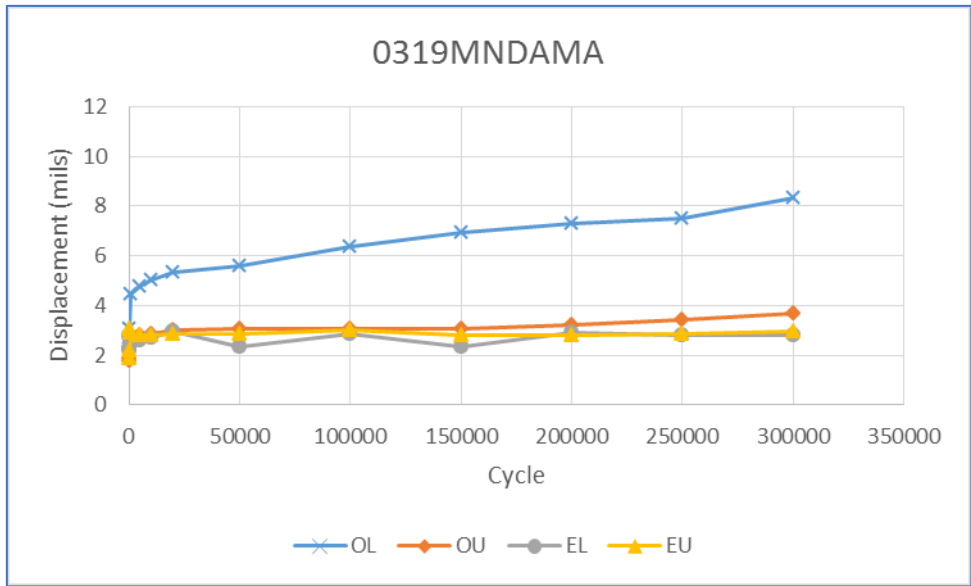
Figure A2.13. MNDAM Displacement vs. Load Cycle (Tested on 4/2/15)
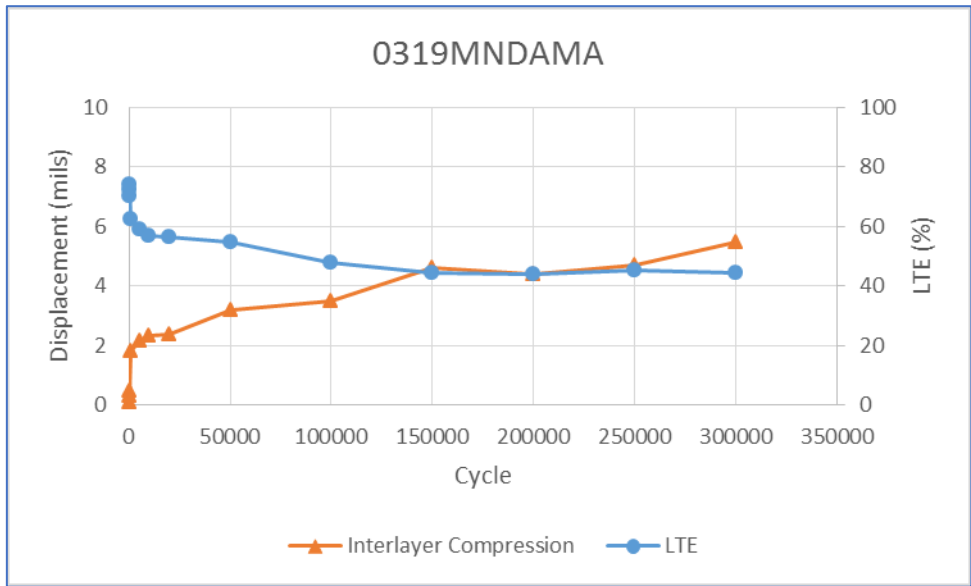
Figure A2.14. MNDAM Interlayer Compression and LTE vs. Load Cycle (Tested on 4/2/15)

A-16
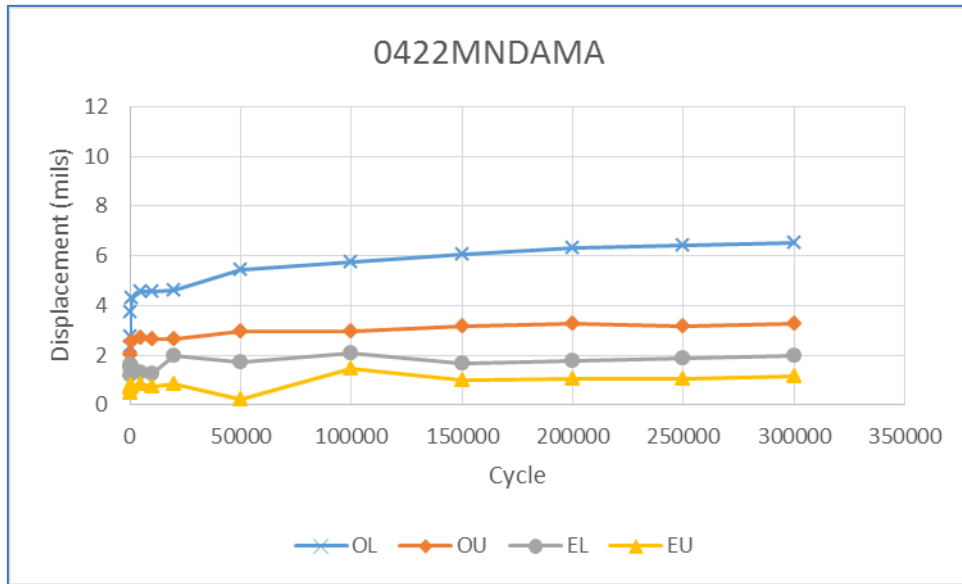
Figure A2.15. MNDAM Displacement vs. Load Cycle (Tested on 4/28/15)
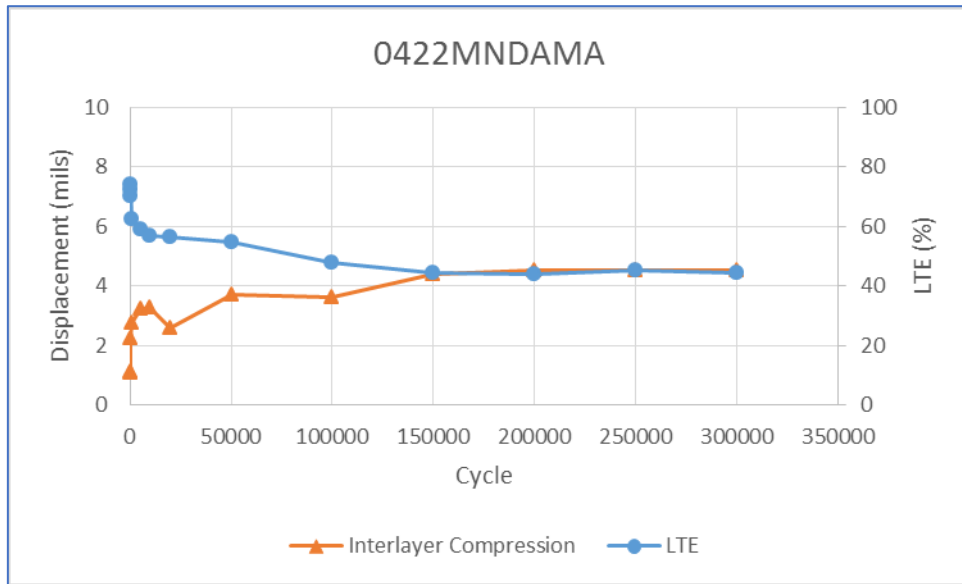
Figure A2.16. MNDAM Interlayer Compression and LTE vs. Load Cycle (Tested on 4/28/15)

A-17
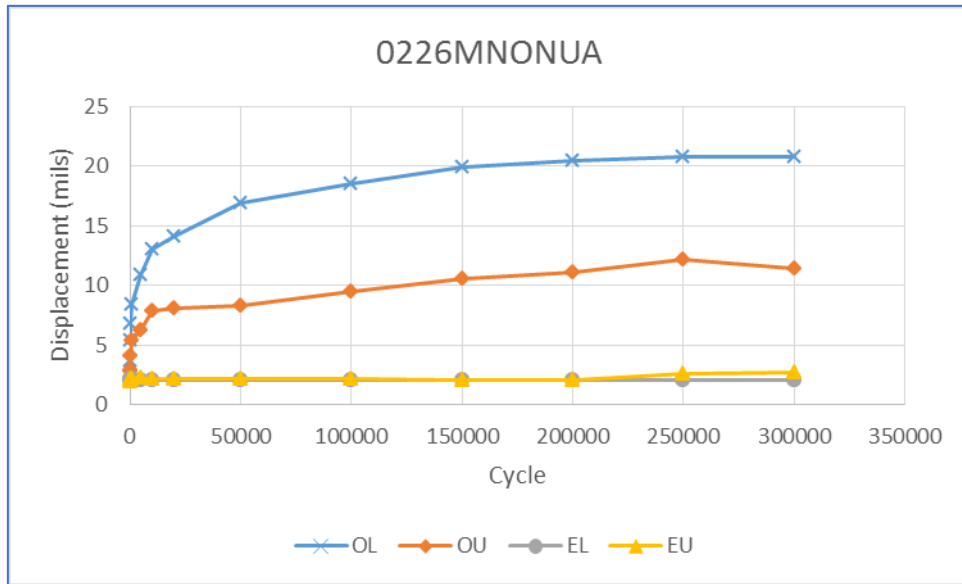
Figure A2.17. MNONU Displacement vs. Load Cycle (Tested on 3/27/15)
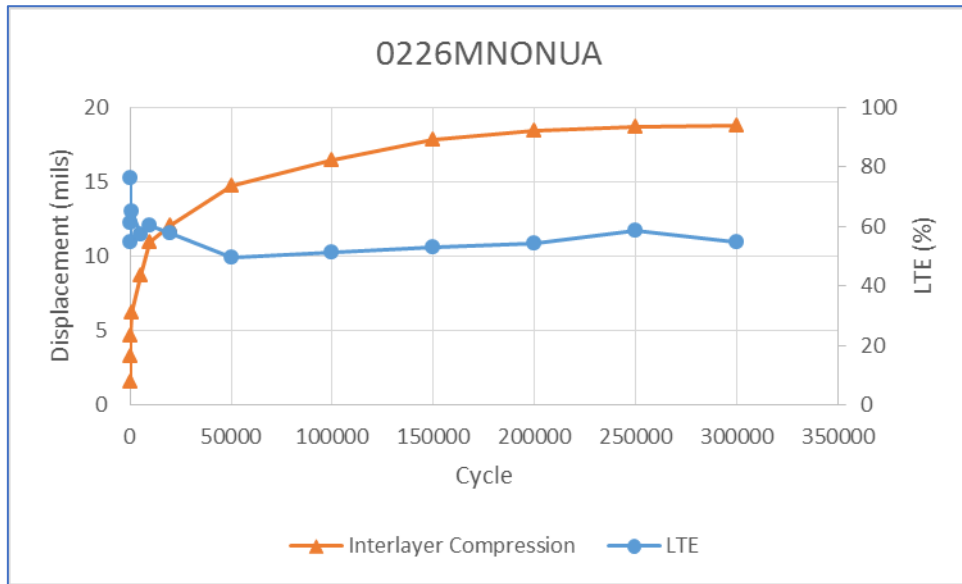
Figure A2.18. MNONU Interlayer Compression and LTE vs. Load Cycle (Tested on 3/27/15)

A-18
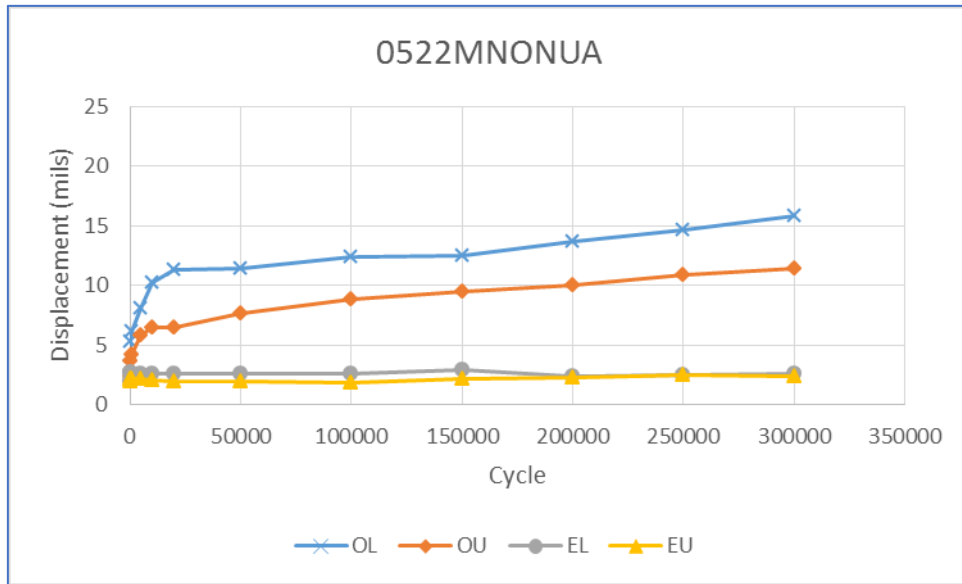
Figure A2.19. MNONU Displacement vs. Load Cycle (Tested on 5/27/15)
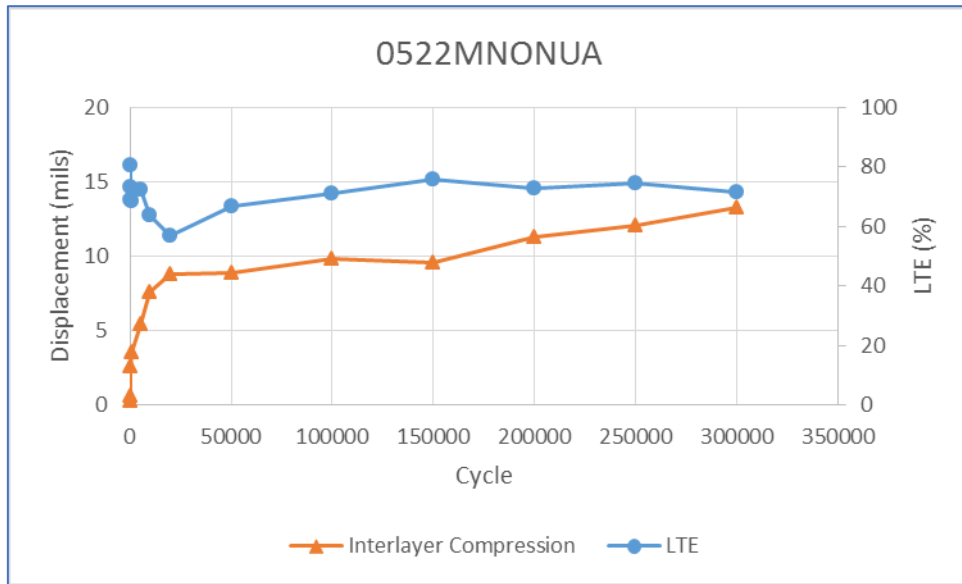
Figure A2.20. MNONU Interlayer Compression and LTE vs. Load Cycle (Tested on 5/27/15)
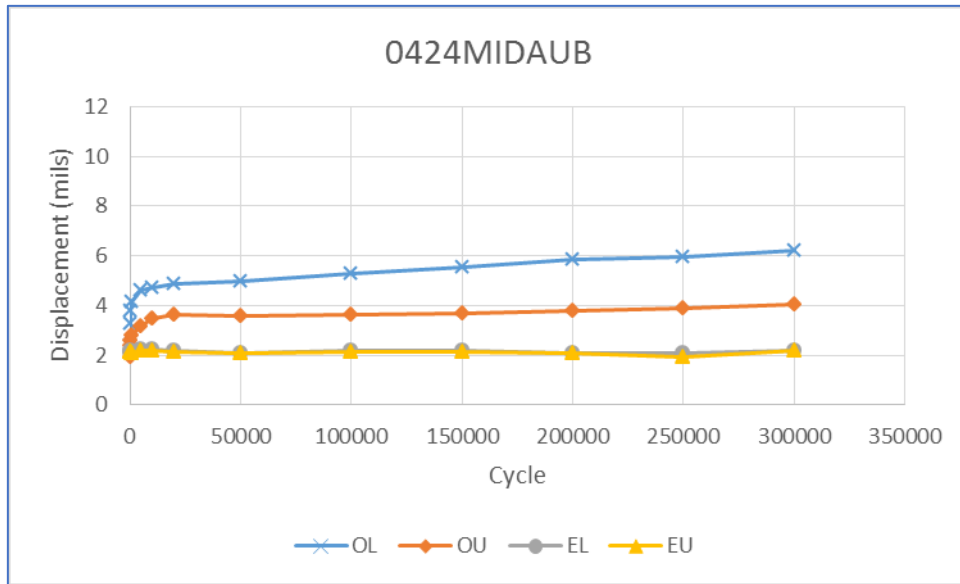
Figure A2.21. MIDAU Displacement vs. Load Cycle (Tested on 4/29/15)
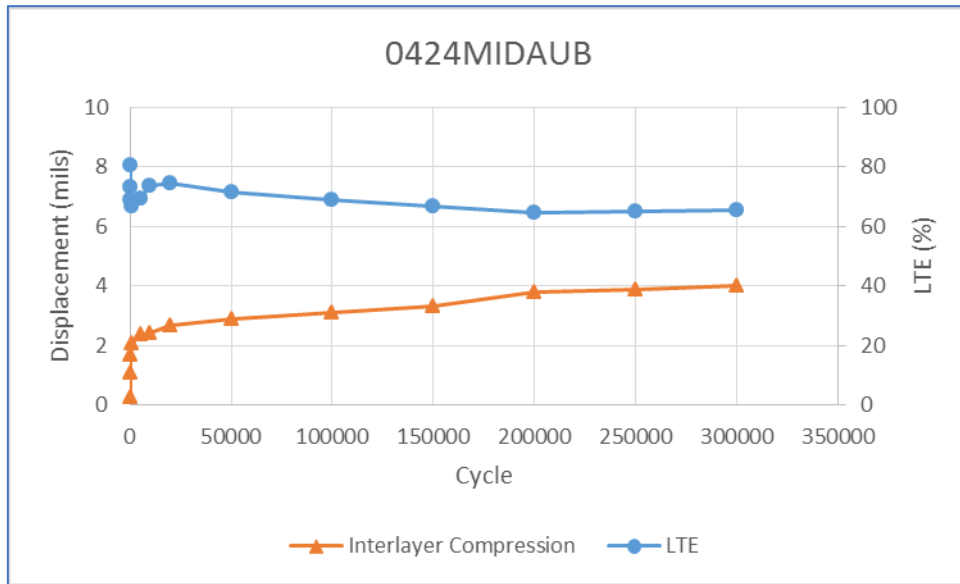
Figure A2.22. MIDAU Interlayer Compression and LTE vs. Load Cycle (Tested on 4/29/15)
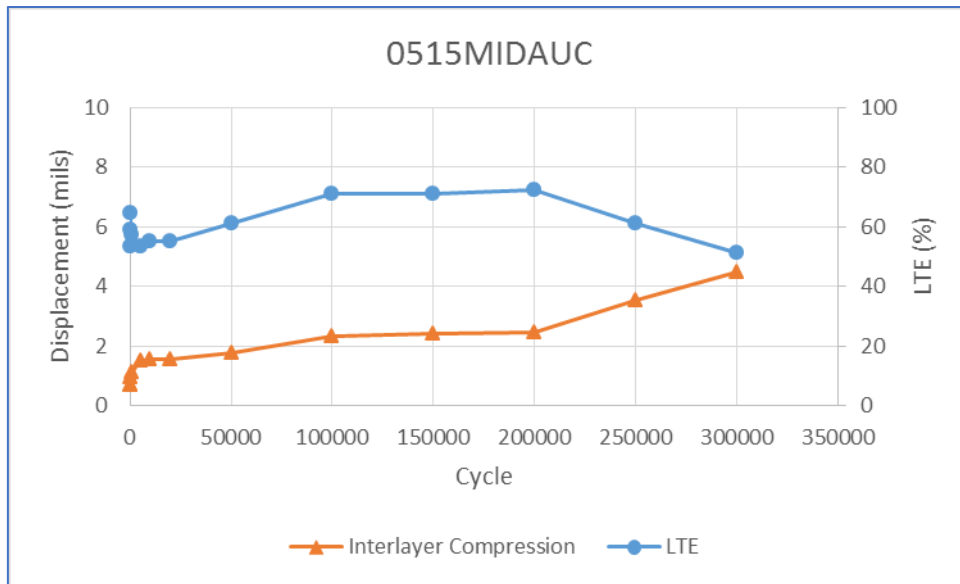
A-20

Figure A2.23. MIDAU Displacement vs. Load Cycle (Tested on 5/20/15)

Figure A2.24. MIDAU Interlayer Compression and LTE vs. Load Cycle (Tested on 5/20/15)

A-21
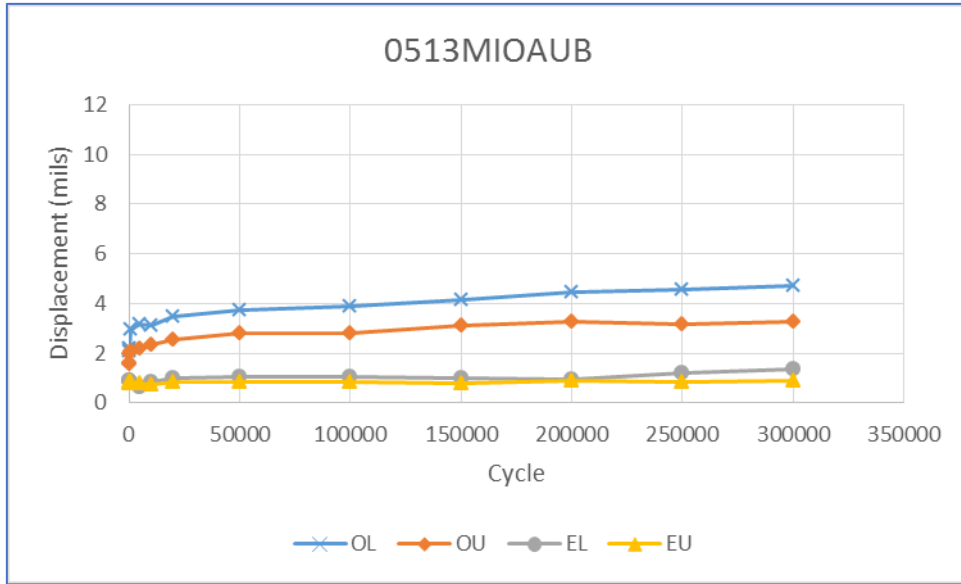
Figure A2.25. MIOAU Displacement vs. Load Cycle (Tested on 5/19/15)
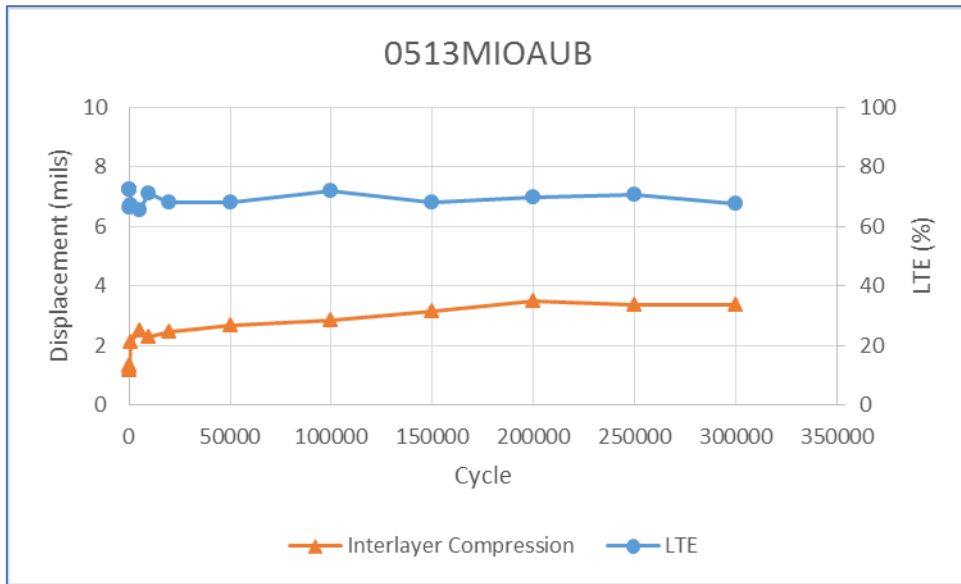
Figure A2.26. MIOAU Interlayer Compression and LTE vs. Load Cycle (Tested on 5/19/15)
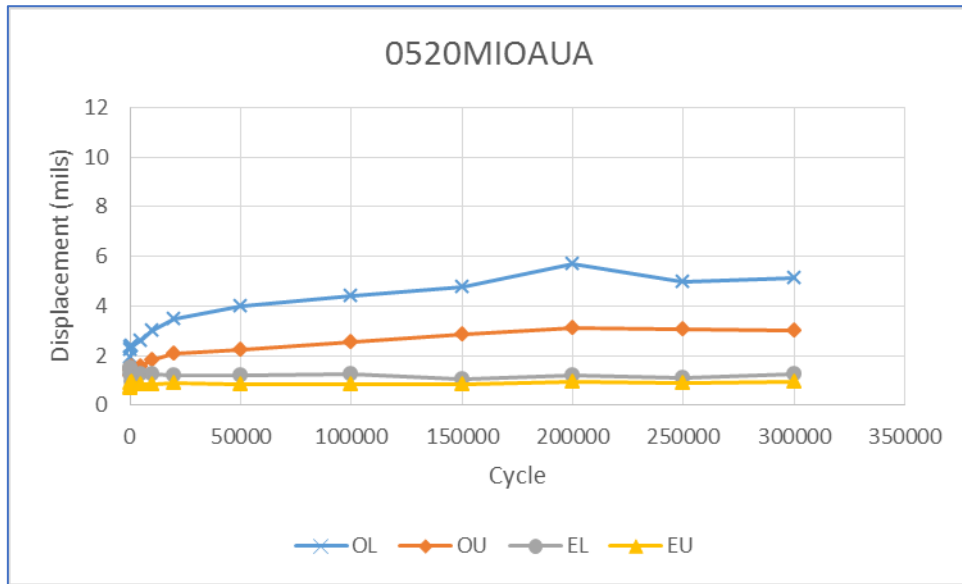
Figure A2.27. MIOAU Displacement vs. Load Cycle (Tested on 5/26/15)
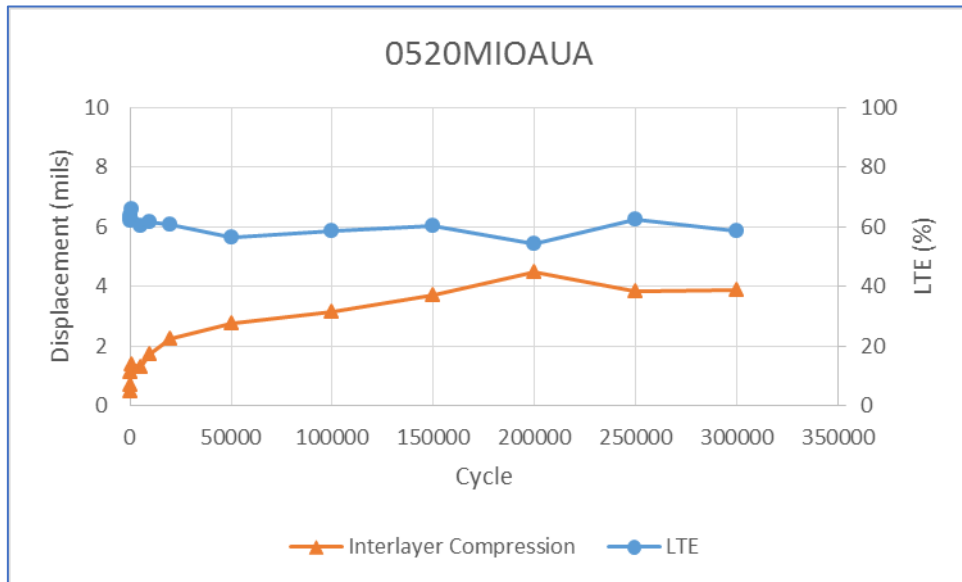
Figure A2.28. MIOAU Interlayer Compression and LTE vs. Load Cycle (Tested on 5/26/15)

This appendix contains two types of plots for the modified push-off test discussed in Section 4.3. Each specimen has two plots, one of each type. The first type of plot shows force and displacement versus time. The second plot shows force versus displacement for each load cycle.
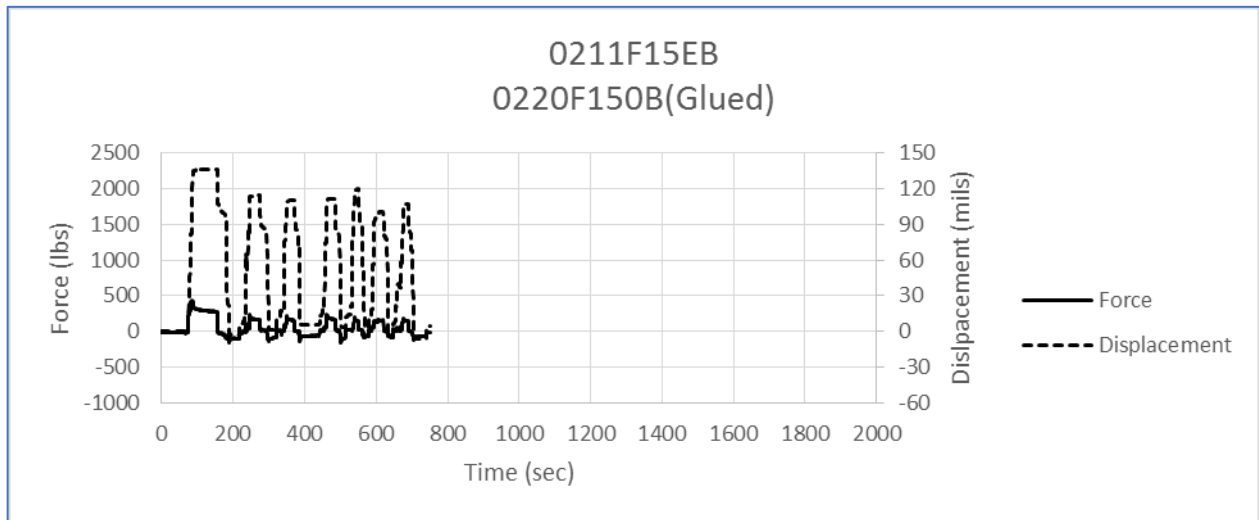
Figure A3.1. F15(Glued) Force and Displacement vs. Time (Tested on 3/20/15)
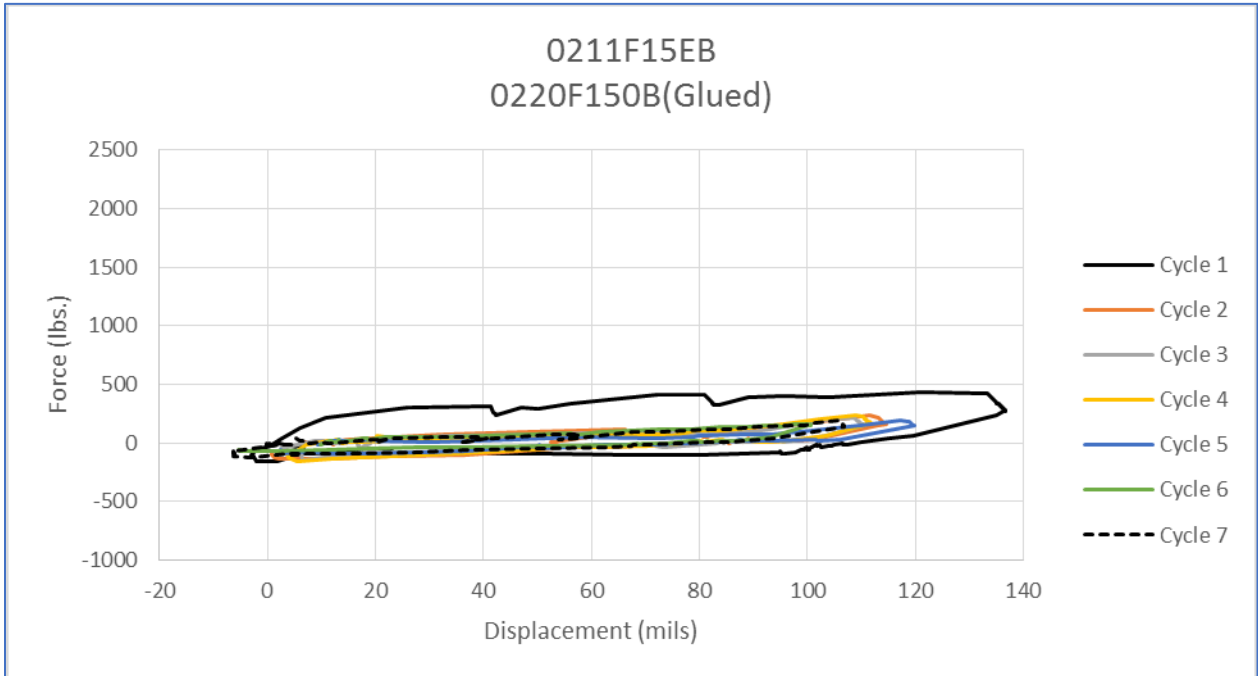
Figure A3.2. F15(Glued) Force vs. Displacement (Tested on 3/20/15)
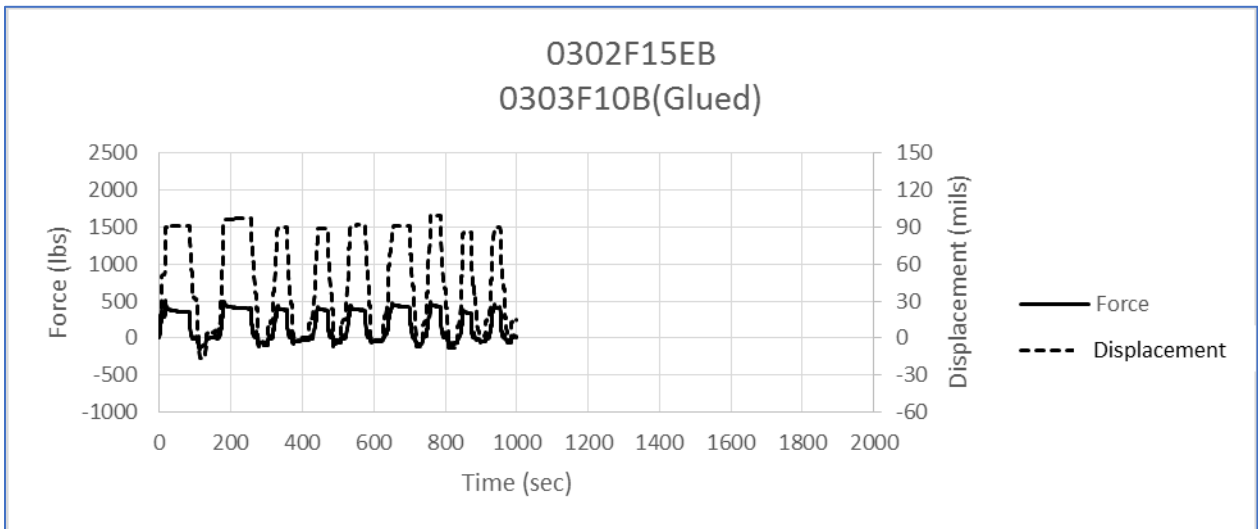
Figure A3.3. F15(Glued) Force and Displacement vs. Time (Tested on 4/1/15)
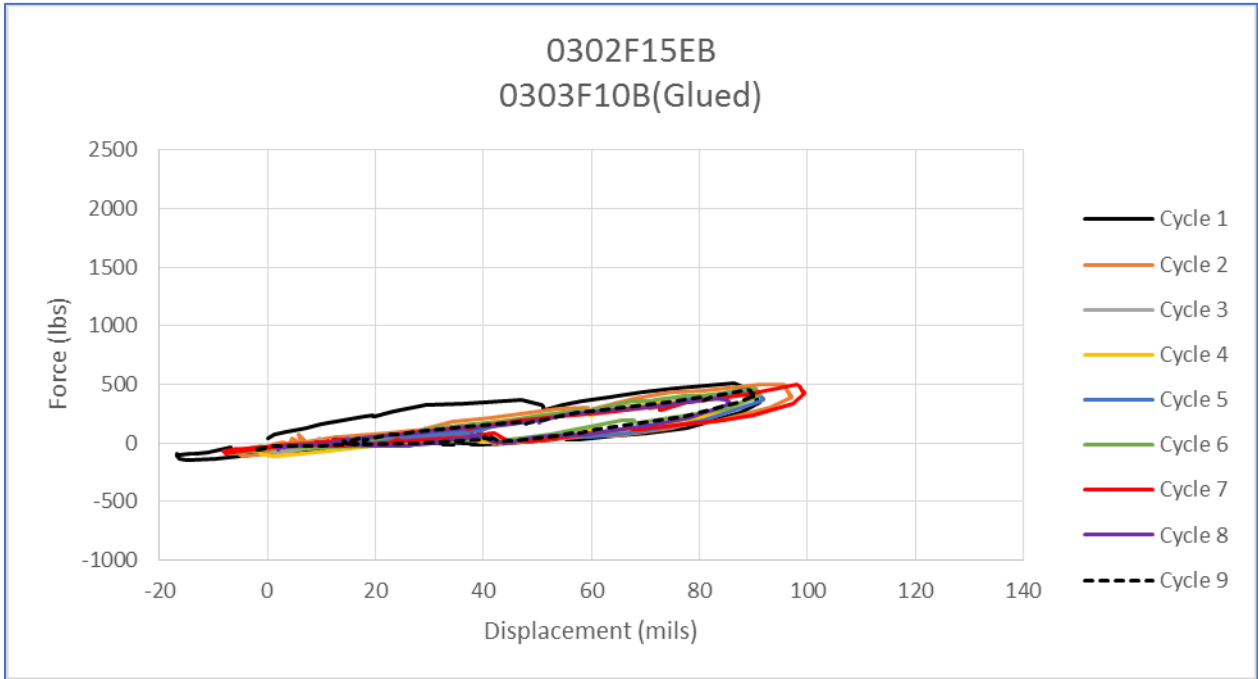
Figure A3.4. F15(Glued) Force vs. Displacement (Tested on 4/1/15)
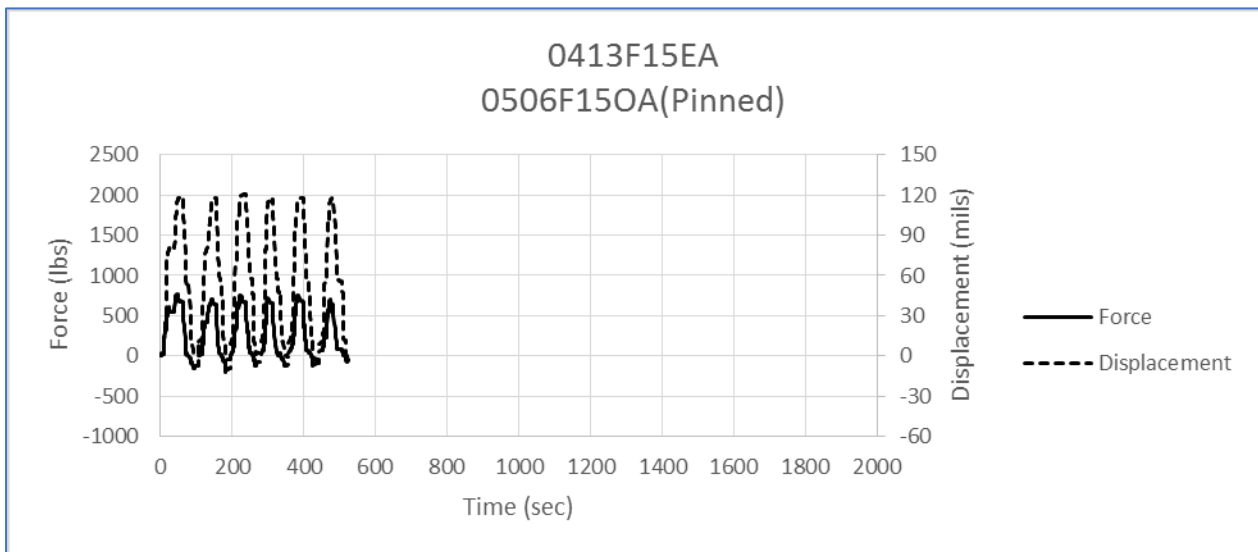
Figure A3.5. F15(Pinned) Force and Displacement vs. Time (Tested on 5/11/15)
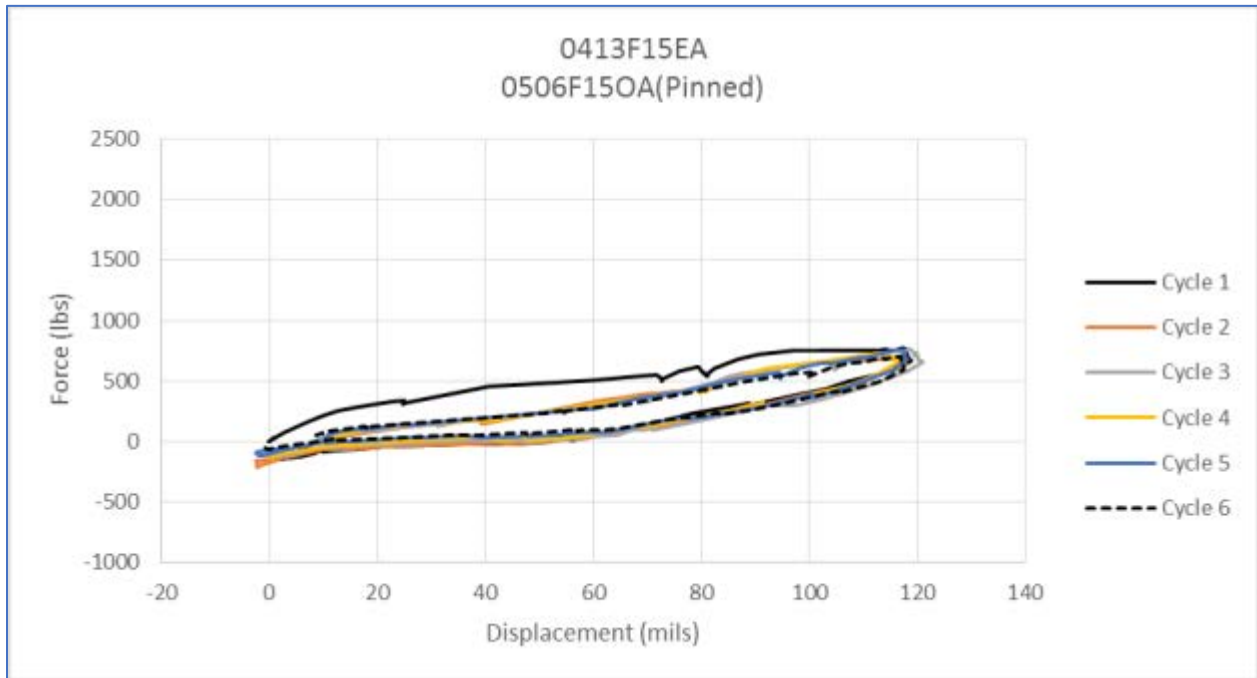
Figure A3.6. F15(Pinned) Force vs. Displacement (Tested on 5/11/15)
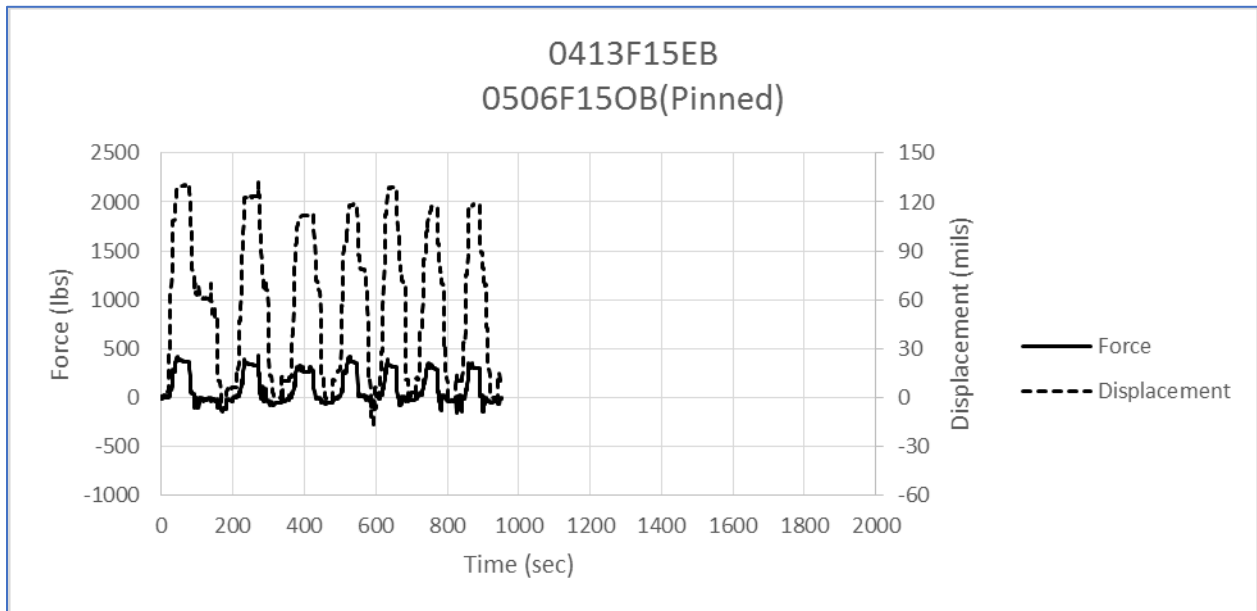
Figure A3.7. F15(Pinned) Force and Displacement vs. Time (Tested on 5/12/15)
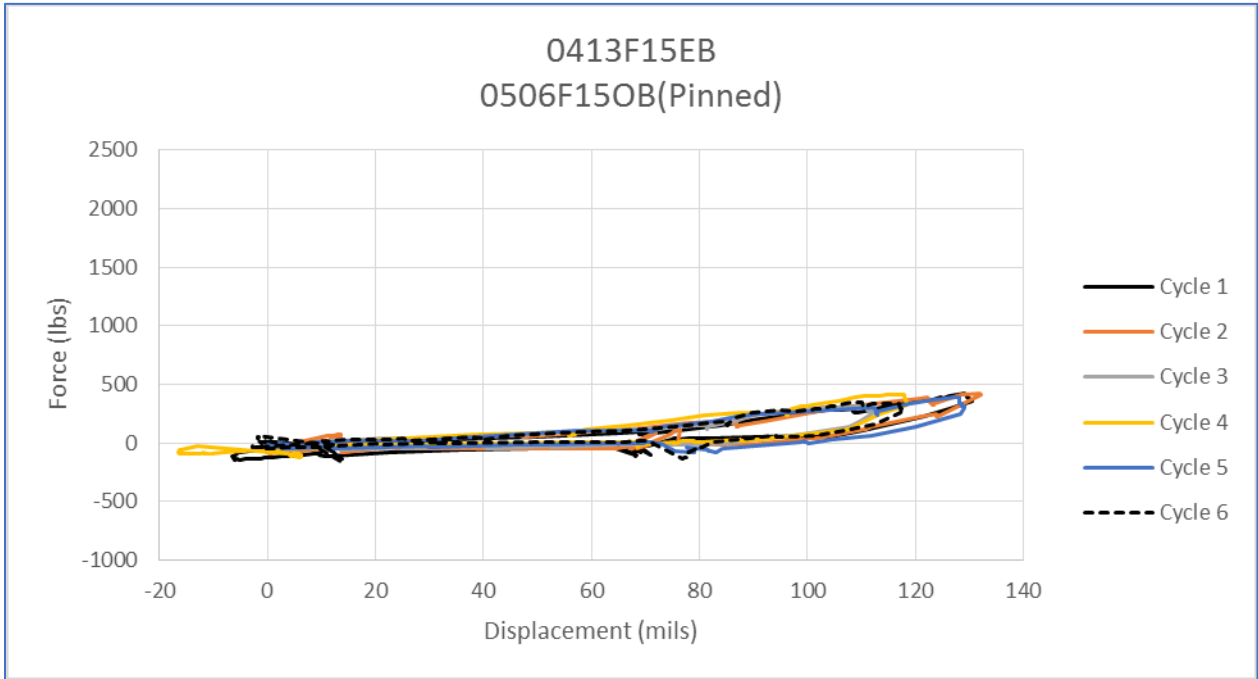
Figure A3.8. F15(Pinned) Force vs. Displacement (Tested on 5/12/15)
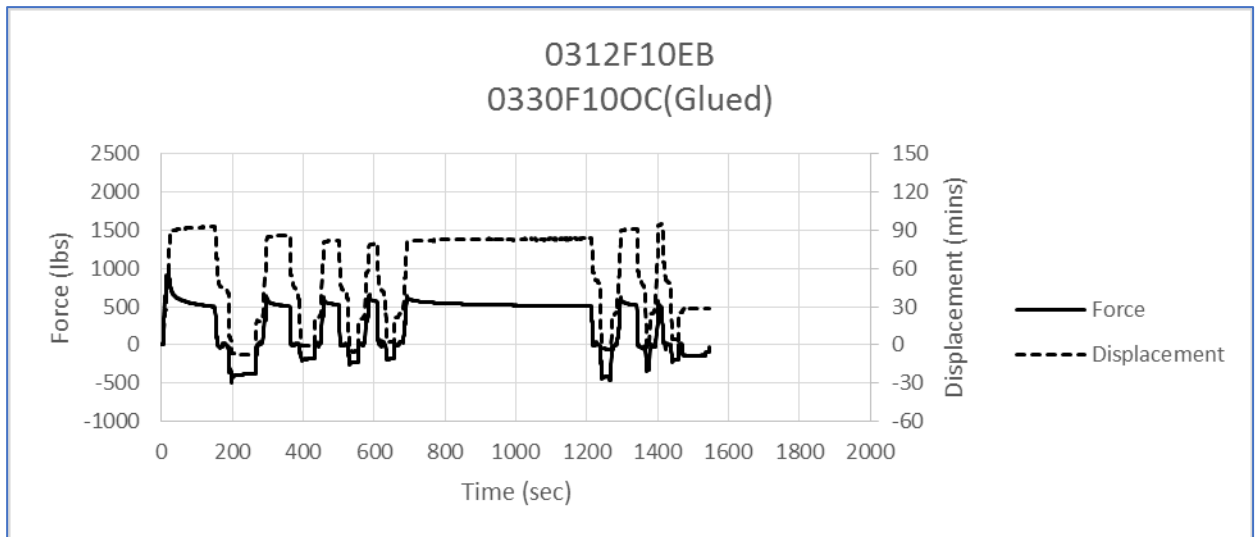
Figure A3.9. F10(Glued) Force and Displacement vs. Time (Tested on 4/10/15)
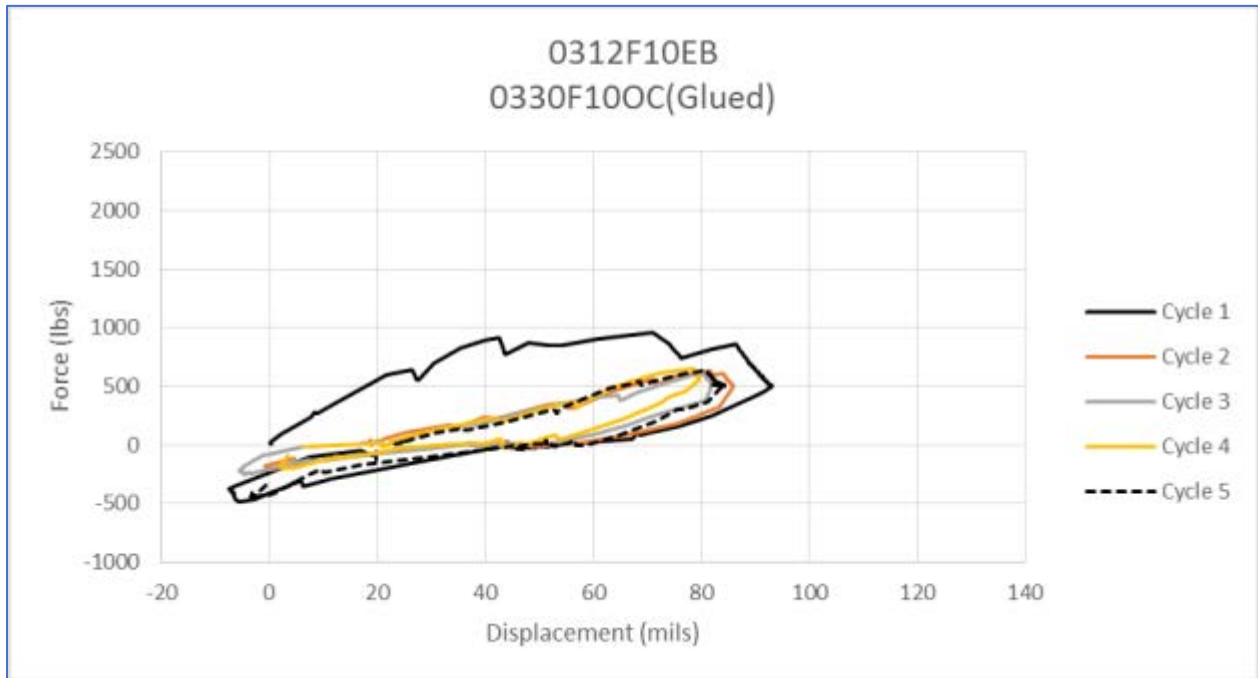
Figure A3.10. F10(Glued) Force vs. Displacement (Tested on 4/10/15)
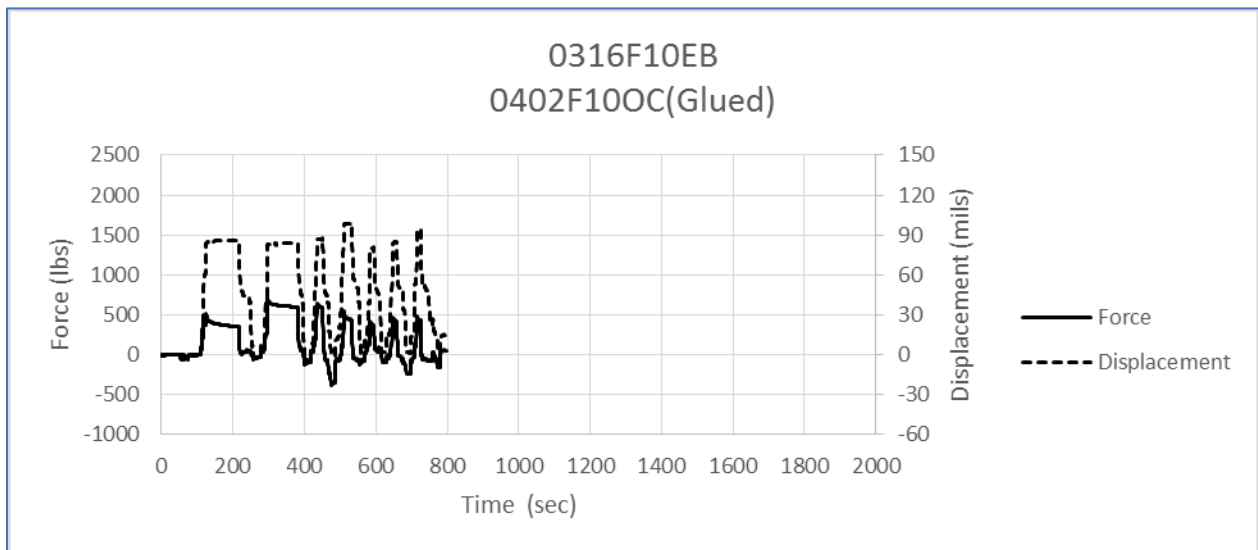
Figure A3.11. F10(Glued) Force and Displacement vs. Time (Tested on 4/10/15)
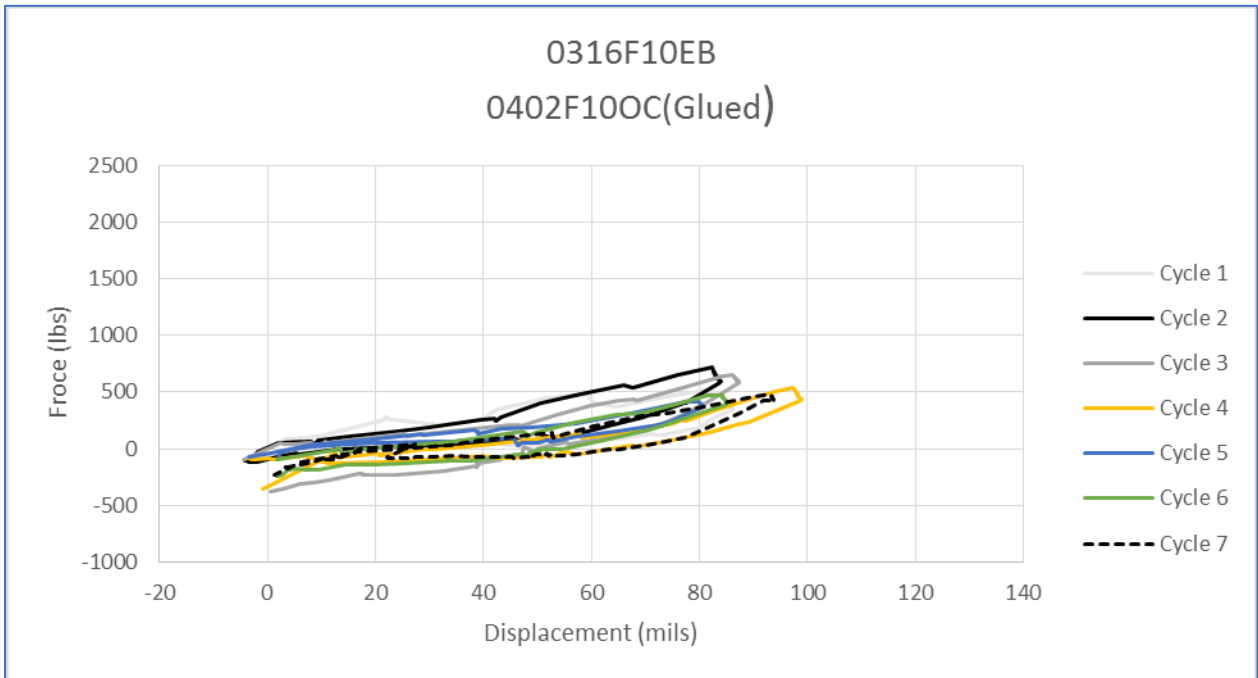
Figure A3.12. F10(Glued) Force vs. Displacement (Tested on 4/10/15)
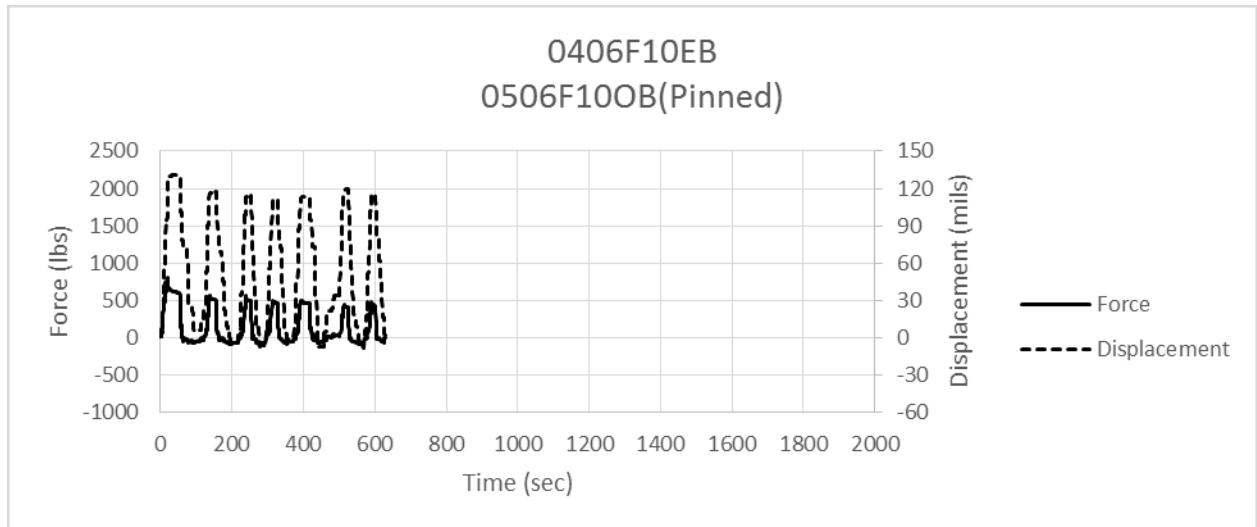
Figure A3.13. F10(Pinned) Force and Displacement vs. Time (Tested on 5/11/15)
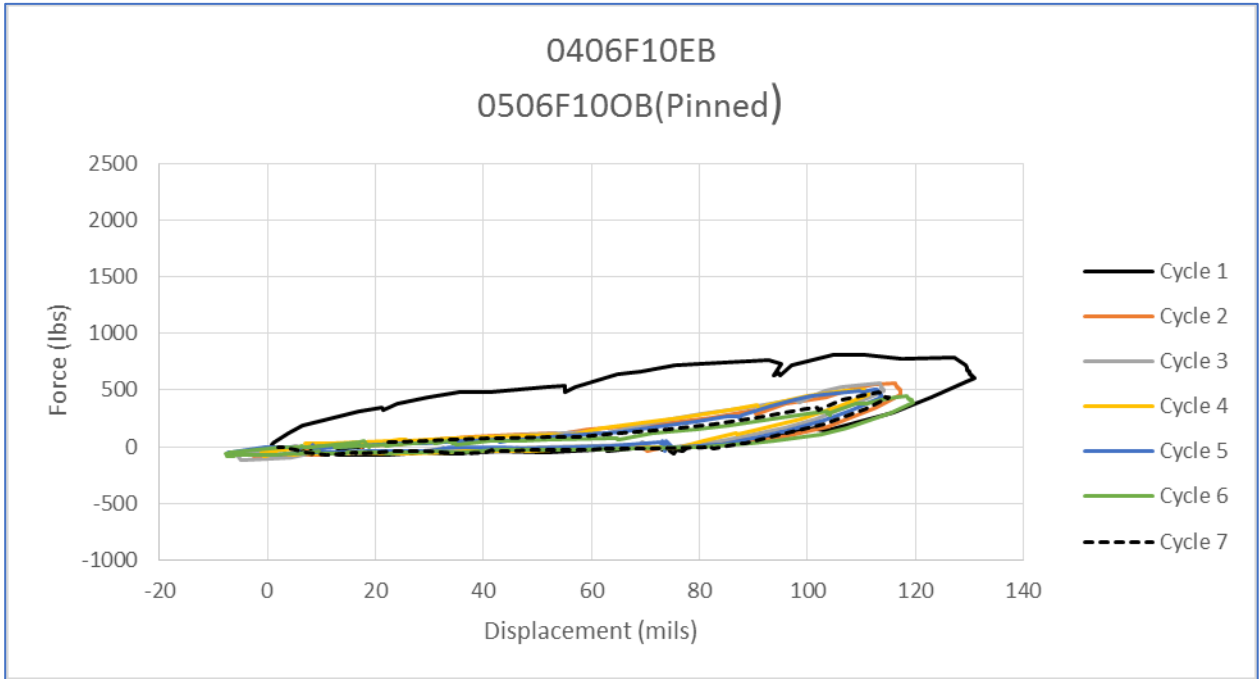
Figure A3.14. F10(Pinned) Force vs. Displacement (Tested on 5/11/15)
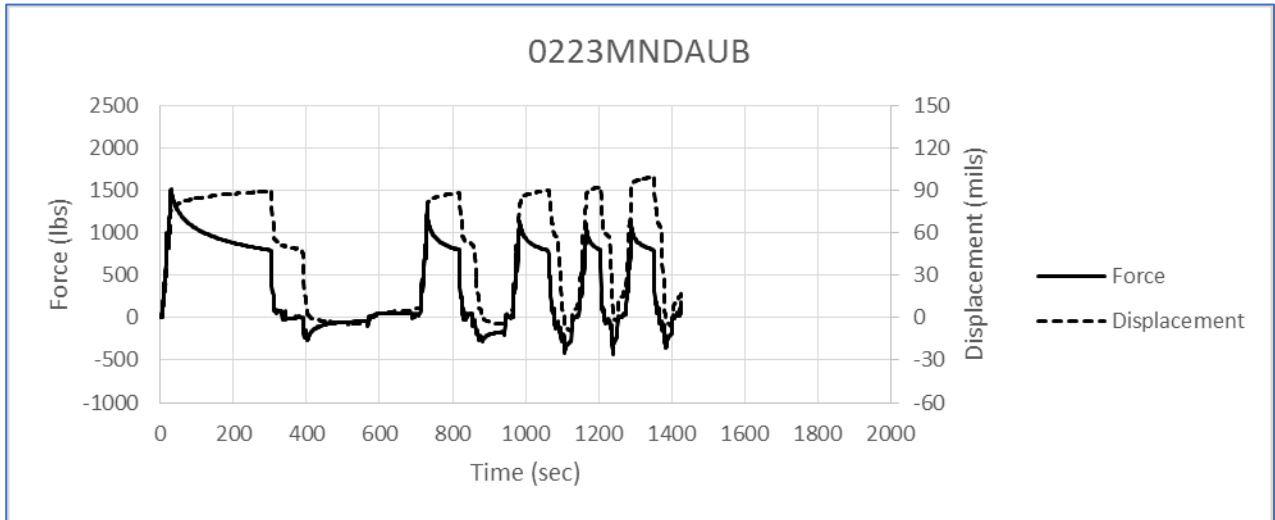
Figure A3.15. MNDAU Force and Displacement vs. Time (Tested on 3/24/15)

A-31
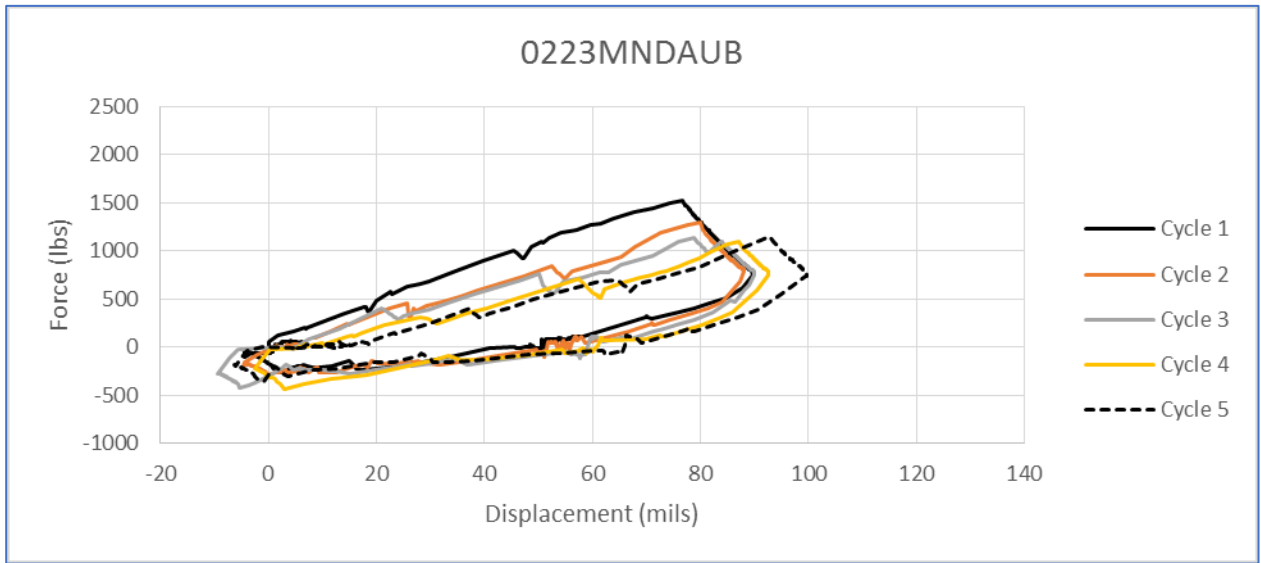
Figure A3.16. MNDAU Force vs. Displacement (Tested on 3/24/15)
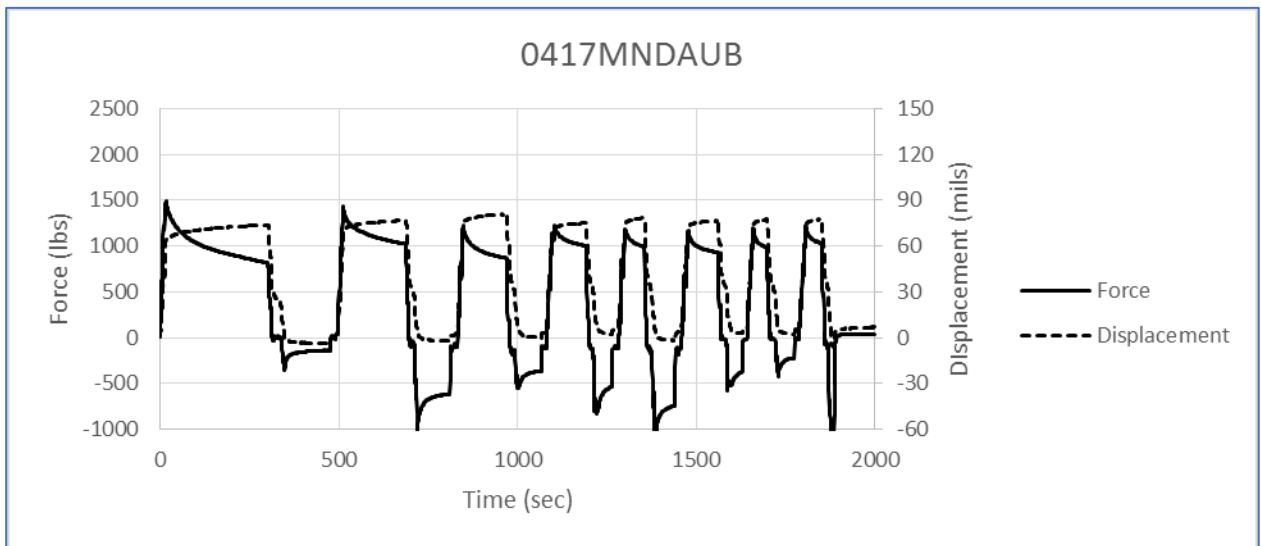
Figure A3.17. MNDAU Force and Displacement vs. Time (Tested on 4/23/15)
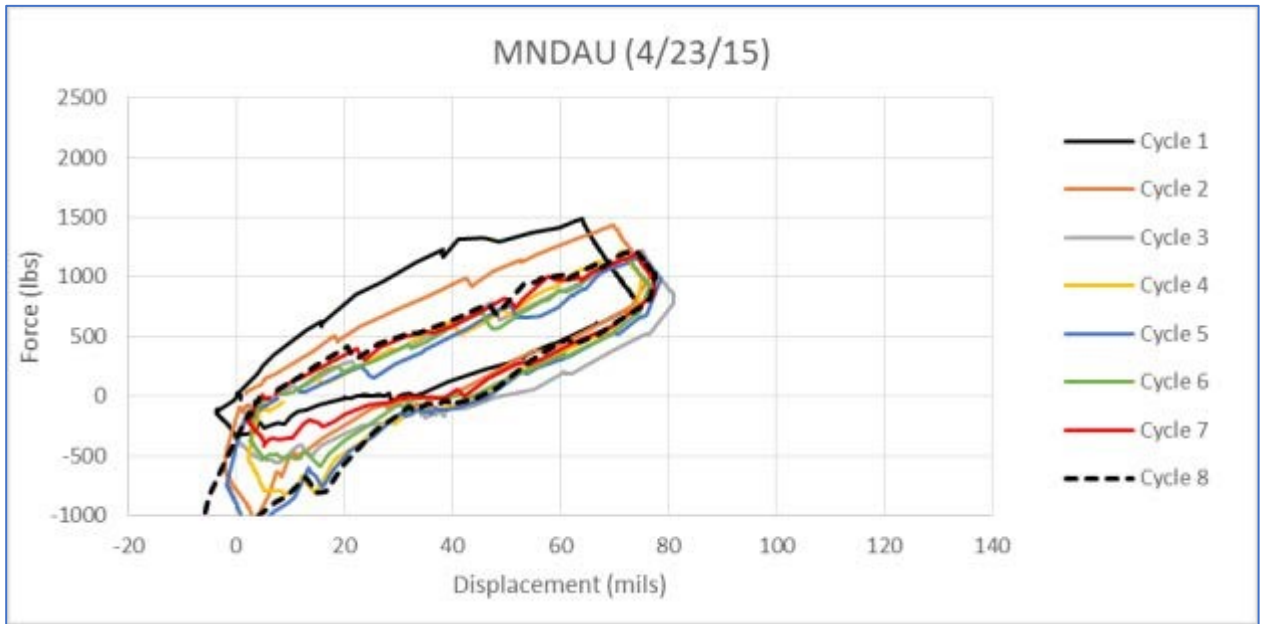
Figure A3.18. MNDAU Force vs. Displacement (Tested on 4/23/15)
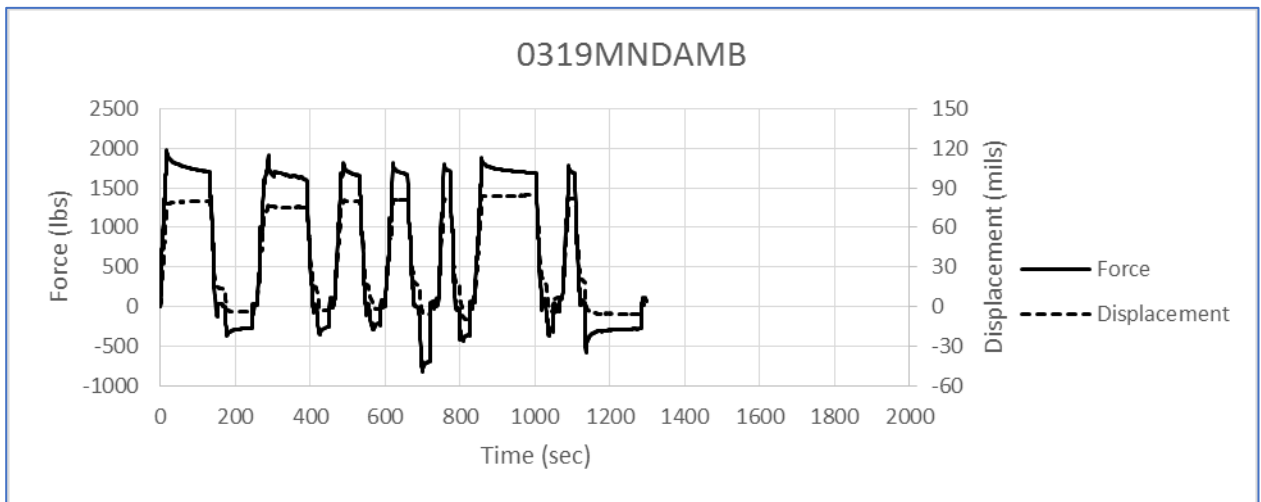
Figure A3.19. MNDAM Force and Displacement vs. Time (Tested on 4/3/15)
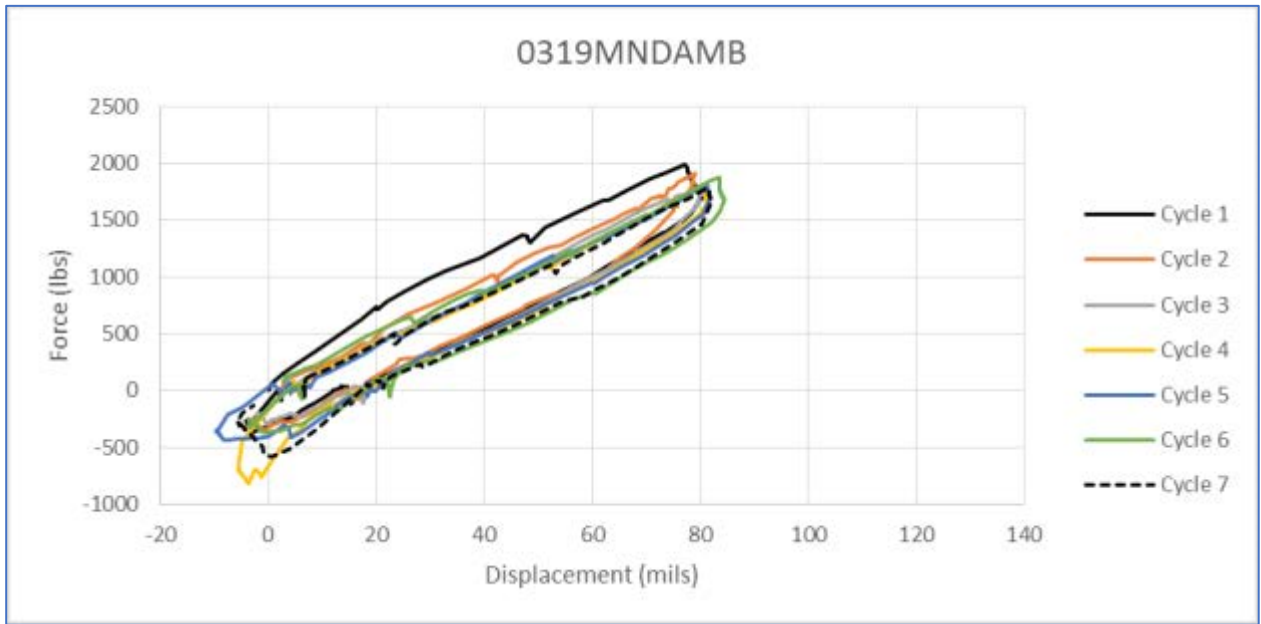
Figure A3.20. MNDAM Force vs. Displacement (Tested on 4/3/15)
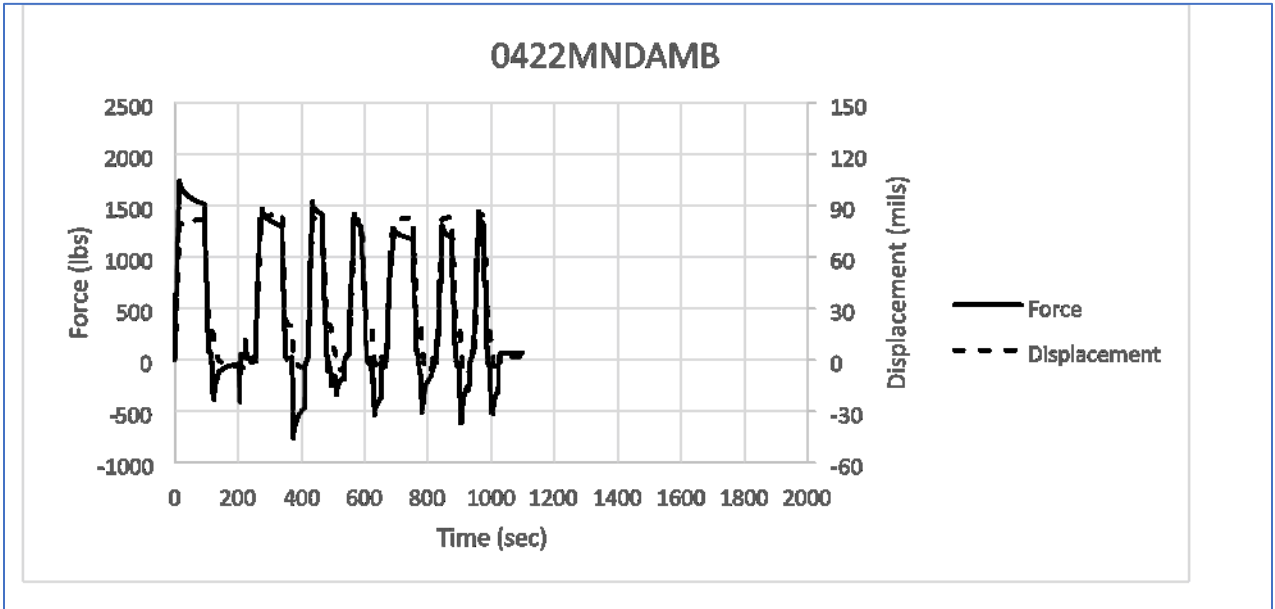
Figure A3.21. MNDAM Force and Displacement vs. Time (Tested on 4/27/15)
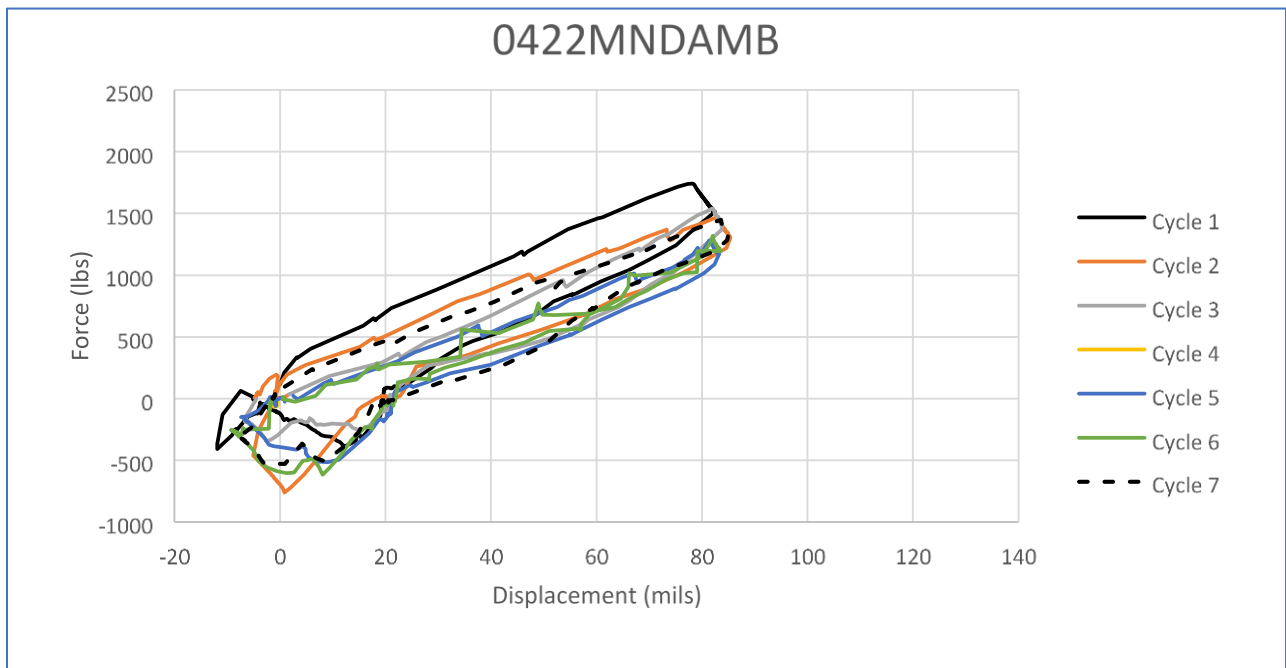
Figure A3.22. MNDAM Force vs. Displacement (Tested on 4/27/15)
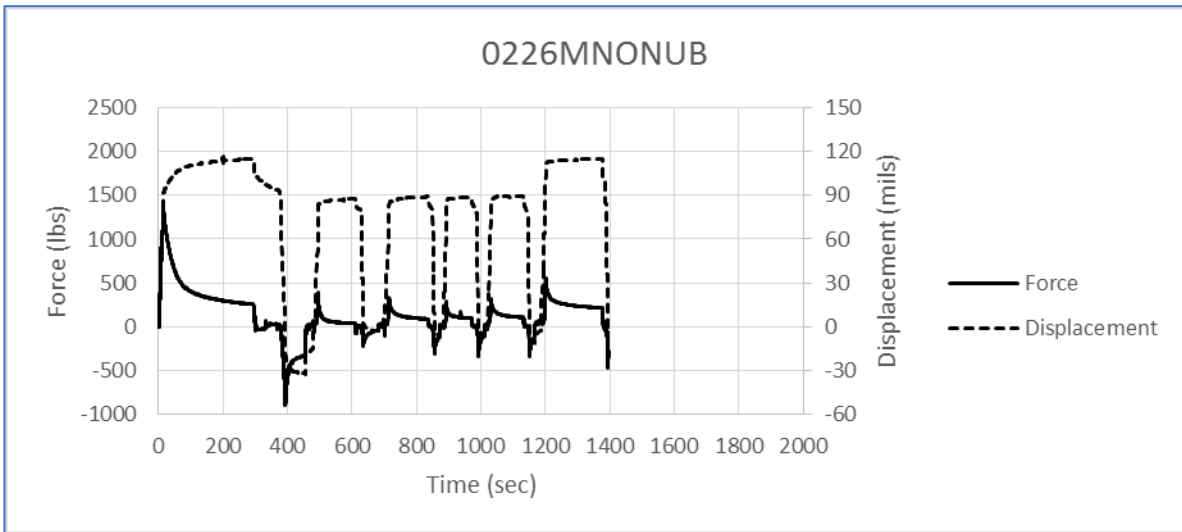
Figure A3.23. MNONU Force and Displacement vs. Time (Tested on 3/30/15)
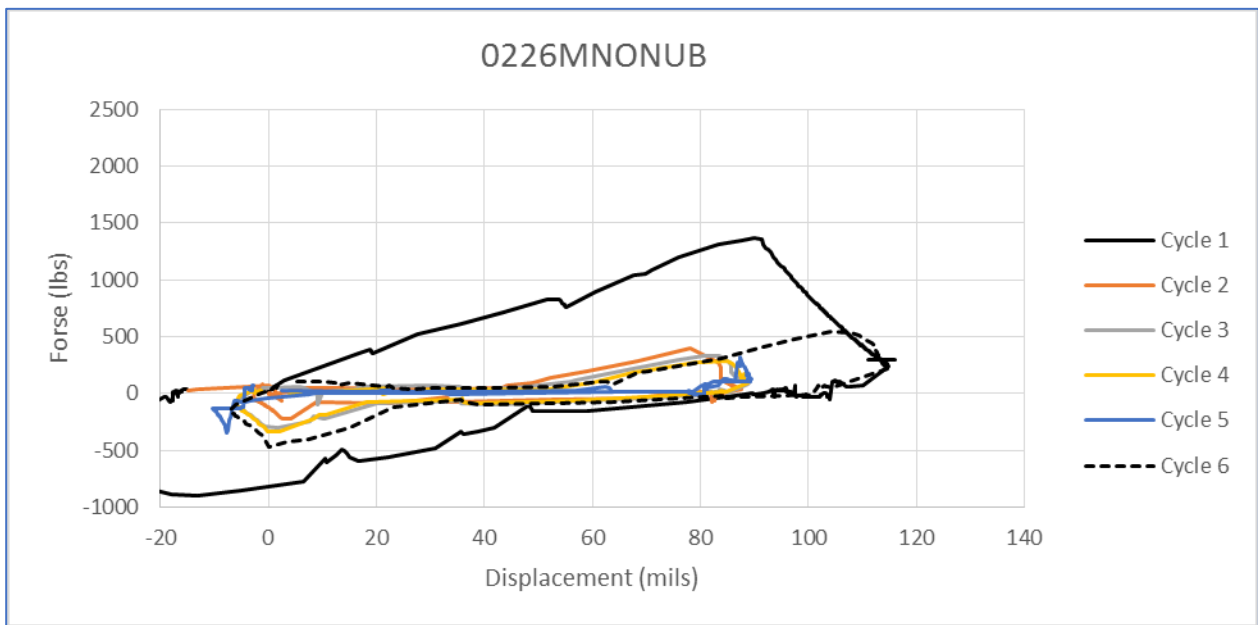
Figure A3.24. MNONU Force vs. Displacement (Tested on 3/30/15)
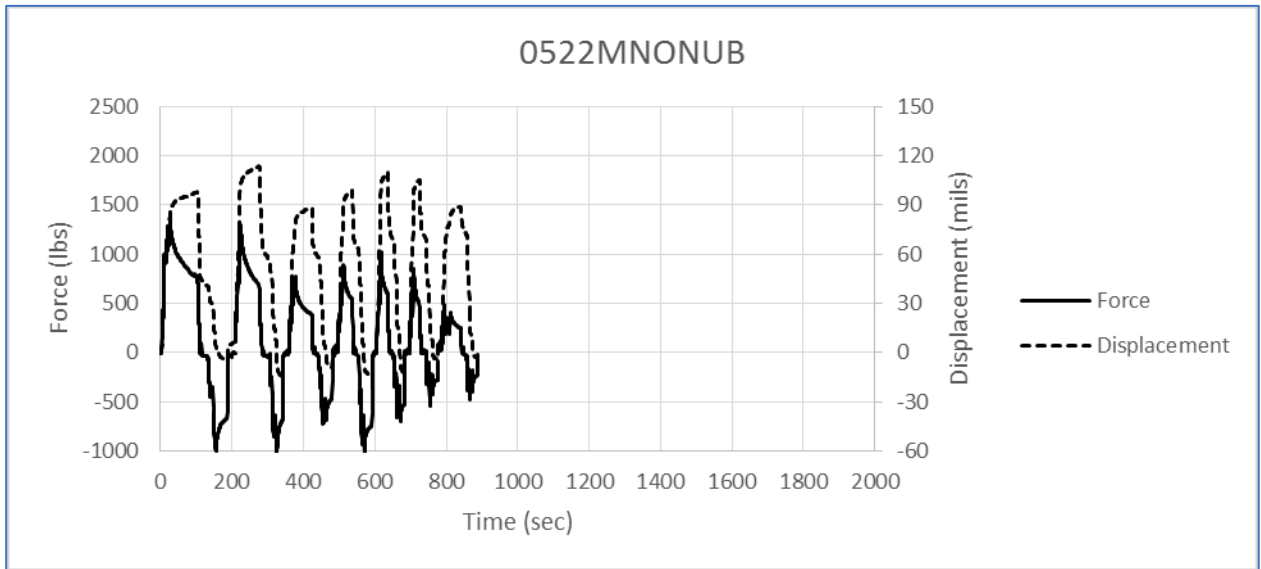
Figure A3.25. MNONU Force and Displacement vs. Time (Tested on 5/26/15)

Figure A3.26. MNONU Force vs. Displacement (Tested on 5/26/15)
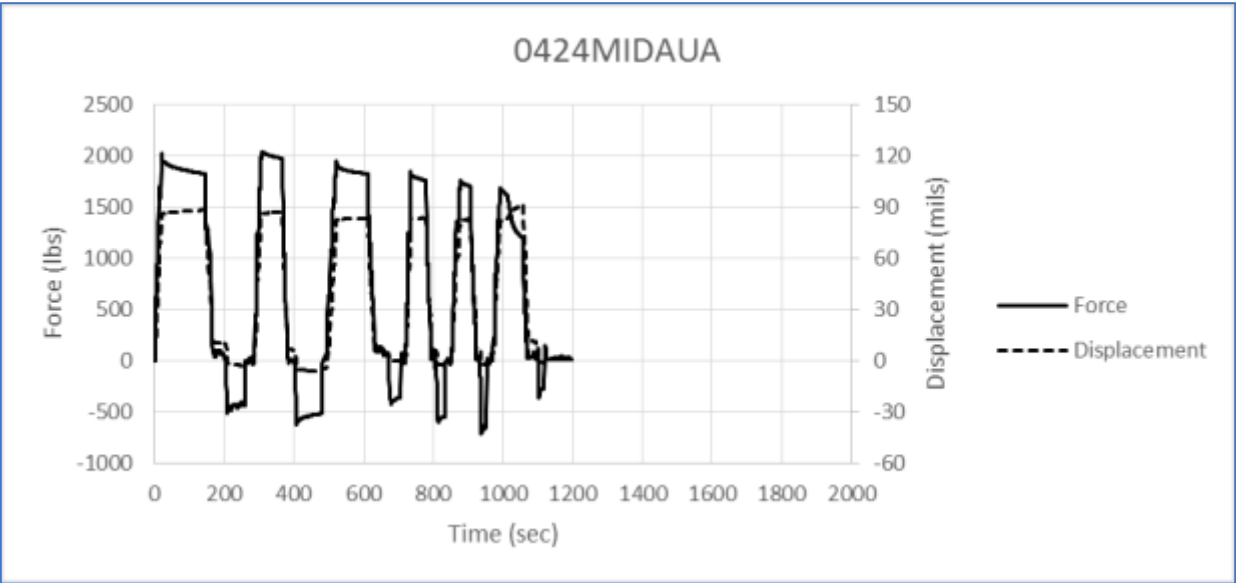
Figure A3.27. MIDAU Force and Displacement vs. Time (Tested on 4/29/15)
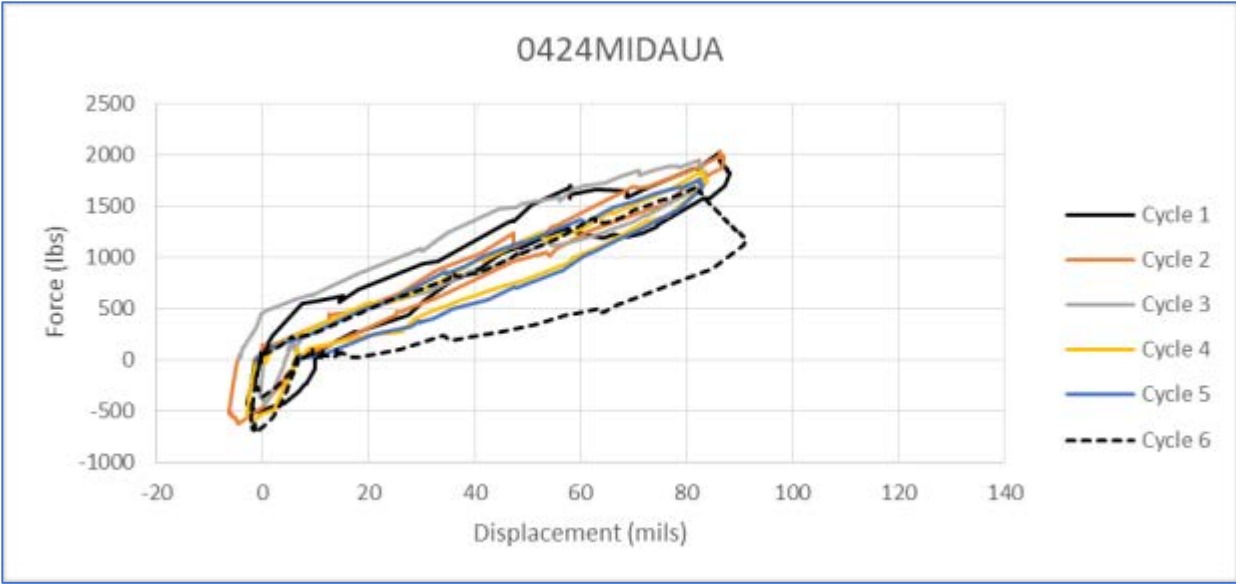
Figure A3.28. MIDAU Force vs. Displacement (Tested on 4/29/15)
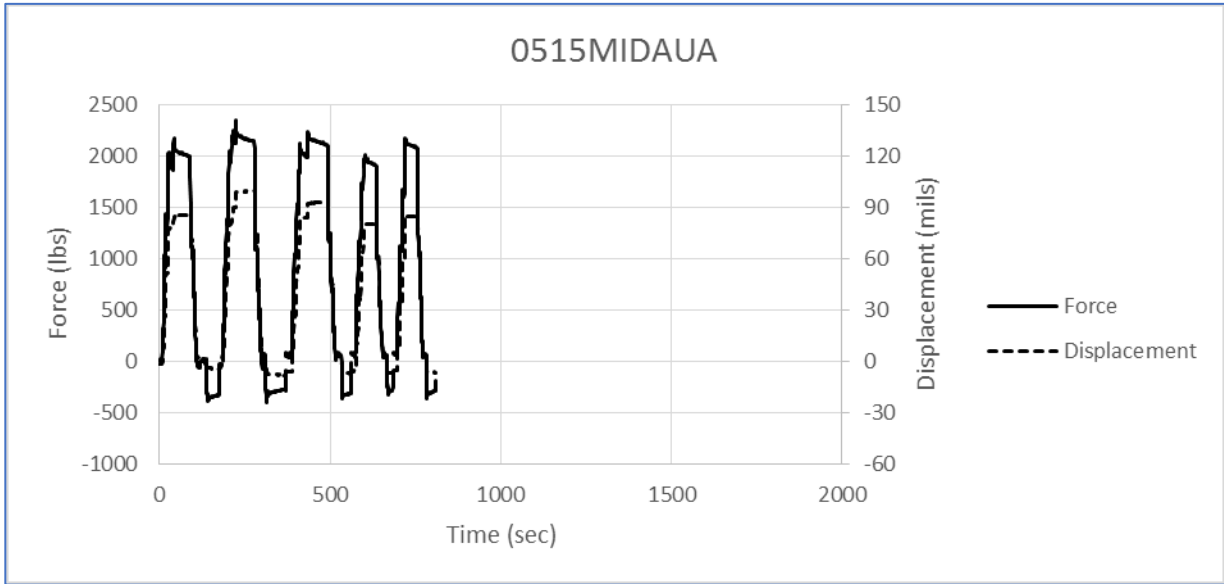
Figure A3.29. MIDAU Force and Displacement vs. Time (Tested on 5/20/15)
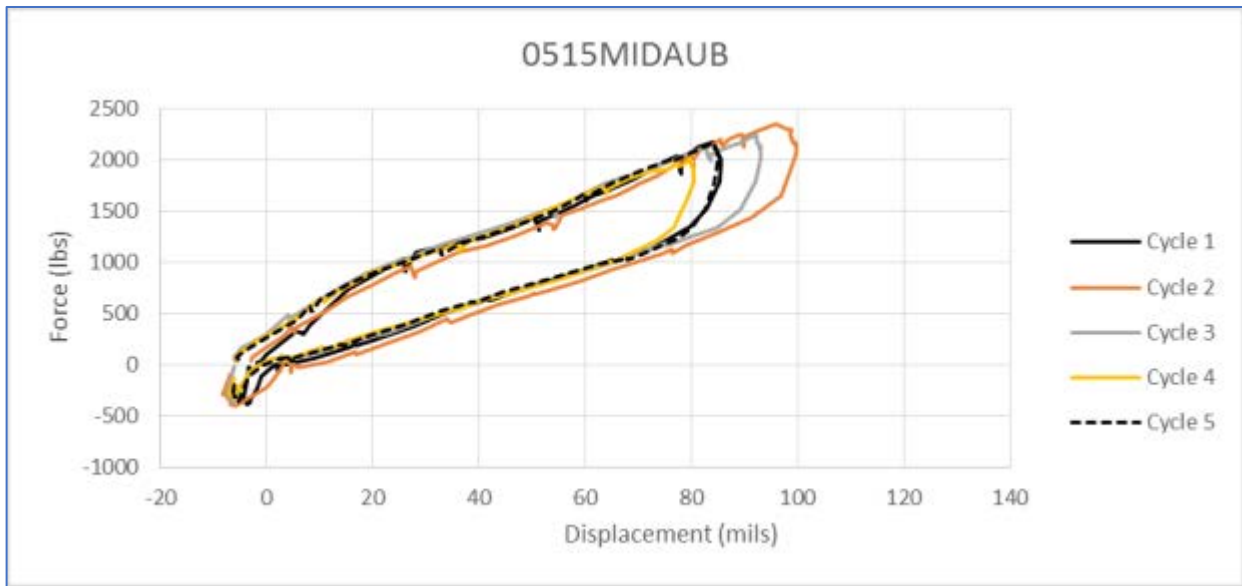
Figure A3.30. MIDAU Force vs. Displacement (Tested on 5/20/15)
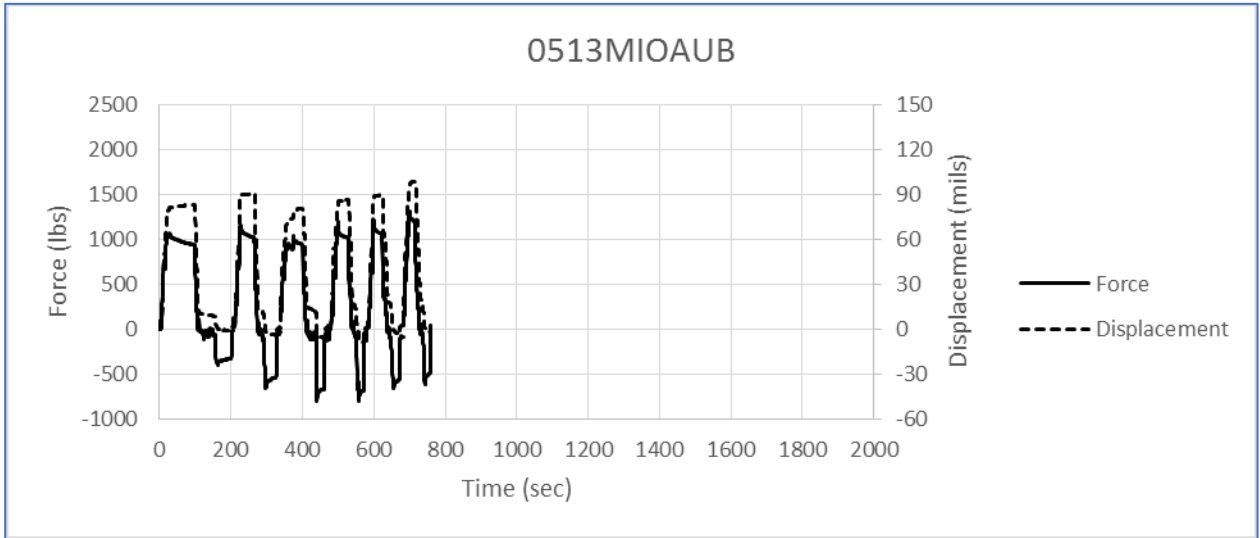
Figure A3.31. MIOAU Force and Displacement vs. Time (Tested on 5/18/15)
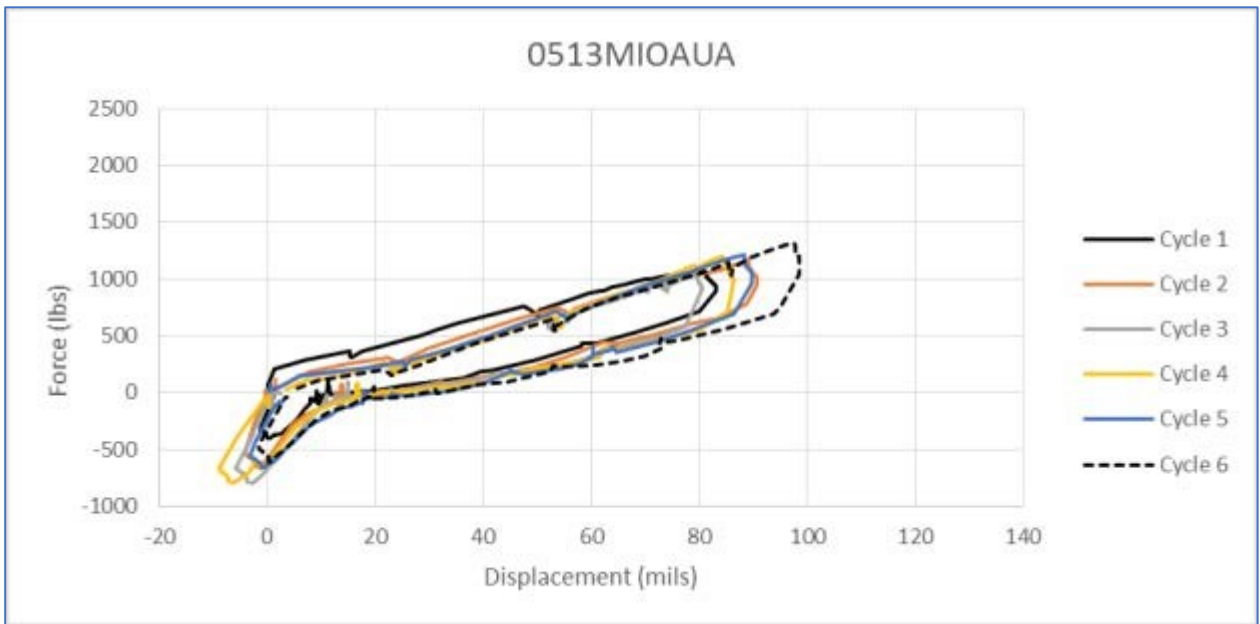
Figure A3.32. MIOAU Force vs. Displacement (Tested on 5/18/15)
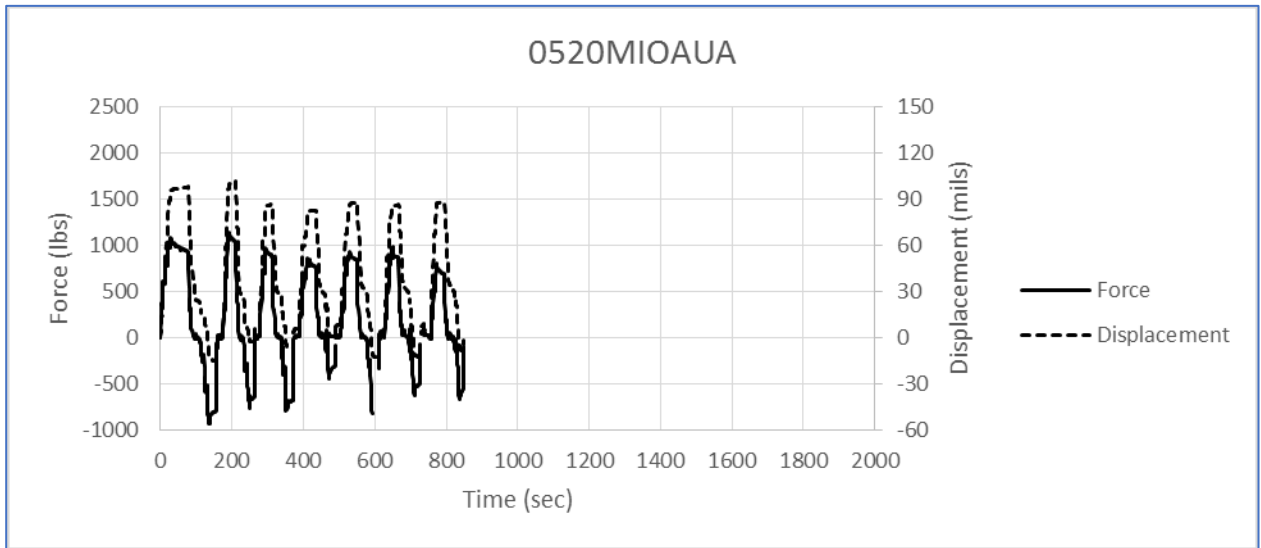
Figure A3.33. MIOAU Force and Displacement vs. Time (Tested on 5/26/15)
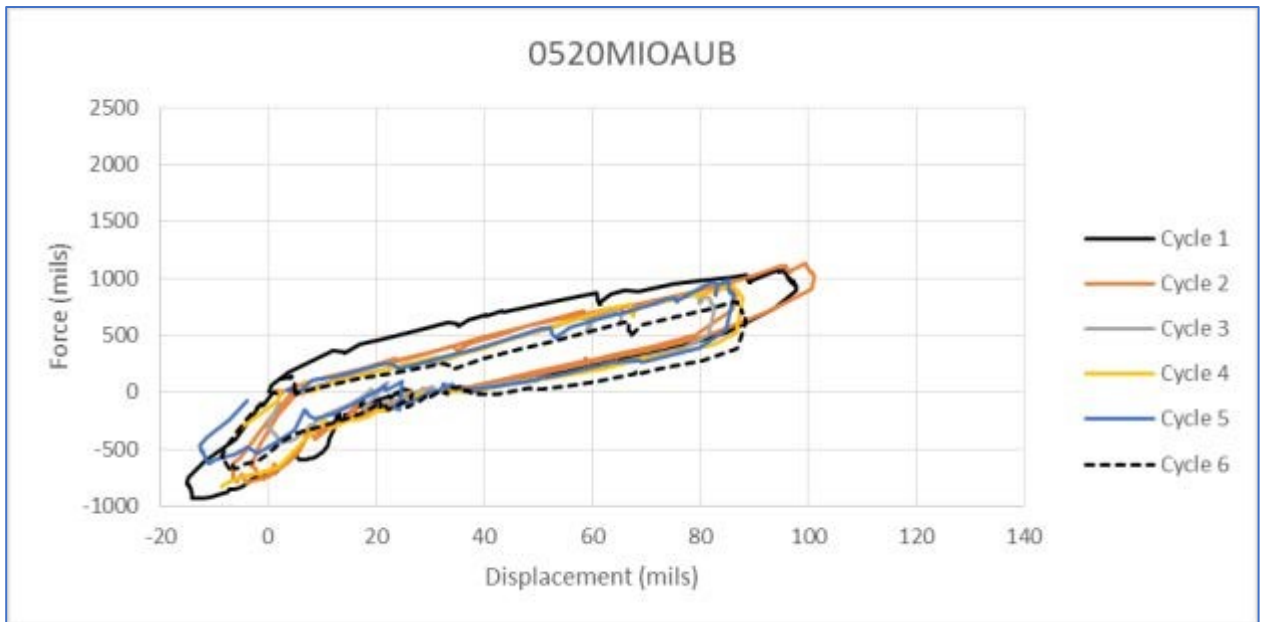
Figure A3.34. MIOAU Force vs. Displacement (Tested on 5/26/15)

The following plots, one for each specimen, show measured displacement of the overlay (TOP(OL)) and the existing (BOT(EXIST)) beam versus the force applied to the beam tested for reflective cracking as discussed in Section 4.4. .
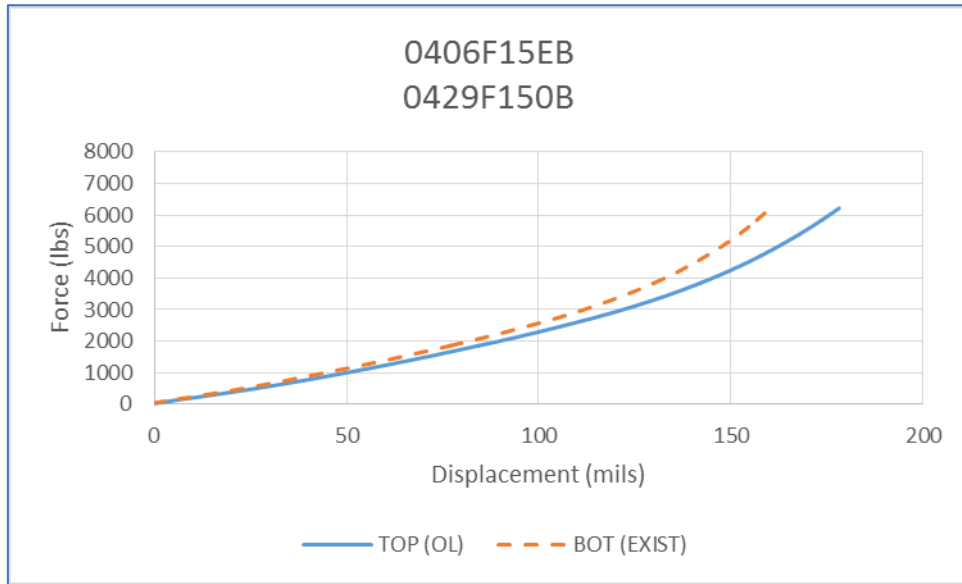
Figure A4.1. F15 Force vs. Displacement (Tested on 5/4/15)
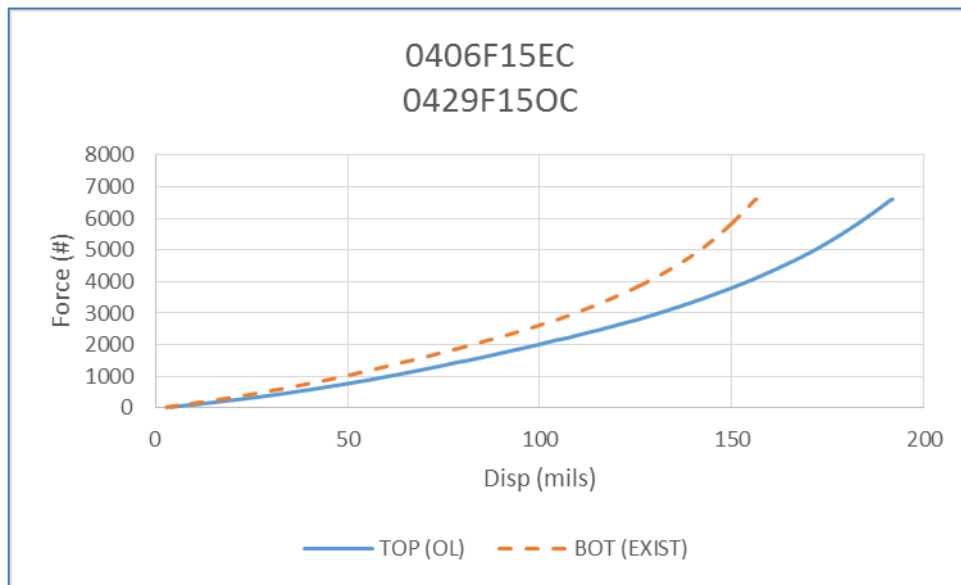
Figure A4.2. F15 Force vs. Displacement (Tested on 5/4/15)
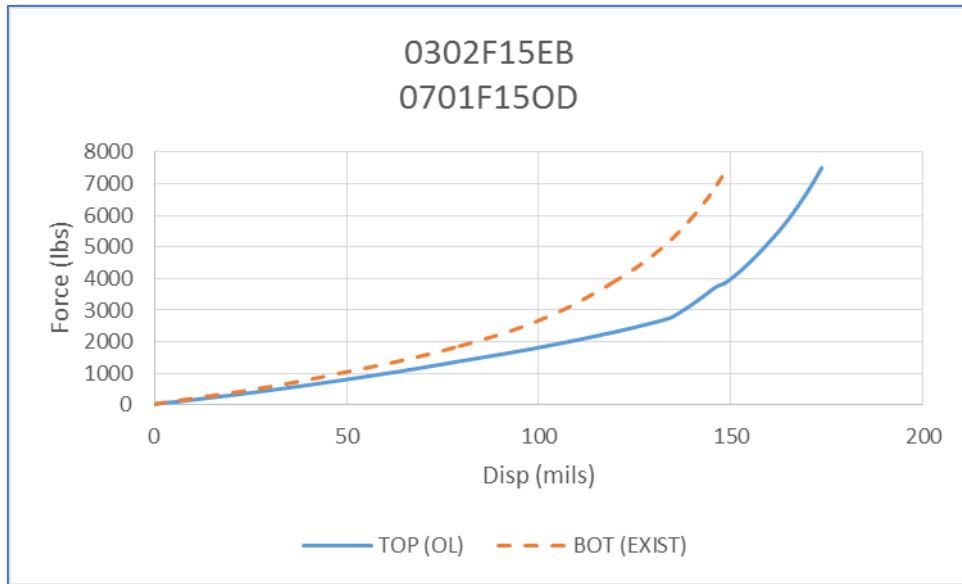
Figure A4.3. F15 Force vs. Displacement (Tested on 7/6/15)
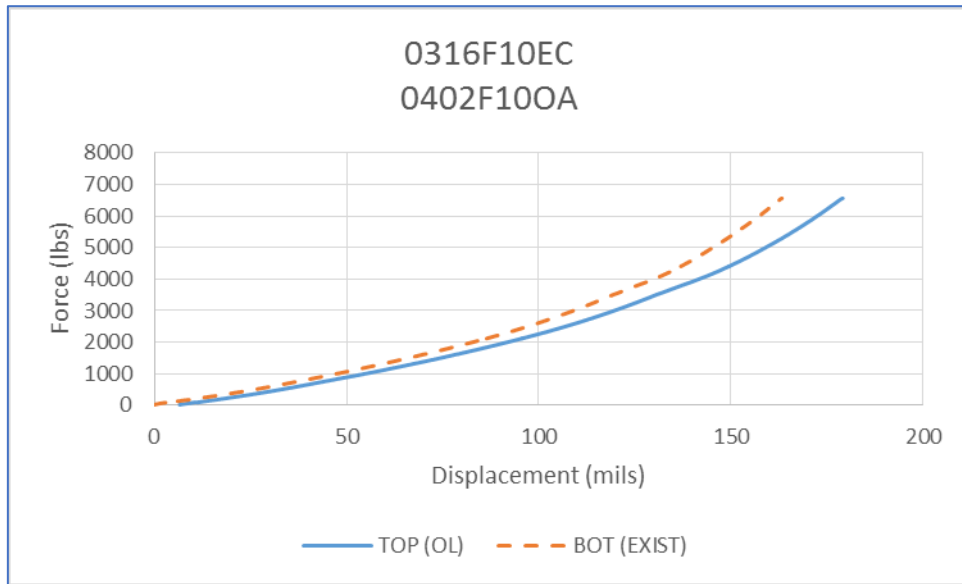
Figure A4.4. F10 Force vs. Displacement (Tested on 4/7/15)
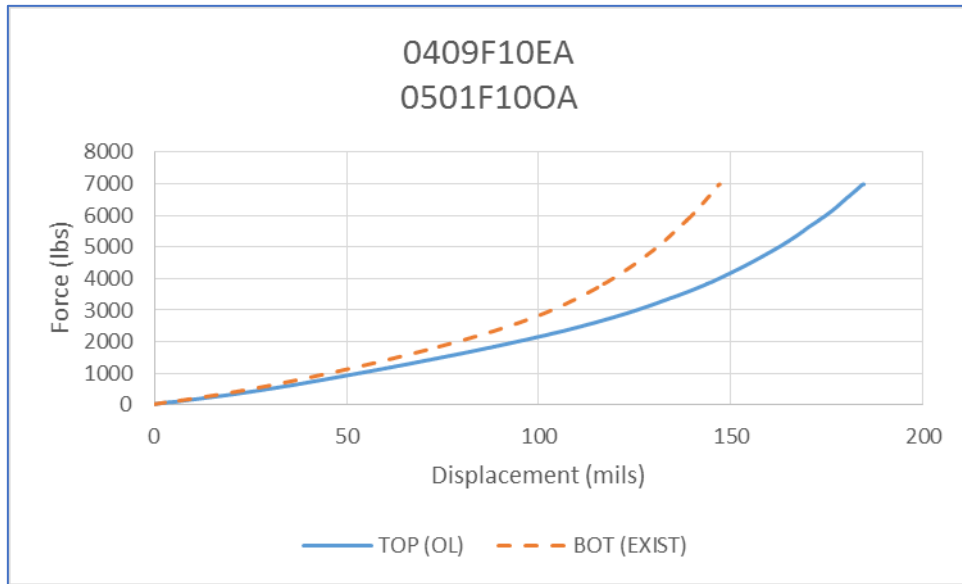
Figure A4.5. F10 Force vs. Displacement (Tested on 5/6/15)
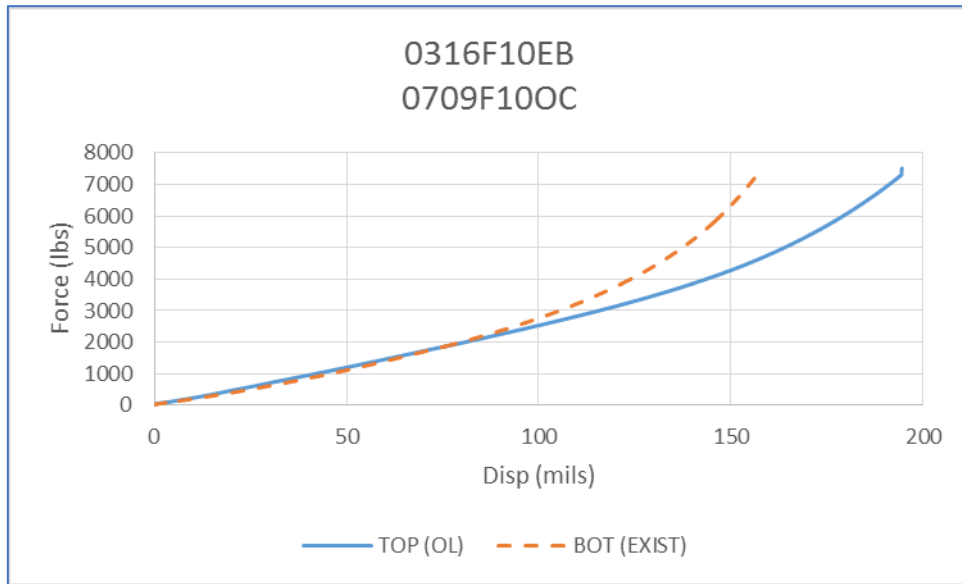
Figure A4.6. F10 Force vs. Displacement (Tested on 7/14/15)
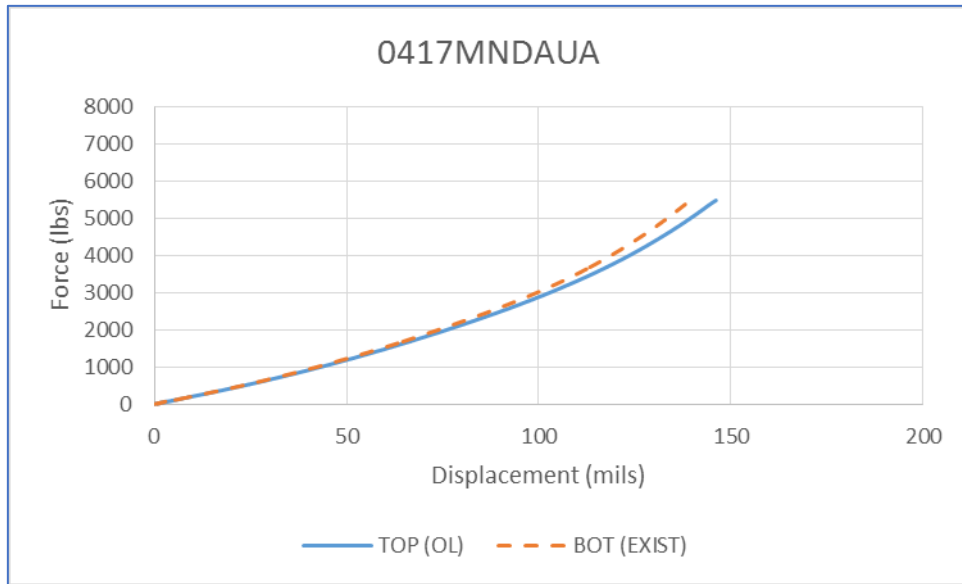
Figure A4.7. MNDAU Force vs. Displacement (Tested on 4/22/15)
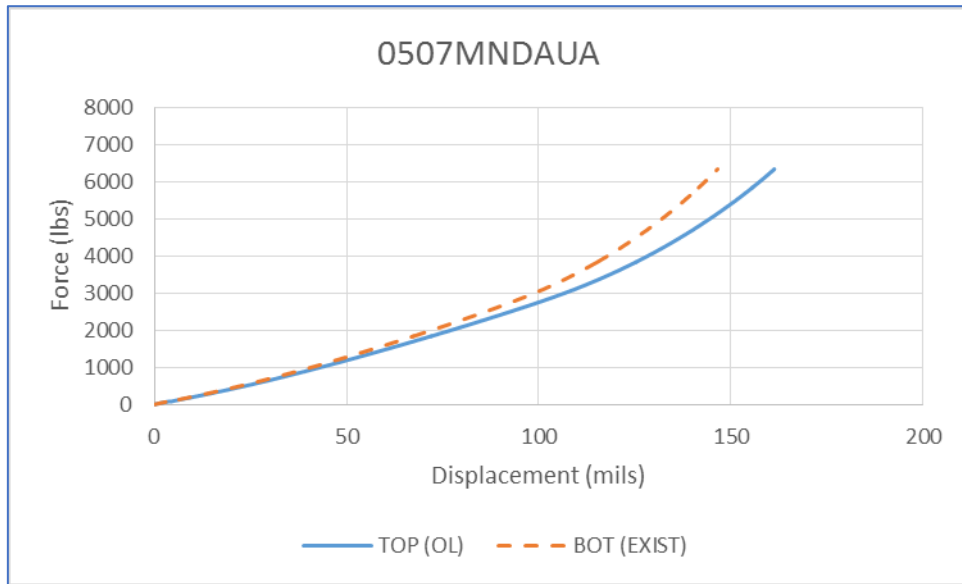
Figure A4.8. MNDAU Force vs. Displacement (Tested on 5/12/15)
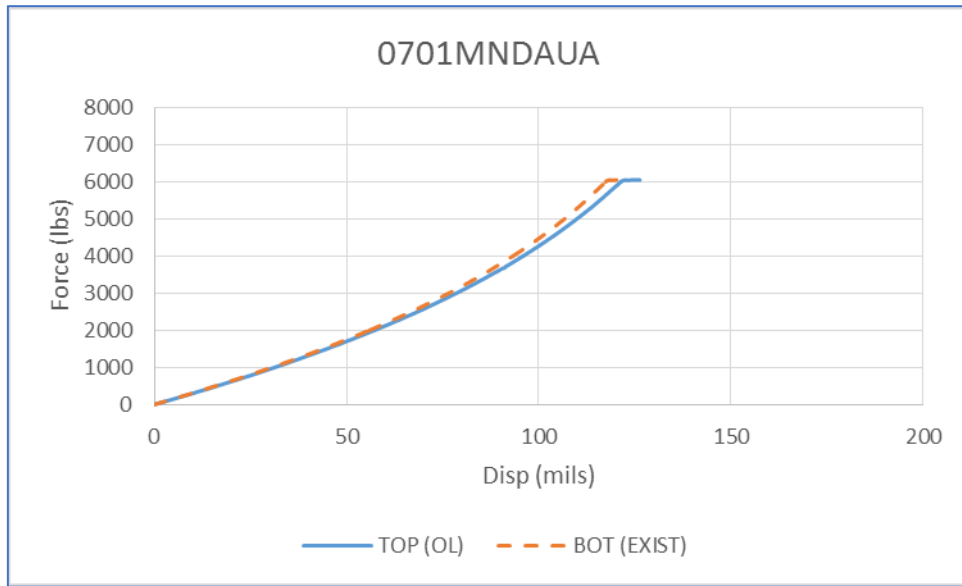
Figure A4.9. MNDAU Force vs. Displacement (Tested on 7/6/15)
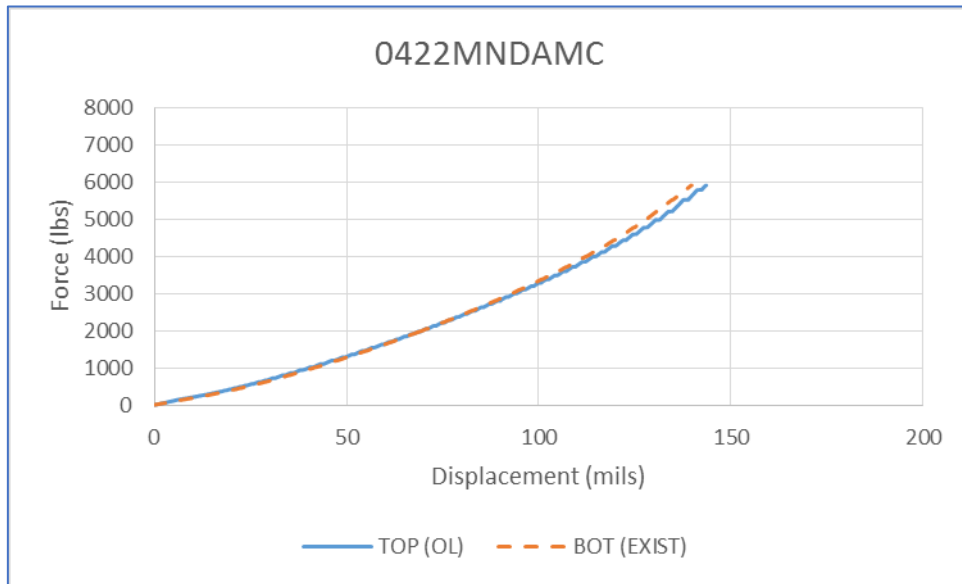
Figure A4.10. MNDAM Force vs. Displacement (Tested on 4/27/15)
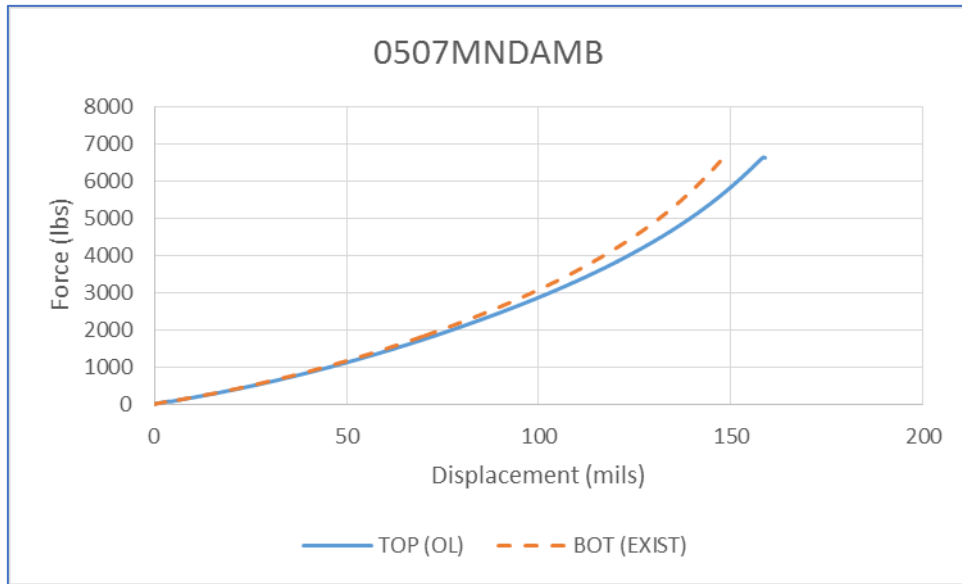
Figure A4.11. MNDAM Force vs. Displacement (Tested on 5/12/15)
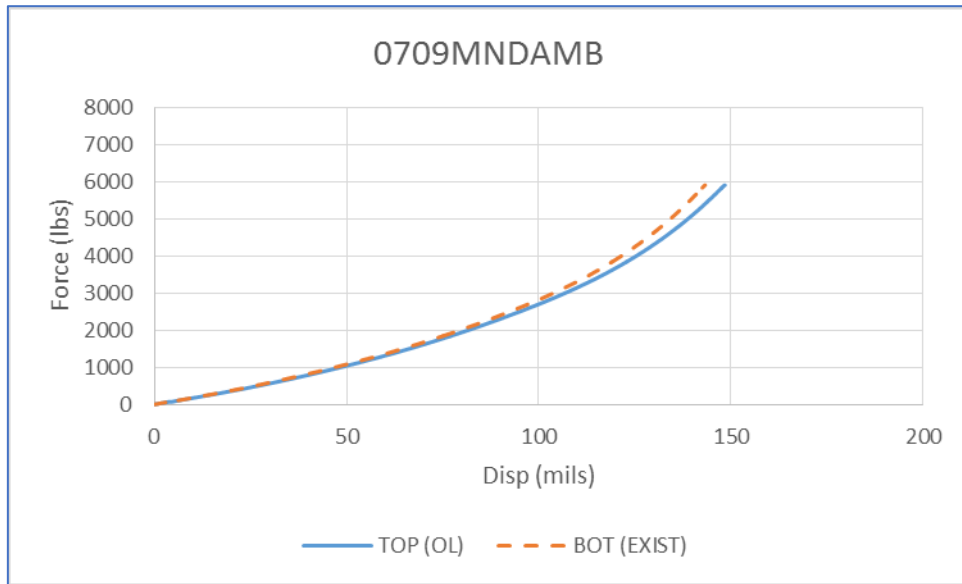
Figure A4.12. MNDAM Force vs. Displacement (Tested on 7/14/15)
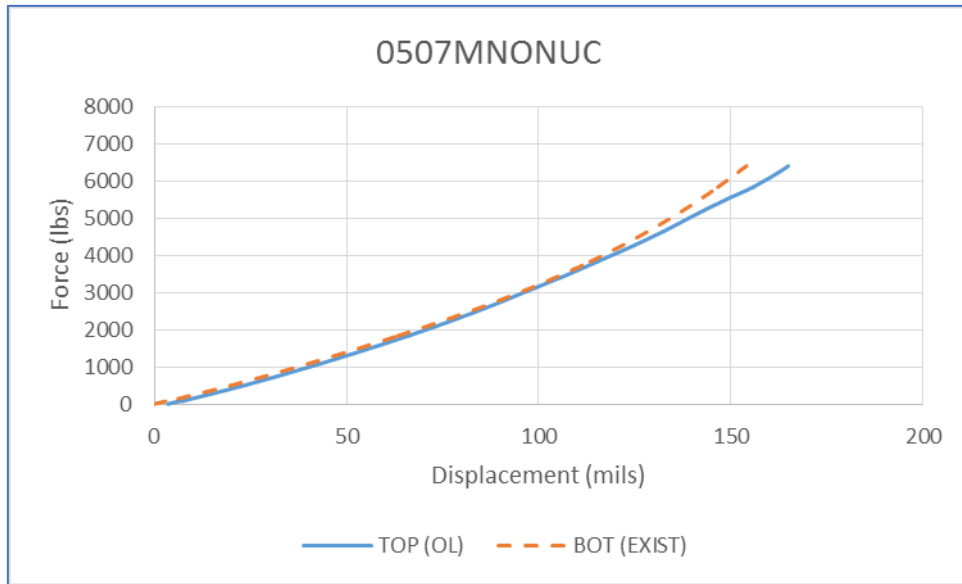
Figure A4.13. MNONU Force vs. Displacement (Tested on 5/12/15)
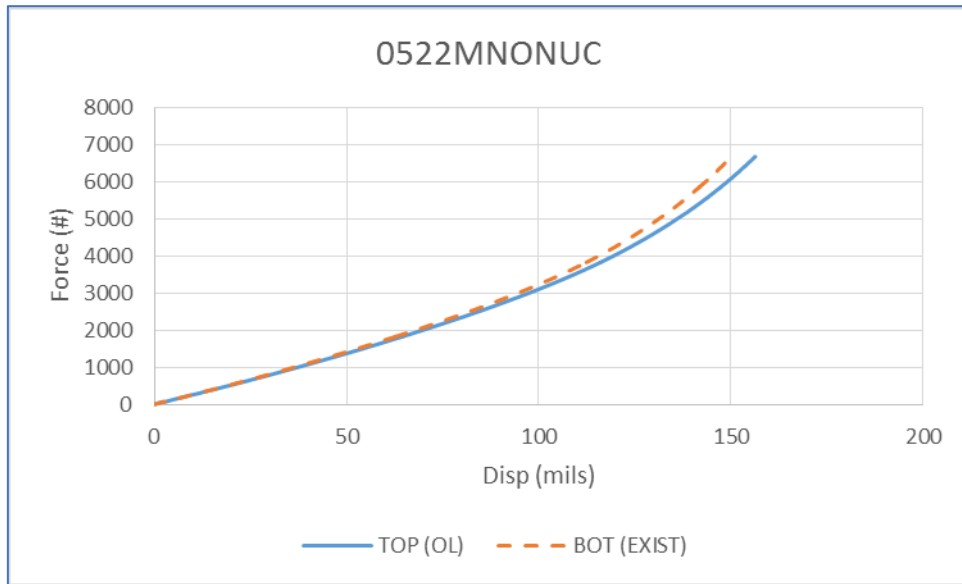
Figure A4.14. MNONU Force vs. Displacement (Tested on 5/27/15)
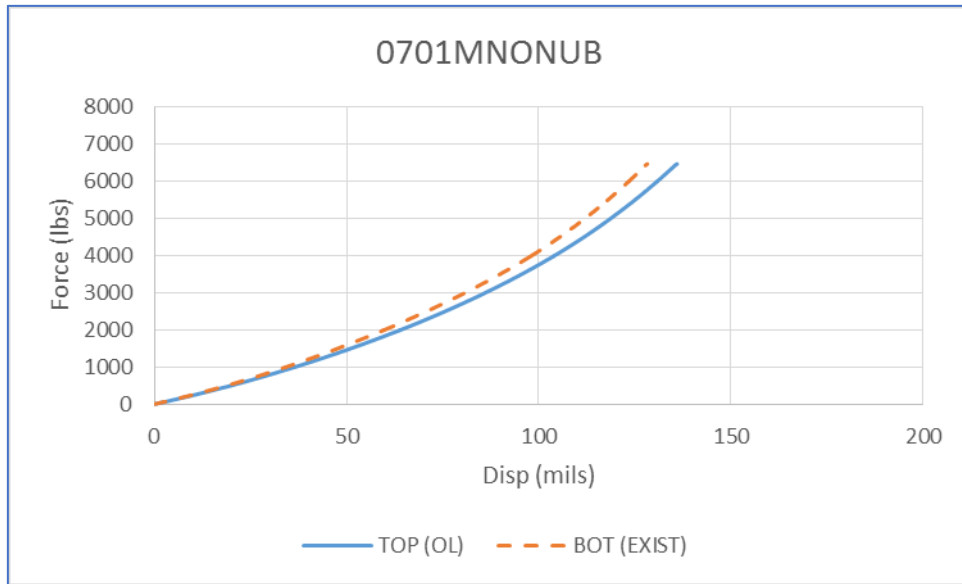
Figure A4.15. MNONU Force vs. Displacement (Tested on 7/6/15)
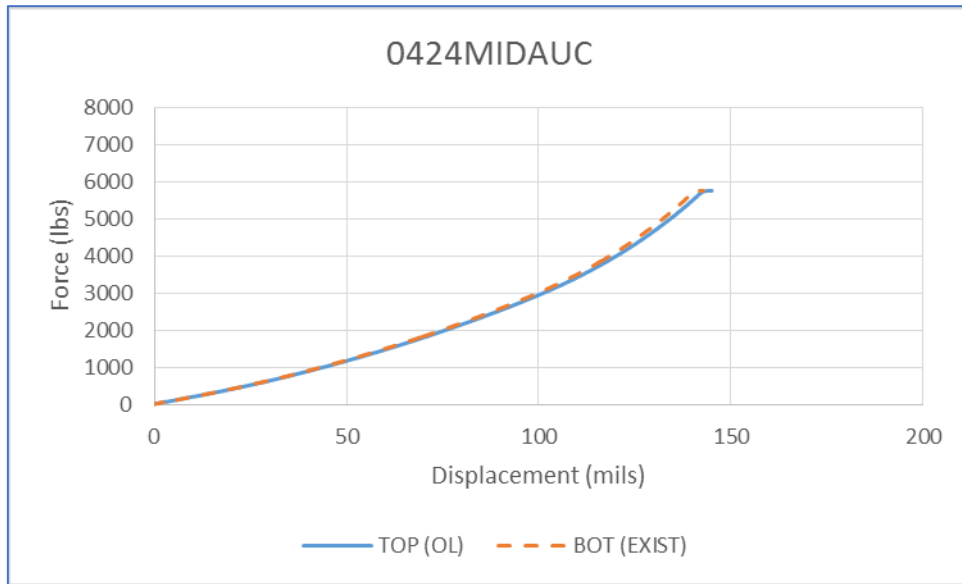
Figure A4.16. MIDAU Force vs. Displacement (Tested on 4/29/15)
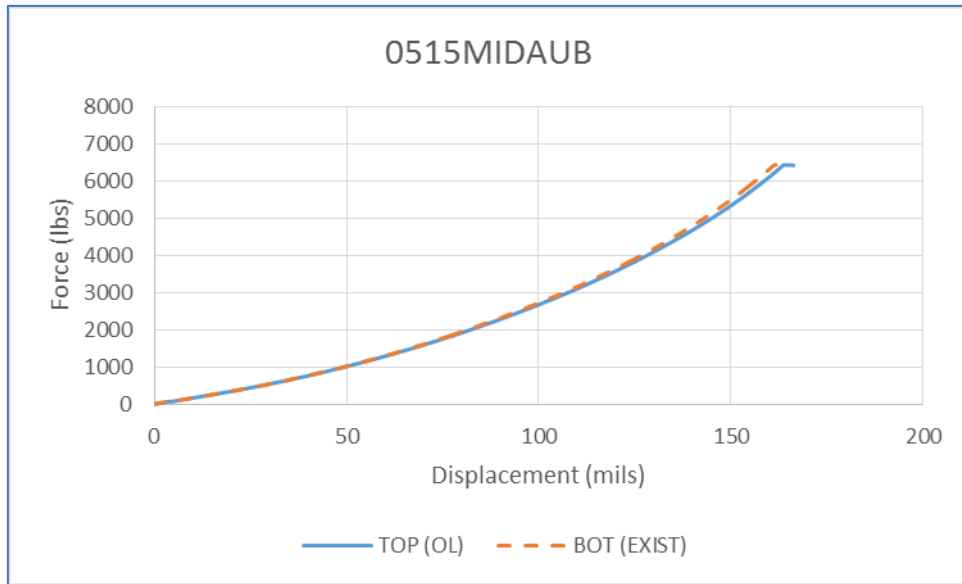
Figure A4.17. MIDAU Force vs. Displacement (Tested on 5/20/15)
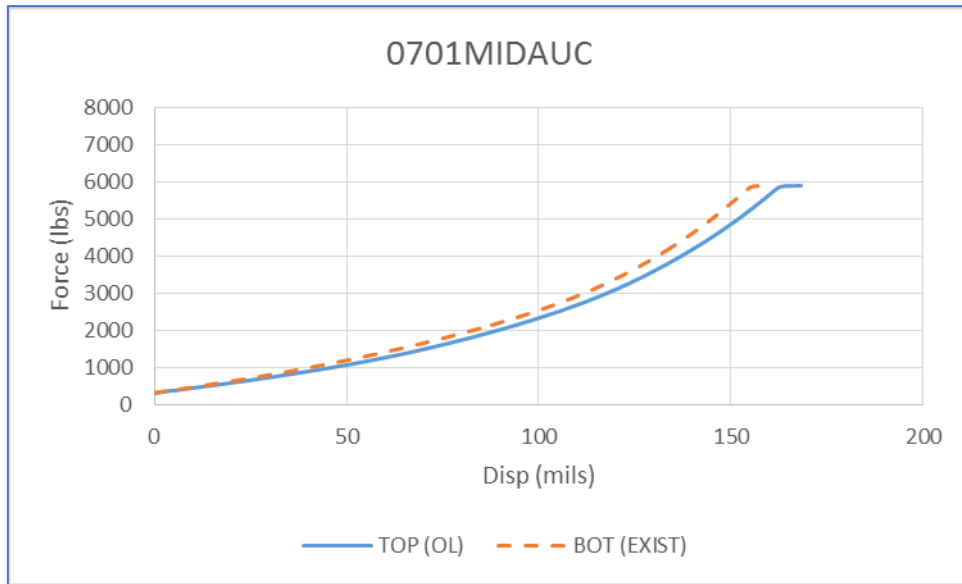
Figure A4.18. MIDAU Force vs. Displacement (Tested on 7/6/15)
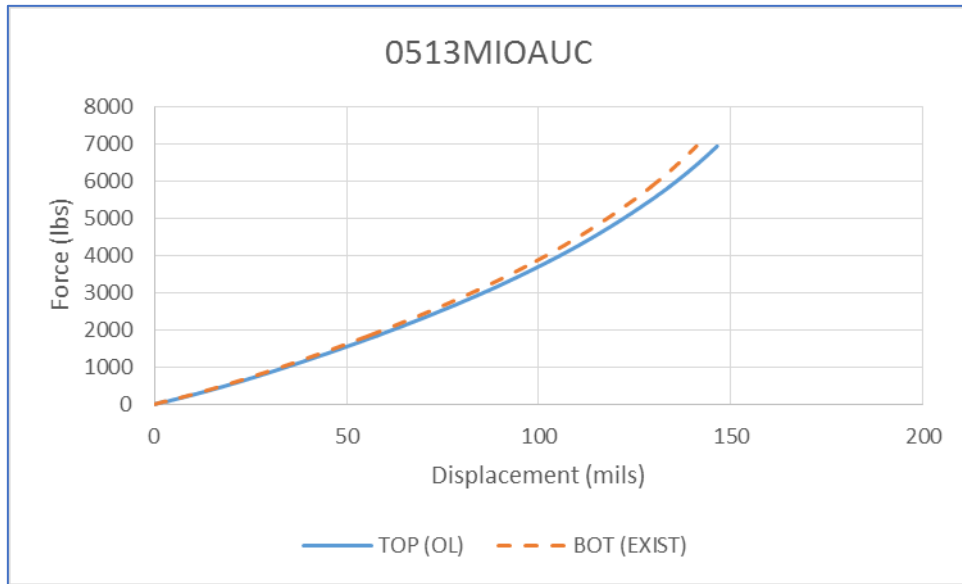
Figure A4.19. MIOAU Force vs. Displacement (Tested on 5/18/15)
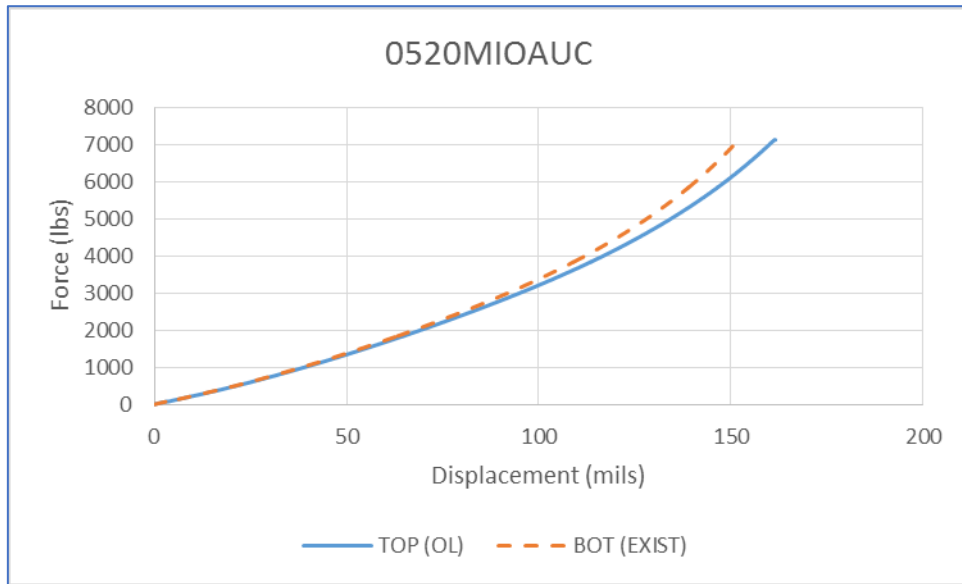
Figure A4.20. MIOAU Force vs. Displacement (Tested on 5/25/15)
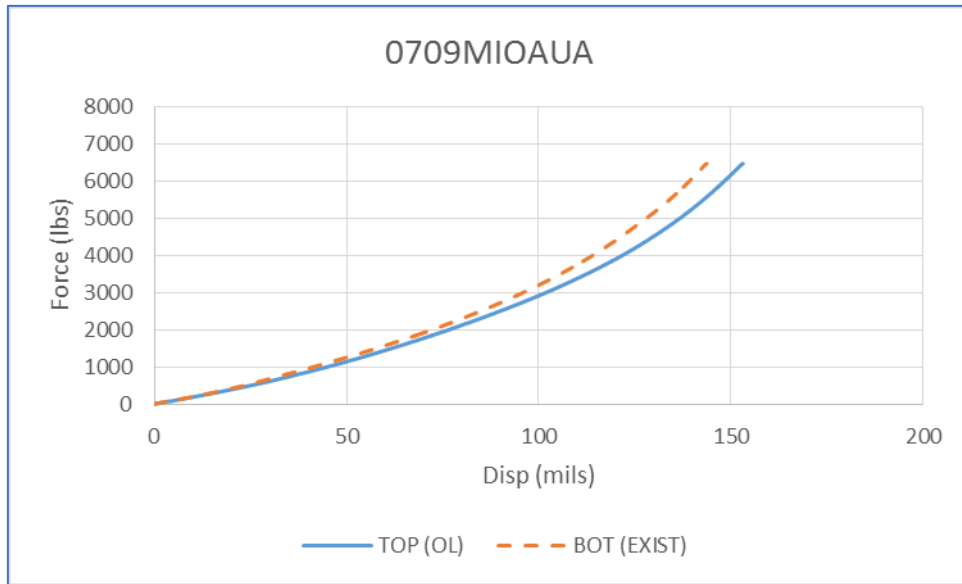
Figure A4.21. MIOAU Force vs. Displacement (Tested on 7/14/15)

The following plots, one for each specimen, show force versus displacement for the displacement controlled direct tension test discussed in Section 4.5.
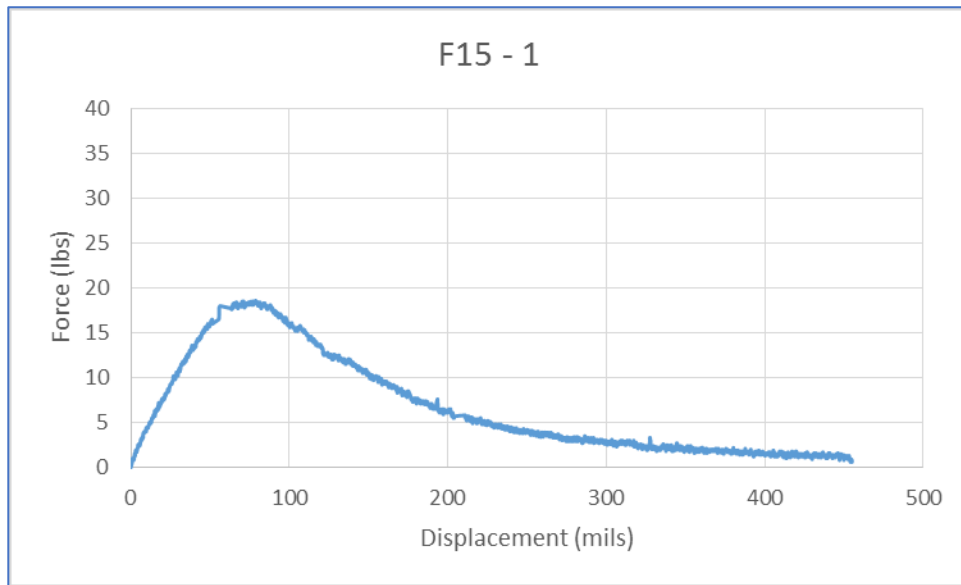
Figure A5.1 F15 Specimen 1 Force vs. Displacement (Tested on 5/18/15)
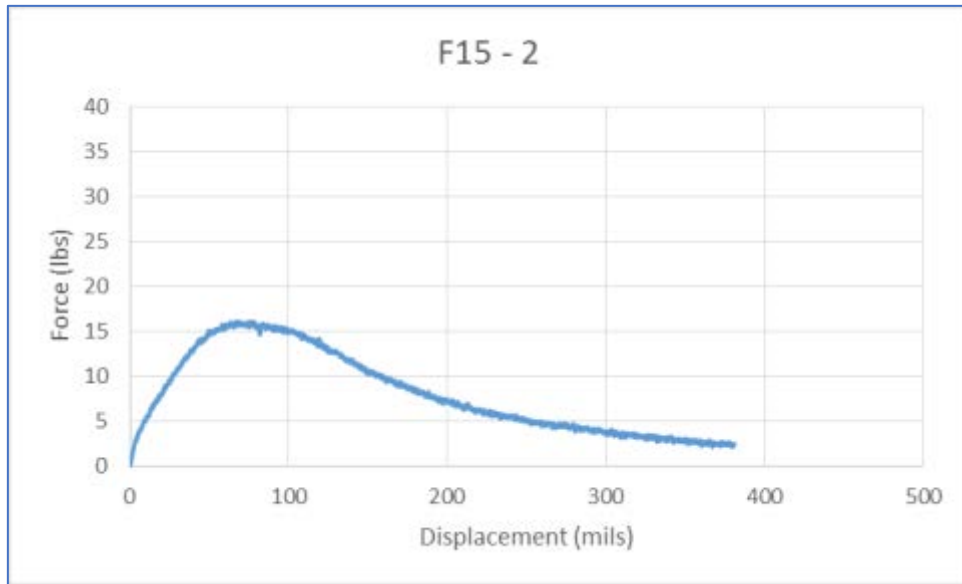
Figure A5.2 F15 Specimen 2 Force vs. Displacement (Tested on 5/18/15)
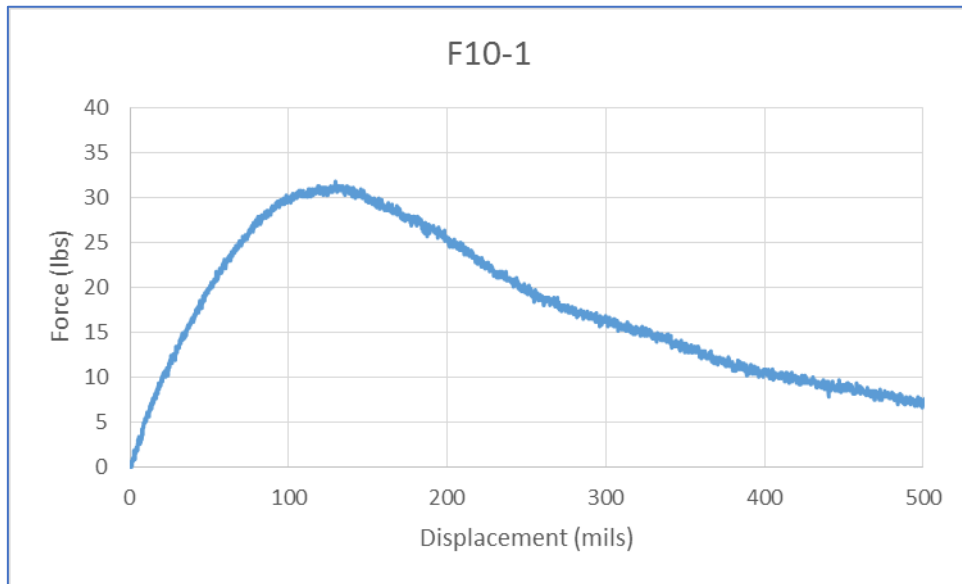
Figure A5.3 F10 Specimen 1 Force vs. Displacement (Tested on 5/18/15)
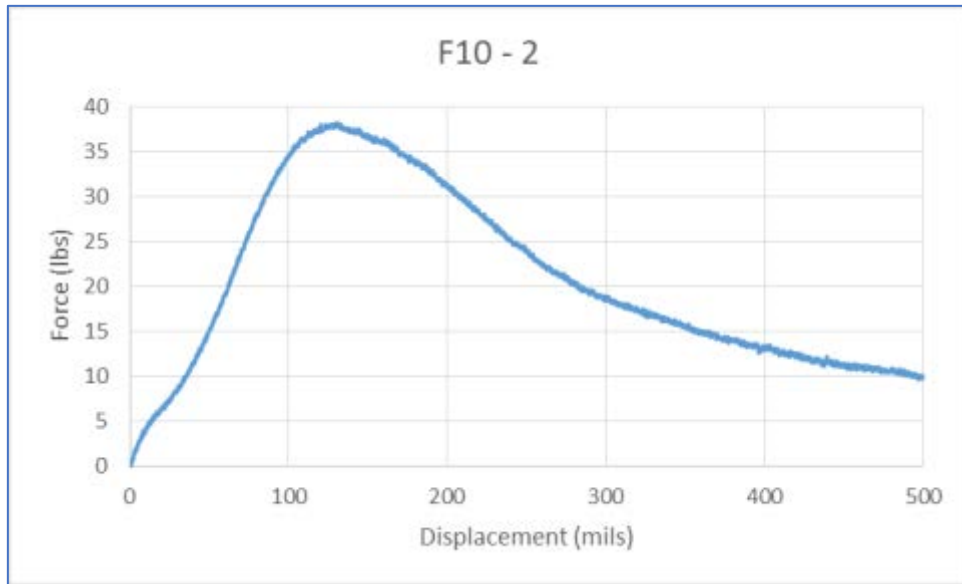
Figure A5.4 F10 Specimen 2 Force vs. Displacement (Tested on 5/18/15)
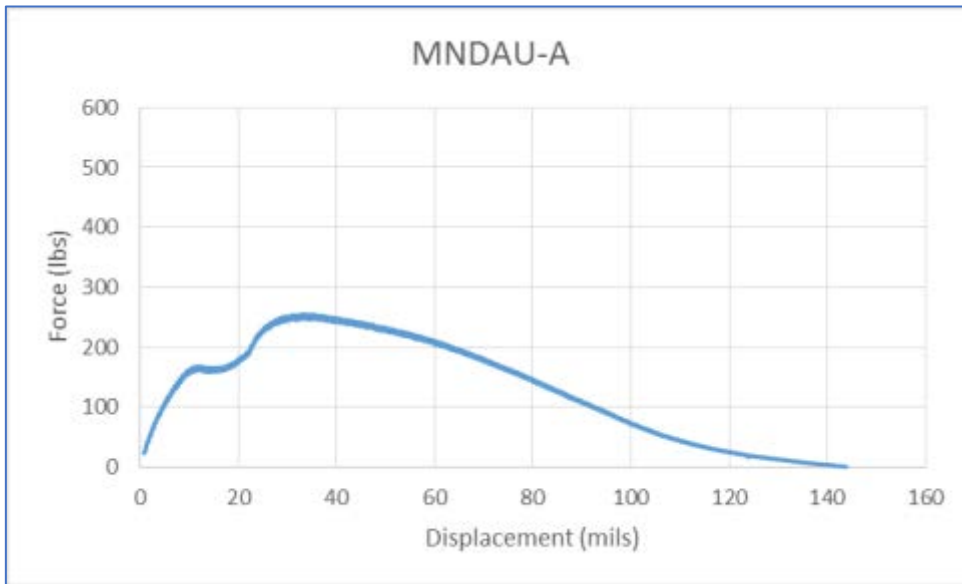
Figure A5.5 MNDAU Specimen A Force vs. Displacement (Tested on 6/17/15)
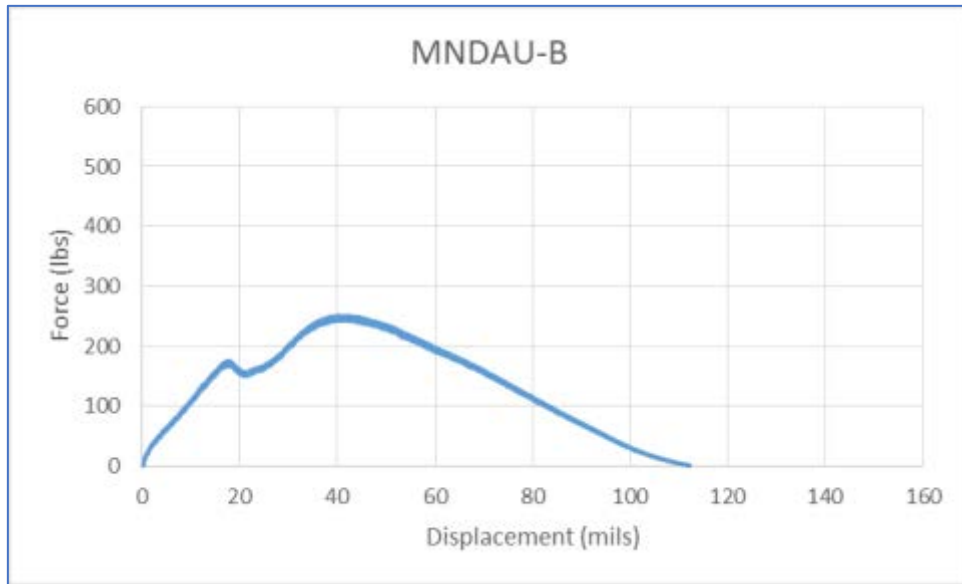
Figure A5.6 MNDAU Specimen B Force vs. Displacement (Tested on 6/17/15)

Figure A5.7 MNDAM Specimen A Force vs. Displacement (Tested on 6/8/15)
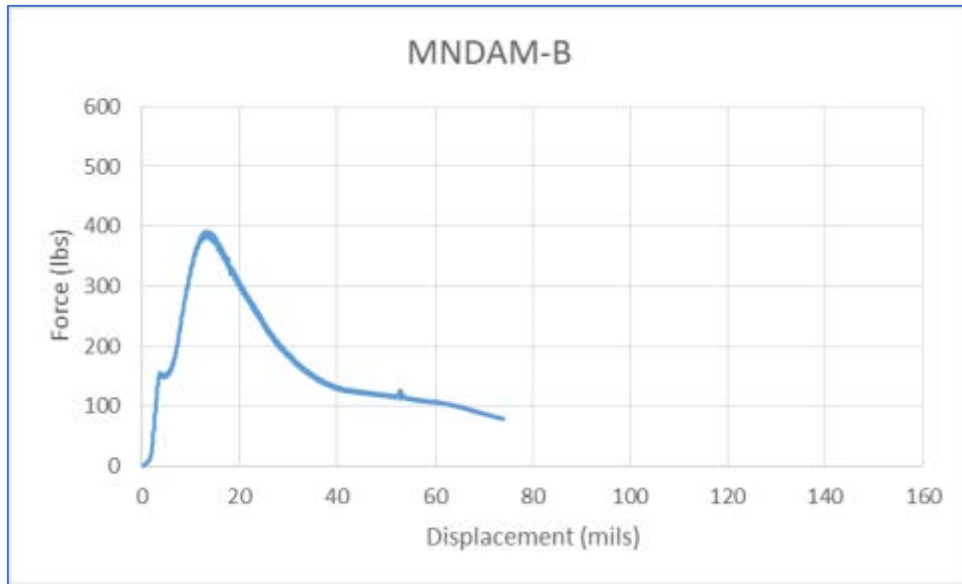
Figure A5.8 MNDAM Specimen A Force vs. Displacement (Tested on 6/17/15)
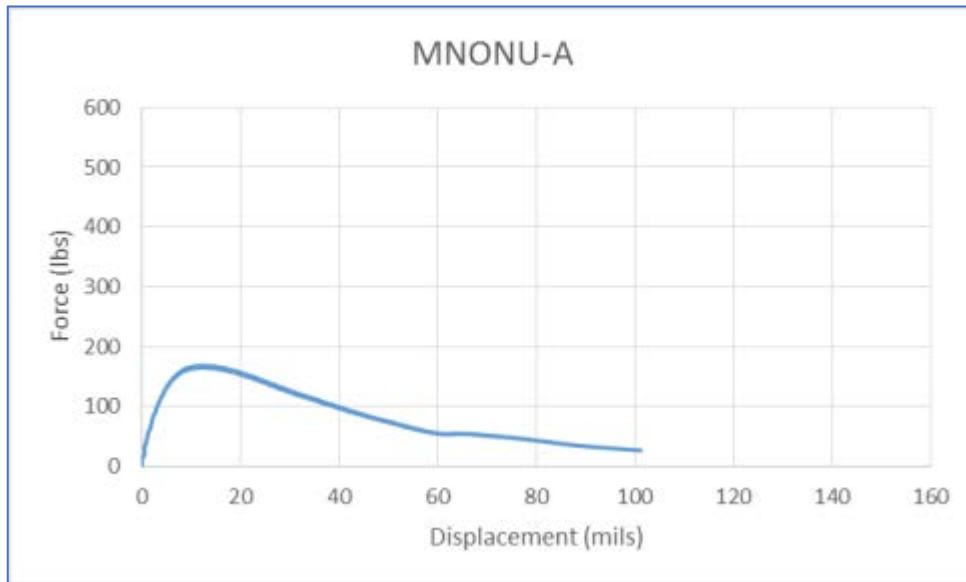
Figure A5.9 MNONU Specimen A Force vs. Displacement (Tested on 6/5/15)
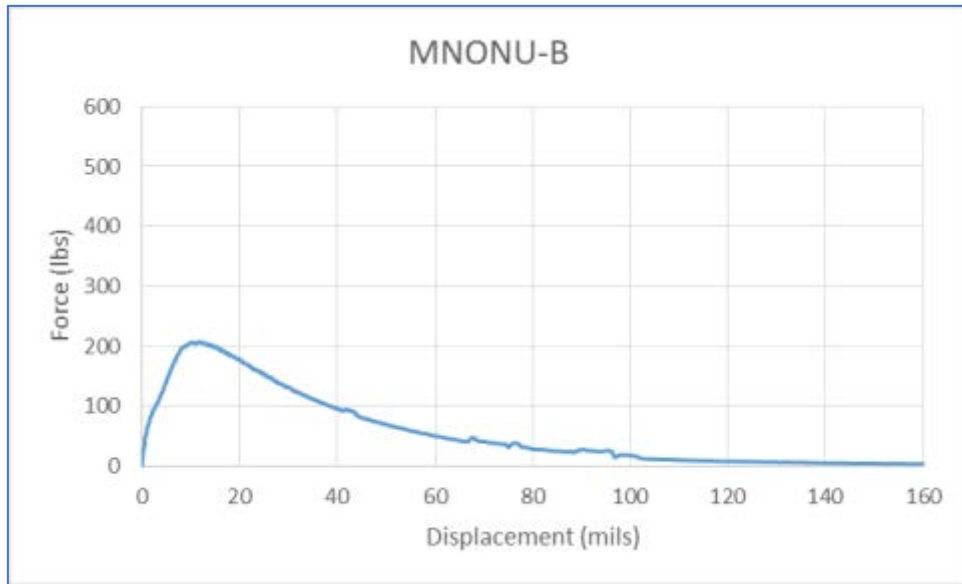
Figure A5.10 MNONU Specimen B Force vs. Displacement (Tested on 6/17/15)
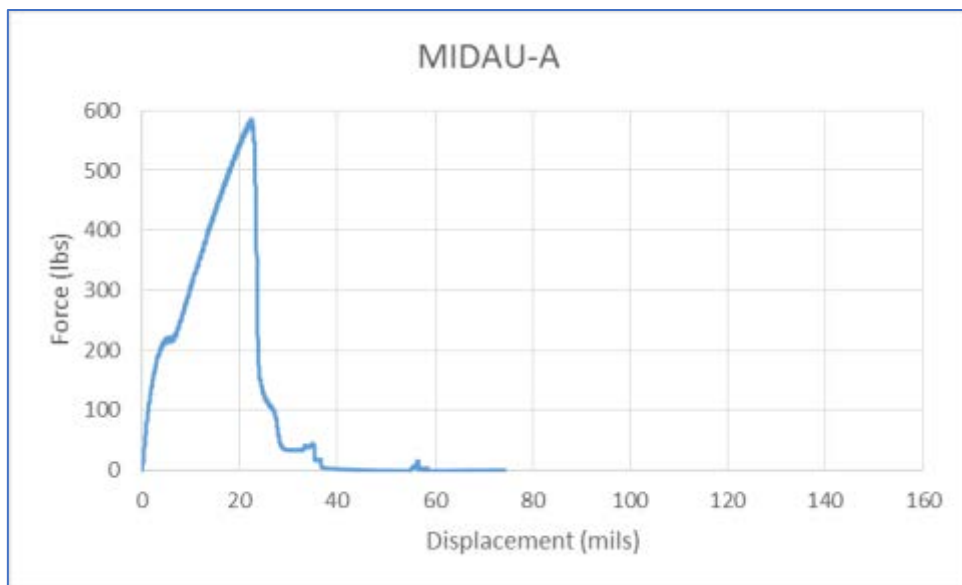
Figure A5.11 MIDAU Specimen A Force vs. Displacement (Tested on 6/5/15)
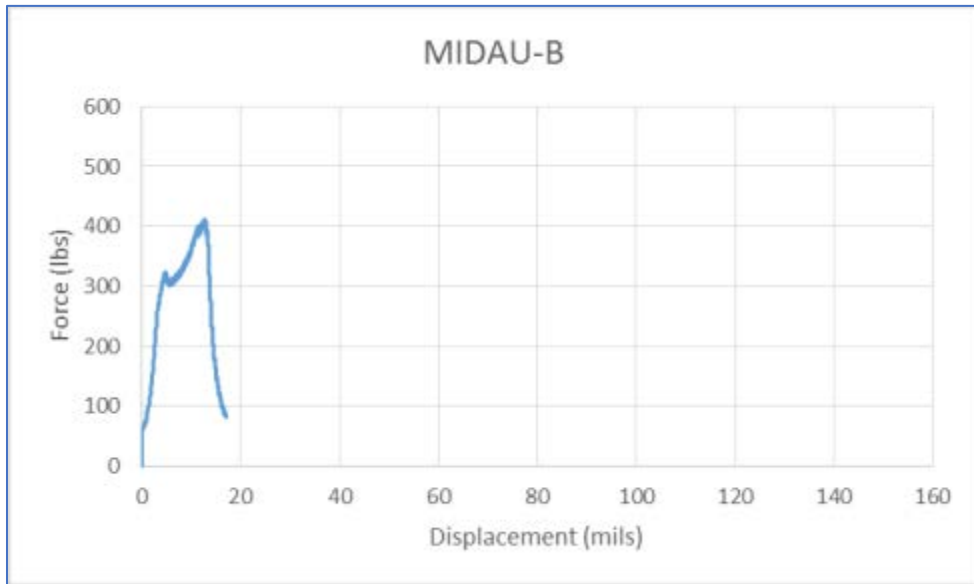
Figure A5.12 MIDAU Specimen B Force vs. Displacement (Tested on 6/17/15)
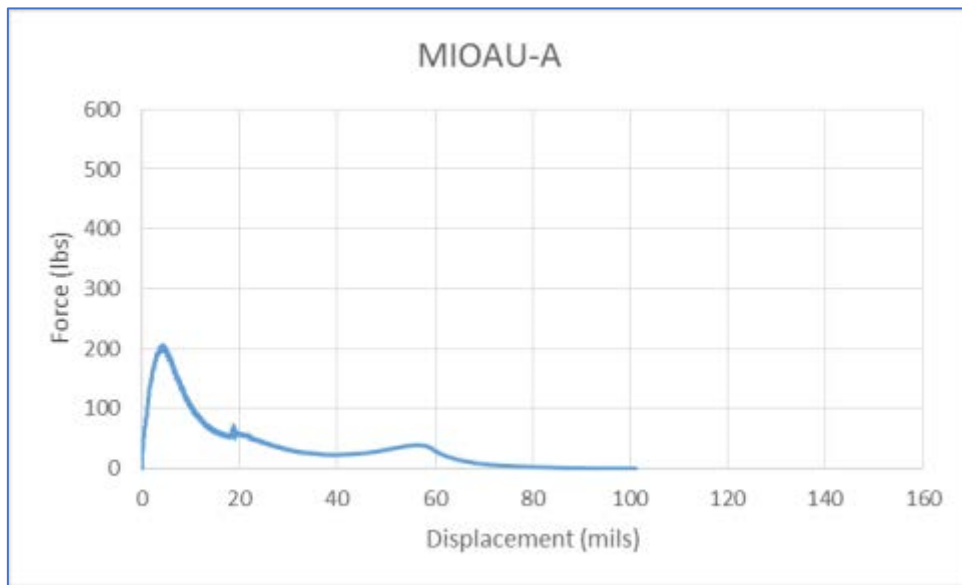
Figure A5.13 MIOAU Specimen A Force vs. Displacement (Tested on 6/10/15)
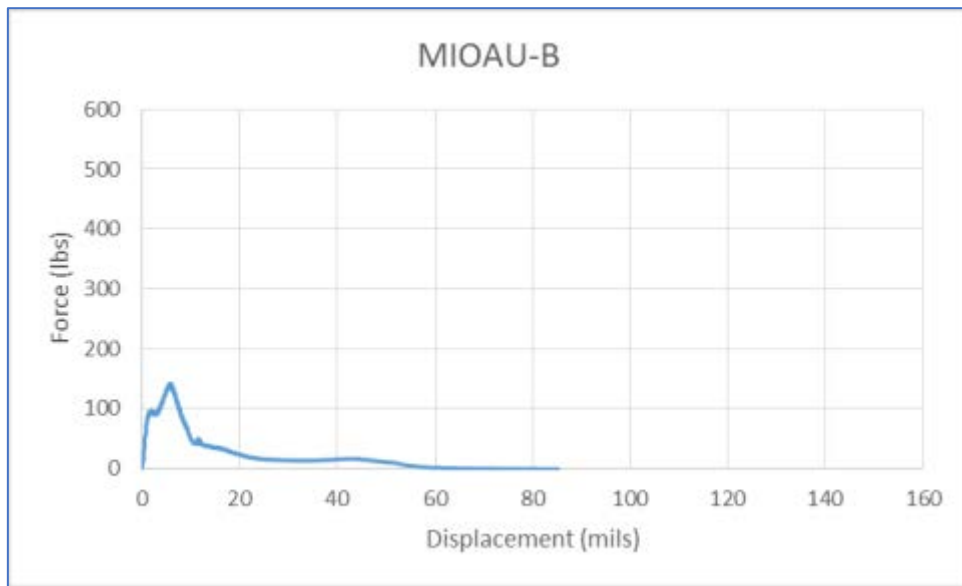
Figure A5.14 MIOAU Specimen B Force vs. Displacement (Tested on 6/10/15)

APPENDIX B: CALIBRATION DATABASE INFORMATION

For each calibration section considered in Chapter 7, detailed information is presented in the following tables which is required for the faulting model calculation.

Table B.1. Calibration sections project information

Source	SHRP_ID or ID	Const. Date	Survey Date	Age, yrs	Est ESALs	Longitude, deg	Latitude, deg
LTPP	6_9107	1-Oct-88	13-Jun-02	13.71	8.45E+06	95.04	44.84
LTPP	8_9020	1-Oct-86	24-Aug-98	11.9	7.69E+06	78.41	41.04
LTPP	18_9020	1-Jan-87	29-Apr-04	17.34	2.45E+07	96.37	31.9
LTPP	28_7012	1-Jul-85	7-Feb-12	26.62	1.71E+07	121.56	38.58
LTPP	42_1627	1-Sep-88	12-Nov-02	14.21	1.79E+07	120.55	39.31
LTPP	48_9167	15-Jun-88	29-Oct-12	24.39	1.50E+07	104.98	40.22
LTPP	48_9355	1-Mar-90	25-Mar-12	22.08	2.24E+07	104.99	40.39
MnROAD	Cell105	30-Oct-08	14-Apr-11	2.45	2.45E+06	93.65	45.24
MnROAD	Cell205	30-Oct-08	14-Apr-11	2.45	2.45E+06	93.65	45.24
MnROAD	Cell305	30-Oct-08	14-Apr-15	6.46	6.46E+06	93.65	45.24
MnROAD	Cell405	30-Oct-08	14-Apr-15	6.46	6.46E+06	93.65	45.24
MnROAD	Cell505	12-Sep-11	16-Apr-15	3.59	3.59E+06	93.65	45.24

MnROAD	Cell605	12-Sep-11	16-Apr-15	3.59	3.59E+06	93.65	45.24
MDOT	3033	2009	2015	6	3.30E+06		
MDOT	3111	2004	2015	11	7.77E+06		
MDOT	16091	2008	2015	7	1.76E+06		
MDOT	39014	2004	2015	11	7.77E+06		
MDOT	41026	2007	2015	8	4.59E+06		
MDOT	56044	2010	2014	4	9.92E+05		
MDOT	70063	2004	2015	11	6.72E+06		
MDOT	71111	2006	2011	5	2.70E+06		

Table B.2. Calibration sections design features

SHRP_ID or ID	Lane Width, ft	Tied PCC Shoulder	Avg Jt Spacing, ft	Dowel Diameter, in	Dowel Spacing, in	Drainage Type
6_9107	12	No, AC	13.5	None	None	Long Edgedrain
8_9020	12	Yes	20	None	None	None
27_9075	12	No, AC	15.5	None	None	None
42_1627	12	Yes	20.5	1.25	12	Long Edgedrain
48_9167	12	Yes	20	1.5	12	Long Edgedrain
48_9355	12	No	15	1.25	12	None
Cell105	14	No, AC	15	None	None	Wick Drains
Cell205	14	No, AC	15	None	None	Wick Drains
Cell305	14	No, AC	15	None	None	Wick Drains
Cell405	14	No, AC	15	None	None	Wick Drains
Cell505	6.5	No, AC	6	None	None	Wick Drains
Cell605	6.5	No, AC	6	None	None	Wick Drains
3033	12	Yes	12	1.25	12	Yes

3111	12	Yes	13	1.25	12	None
16091	12	Yes	12	1.25	12	Yes
39014	12	Yes	12	1.25	12	None
41026	12	Yes	14	1.25	12	18" PDS at EOP
56044	12	Yes	12	1.25	12	18" PDS at EOP
70063	12	Yes	14	1.25	12	18" PDS at EOP
71111	12	Yes	14	1.25	12	6" open graded underdrain

Table B.3. Calibration sections structural details

SHRP_ID or ID	Overlay thickness, in	Overlay EMOD, psi	Overlay MOR, psi	Interlayer thickness, in	Existing thickness, in	Existing EMOD, psi	Overlay Cement Content, lbs
6_9107	8.8	3.09E+06	530	1	7.6	4.75E+06	594.5
8_9020	8	3.44E+06	541	0.5	7.7	3.68E+06	565
27_9075	5.9	4.25E+06	714	0.8	8.5	3.7E+06	555
42_1627	10.3	3.31E+06	696	3.3	9.7	4.25E+06	541

48_9167	10.2	4.33E+06	858	8.6	8.4	4.85E+06	414
48_9355	10.3	4.85E+06	877	1.4	9.9	4.98E+06	354
Cell105	4.5	4.00E+06	660	1.75	7.1	4.63E+06	550
Cell205	4.5	4.00E+06	660	1.75	7.1	4.63E+06	550
Cell305	5	4.00E+06	660	1.75	7.1	4.63E+06	550
Cell405	5	4.00E+06	660	1.75	7.1	4.63E+06	550
Cell505	5	4.00E+06	660	NWGF	7.1	4.63E+06	550
Cell605	5	4.00E+06	660	NWGF	7.1	4.63E+06	550
3033	7	4.00E+06	625	1	9	4.50E+06	550
3111	7	4.00E+06	625	1	9	4.50E+06	550
16091	7	4.00E+06	625	1	9	4.50E+06	550
39014	7	4.00E+06	625	1	9	4.50E+06	550
41026	7	4.00E+06	625	1	9	4.50E+06	550
56044	7	4.00E+06	625	1	9	4.50E+06	550
70063	7	4.00E+06	625	1	9	4.50E+06	550
71111	7	4.00E+06	625	1	9	4.50E+06	550
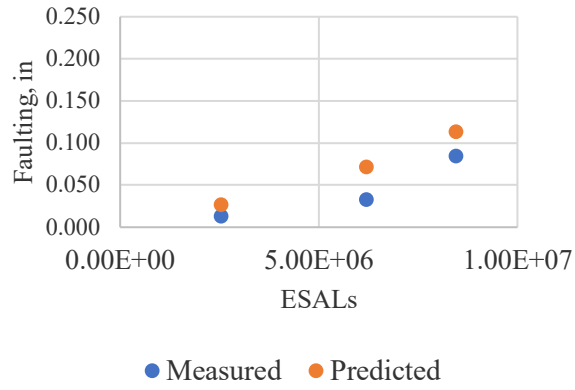
a)   LTPP 06_9107
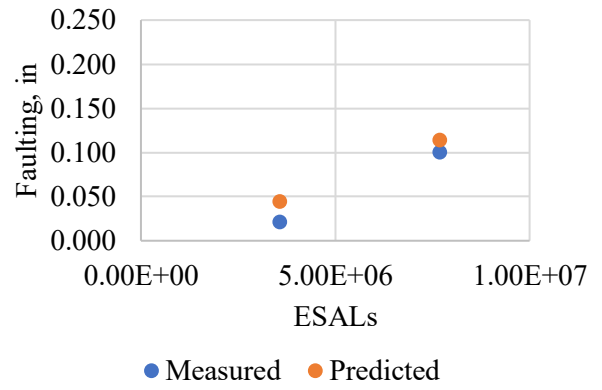
b)   LTPP 08_9020
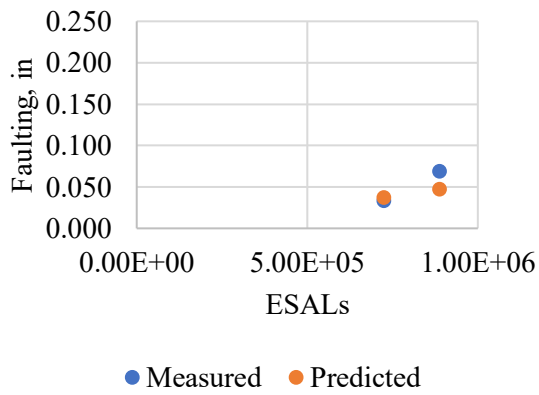
c)   LTPP 27_9075

d)   LTPP 48_9167

B-6
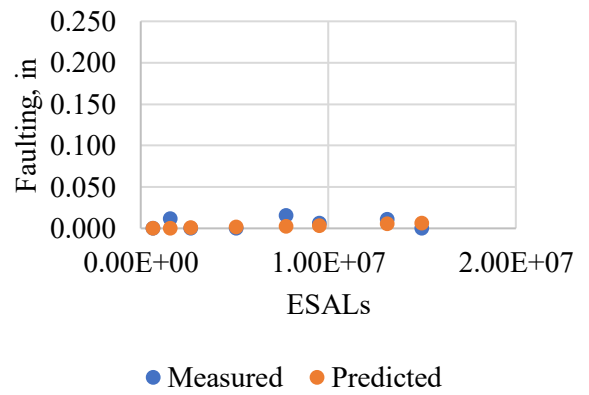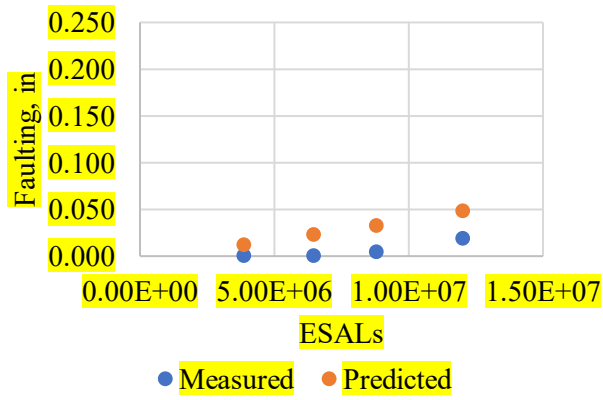
e) LTPP 42_1627
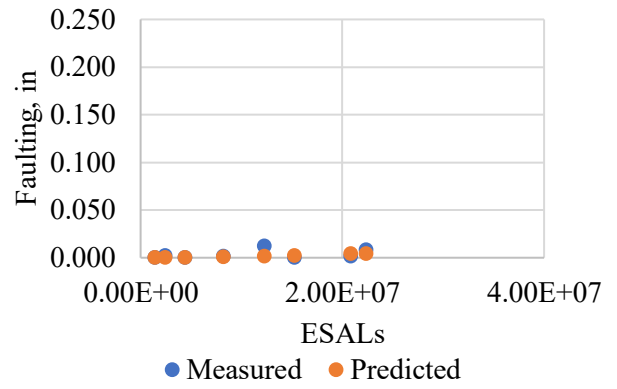
f) LTPP 48_9355
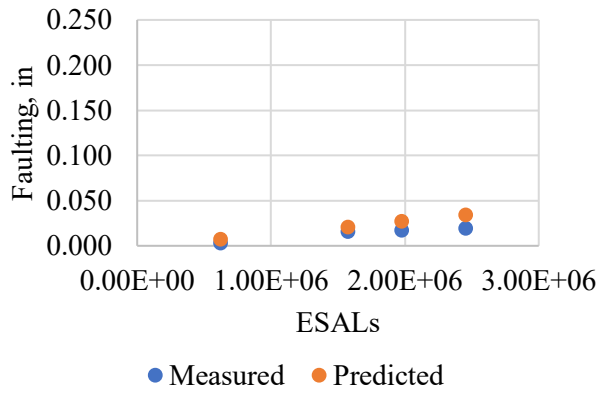
g) MnROAD Cell 105
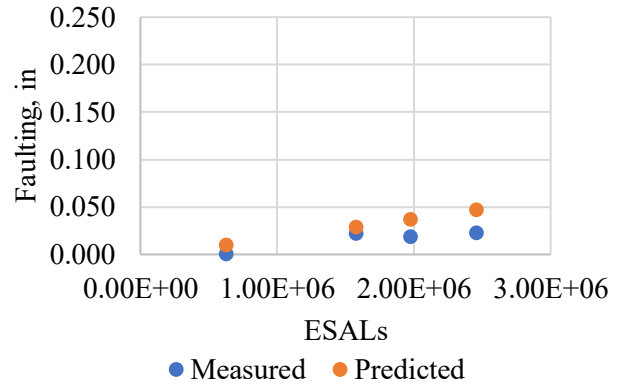
h) MnROAD Cell 205
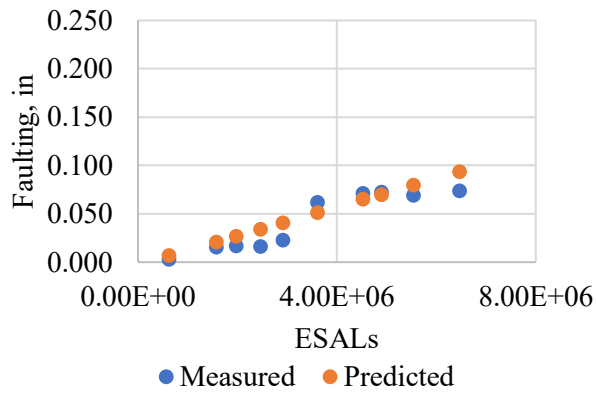
i) MnROAD Cell 305
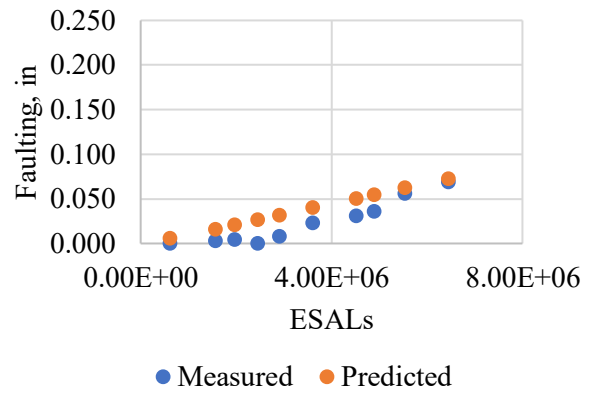
j) MnROAD Cell 405
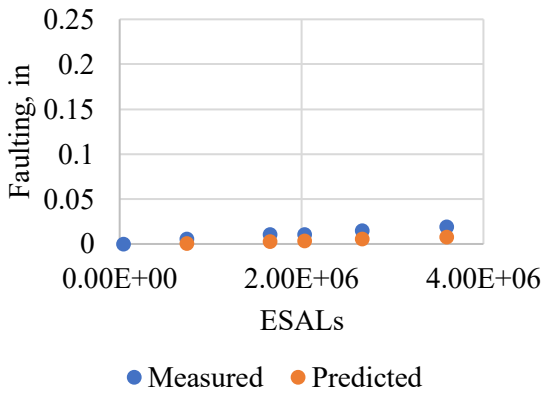
k) MnROAD Cell 505

l) MnROAD Cell 605

B-8
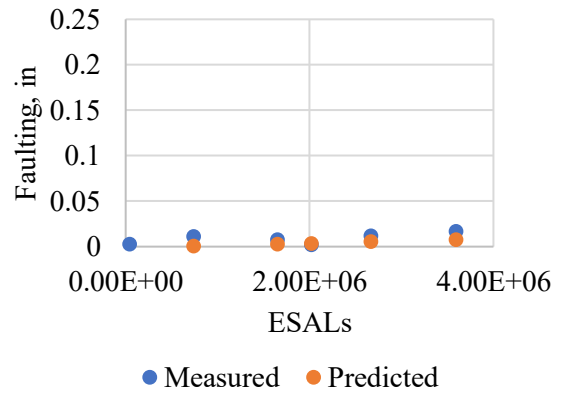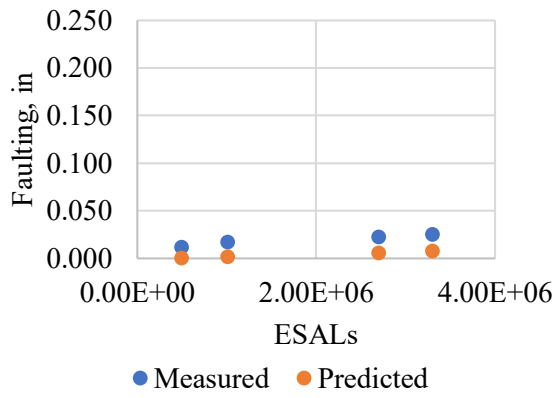
m) MDOT 3033
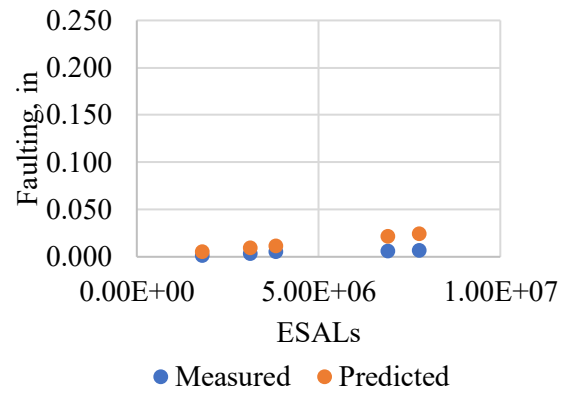
n) MDOT 3111
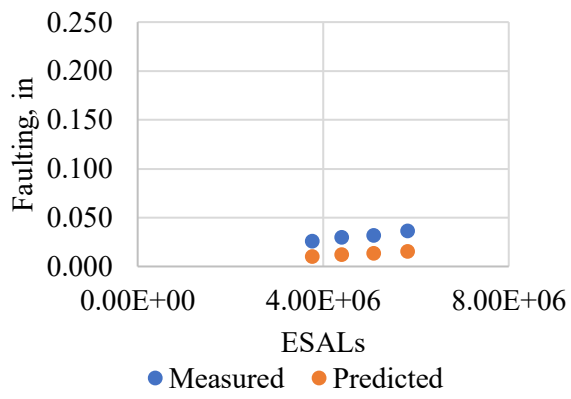
o) MnDOT 9101
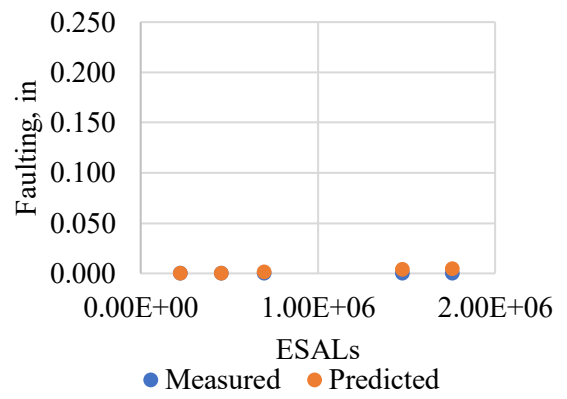
p) MnDOT 16091
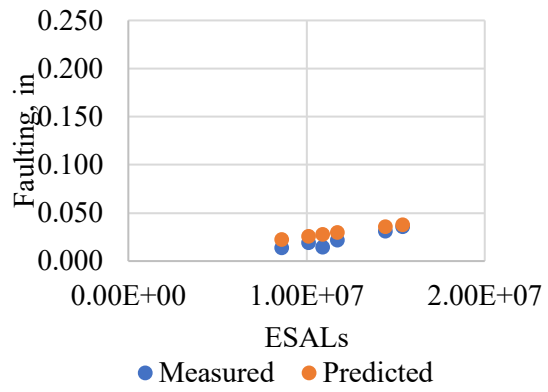
q) MnDOT 19022
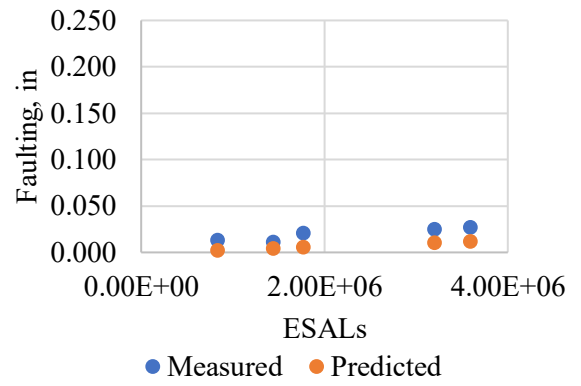
r) MnDOT 25032
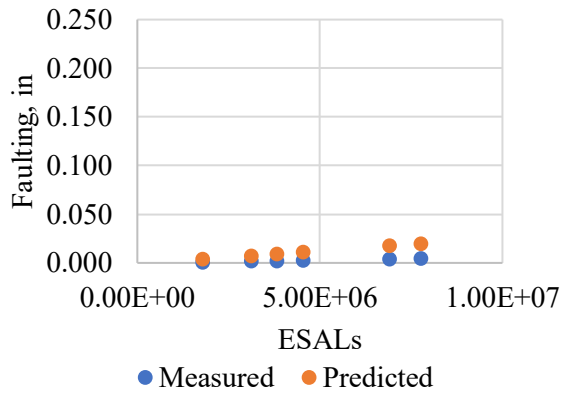
s) MnDOT 39014
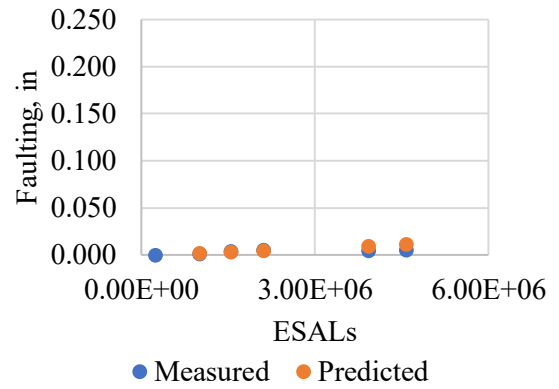
t) MnDOT 41026
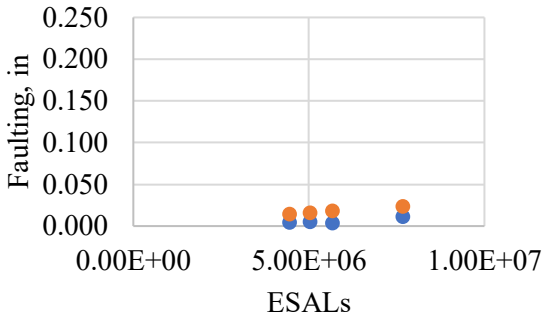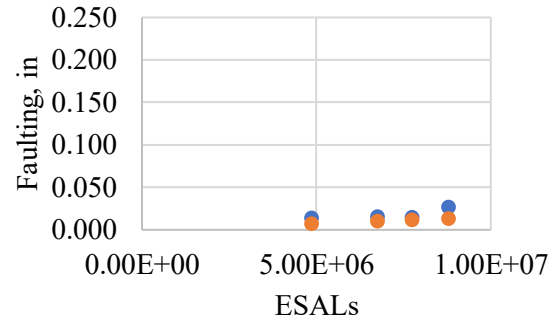
u) MnDOT 41132

v) MnDOT 47014
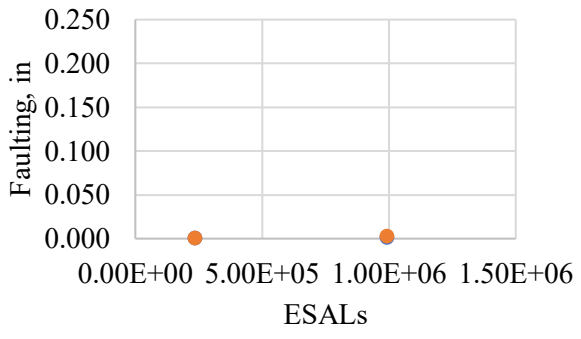
w) MnDOT 56044
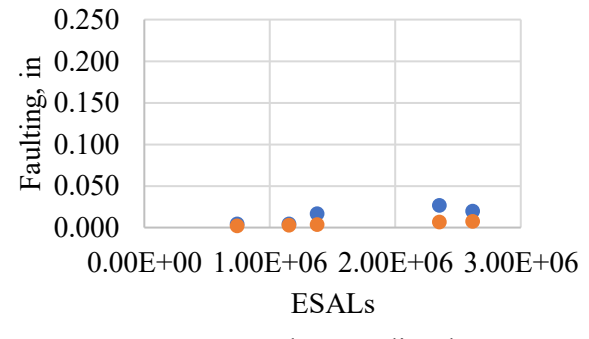
x) MnDOT 65041
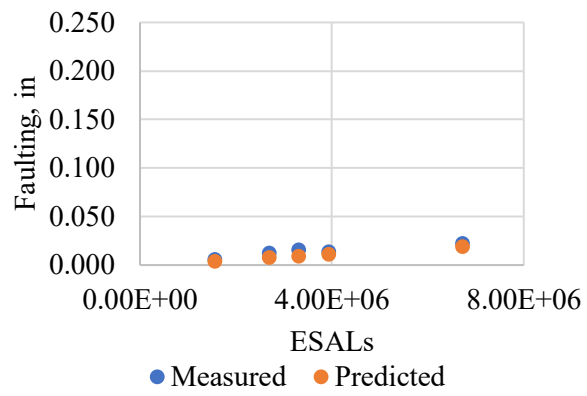
y)   MnDOT 70063
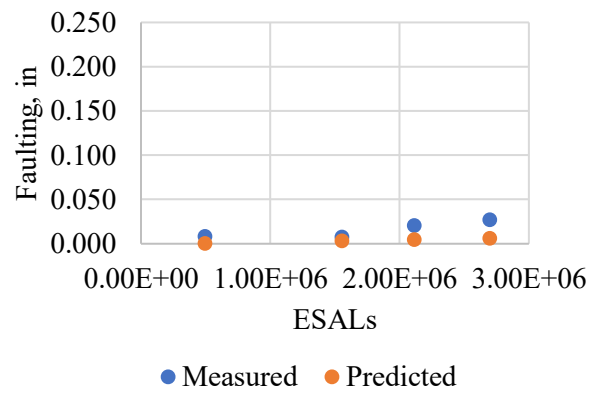
z)   MnDOT 7111

Figure B.1. Calibration section plots

APPENDIX C: USER GUIDE

TABLE OF CONTENTS

The program performs design and analysis of unbonded concrete overlays using the procedure developed under TPF-5(269) project "Development of an Improved Design Procedure for Unbonded Concrete Overlays Setup Instructions

From Windows Explorer, double click on "setup.exe" file. The following screen will appear:

Click "Next". The Installation Wizard will prompt the user to select a destination directory for the UNOLDesign program.
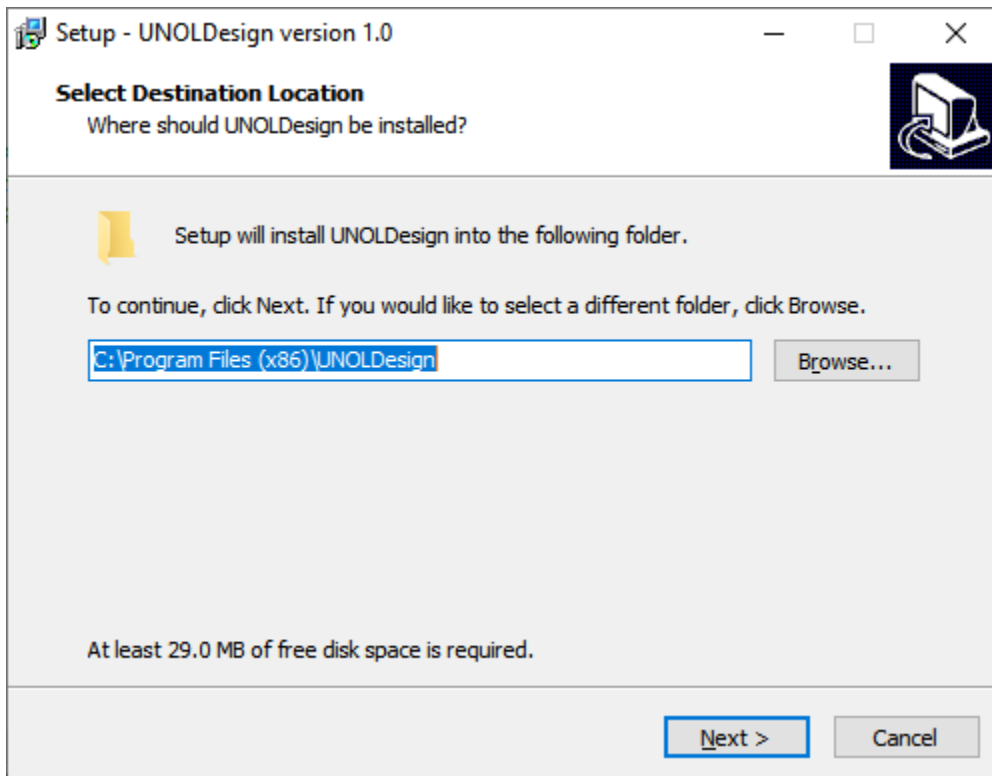
If the destination location is not already the root directory of one of the hard drives on your computer, it is recommended to change the directory using the "Browse" option as shown in the example below:

Setup - UNOLDesign version 1.0

Select Destination Location
Where should UNOLDesign be installed?

Setup will install UNOLDesign into the following folder.

To continue, click Next. If you would like to select a different folder, click Browse.

C:\UNOLDesign   Browse...

At least 29.0 MB of free disk space is required.

Next >   Cancel
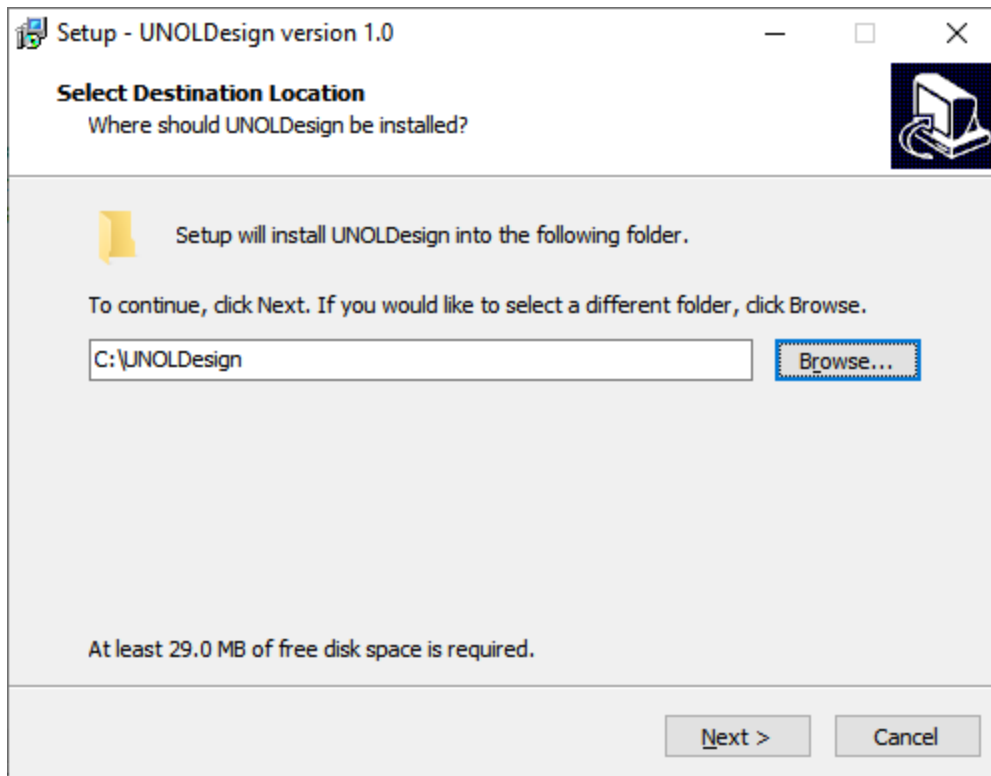
After clicking "OK", the following screen appears:
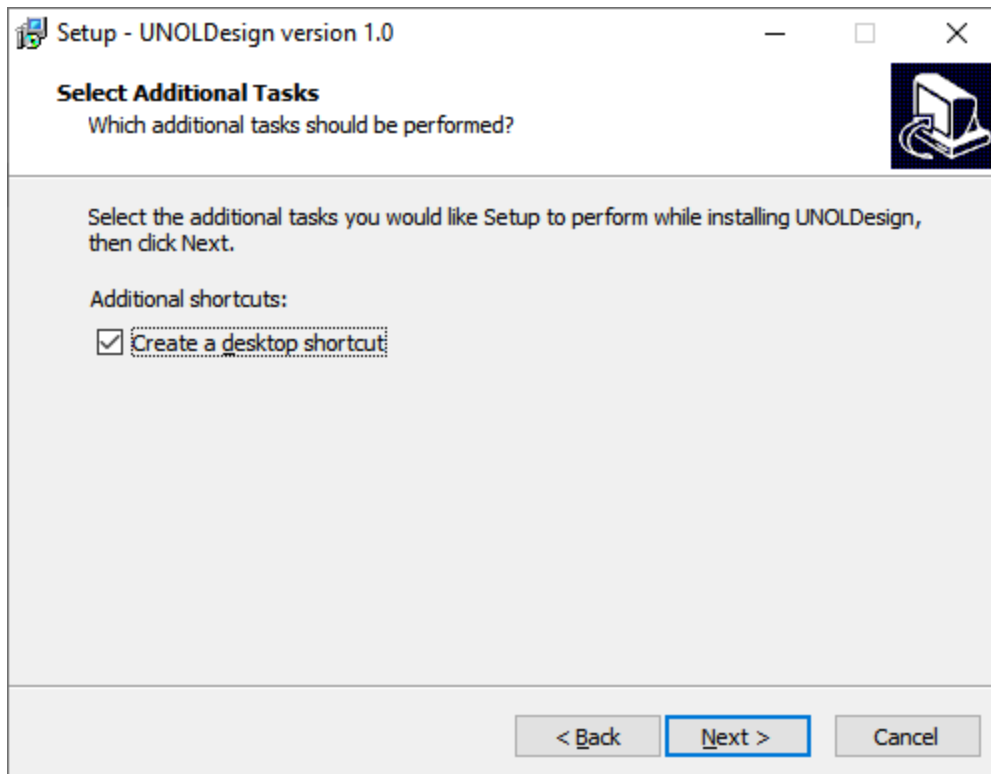
Click "Next", and then follow the on-screen instructions to complete the installation.

1. EXECUTING THE UNOLDESIGN PROGRAM

1.1 Design Inputs

The application starts with the following screen:

By default, a new empty project is created. The user should modify the default parameters. The following ranges of the input values can be analyzed by the current version of the programs:

- Reliability level: 40 to 99 %.

- Overlay thickness: from 6 to 12 in for convention slab width overlays and from 4 to 10 in for short slabs (6 ft by 6 ft) overlays

- Design life: from 1 to 100 years. Must be an integer value.

- Two-way annual average daily truck traffic (AADTT): from 0 to 10,000 (do not enter comma in the input).

- Joint spacing: either 6 ft or from 12 to 16 ft.

- Existing PCC thickness: from 6 to 16 in.

Existing PCC elastic modulus: from 500,000 to 10,000,000 psi (do not enter commas in the input).

Two types of analyses can be performed: reliability or cracking prediction.

If the reliability checkbox is checked, the user should provide the target design reliability, and the program will find the corresponding overlay thickness meeting this reliability level.

☑ Reliability analysis

Climate Station   MOBILE AL ▾

Reliability, percent   90

If the reliability checkbox is unchecked, the user should provide the overlay thickness, and the program will predict the cracking level at the end of the pavement design life.

☐ Reliability analysis

Climate Station   MOBILE AL ▾

Overlay Thickness, in   7

Two types of interlayers can be analyzed: hot mix asphalt (HMA) or geotextile fabric. If the HMA option is selected, the user is prompted to provide the following HMA layer parameters:
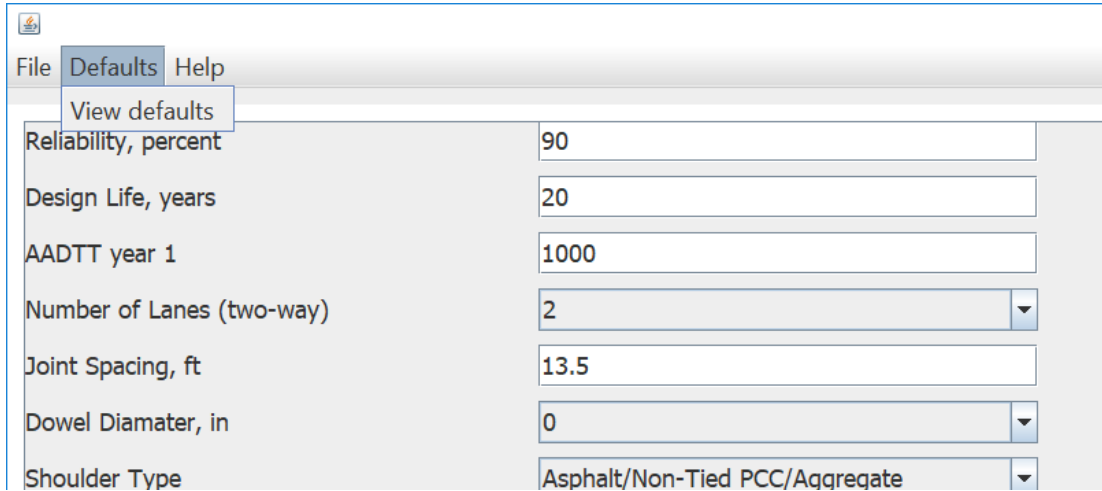
- Effective binder content

- Percent passing #200 sieve

- Percent of air voids

Effective binder content by volume, %   5   Percent air voids   5

Percent passing #200 sieve in interlayer   3
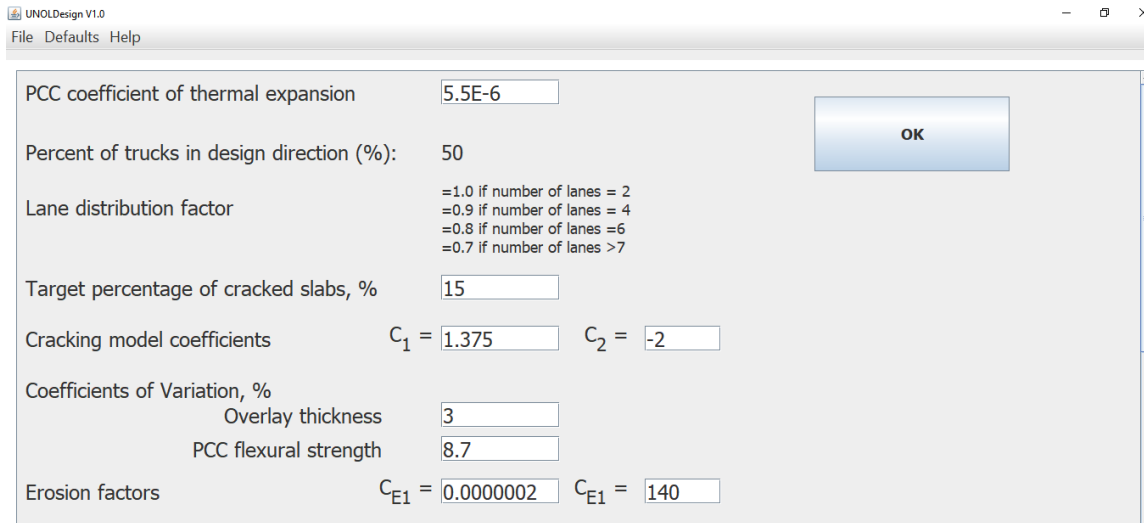
1.2 View/Modify Defaults

To view or modify default, select Defaults->View defaults option.

File **Defaults** **Help**	
View defaults	
Reliability, percent	90
Design Life, years	20
AADTT year 1	1000
Number of Lanes (two-way)	2
Joint Spacing, ft	13.5
Dowel Diamater, in	0
Shoulder Type	Asphalt/Non-Tied PCC/Aggregate

The following screen should appear:

UNOLDesign V1.0

File Defaults Help

PCC coefficient of thermal expansion	5.5E-6
Percent of trucks in design direction (%):	50
Lane distribution factor	=1.0 if number of lanes = 2 =0.9 if number of lanes = 4 =0.8 if number of lanes =6 =0.7 if number of lanes >7
Target percentage of cracked slabs, %	15

OK

Cracking model coefficients C_1 = 1.375 C_2 = -2

Coefficients of Variation, %

Overlay thickness   3

PCC flexural strength   8.7

Erosion factors C_{E1} = 0.0000002 C_{E1} = 140

If the screen is scrolled down then the remaining portion of the options will appear:

Coefficients of Variation, %

Overlay thickness   3

PCC flexural strength   8.7

Erosion factors C_{E1} = 0.0000002 C_{E1} = 140

a = 0.14

b = 0.15

c = 0.04

Target mean joint faulting, in   0.15

Faulting model coefficients

C_1 = 1.25 C_2 = 1.5 C_3 = 0.75 C_4 = 0.015 C_5 = 0.01 C_6 = 1.45 C_7 = 0.85

The user has an option to change the target percentage of cracked slabs and mean joint faulting, cracking and faulting model coefficients (see Equations 75 and Equations 116 through 119, respectively), default coefficients of variation in reliability analysis, and erosion model coefficients (see Equation 60). It is recommended that only advanced users modify these parameters.

Click "OK" button to return to the main screen.

1.3 Executing the Analysis

Once the files and data options have been selected, user can press the "Run" button. If the "Run" button does not appear on the screen, scroll the window to the bottom.

Joint spacing, ft	13.5
Dowel diamater, in	0
Shoulder type	Asphalt/Non-Tied PCC/Aggregate
Flexural strength, psi	650
Existing PCC thickness, in	10
Existing PCC modulus, psi	4000000
Interlayer type	Asphalt

Effective binder content by volume, %   5   Percent air voids   5   Run
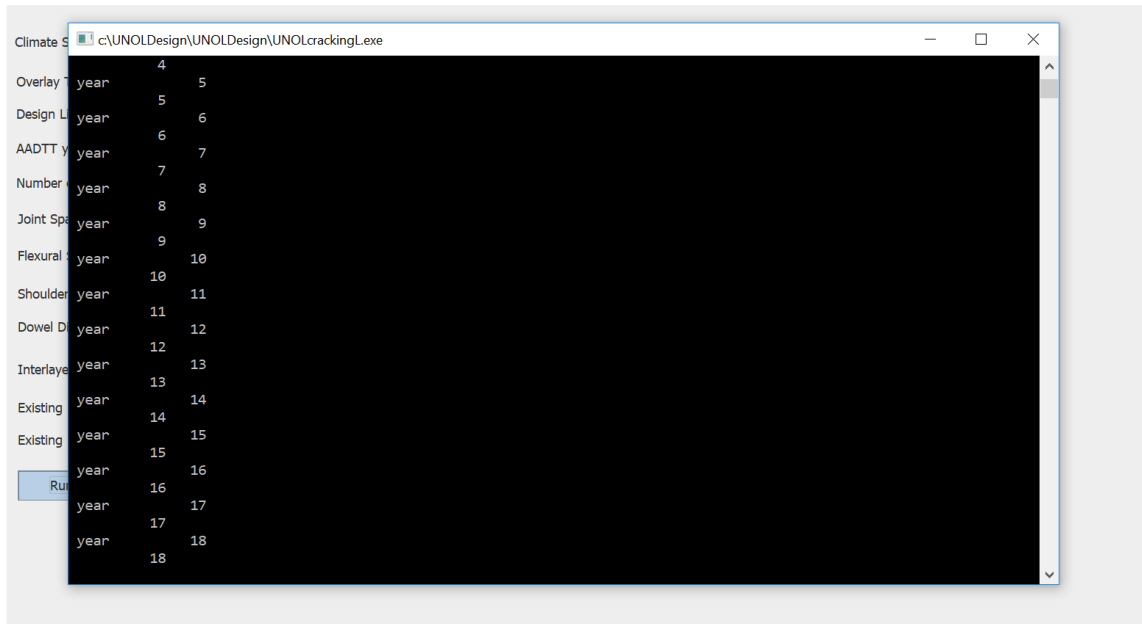
Percent passing #200 sieve in interlayer   3

If the input value is out or range or of a wrong type, an error message will appear, for example:
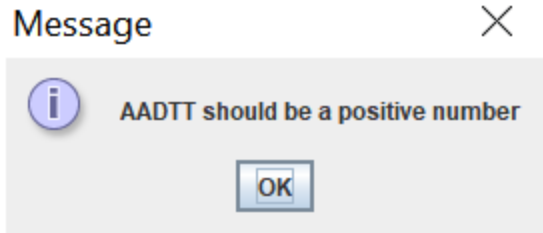
After the user clicks OK, the background of the corresponding input cell will turn red:

The user will need to correct the input(s) and press the Run button again. If all the input values are acceptable, the MS DOS window will appear.

Once the cracking analysis is completed, the MS DOS window will disappear and another MS DOS window with the faulting analysis will appear. After the faulting analysis is completed, the results of the analysis will appear. If the reliability analysis is being performed, the resulting PCC overlay thickness satisfying slab cracking requirements at the specified reliability level is displayed along with the predicted slab cracking and joint faulting at the specified reliability level and at 50% reliability.
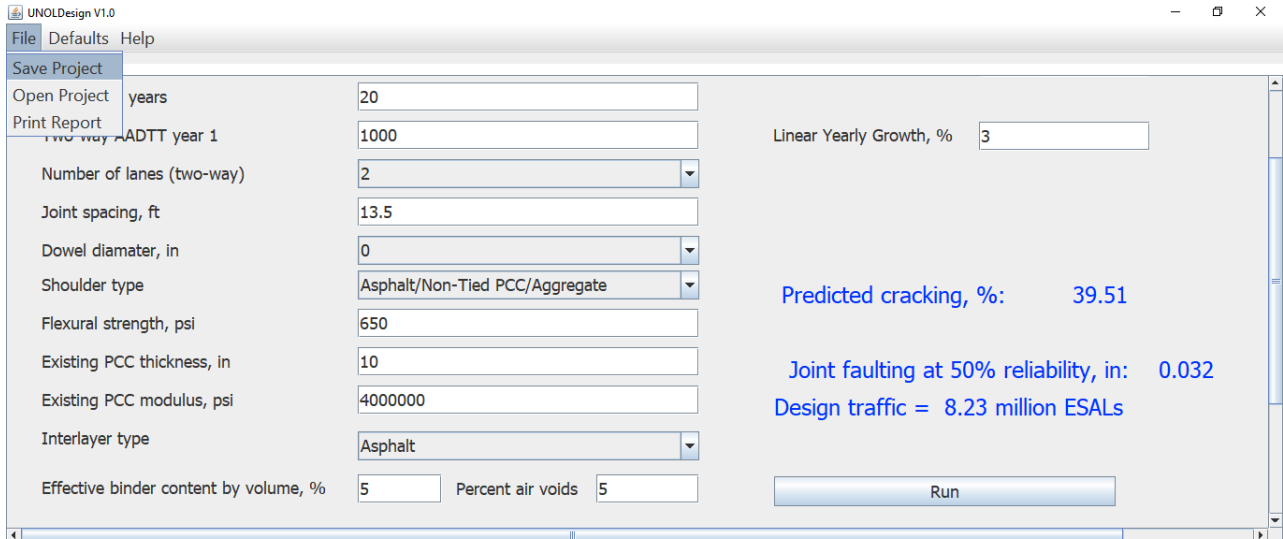

If the reliability analysis option is not selected, the predicted **percentage of cracked slabs and mean joint faulting at 50% reliability level** are displayed.
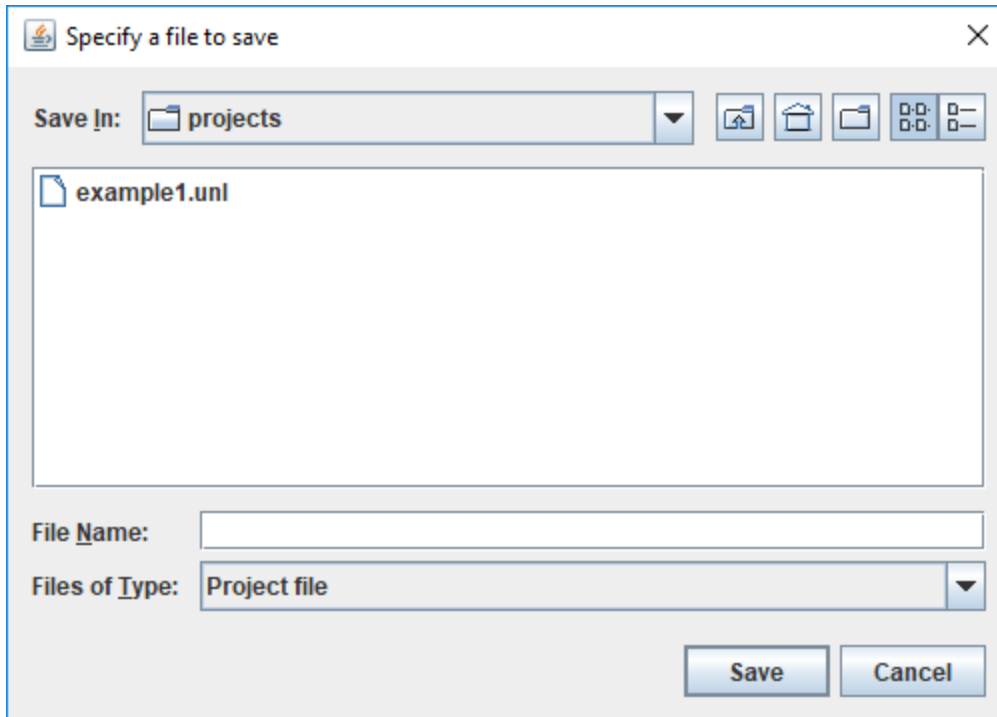
Design life, years	20		
Two-way AADTT year 1	1000	Linear Yearly Growth, %	3
Number of lanes (two-way)	2		
Joint spacing, ft	13.5		
Dowel diamater, in	0		
Shoulder type	Asphalt/Non-Tied PCC/Aggregate		
Flexural strength, psi	650		
Existing PCC thickness, in	10		
Existing PCC modulus, psi	4000000		
Interlayer type	Asphalt		
Effective binder content by volume, %	5 Percent air voids 5		

Predicted cracking, %:   39.51

Joint faulting at 50% reliability, in: 0.032
Design traffic = 8.23 million ESALs

Run

1.4 Saving the Project

To save the project, select from the menu File->Save Project option:

UNOLDesign V1.0   — ☐ ✕

File Defaults Help

Save Project
Open Project   years   20
Print Report   1000   Linear Yearly Growth, %   3
Two-way AADTT year 1
Number of lanes (two-way)   2
Joint spacing, ft   13.5
Dowel diamater, in   0
Shoulder type   Asphalt/Non-Tied PCC/Aggregate
Flexural strength, psi   650   Predicted cracking, %:   39.51
Existing PCC thickness, in   10
Existing PCC modulus, psi   4000000   Joint faulting at 50% reliability, in: 0.032
Interlayer type   Asphalt   Design traffic = 8.23 million ESALs
Effective binder content by volume, %   5   Percent air voids 5   Run
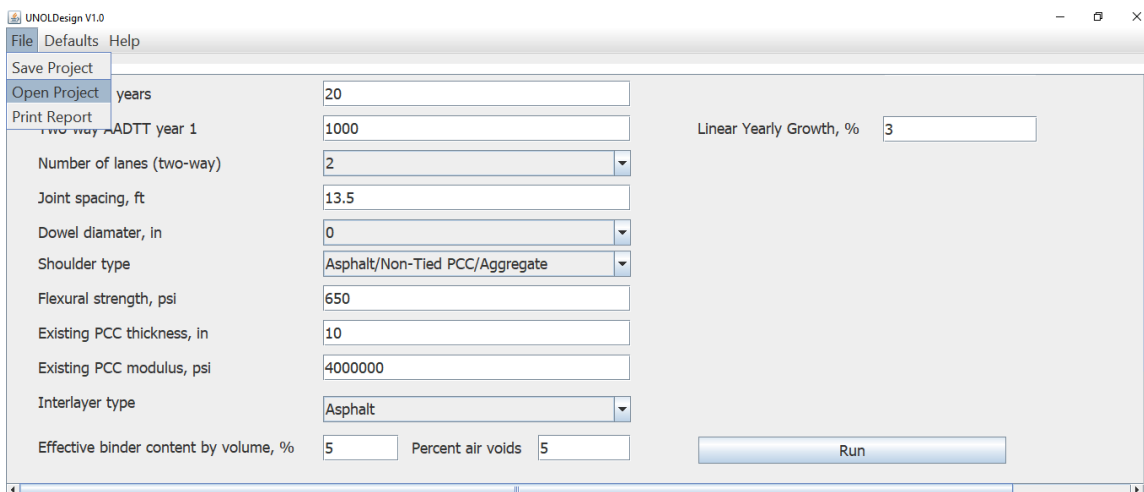
The following dialog box will appear:

Navigate to the desired location, provide the file name and click "Save" button.
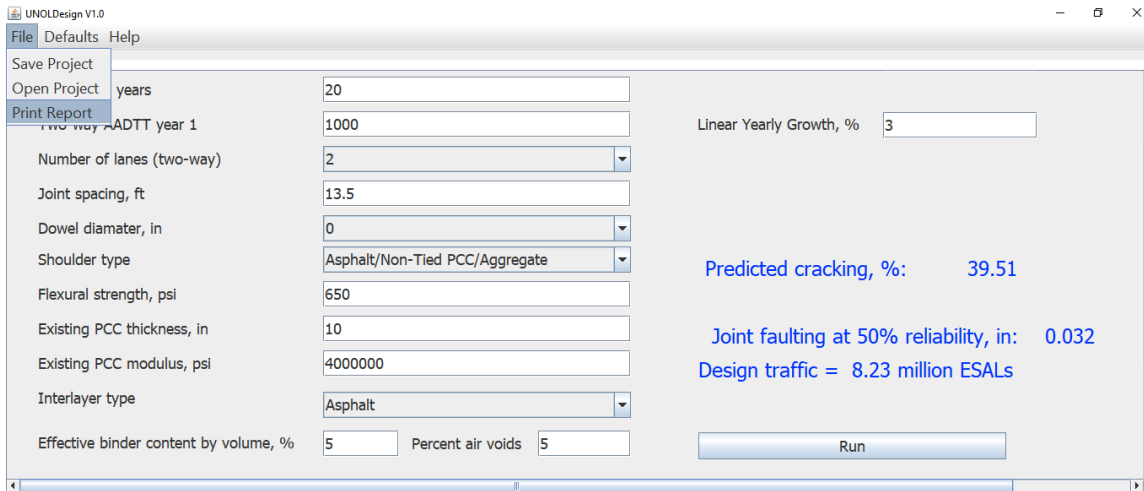
1.5 Opening Project

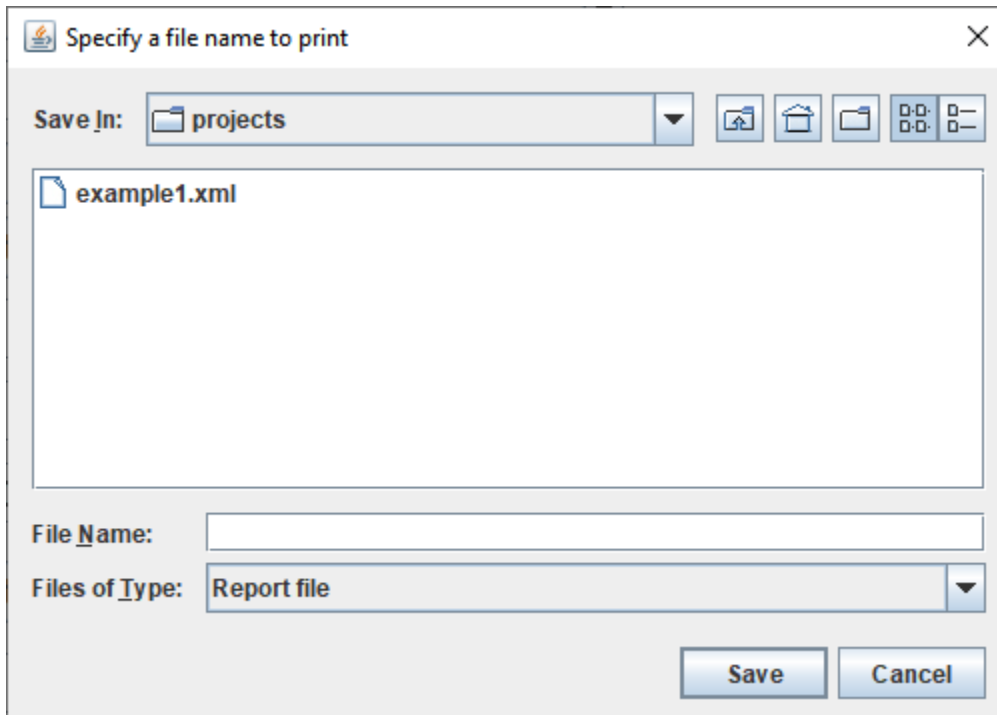To open an existing project, select from the menu File->Open Project option.

Find the desired file and click "OK" button.

1.6 Printing Report

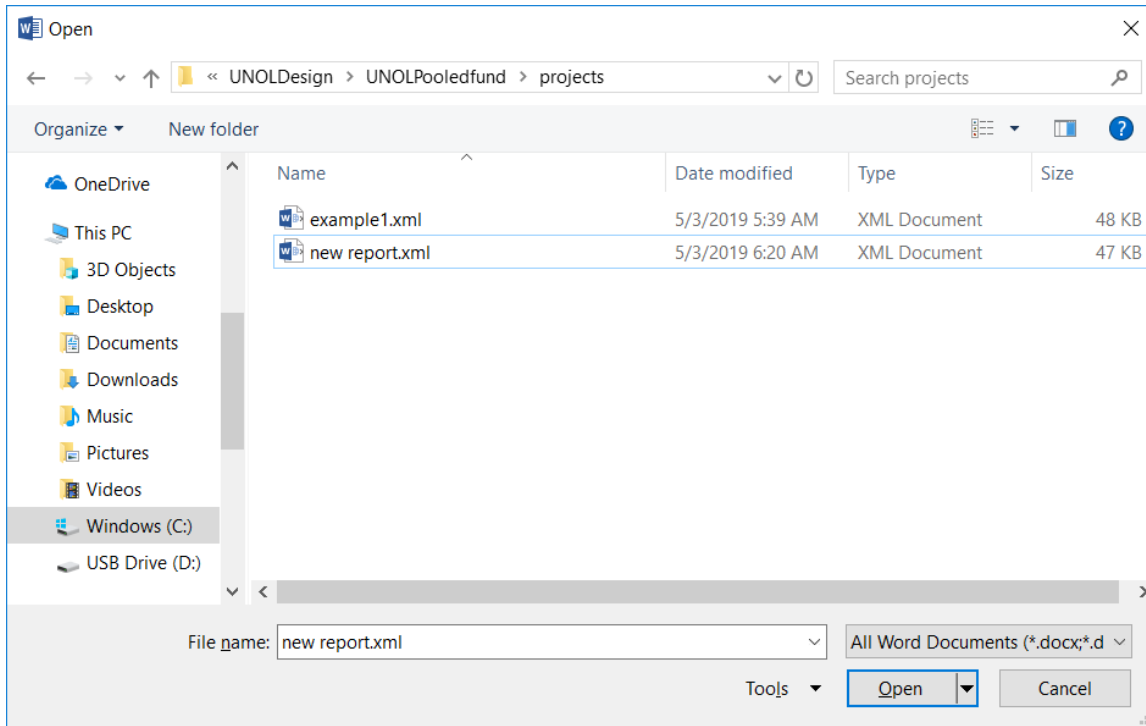To create a report, select from the menu File->Open Project option.

The following dialog box will appear:

Navigate to the desired location, provide the file name and click "Save" button.

The file will be saved with an extesion ".xlm".

The report can be later opened using MS WORD. When open the document, the file type option "All Word Documents (*.docx, *.docm, …) should be selected.

An example of an output file is shown below:

Unbonded Overlay Design

01-12-2019 00:32:06

Inputs:

Location: MOBILE AL

Design life, years: 20

First year AADTT: 1000   Linear growth, %: 3

Number of lanes: 2

Overlay cracking reliability, %: 90

PCC overlay 28 days flexural strength, psi: 650

Joint spacing: 13.5

Dowel diameter, in: 0

Shoulder type: Asphalt/Non-Tied PCC/Aggregate

Existing PCC thickness, in: 10   Existing PCC modulus of elasticity, psi: 4000000

Interlayer type: Asphalt

    Interlayer effective binder, %: 5

    Air void content, %: 3

    P200 content, %:5

Outputs:

Required PCC overlay thickness, in : 8.30

Cracking at specified reliability, %: 12.65

Cracking at 50 reliability, %:   2.44

Joint faulting at specified reliability, in: 0.046

Joint faulting at 50% reliability, in: 0.022

Design traffic = 10.56 million ESALs